Government of Western Australia

Department of
**Mines and Petroleum**

REPORT
149

# CHARACTERIZATION AND CORRELATION OF LOWER PERMIAN STRATA, CANNING BASIN, WESTERN AUSTRALIA, AND IMPLICATIONS FOR $CO_2$ SEQUESTRATION

by LM Dent

Geological Survey of Western Australia

Government of Western Australia
Department of Mines and Petroleum

REPORT 149

# CHARACTERIZATION AND CORRELATION OF LOWER PERMIAN STRATA, CANNING BASIN, WESTERN AUSTRALIA, AND IMPLICATIONS FOR $CO_2$ SEQUESTRATION

by
LM Dent

Perth 2016

Geological Survey of
Western Australia

**MINISTER FOR MINES AND PETROLEUM**
**Hon. Sean K L'Estrange MLA**

**DIRECTOR GENERAL, DEPARTMENT OF MINES AND PETROLEUM**
**Richard Sellers**

**EXECUTIVE DIRECTOR, GEOLOGICAL SURVEY OF WESTERN AUSTRALIA**
**Rick Rogerson**

**REFERENCE**
**The recommended reference for this publication is:**
Dent, LM 2016, Characterization and correlation of lower Permian strata, Canning Basin, Western Australia, and implications for $CO_2$ sequestration: Geological Survey of Western Australia, Report 149, 104p.

**National Library of Australia Cataloguing-in-Publication entry:**

| | |
|---|---|
| **Creator**: | Dent, L., author. |
| **Title:** | Characterization and correlation of lower Permian strata, Canning Basin, Western Australia and implications for CO2 sequestration / L.M. Dent. |
| **ISBN:** | 9781741686678 (ebook) |
| **Subjects:** | Sedimentology--Western Australia--Canning Basin.<br>Carbon sequestration--Western Australia--Canning Basin.<br>Geology--Western Australia--Canning Basin. |
| **Other Authors/Contributors:** | Geological Survey of Western Australia, issuing body |
| **Dewey Decimal Classification:** | 552.5099411 |

**ISSN 0508–4741**

Grid references in this publication refer to the Geocentric Datum of Australia 1994 (GDA94). Locations mentioned in the text are referenced using Map Grid Australia (MGA) coordinates, Zones 51 and 52. All locations are quoted to at least the nearest 100 m.



**Published 2016 by Geological Survey of Western Australia**
This Report is published in digital format (PDF) and is available online at <www.dmp.wa.gov.au/GSWApublications>.

**Further details of geological publications and maps produced by the Geological Survey of Western Australia are available from:**
Information Centre
Department of Mines and Petroleum
100 Plain Street
EAST PERTH WESTERN AUSTRALIA 6004
Telephone: +61 8 9222 3459 Facsimile: +61 8 9222 3444
**www.dmp.wa.gov.au/GSWApublications**

**Cover photograph:** Grant Group and Poole Sandstone outcrop at St George Ranges

# Contents

# Appendices



# Figures



# Table



# Plates

Plates 1–6 accompany this Report

# Characterization and correlation of lower Permian strata, Canning Basin, Western Australia, and implications for $CO_2$ sequestration

**by**

**LM Dent**

## Abstract

The Poole Sandstone and Noonkanbah Formation are recognized as part of the first-order Late Carboniferous – Permian Megasequence. Within this megasequence, the two formations are part of the second-order Early–Late Permian Supersequence I. This Report presents facies analysis and well-log data that allow further subdivision into two third-order sequences in the Noonkanbah Formation and eight fourth-order sequences between the uppermost Grant Group and top of the Noonkanbah Formation. Third- and fourth-order sequences comprise a series of stacked, high-frequency cycles, the formation of which may be related to Milankovitch processes.

The Poole Sandstone displays a major facies variation from northwest to southeast. Five facies associations are identified in outcrop and cored sections: fluvial (FA1), tidal flat (FA2), shoreface (FA5), shallow marine carbonate ramp (FA9) and offshore (FA7). The formation is typically sandstone-dominated but mudstone facies become more prevalent at the base of the Poole Sandstone in the northwest of the study region. The Noonkanbah Formation is dominated by mudstone facies across the study area. Four major facies associations are identified in cored sections: tidal flat (FA3), shoreface (FA5), offshore transitional (FA6) and offshore (FA7). Facies associations in the Noonkanbah Formation have a consistent stratigraphic position across large areas. The depositional setting and character of the uppermost Grant Group (G1) are also discussed in this Report to assist stratigraphic subdivision and correlation, and tidal and fluvial facies associations are identified (FA1, FA4, and FA8).

Subsurface carbon dioxide ($CO_2$) sequestration is now considered a significant climate change mitigation strategy, as a result of which, a prospective $CO_2$ sequestration site was investigated in the northern Canning Basin near James Price Point. The Permo-Carboniferous Grant Group and Poole Sandstone are possible reservoirs, sealed by the Noonkanbah Formation. The lateral facies changes, abundant mudstone facies, and the presence of an extensive basal carbonate facies in the region around James Price Point suggest the lowermost Poole Sandstone has limited potential as a reservoir. Reservoir potential increases with increase in sandstone facies; for example, up-section and to the southeast, with high porosities (up to 32%). Heterogeneity produced by cyclicity on large and small scales, variable clay and cement distributions, and locally pervasive bioturbation in the Noonkanbah Formation may have significant implications for the integrity of the unit as a regional $CO_2$ sequestration seal. Variation in formation thickness due to basin structure and local structural features may also affect the formation's suitability as a sealing unit.

**KEYWORDS**: facies analysis, regressive sediments, sequence stratigraphy, stratigraphic correlation, transgressive sediments, well log interpretation

## Introduction

Recent discoveries of conventional and unconventional petroleum resources in the Canning Basin have led to a significant increase in interest and research into the basin's geological history and fill (Zhan and Mory, 2013; Kingsley and Streitberg, 2013; Al-Hinaai and Redfern, 2013; Parra-Garcia et al., 2014). Proposals for geological $CO_2$ sequestration in the late Carboniferous – early Permian Grant Group near James Price Point (Fig. 1) have increased the group's economic significance along with the overlying early Permian Poole Sandstone and Noonkanbah Formation (Dentith et al., 2015). The Grant Group has been extensively studied due to its potential as a petroleum reservoir (Crostella, 1998; O'Brien et al., 1998; Eyles et al., 2001). The Noonkanbah Formation is the proposed major seal for the $CO_2$ storage site, but its sealing potential and the potential influence of the underlying Poole Sandstone on $CO_2$ migration are largely unknown due to limited previous characterization. Both formations were deposited during the final stages of the Gondwanan deglaciation and are widely distributed across the Canning Basin. This Report describes the sedimentology, well-log characteristics and stratal geometry of the Poole Sandstone and Noonkanbah Formation, which are used to interpret depositional history controlled by global climatic changes and tectonic activity.

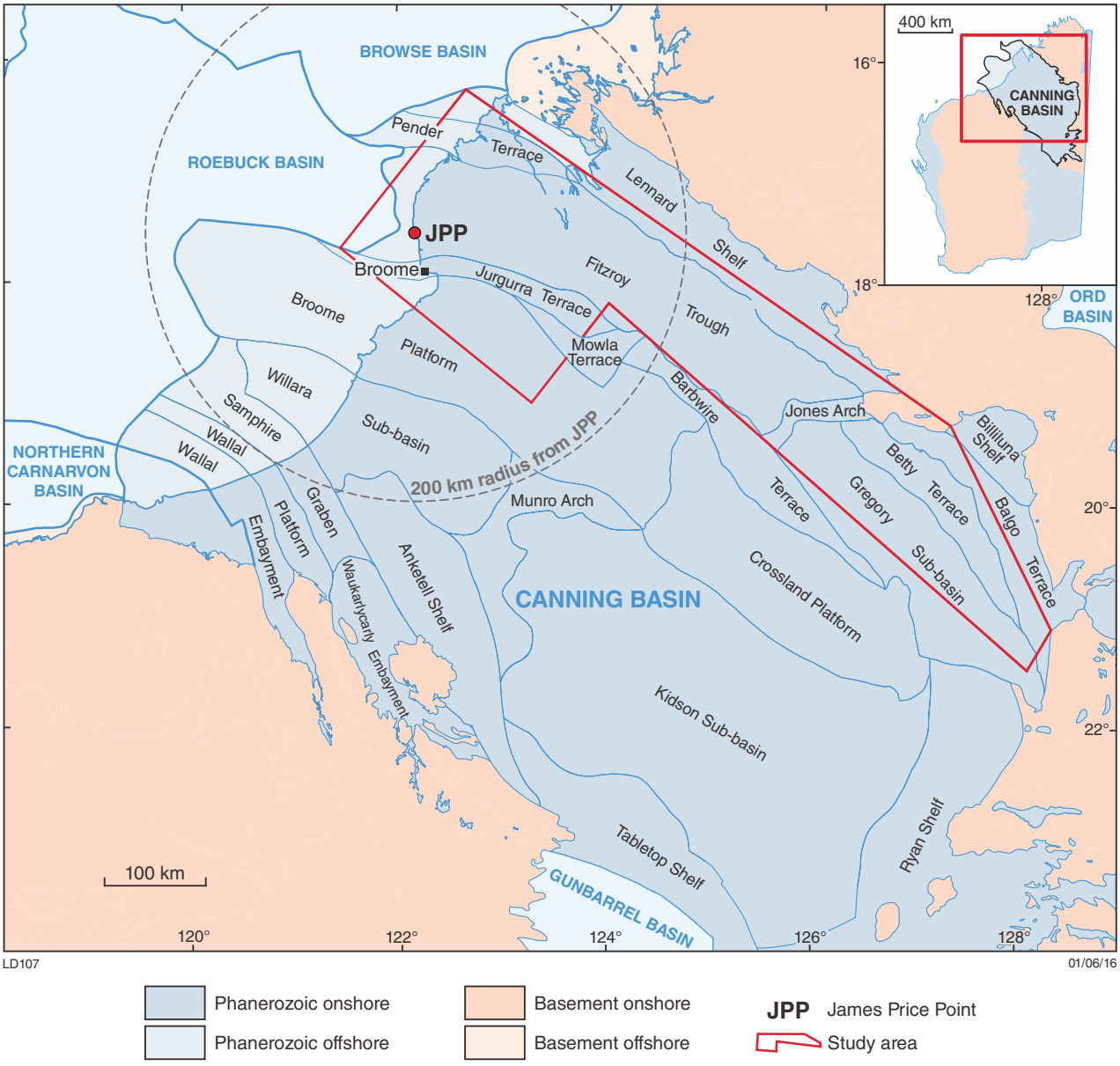


**Figure 1. Structural subdivisions of the Canning Basin (after Martin et al., 2015) displaying the extent of the study area and location of James Price Point. Inset shows location in Western Australia.**

Excessive anthropogenic $CO_2$ in the atmosphere as a significant contributor to global climate change is now widely, though not universally, accepted (Bachu, 2008; Ghommem et al., 2012). The role of $CO_2$ in the atmosphere was originally identified in 1896 by Swedish physicist–chemist Svante Arrhenius (Arrhenius, 1896). He proposed that $CO_2$ affected the activity of incident radiation and atmospheric temperature, an idea that was pursued for almost a century with concern that human activities would cause significant changes in Earth's climate. In 1987 the World Meteorological Organization (WMO) identified the need for a global scientific assessment of climate change. The Intergovernmental Panel on Climate Change (IPCC) was subsequently formed in 1988. The IPCC's first report in 1990 identified that levels of greenhouse gases in the atmosphere, including $CO_2$, were being increased by human activities with the potential to cause changes in global climate (Houghton et al., 1990). Carbon dioxide separation and geological storage (geosequestration) were identified as a potential avenue for greenhouse mitigation (Houghton et al., 1990). The first $CO_2$ sequestration project was initiated at the Sleipner gasfield in the North Sea in 1996 (Chadwick et al., 2004). In 2005 the IPCC produced a special report on detailed methods, criteria and analysis of different styles of sequestration including geological storage (Metz et al., 2005). Australia currently hosts five sequestration projects (Table 1; Cook, 2006; Varma et al., 2011; Jenkins et al., 2012). A sixth project in the northwest Canning Basin was proposed to store

**Table 1. Location, operational stage and $CO_2$ source of current $CO_2$ sequestration projects in Australia**

| *Project* | *State* | *Basin* | *$CO_2$ source* | *Stage* |
|---|---|---|---|---|
| Collie Hub | Western Australia | South-central Perth Basin | Collie and Kwinana fertiliser production | Evaluation |
| Carbon Net | Victoria | Gippsland Basin | Latrobe Valleys coal-fired power stations | Evaluation |
| Wandoan Power | Queensland | Surat Basin | Future Wandoan Power IGCC project | Evaluation |
| Gorgon Project | North West Shelf | | | |
| Western Australia | Browse Basin | Natural gas processing | Execution | |
| Otway Project | Victoria | Otway Basin | Petroleum production | Execution |

$CO_2$ waste from potential liquefied natural gas (LNG) production and processing at an onshore facility planned at James Price Point. Based on integration of well-log and sedimentological data for the Poole Sandstone and Noonkanbah Formation, within a sequence stratigraphic framework, the current Report examines the suitability of these formations for the proposed $CO_2$ sequestration site within a 200 km onshore radius of James Price Point (Fig. 1).

# Geological setting

## Canning Basin

The Canning Basin has the largest onshore area of any Australian basin, covering ~530 000 km$^2$, with a further 110 000 km$^2$ extension offshore to the northwest (Fig. 1). The basin is bounded by the Kimberley Craton to the northeast and the Pilbara Craton to the west. Basin formation was initiated by extension and subsidence in the Early to Middle Ordovician. A further five major tectonic events between the Middle Devonian and Triassic significantly contributed to the structural development of the basin (Drummond et al., 1991; Kennard et al., 1994; Shaw et al., 1994; Fig. 2). The basin is composed of four large sub-basins: the Fitzroy Trough, Gregory Sub-basin, Kidson Sub-basin and the Willara Sub-basin, each flanked by a series of platforms and shelves (Hocking, 1994; Shaw et al., 1994; Fig. 1). A dominant northwest trend is displayed by these major structural components, controlled by regional, northwest-trending, extensional faults (Kennard et al., 1994; Shaw et al., 1994).

The Fitzroy Trough hosts up to 15 km of sedimentary fill of Ordovician age and younger (Forman and Wales, 1981; Drummond et al., 1991; Shaw et al., 1994; Fig. 2). Isopach models of the Permo-Carboniferous basin fill indicate that the thickest deposits of both the Poole Sandstone and the Noonkanbah Formation are in the Fitzroy Trough, up to 160 m and 640 m, respectively (Mory, 2010). Sedimentary successions are thinner on basement highs flanking the Fitzroy Trough, including the Broome Platform and Crossland Platform, and are up to about 5 km thick on the Lennard Shelf (Kennard et al., 1994; Shaw et al., 1994).

## Gondwanan deglaciation

The early Permian Earth was in a major transitional phase as the Permo-Carboniferous glaciation came to an end. Deglaciation began at c. 300 Ma as the ice sheets that covered Gondwana since c. 330 Ma rapidly receded, filling neighbouring basins with glacially derived detritus (Veevers, 2006). Previous work by Powell and Veevers (1987), Veevers (2006) and Isbell et al. (2012) indicated the presence of glaciers over central and northern Western Australia. The provenance of glacially derived sedimentary rocks in the Canning Basin has not been extensively studied; a north-northwest movement of ice sheets has been interpreted based on the striated pavements on Devonian limestone (Playford, 2001, 2002). More recent work by Haines et al. (2013) suggested the Alice Springs Orogeny generated the major sediment source for the basin.

Eyles et al. (2002) defined a three-part sedimentary succession or 'deglaciation sequence' that can be correlated between Western Australian sedimentary basins (Fig. 3). Typically this succession constitutes: a coarse, clastic, basal glacial deposit; a middle shale unit; and an upper, sandy deltaic succession (Eyles et al., 2002). The Poole Sandstone and Noonkanbah Formation represent the third phase of this sequence in the Canning Basin (Fig. 3). These deglaciation sequences are well correlated between basins but the sequence is diachronous, most notably in the Southern Carnarvon and northern Perth Basins (Fig. 3; Backhouse, 1993; Eyles et al., 2002, 2003).

Permo-Carboniferous deglaciation triggered a first-order eustatic sea-level rise that can be correlated between Gondwanan basins worldwide (Dickins, 1996; Wopfner, 1999). Coeval deglaciation sequences in the Western Australian basins are also observed in the Paraná Basin in Brazil and the Karoo and Kalahari Basins in South Africa (Visser, 1997; Vesely and Assine, 2006). Veevers (2006) interpreted shoreline incursion in the Canning Basin in the early Permian resulting from this global sea-level rise (Fig. 4). In addition to the three-part sequence of Eyles et al. (2002), numerous Permo-Carboniferous deglaciation sequences are overprinted by a high-frequency cyclicity. This signature is observed worldwide in the mid-continental sedimentary basins in the US (Heckle, 1986), Karoo and Kalahari Basins, South Africa (Visser, 1997), eastern Australia (Fielding et al., 2008), and the Kennedy Group in the Carnarvon Basin (Lever, 2004).

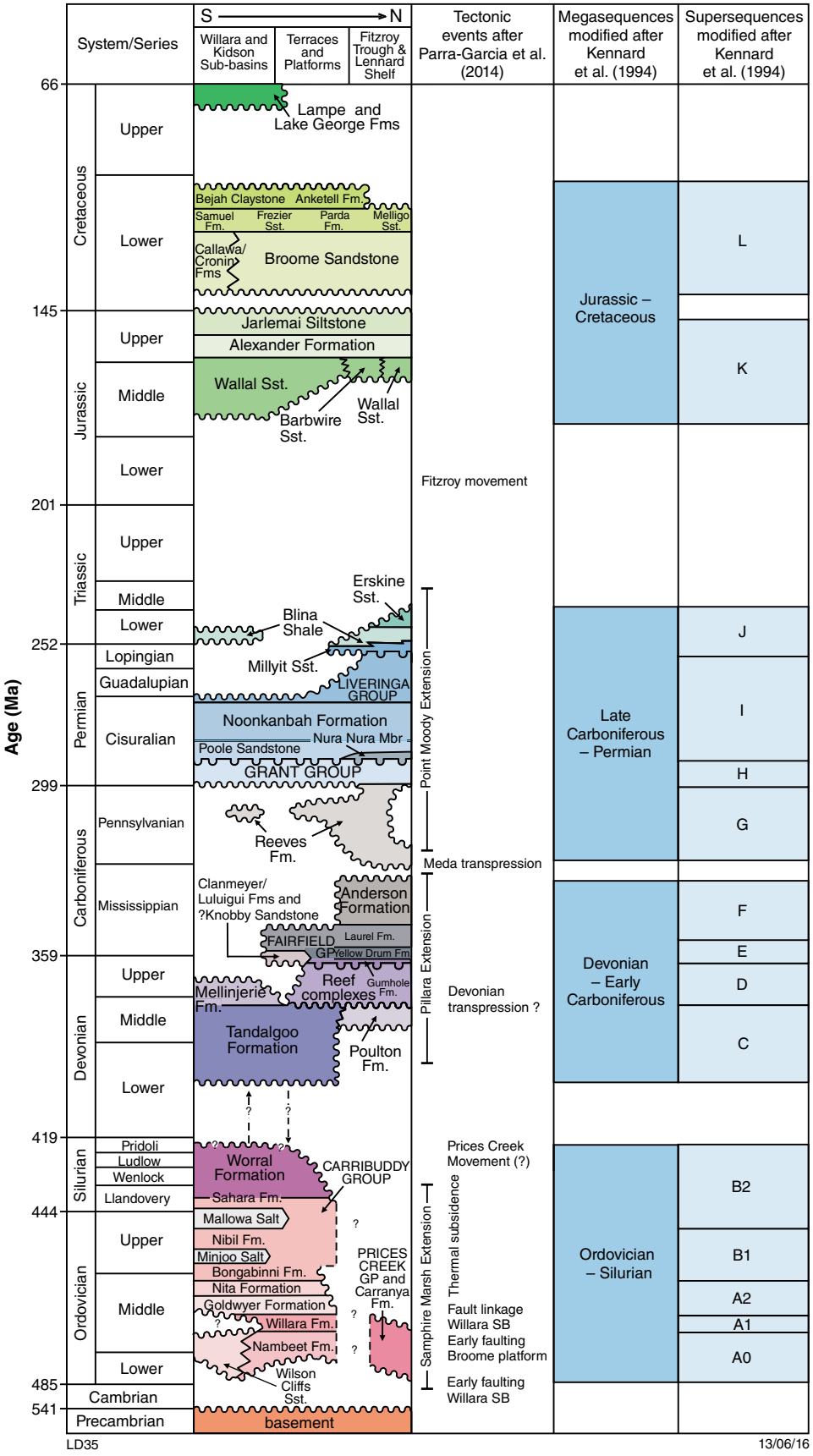


**Figure 2. Summary of Canning Basin stratigraphy (revised from Shaw et al., 1994), major tectonic events that have affected the Canning Basin (after Parra-Garcia et al., 2014), and depositional megasequences and supersequences (modified after Kennard et al., 1994). Fm.. – Formation; Gp – Group; Sst. – Sandstone**

Adkins (2003) proposed similar high-frequency cyclicity in the Poole Sandstone. This Report also describes such cycles in the Poole Sandstone, and throughout the Noonkanbah Formation.

## Sequence stratigraphic framework

The sequence stratigraphic framework for the Canning Basin, proposed by Kennard et al. (1994), divides the basin fill into four first-order megasequences: Ordovician–Silurian, Devonian – Early Carboniferous, Late Carboniferous – Permian, and Jurassic – Cretaceous (Fig. 2). Each megasequence represents approximately 70–80 Ma and is correlated with a major tectonic event in the basin history (Kennard et al., 1994). The four megasequences are further divided into 15 second-order supersequences (Fig. 2). Supersequences are transgressive–regressive cycles of ~10–20 Ma duration, attributed to the interplay between subsidence and eustacy (Kennard et al., 1994).

Division of supersequences into component third-order sequences has been undertaken for the Ordovician–Silurian (Romine et al., 1994) and Devonian – Early Carboniferous megasequences (Southgate et al., 1993; George et al., 2013). Third-order cycles have not been identified in the upper Carboniferous strata; however, this Report proposes third-order cycles for the lower Permian Noonkanbah Formation.

The Grant Group, Poole Sandstone and Noonkanbah Formation belong to the Late Carboniferous – Permian Megasequence deposited from c. 330 to 243 Ma (Kennard et al., 1994). The base of this megasequence is defined by a basinwide unconformity related to the Meda Transpression, with accommodation in the basin generated by the ensuing Point Moody Extensional Event (Kennard et al., 1994; Parra-Garcia et al., 2014).

The Poole Sandstone, Noonkanbah Formation, and Liveringa Group are assigned to the early–late Permian Supersequence I (Fig. 2). Transgression following the end of glaciation has been interpreted at the base of this supersequence leading to deposition of the Poole Sandstone (Yeates et al., 1975; Towner et al., 1976; Middleton, 1990; Kennard et al., 1994). However, Crowe and Towner (1976a) and Adkins (2003) interpreted a locally regressive character for the Poole Sandstone, and Warris (1993) suggested both transgressive and regressive conditions during deposition, for which the transgressive phase is represented by the basal Nura Nura Member of the Poole Sandstone. The order of sequences defined by Crowe and Towner (1976a) and Warris (1993) is not specified; however, their descriptions may refer to third-order transgressive–regressive events within Supersequence I.

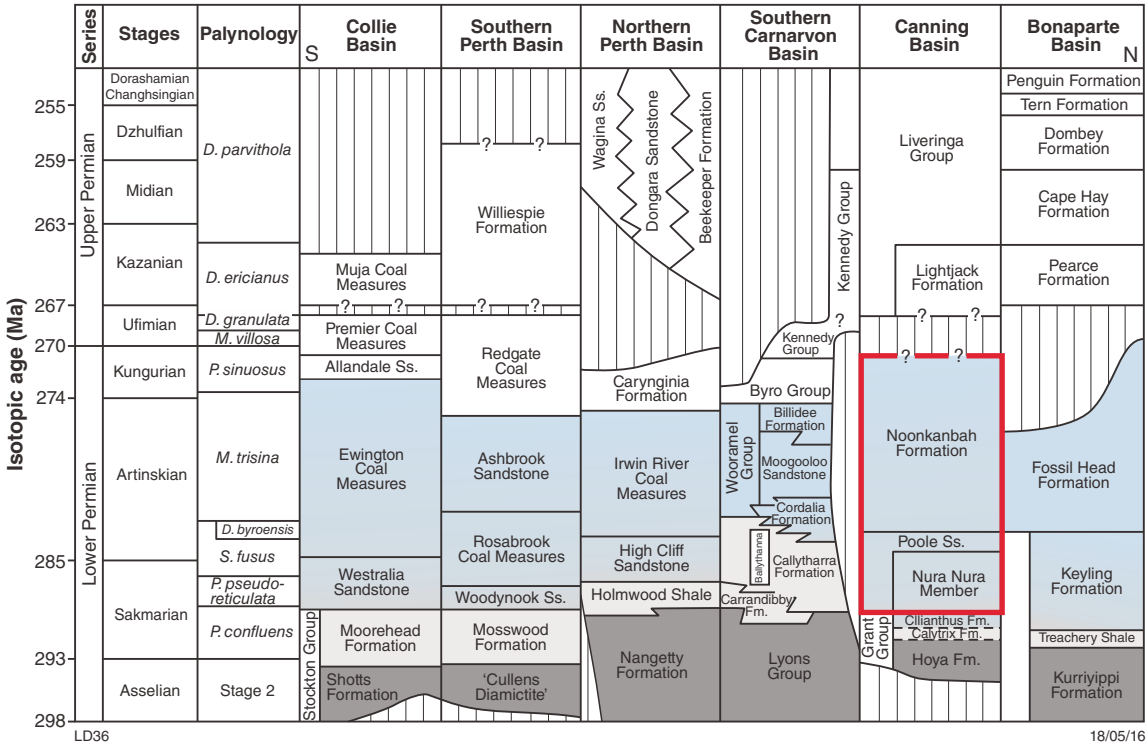


**Figure 3. Correlation of 'deglaciation' sequences in Western Australian sedimentary basins adapted from Eyles et al. (2002). Dark grey units represent the first of three deposits in the deglaciation sequence. The middle deposits are illustrated in pale grey, and pale blue units represent the final deglaciation deposits, including the Poole Sandstone and Noonkanbah Formation.**

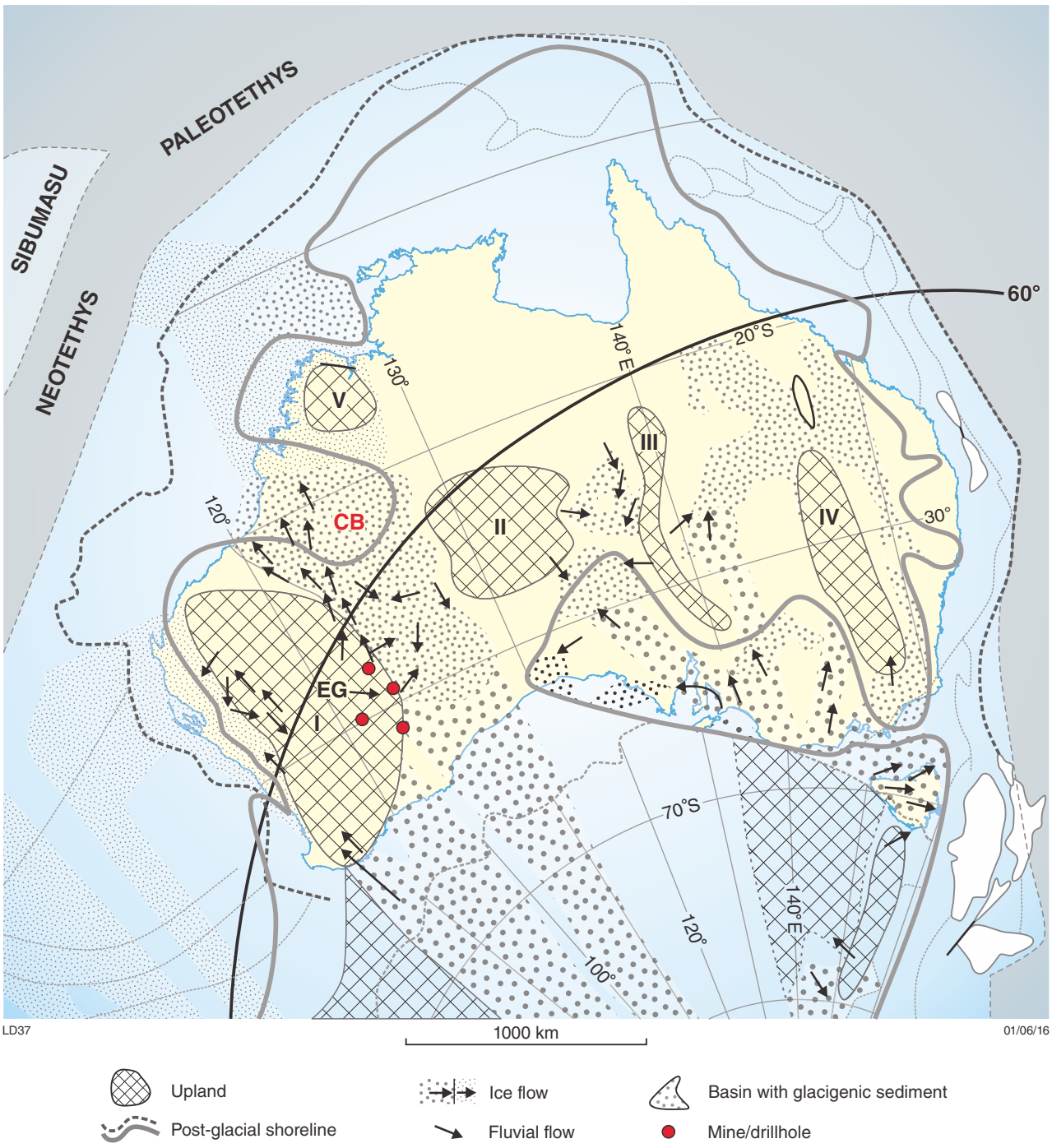


**Figure 4.** **Location of Australia, 302–280 Ma focusing on the early Sakmarian (early Permian; ~290 Ma) indicating position of the coastline after deglaciation (adapted from Veevers, 2006). CB – Canning Basin; EG – Eastern Goldfields. Uplands: I – ancestral Great Western Plateau, II – Central Australia, III – Central-eastern Highlands, IV – ancestral eastern Australian foreswell, V – Kimberley**

# Permian lithostratigraphy: previous work

## Poole Sandstone

The Poole Sandstone is a predominantly siliciclastic succession with a basal lenticular carbonate unit, the Nura Nura Member (Crowe and Towner, 1975; Apak, 1996; Adkins, 2003; Mory, 2010; Mory and Hocking, 2011). In the current Report, the Poole Sandstone above the basal Nura Nura Member is considered as a single package referred to as P1.

### Lithostratigraphy

Originally described by Blatchford (1927) as the 'Poole Range Beds', the unit underwent numerous revisions until its designation by Guppy et al. (1951) as the Poole Sandstone. This name was adopted in later work (Guppy et al., 1958; Veevers and Wells, 1961; Yeates et al., 1975; Forman and Wales, 1981). The type section was defined by Guppy et al. (1958) at Grant Range (17°46'S, 125° 51'E), and Traves et al. (1956) identified the Cuncudgerie Sandstone as a lateral equivalent in the basin's south on Patterson Range 1:250 000. This name was later abandoned by Towner et al. (1976) in favour of the Poole Sandstone as a basinwide unit.

The earliest subdivision of the Poole Sandstone was by Wade (1936) with identification of a basal limestone member, the 'Nura Nura Limestone', which unconformably overlies glacial Grant Group deposits near Nura Nura Ridge. This unit was reclassified by Guppy et al. (1951) to the Nura Nura Member. The type section is at Nura Nura Ridge (18°05'09"S, 124°24'34"E; coordinates determined by Mory, 2010, based on the original report by Guppy et al., 1958). The Nura Nura Member is the only subdivision of the Poole Sandstone to remain in formal use.

Crowe and Towner (1976a,b) proposed two additional members: the middle Tuckfield Member and the uppermost Christmas Creek Member. These divisions were recognized but not unanimously used in following work (Towner and Gibson, 1980, 1983; Adkins, 2003), and a later revision by Mory (2010) suggested that these subdivisions were unnecessary. The whole sedimentary package above the Nura Nura Member is here referred to as P1.

### Nura Nura Member

Traditionally the Nura Nura Member was defined as the basal unit of the Poole Sandstone (Guppy et al., 1958; Veevers and Wells, 1961; Forman and Wales, 1981; Towner and Gibson, 1983) but more recent definitions have specified a lenticular basal carbonate (Hocking et al., 2008; Mory and Hocking, 2011), and Mory (2010) questioned the equivalence of non-marine facies at St George and Poole Ranges. Early work described a facies shift from carbonate in the northwest to increasingly clastic deposits in the southeast indicative of a transition from shallow marine to non-marine settings (Crowe and Towner, 1976a; Forman and Wales, 1981; Towner and Gibson, 1983).

Confusion arises in identification and correlation of this unit due to its onshore transitional character. In the strictest lithostratigraphic sense, the Nura Nura Member refers to carbonate facies only. In this Report, however, the basal portion of the Poole Sandstone is described as a system, and thus incorporates non-marine siliciclastic correlatives of this carbonate in discussion of the Nura Nura Member.

The basal contact with the Grant Group is interpreted as unconformable (Guppy et al., 1951; Yeates et al., 1975; Crowe and Towner, 1976a). The upper contact with P1 is conformable (Yeates et al., 1975; Crowe and Towner, 1976a,b).

## P1

P1 is a sandstone-dominated succession with minor, interbedded siltstone comprising up to three coarsening-up cycles (Veevers and Wells, 1961; Yeates et al., 1975, 1984; Crowe and Towner, 1976a; Towner and Gibson, 1983; Apak, 1996; Mory, 2010; Mory and Hocking, 2011). Root beds, plant material including fossilized wood, and thin coal beds have been recorded in the basin's east (White and Yeates, 1976; Yeates et al., 1984; Adkins, 2003; Mory, 2010; Mory and Hocking, 2011). Basinwide shallow marine settings have been inferred for P1, with nearshore settings in southern basin areas (Towner et al., 1976), and shore-zone (Adkins, 2003), intertidal, fluvio-deltaic to deltaic and lagoonal settings have been interpreted in the northeastern Fitzroy Trough (Yeates et al., 1984; Mory and Hocking, 2011) and Gregory Sub-basin areas (Yeates et al., 1975). A regressive transition up-sequence to fluvial settings has also been interpreted in the Fitzroy Trough (Towner and Gibson, 1983; Yeates et al., 1984).

Whereas Guppy et al. (1958), Towner et al. (1976), Mory (2010), and Mory and Hocking (2011) considered the basal contact with the Grant Group to be disconformable, Towner and Gibson (1983) and Yeates et al. (1984) suggested an unconformable relationship in the Fitzroy Trough, with disconformable and conformable relationships in other areas. P1 is conformably overlain by the Noonkanbah Formation (Guppy et al., 1958; Veevers and Wells, 1961; Yeates et al., 1975, 1984; Towner et al., 1976; Towner and Gibson, 1983; Mory, 2010), except between the Poole and St George Ranges, where Guppy et al. (1958) proposed a disconformable relationship based on the presence of a basal conglomerate in the Noonkanbah Formation.

## Age

### *Nura Nura Member*

Initial investigations by Wade (1936) recovered ammonoids that indicated a middle Permian age for the Nura Nura Member. Later work by Guppy et al. (1951) uncovered a richly fossiliferous bed near the base of the Poole Sandstone at Mount Wynne, St George Ranges, and further work by Guppy et al. (1958) identified equivalents of the Nura Nura Ridge deposits at both St George Ranges and Grant Range. Ammonoids, brachiopods, bryozoan, foraminifera and molluscs from these localities indicate a lower Artinskian (early Permian) age (Guppy et al., 1958; Archbold, 1982). This age was supported by later paleontological work by (Archbold, 1982, 1998, 2002) and Glenister et al. (1993) that identified the member as upper Sakmarian to lower Artinskian (early–middle Permian).

### *P1*

Macrofossils in P1, brachiopods and bivalves, are recorded only in the basins to the south and indicate an early Permian, Artinskian, age (Towner et al., 1976; Yeates et al., 1984). An early Permian age is also determined from the *Glossopteris* floras recovered from Mount Bannerman (White and Yeates, 1976). This age is consistent with subsurface palynological data that records deposition in the *Pseudoreticulatispora pseudoreticulata* (*P. pseudoreticulata*) zone, middle Sakmarian (Fig. 5).

The boundary of the *P. confluens* zone with the overlying *P. pseudoreticulata* zone is well defined in Western Australian sedimentary basins and commonly signifies the end of glacial conditions (Eyles et al., 2002). In the Canning Basin it has been used to differentiate the Poole Sandstone from the underlying Grant Group (Eyles et al., 2002).

The upper age constraint for P1 is ambiguous and possibly diachronous. The *P. pseudoreticulata* zone is recorded in the lower parts of the Noonkanbah Formation in Padilpa 1 and Point Moody 1 (Plate 1), but Mory (2010) noted that palynomorphs typically assigned to the upper Artinskian are present at the top of the Poole Sandstone in BHP PND1.

# Noonkanbah Formation

The Noonkanbah Formation is siltstone to claystone dominated with local calcareous sandstone and limestone interbedded throughout the formation (Guppy et al., 1951; McWhae et al., 1956; Veevers and Wells, 1961; Mory, 2010; Mory and Hocking, 2011). The formation hosts a highly abundant, diverse range of fossil material and shelly limestones are present locally (Guppy et al., 1951; Yeates et al., 1975). Exposure is typically poor and the formation is commonly represented by large expanses of ferruginized platy scree.

### *Lithostratigraphy*

Initially defined as the Noonkanbah Series by Wade (1936), and later as the Noonkanbah Shale, the current status as the Noonkanbah Formation was set by Guppy et al. (1951) and assumed in all subsequent work (Guppy et al., 1958; Veevers and Wells, 1961; Towner and Gibson, 1980, 1983; Forman and Wales, 1981; Mory, 2010; Mory and Hocking, 2011). The type section near Noonkanbah Homestead (18°30'S, 124° 48'E) defined by Guppy et al. (1958) from the records of Wade (1936) was later revised by McWhae et al. (1956) to Brutens Hill (18°42'11"S, 125°36'22"E; coordinates updated by Mory, 2010). The Noonkanbah Formation was originally identified by Traves et al. (1956) in the southeast Canning Basin as the Dora Shale; however, foraminifera within the shale later allowed it to be identified as equivalent to the Noonkanbah Formation (Veevers and Wells, 1961).

A shallow marine depositional setting is inferred from faunal assemblages, with warm to tropical conditions suggested by the abundance and diversity of faunas (Wade, 1936; Yeates et al., 1975; Forman and Wales, 1981). Shallow marine conditions are interpreted to extend as far southeast as the Balgo Hills area based on the presence of goniatites (Forman and Wales, 1981). The presence of shelly limestones, limonite, and associations of non-marine faunas — including freshwater fish — with marine faunas, have been used as evidence to suggest strandlines (Casey and Wells, 1964), nearshore settings (Yeates et al., 1975), and nearby riverine settings (Forman and Wales, 1981) possibly marking the extent of marine conditions. The Noonkanbah Formation is typically conformable on the Poole Sandstone and conformably to gradationally overlain by the Liveringa Group (Guppy et al., 1951, 1958; Veevers and Wells, 1961; Casey and Wells, 1964; Yeates et al., 1975), although (Mory, 2010) suggested that the upper contact may be locally disconformable.

### *Age*

The Noonkanbah Formation hosts a diverse macro- and microfossil assemblage including bryozoa, brachiopods, bivalves, crinoids, corals, arthropods, gastropods and foraminifera. Fossil assemblages indicate an Artinskian age for the formation; full details of genus and species identifications can be found in Guppy et al. (1951, 1958). This age is consistent with the *S. fusus – M. trisina* zone palynomorphs recorded from subsurface formation samples (Fig. 5, Plate 1). A Kungurian (latest early Permian) age is indicated for the uppermost section of the formation based on records of the *Nechoneies nalbiaensis* brachiopod zone and the *P. sinuosus* palynological zone (Archbold, 1999; Fig. 5). Recovery of *P. pseudoreticulata* zone palynomorphs suggests a Sakmarian age for the lowermost part of the formation in some wells (e.g. Padilpa 1; Plate 1).

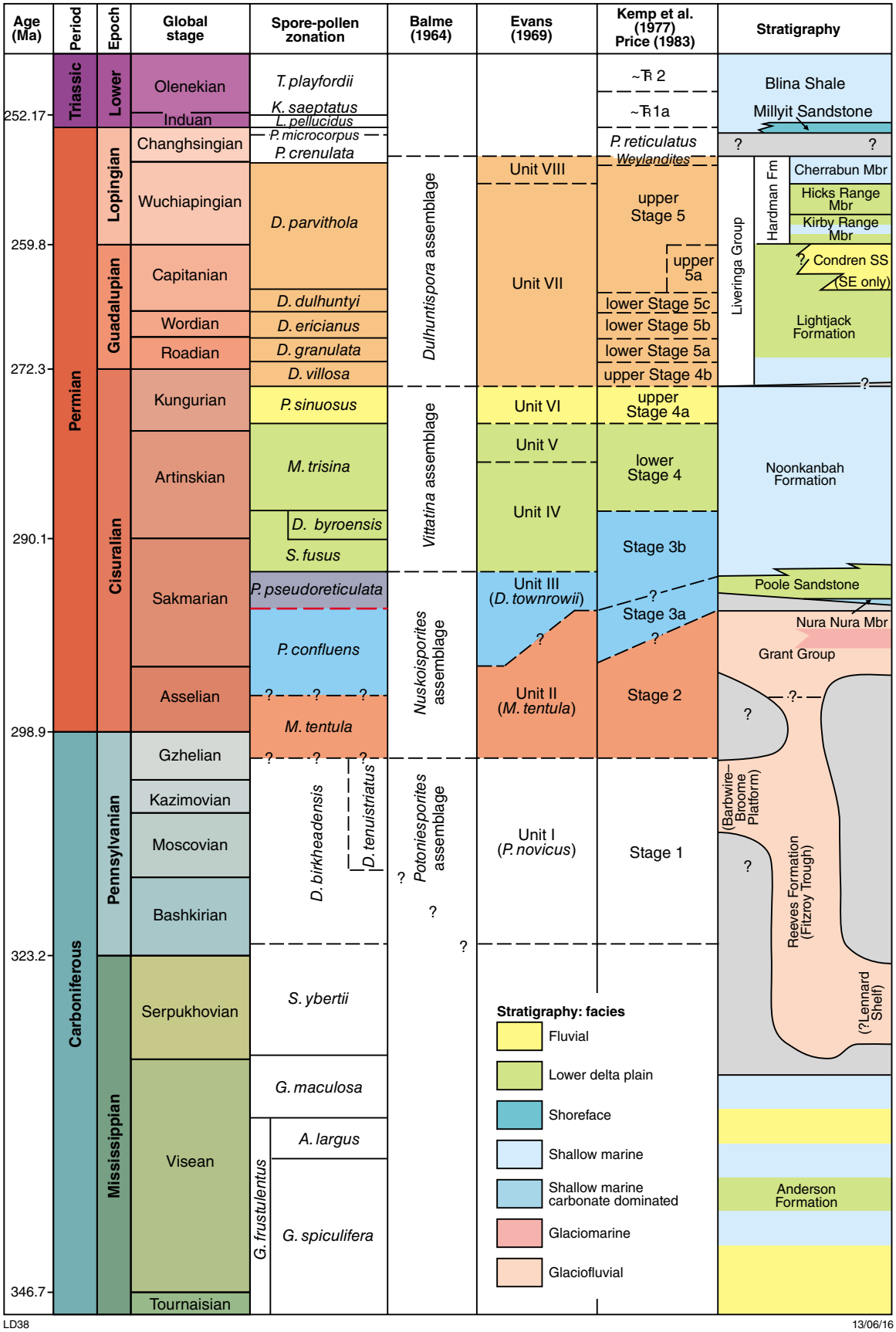


**Figure 5. Biostratigraphic zonal schemes applied to the Canning Basin, adapted from Mory (2010). Ages have been revised according to Cohen et al. (2013). Red dashed line is the *P. confluens* – *P. pseudoreticulata* boundary.**

# This study

## Data sources and methods

New work described in this Report used drillcore and outcrop sections to establish major facies and facies associations present in the uppermost Grant Group, Poole Sandstone and Noonkanbah Formation (Appendix 1). Facies associations, in combination with well logs and supplementary well data, were used for sedimentological characterization across the study area (Appendix 2). Classification of carbonate facies uses Dunham's (1962) classification and descriptions of bioturbation in siliciclastic facies follow the Taylor et al. (2003) classification system.

### Petrographic analysis

Twenty-one thin sections were made from available core samples. These and existing thin sections were analysed to support facies descriptions through more detailed examination of composition, texture and diagenetic features. Blue epoxy resin was used to highlight porosity and samples were stained with sodium cobaltinitrite to highlight the presence of alkali feldspars and differentiate ferroan from nonferroan calcite. Petrographic analysis was carried out by conventional polarizing microscopy. Classification and naming of sandstones follows Folk et al. (1970). Full details for each thin section are presented in Appendix 3.

### Well data

Subsurface study of the Poole Sandstone and Noonkanbah Formation incorporated 89 well logs and nine cored sections (Appendix 4; Fig. 6). Well data are clustered on the Lennard Shelf, Jurgurra Terrace and Crossland Platform, and are limited in the Fitzroy Trough. Outcrop sites and sections were used to provide continuity across the study region. Well and outcrop data from the Poole Sandstone and Noonkanbah Formation are sparse in the remainder of the Canning Basin (Fig. 6), restricting in-depth analysis and characterization of sediments to the study area.

### Dynamic-INPEFA

Dynamic Integrated Prediction Error Filter Analysis (D-INPEFA) (Nio et al., 2006) assesses variation in sedimentary sequences and interprets these variations in a climate-stratigraphic context. The D-INPEFA curve represents variations in spectral properties. Variations highlight trends or cyclicity that may be subtle or masked in the original log data. Climatic variation is intrinsically linked to lithology so gamma ray log data (GR) are analysed to best represent lithological changes. The D-INPEFA uses a prediction model that incorporates all points in the selected dataset. Accordingly, an analysis of the whole dataset will highlight different trends compared with analysis of a small interval (Fig. 7). Assessment of larger and smaller intervals is used to highlight different orders of cyclicity.

Geological interpretation of the D-INPEFA curve is based on identification of major trends and turning points (Fig. 7). Negative trends (NT) represent coarsening-up trends and are interpreted as shallowing or lowering base-level conditions. Positive trends (PT) represent fining-up trends and can be interpreted as deepening or rising base-level conditions.

Turning points indicate change from one trend to another. Major negative turning points (NTP) show a switch to increasingly shallow or sandy environments and may represent sequence boundaries. Major positive turning points (PTP) represent transition into more shaly conditions and can be interpreted as flooding surfaces (Nio et al., 2006).

### Correlation charts

The key findings and interpretations of this study are supported by a series of correlation charts (Figures 27–29; Plates 1–6). These charts present a representative selection of data that help illustrate important interpretations made from the larger dataset. The locations of the correlation charts that support these interpretations are illustrated in Figure 8. Palynological data represented on correlation charts is coloured according to Figure 5.

## Facies analysis

Twenty-one facies were identified in nine wells and six outcrop sections from the uppermost Grant Group, Poole Sandstone and Noonkanbah Formation. The facies described herein are defined by their lithological features, physical sedimentary structures, trace fossils, and bioclasts. Facies and corresponding facies codes are summarized in Appendix 2, Table 2.2 with an interpretation of depositional processes. Facies are grouped into nine facies associations representing different depositional environments. Representation of facies and facies associations in core and outcrop sections are illustrated in log sections (Appendix 2). Bioturbation index (BI) describes the relative level of bioturbation in terms of burrow density, overlap and proportion or primary sedimentary structures preserved, on a scale of 0 to 6 (Taylor et al., 2003; Buatois and Mángano, 2011). According to the scheme of Taylor and Goldring (1993), a BI of zero represents sediment with no bioturbation and BI 6 represents complete biological reworking with no preservation of primary sedimentary structure.

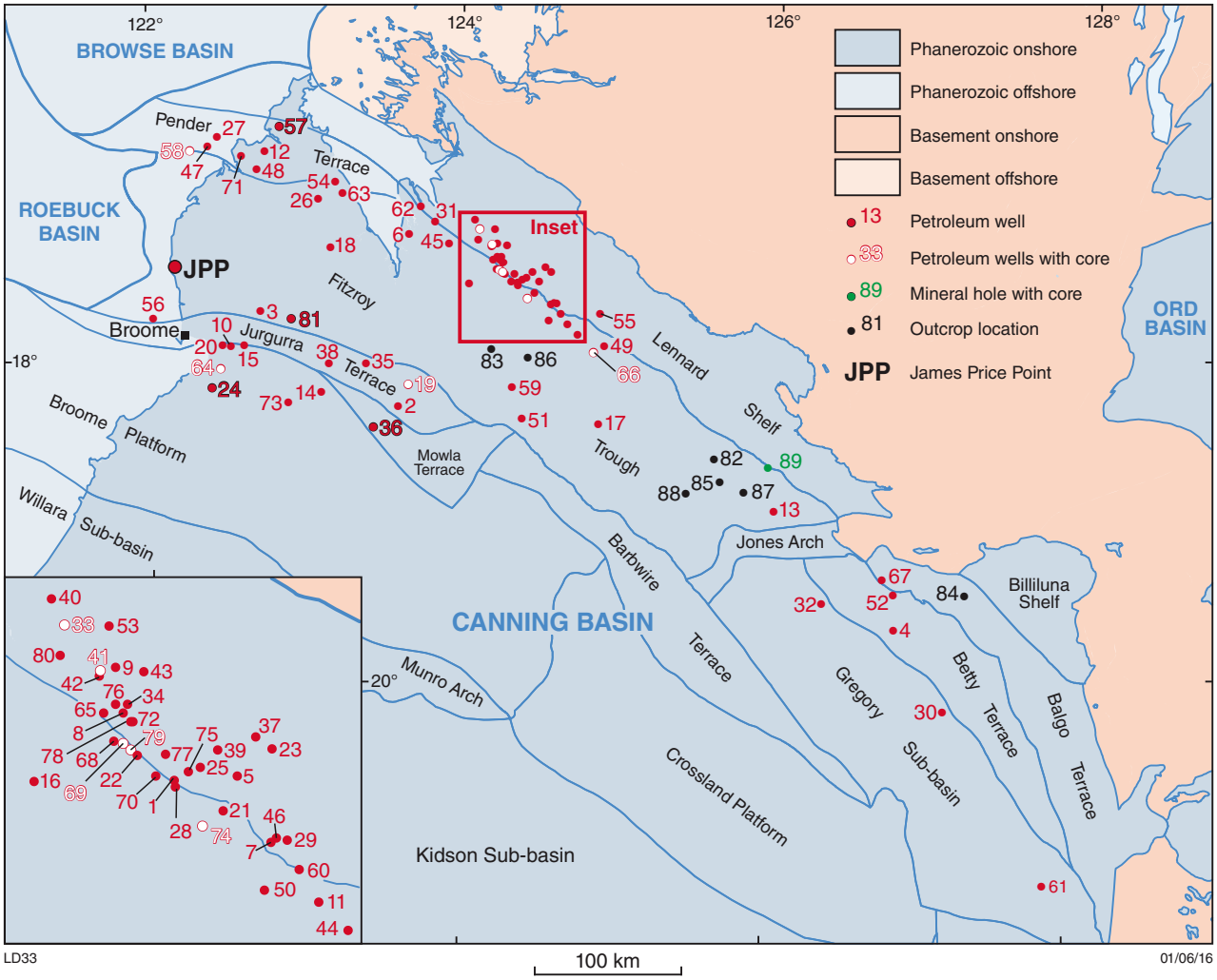


1 Aquanita 1
2 Babrongan 1
3 Barlee 1
4 Bindi 1
5 Blina 1,2,3,4,5,6,7,8
6 Booran 1
7 Boronia 1
8 Boundary 1
9 Canegrass 1
10 Crab Creek 1
11 Crimson Lake 1
12 Curringa 1
13 Cycas 1
14 Dampier Downs 1
15 East Crab Creek 1
16 East Yeeda 1
17 Fitzroy River 1
18 Fraser River 1
19 Frome Rocks 2
20 Freney 1
21 Hakea 1
22 Hangover 1
23 Harold 1
24 Hedonia 1
25 Janpam 1
26 Jum Jum 1
27 Kambara 1
28 Katy 1
29 Kennedia 1
30 Kilang Kilang 1
31 Kora 1
32 Lake Betty 1
33 Langoora 1
34 Lloyd 2
35 Logue 1
36 Lovells Pocket 1
37 Lukins 1
38 Mahe 1
39 Mariana 1
40 May River 1
41 Meda 1
42 Meda 2
43 Mellany 1
44 Metters 1
45 Millard 1
46 Mimosa 1
47 Minjin 1
48 Moogana 1
49 Mt Hardman 1
50 Nemile 1
51 Nerrima 1
52 Olios 1
53 Orange Pool
54 Padilpa 1
55 Palm Spring 1
56 Pearl 1
57 Pender 1
58 Perindi 1
59 Petaluma 1
60 Philydrum 1
61 Point Moody 1
62 Point Torment 1
63 Puratte 1
64 Roebuck Bay 1
65 Runthrough 1
66 Scarpia 1
67 Selenops 1
68 Sundown 1,2,3,4,5
69 Sundown 3H
70 Sunup 1
71 Tappers Inlet 1
72 Terrace 1
73 Thangoo 1
74 The Sisters 1
75 Thompsons 1
76 Wattle 1
77 West Blackstone 1
78 West Terrace 1
79 Whitewell 1
80 Yarrada 1
81 Yulleroo 1
82 Brutens Yard
83 Liveringa
84 Mount Bannerman
85 Mount Hutton
86 Nura Nura Ridge
87 Poole Range
88 St George Ranges (E)
89 PND 1

**Figure 6. Map showing the distribution of petroleum well, mineral drillcore, and outcrop data used in this Report**

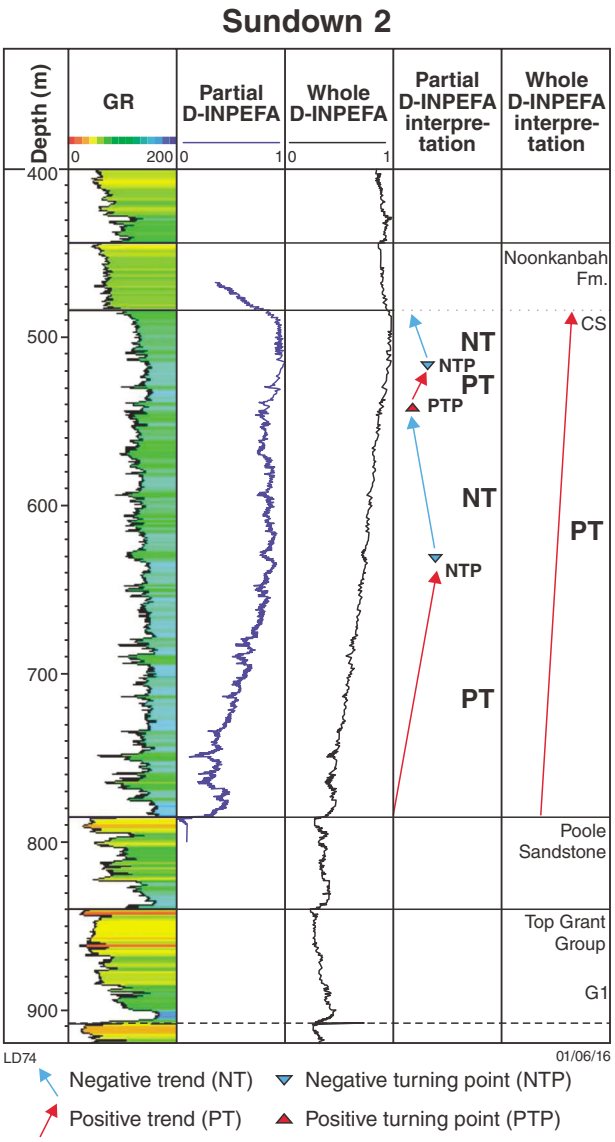


**Figure 7.** **D-INPEFA log and corresponding gamma ray (GR) log from Sundown 2, illustrating positive and negativetrends and turning points. CS – casing shoe; G1 – Grant Group**

## Facies association 1 (FA1) – fluvial channel fills and bars

### *Description*

FA1 is dominated by tabular to trough cross-stratified, fine to very coarse sandstone (*St*, *Sx*) with abundant ripple cross-laminated (*Sr*) and planar-laminated (*Sp*) sandstone beds. Very coarse-grained facies transitionally overlie fine- to medium-grained facies or truncate them in thick scour and fill sequences (Fig. 9). Concave-up scours overlain by quartz-pebble lags or intraformational breccias (*Bm*) are common in outcrop (Fig. 9d). Scours are typically filled by cross-bedded St or Sp facies that are arranged into fining-up packages or grade upward into Sp and Sr facies. Small scour and fill packages are between 1–10 m wide and 1–5 m deep; large sequences are up to approximately 50 m wide and >10 m deep (Fig. 9). Locally, small packages are stacked and laterally offset (Fig. 9b). Mudstone rip-up clasts are commonly aligned along the basal foresets of St and Sp beds. Sharp-based Sx, thinly bedded Sp, and thickly bedded Sr facies are also observed, stacked in fining-up packages (Fig. 10). Rootlet beds are common and small fragments of carbonaceous material are commonly concentrated along St and Sx foresets. Plant material is locally abundant (Fig. 11). Trace fossils are typically absent in facies infilling scours; however, moderate abundance, low-diversity assemblages are recorded.

### *Interpretation*

FA1 is interpreted as a fluvial depositional setting with channel scours, point bar, and interchannel bars. Concave-up erosional scours overlain by lags or breccia facies are indicative of high-energy flow events. The association of St, Sx, Sr, and Sp in fining-up and transitional packages suggests bedform accretion and waning current energy conditions, classically associated with fluvial channel fill (Amorosi and Milli, 2001; Miall, 2010). The multistorey and laterally offset structure of channel features observed in outcrop suggests unstable, avulsing channels akin to a braided-type system (e.g. Midtkandal et al., 2007; Tedesco et al., 2010). This is supported by the dominance of sandstone, the absence of any demonstrable floodplain siltstone and mudstone deposits, and the abundance of rootlet beds in channel margin or interchannel areas with bars or islands.

## Facies association 2 (FA2) – sandy tidal flats

### *Description*

FA2 is characterized by thick, ripple cross-laminated sandstone beds (*Sr*) interbedded with small-scale, trough cross-bedded sandstones (*St*) and thinly planar bedded, parallel-laminated sandstones (*Sp*) (Fig. 12a–d). Combined flow ripples are common, and sigmoidal, climbing and ladder-back ripples are locally present (Fig. 12a,b). Minor convolute sandstones (*Sfc*), thick, tabular cross-bedded sandstones (*Sx*), and intraformational breccias (*Bm*) are interbedded with the major facies (*Sr*, *St* and *Sp*) (Fig. 12e,f). Wavy-bedded sandstone and thin siltstone layers (*Sfw*) are locally present interbedded with ripple cross-laminated and planar-laminated sandstones (*Sr*, *Sp*). Channels with scoured bases are locally present, commonly with fill 1–2 m deep of thin, basal breccia (*Bm*) overlain by tabular to trough cross-bedded sandstones (*St*, *Sx*; Fig. 13). Rip-up clast moulds are common in sandstone, and large moulds after woody fragments are abundant. Thin rootlet beds are present, most commonly at the top of sections. Locally, sandy rootlet beds fine upwards into carbonaceous siltstones, forming stacked successions. Overall, bioturbation is very low, with rare horizontal traces. Extreme low-diversity, high-abundance trace-fossil assemblages are found in Sr facies with bioturbation indices of BI 5–6, dominated by horizontal traces (Fig. 12g). Synaeresis cracks are common.

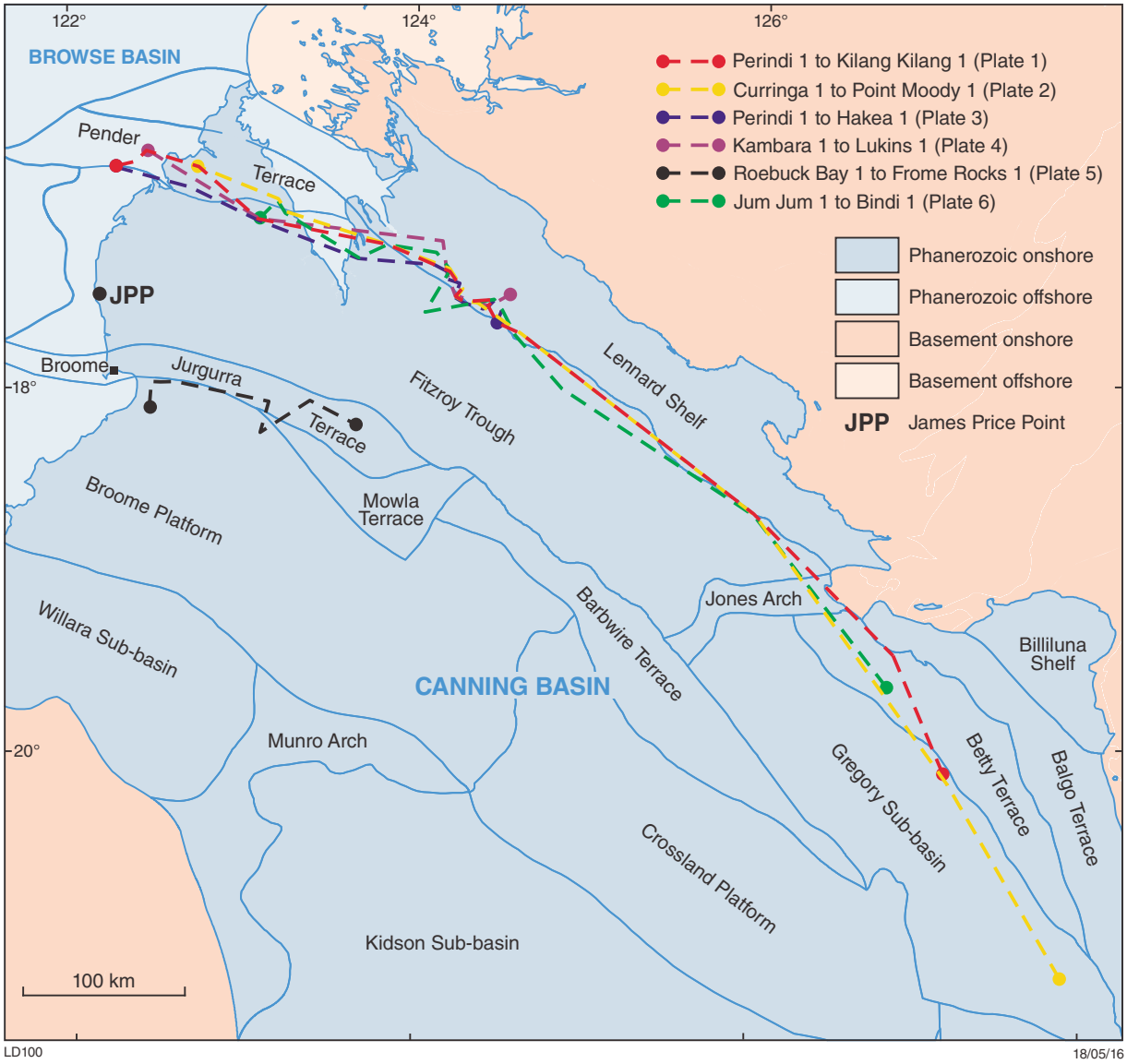


**Figure 8. Location of key sections represented in correlation panels (Plates 1–6). Lines are labelled according to corresponding plates.**

## *Interpretation*

The combination of facies Sp, St and Sr, and their characteristics indicates a shallow marine setting with alternating upper- and lower-flow regime conditions. Deposition along subhorizontal surfaces, high sediment loads and the interplay of opposing currents are commonly associated with sandy tidal-flat environments (Dalrymple et al., 1990; Chakrabarti, 2005; Santos and Rossetti, 2006). Convolute-laminated sandstones, rootlet beds and mud rip-up clasts are also consistent with a tidal setting (Chakrabarti, 2005; Rebata Hernani et al., 2006; Donselaar and Geel, 2007). The presence of channels supports this interpretation, as such features are often abundant, and commonly dissect tidal flats (e.g. Dalrymple et al., 1990; Martinius et al., 2001; Donselaar and Geel, 2007). Sx facies not associated with breccias and lacking scoured bases as seen in channels, and their association with Sp, Sr and St, may indicate compound dune formation, which is common in tidal settings (Dalrymple and Choi, 2007; Dalrymple, 2010; Desjardins et al., 2012). Overall low to absent bioturbation, with the exception of locally abundant, opportunistic colonization, is often a feature of sandy tidal-flat environments as upper-flow regimes and dune migration make colonization difficult (Dalrymple et al., 1990; Mángano and Buatois, 2004). The association of scour and fill channels, rootlet beds, and large wood fragments suggests shallow, near-terrestrial subaqueous conditions, or possibly with switching between the two conditions. Cyclical rootlet bed to carbonaceous siltstone fining-up sequences may represent a more proximal expression of this association.


a)


b)


c)
d)
FA1
FA2
50 m
Poole Sandstone
Grant Group

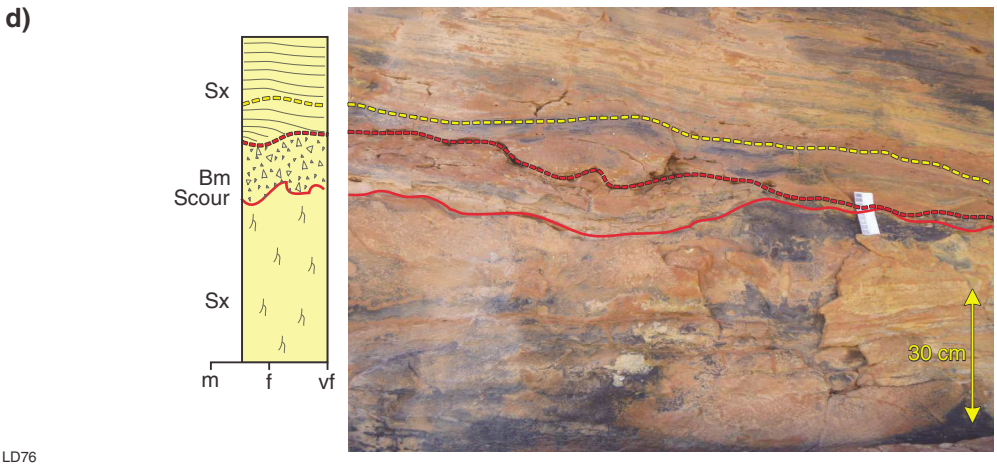
d)
Sx
Bm
Scour
Sx
m
f
vf
30 cm

LD76

18/05/16

**Figure 9.** **(opposite) Field photographs of FA1 scour and fill in the Poole Sandstone: a) large erosional scour filled with very coarse-grained, thickly bedded, cross-stratified sandstone incising a succession of fine- to medium-grained sandstone facies at Mount Bannerman; b) stacked and laterally offset channel forms and fill at Mount Bannerman; c) FA1 overlying FA2 at Mount Hutton with channel form outlined; d) detail from (c) showing basal erosional scour (red line), at the base of FA1 and overlying channel-fill facies succession from intraformational breccia (Bm) to cross-bedded sandstone (Sx).**

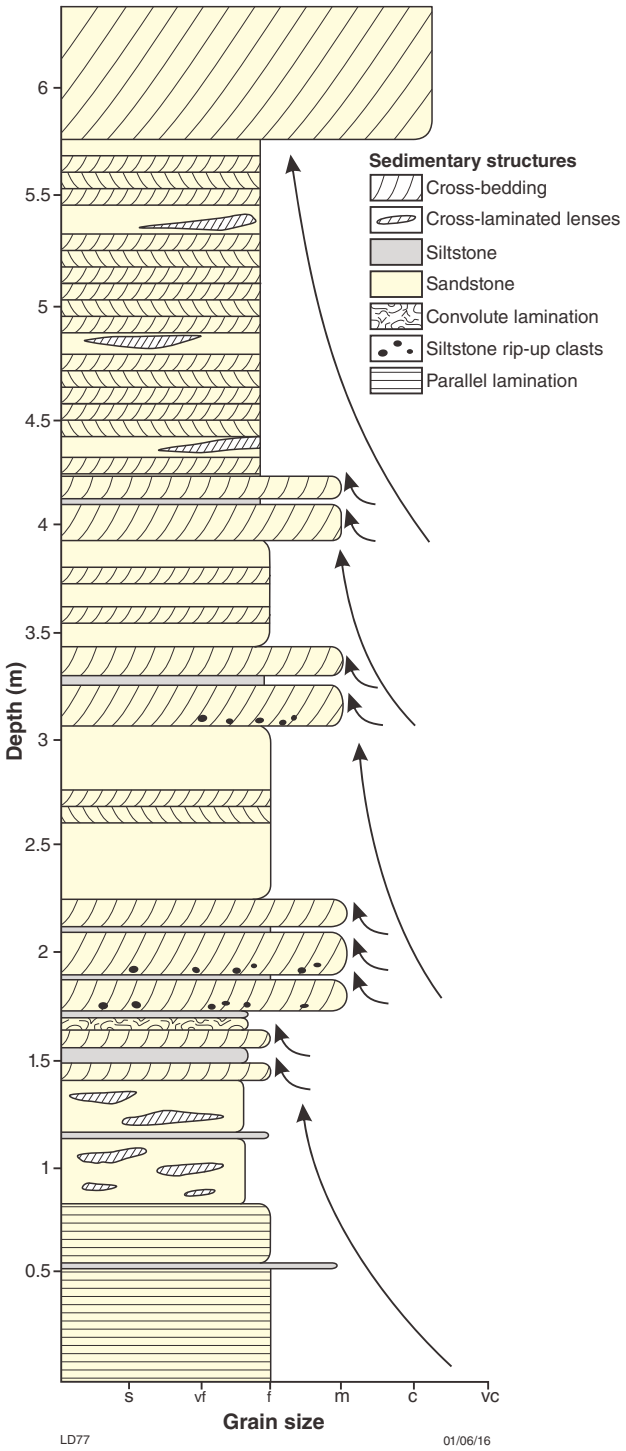


**Figure 10.** **Log representation of stacked fining-up trends in FA1 in Poole Sandstone at Mount Bannerman. Arrows indicate normally graded packages on centimetre to metre scales. On horizontal grain size axis, s is siltstone, vf – vc is very fine-grained to very coarse-grained sandstone.**

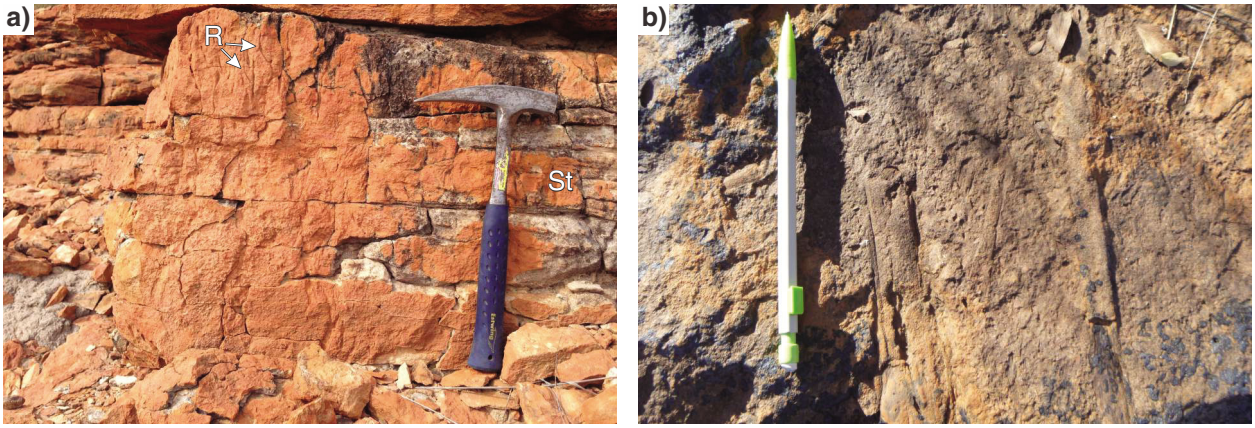


**Figure 11. Outcrop photographs of relict plant fossils and rootlet beds: a) rootlet bed with root traces (R) in trough cross-bedded sandstone (St), at Mount Bannerman; b) remnants of plant fragments in sandstones at Mount Bannerman**

## Facies association 3 (FA3) – mixed tidal flats

### *Description*

FA3 is characterized by thin to medium, flaser- and wavy-bedded, heterolithic sandstone and siltstone facies (*Sff*, *Sfw*; Fig. 14). Reactivation surfaces and bidirectional ripple cross-lamination are common in Sfw. Thin massive mudstones and siderite bands, <10 cm thick, and clasts are present throughout FA3. Very low levels of bioturbation (BI 1) are present in Sfw and Sff; typically assemblages constitute only sparse *Planolites*. Sharp-based, clast-supported pebble conglomerates and mud rip-up clast breccias (*Gm*, *Bm*) are interbedded with heterolithic facies Sff and Sfw. Thin, planar-laminated beds (*Sp*) with ripple cross-laminated tops are present. These beds are composed of sandstone, with laminations defined by small, highly abundant flakes of carbonaceous material (Fig. 14). Locally, wavy-bedded facies coarsen-up to cross-bedded sandstones (*Sx*).

### *Interpretation*

Heterolithic units of sandstone and siltstone dominated by flaser and wavy bedding with planar-laminated sandstones that have rippled tops, bidirectional ripple cross-lamination and reactivation surfaces are commonly associated in tidal settings (Martinius et al., 2001; Donselaar and Geel, 2007). Low-abundance, low-diversity trace-fossil assemblages provide further evidence for stressed conditions; in this case, due to brackish water in tidal environments (Dreyer, 1994; Donselaar and Geel, 2007; Dalrymple, 2010; Buatois and Mángano, 2011). Fine-scale lamination grading to ripple lamination indicates waning flow velocities commonly associated with tidal currents (Plink-Björklund, 2012). In association with these features, the abundant carbonaceous material suggests proximity to terrestrial settings, and massive mudstones deposited during slack-water episodes suggest tidal-flat environments (Dalrymple, 2010). Mudstone rip-up clast breccias indicate reworking of muddy substrate and higher energy flows, which are consistent with a channelized tidal environment (Rebata Hernani et al., 2006; Dalrymple and Choi, 2007; Ponten and Plink-Björklund, 2007). Interbedded, sharp-based pebble conglomerates indicate episodic high-energy flows and bed load deposition, probably also associated with small-scale channels.

## Facies association 4 (FA4) – heterolithic tidal channel

### *Description*

FA4 consists of thinly interbedded, convolute-laminated sandstones (*Sfc*), planar- and ripple-laminated sandstones (*Sp*, *Sr*), and locally bioturbated siltstones (*Hxs*) (Fig. 15). Bed bases are sharp and commonly contain mudstone rip-up clasts (Fig. 15a,c). Planar-laminated sandstone is commonly gradationally overlain by ripple cross-laminated sandstones with thick mudstone drapes. Climbing ripples and double mud drapes are common, as are synaeresis cracks and small-scale synsedimentary faults (Fig. 15b). Heterolithic Hxs facies are moderately bioturbated (BI 2-3; Fig. 15a). *Zoophycos* and *Teichichnus* traces are present but typically bioturbation is represented by indistinct mottling with sandy backfill. This style of bioturbation is confined to Hxs beds; elsewhere bioturbation is low (BI 1) with low-abundance, low-diversity assemblages including small *Planolites* and *Teichichnus*.

### *Interpretation*

Climbing ripples and soft-sediment deformation indicate high sediment supply and rapid deposition (Owen and Moretti, 2011). Double mud drapes and climbing ripples are common and are diagnostic features of tidally influenced deposition (Fenies and Faugeres, 1998; Dalrymple et al., 2012). Repetition of thin, sharp-based, sandstones suggests high-energy flows, and transition

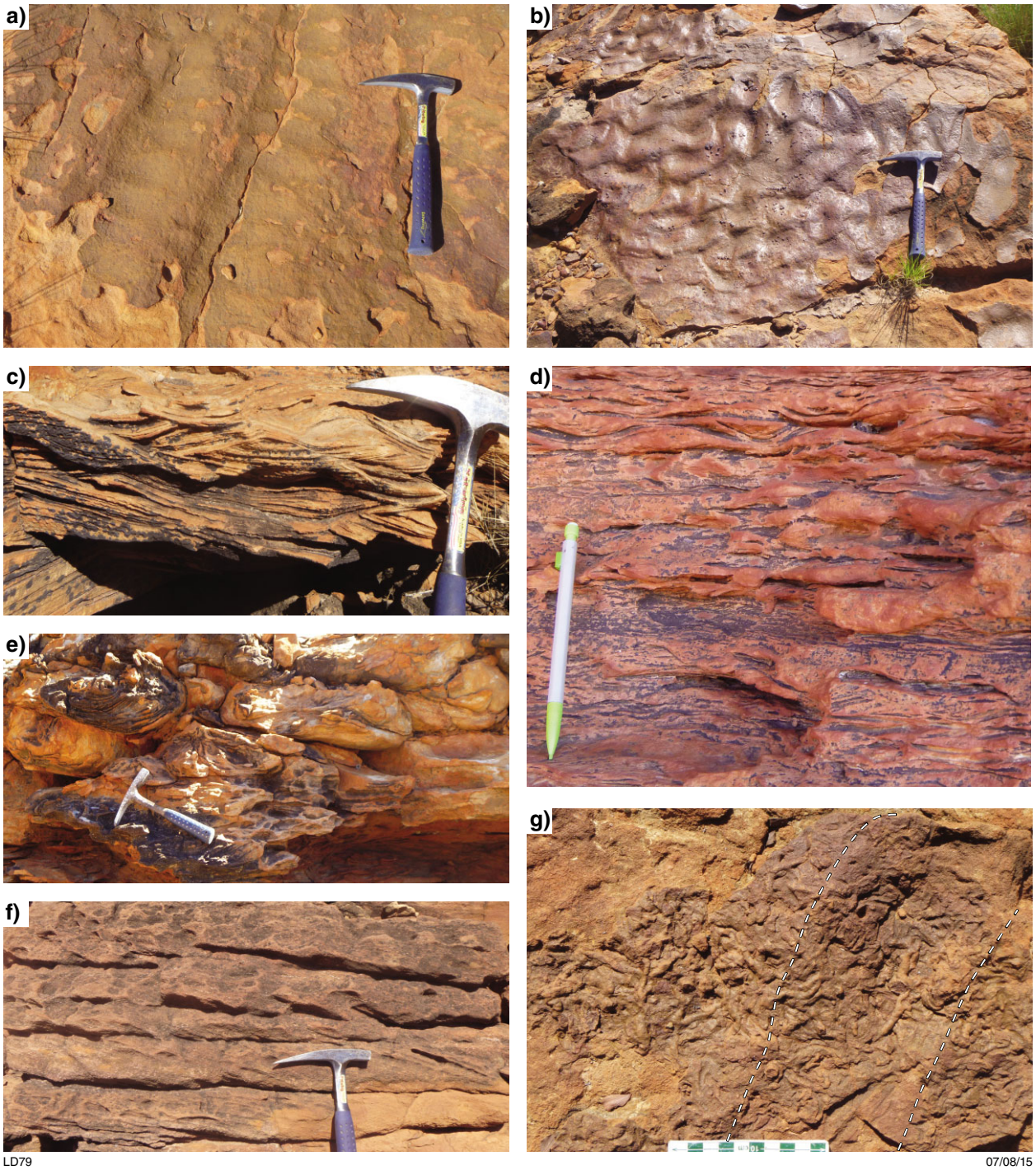


**Figure 12. Component facies of FA2 in Poole Sandstone outcrop sections, localities indicated in Figure 6: a) ladder-back ripples in outcrop at Liveringa; b) interference ripples preserved on a trough surface at Liveringa; c) small-scale trough cross-bedding (St) at Poole Range; d) amalgamated ripple cross-laminated section (Sr) at Poole Range; e) convolute sandstone bed (Sfc) displaying ball and pillow structures at Poole Range; f) tabular cross-bedding (Sh) at Poole Range; g) intense, low-diversity bioturbation on a rippled surface. Ripple crests indicated by dashed lines at east St George Ranges.**

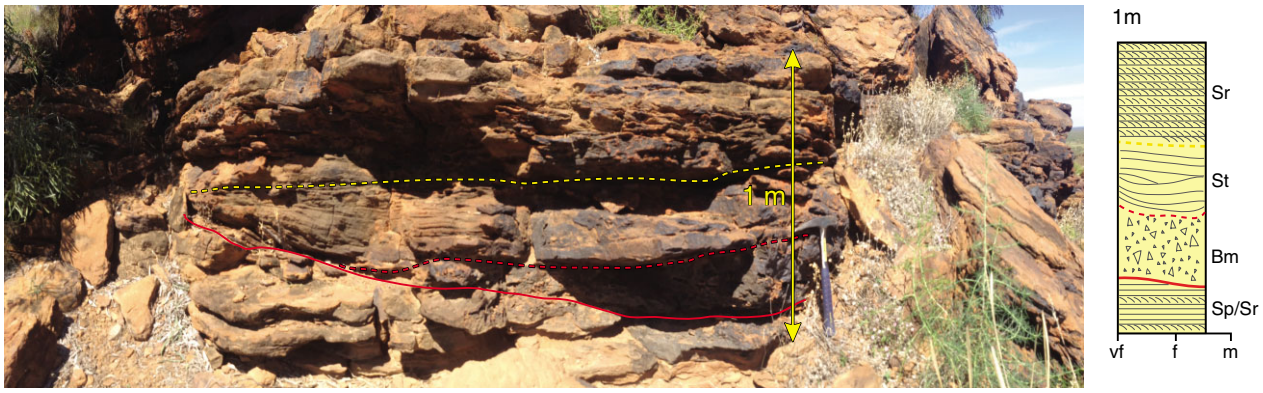


**Figure 13. Small channel in FA2 at Liveringa outcrop section, location 83 in Figure 6. Channel fill is depicted in sketched section at right, scale for which is same as photograph. The sharp basal surface (red line) is overlain by breccia (Bm) then cross-bedded sandstone (St) and ripple cross-laminated facies (Sr).**

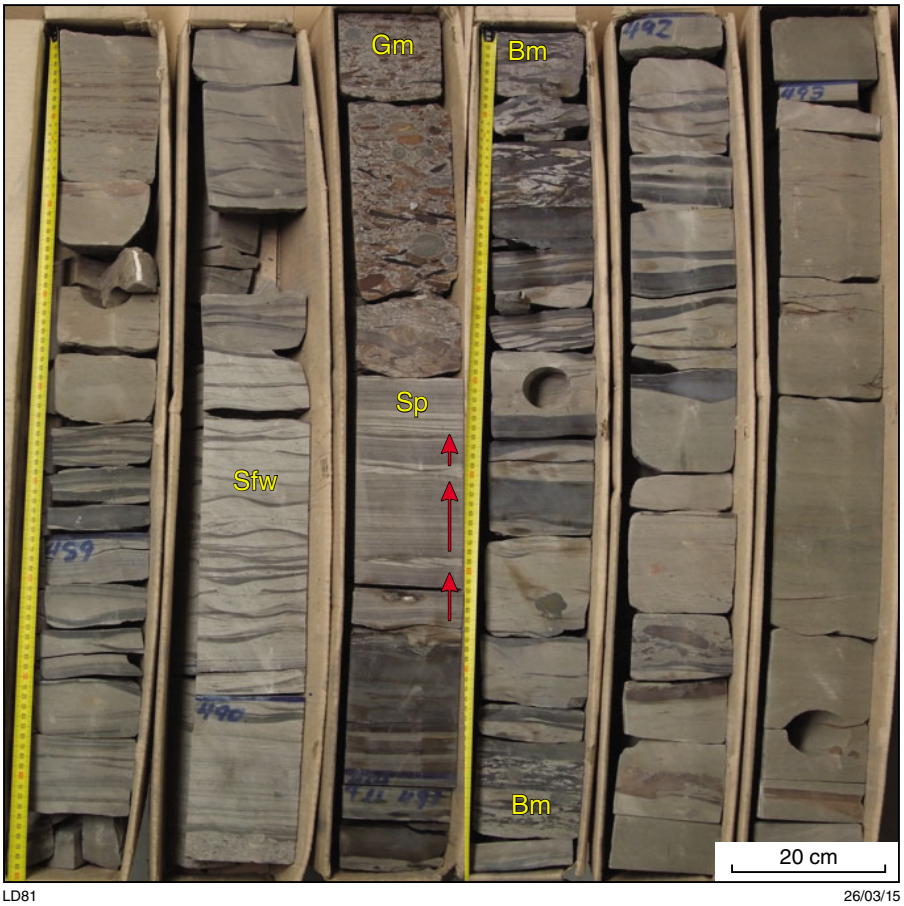


**Figure 14. FA3 in the Noonkanbah Formation, Scarpia 1 core. Distinct wavy bedding (Sfw) with pinstripe planar lamination (Sp), a conglomerate bed (Gm), and mud rip-up clast breccia (Bm). Red arrows indicate structural gradation from planar to ripple carbonaceous lamination.**

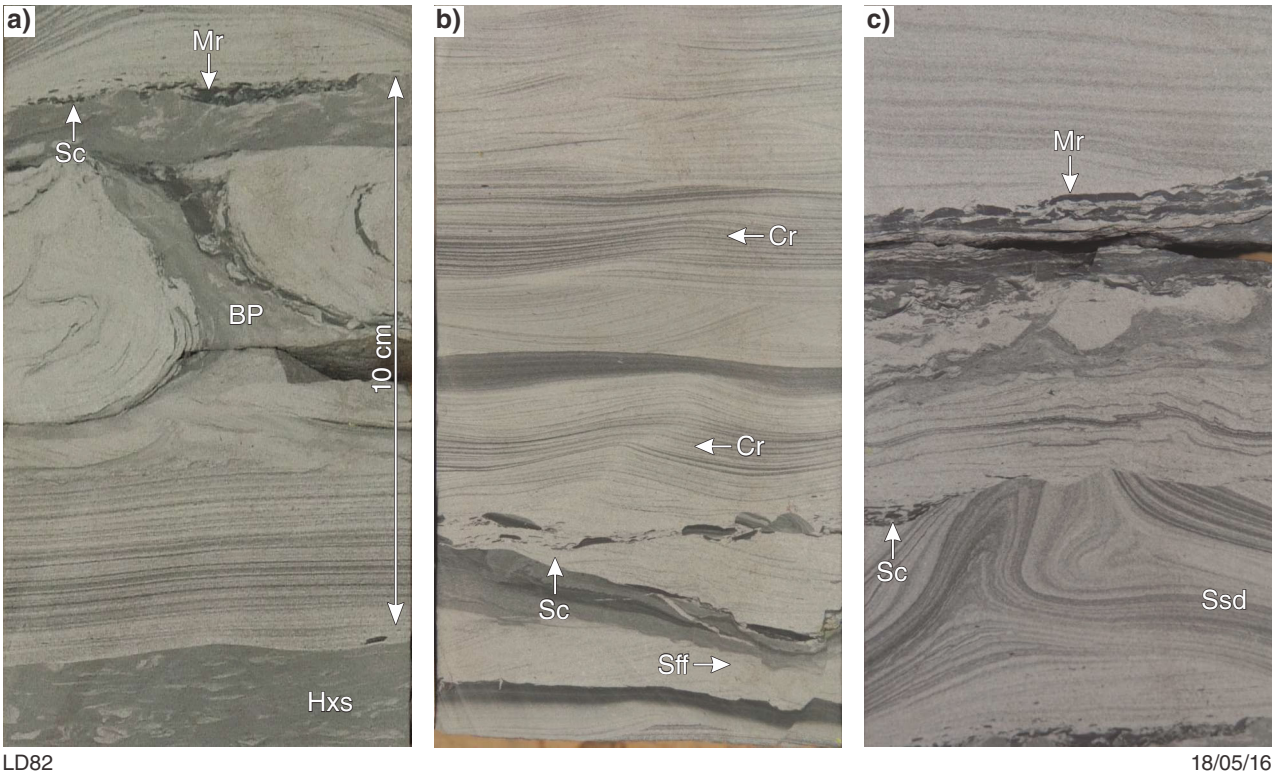


**Figure 15. FA4, present only in Sundown 3H core, location 69 in Figure 6. a), b), c) Common sedimentary structures of the heterolithic tidal channel facies association. Cr – climbing ripples, Hxs – bioturbated heterolithic facies, Sc – scoured bedding surfaces, Sff – synsedimentary faulting, Mr – mud rip-up clast lags and Ssd – soft-sediment deformation including ball and pillow structures (BP). Scale in (a) applies to all.**

from planar lamination to ripple cross-lamination and mud drapes indicates waning flow conditions (Dalrymple, 2010). Sediment-laden flows with scoured bases and mud rip-up clast lags suggest a tidal-channel setting (Dalrymple and Choi, 2007; Ponten and Plink-Björklund, 2007). Synaeresis cracks coupled with low-abundance trace-fossil assemblages, and small size of traces in those assemblages, suggest biologically stressful conditions consistent with salinity fluctuations (Buatois and Mángano, 2011; Gingras et al., 2012b). In combination, these features suggest deposition in a tidal setting, which is commonly brackish (Dalrymple, 2010; Buatois and Mángano, 2011).

## Facies association 5 (FA5) – lower shoreface

### *Description*

FA5 is characterized by sparsely bioturbated, planar-laminated and ripple cross-laminated siltstone and sandstone (*Hm*) interbedded with abundantly bioturbated sandstone facies (*Smb*). Planar-laminated and ripple cross-laminated sandstone beds in Hm are sharp based and typically fine upwards to siltstone. Rippled to hummocky–swaley cross-stratified sandstone (*Sfx*, *Sxs*) with sharp contacts are interbedded with Hm. Sfx facies occur as single, event beds or stacked sets. Low-level bioturbation (BI 0–2) is present in Hm with predominantly horizontal traces including *Thalassinoides*, *Phycosiphon*, *Planolites*, and *Teichichnus*. In contrast, bioturbated sandstones (*Smb*) contain a high-abundance, high diversity trace-fossil assemblage (Fig. 16a). Silt-lined, sand-filled, vertical burrows dominate the assemblage with common overprinting. Intense bioturbation (BI 4–6) has removed nearly all primary sedimentary structures. *Diplocraterion*, *Thalassinoides*, *Rosselia* and *Palaeophycus*, with possible *Ophiomorpha* and *Skolithos*, were identified, in addition to abundant, indistinct mottling (Fig. 16a). *Rosselia* and *Skolithos* traces are overprinted by *Palaeophycus* and *Thalassinoides*.

### *Interpretation*

Hummocky–swaley cross-stratified sandstones with scoured surfaces indicate high-energy wave action and likely storm activity (Dumas and Arnott, 2006). Repeated fining-up beds with basal scoured surfaces indicate repetitive high-energy waning flows possibly related to tidal activity (Dalrymple, 2010). *Teichichnus* and *Rosselia* trace fossils identify marine conditions (Buatois and Mángano, 2011). *Skolithos* and *Ophiomorpha* are opportunistic traces that are commonly, but not exclusively, associated with shifting sandy substrates (Buatois and Mángano, 2011). Overprinting of these

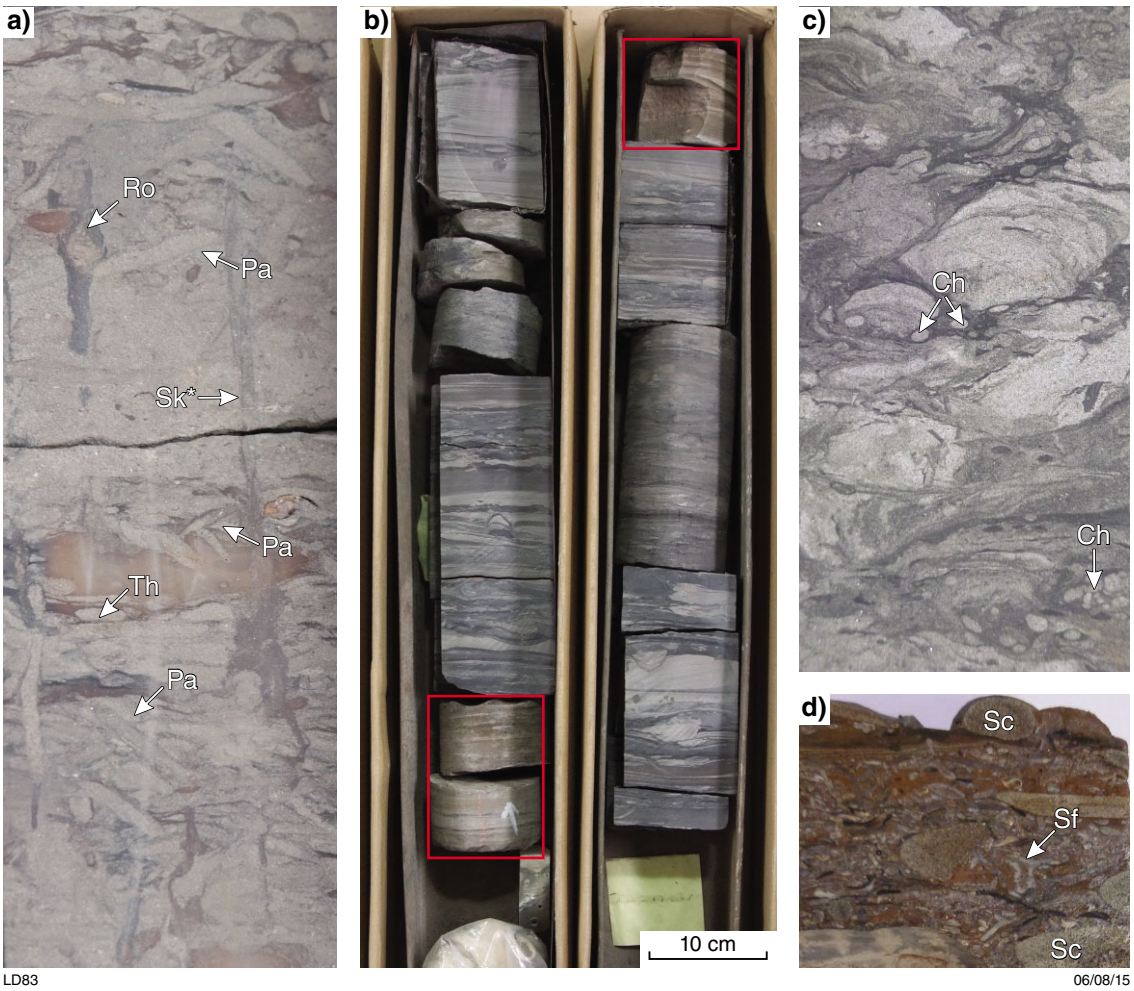


**Figure 16. Images of trace-fossil genera and facies associations from core sections, localities indicated in Figure 6: a) FA5 Smb from Scarpia 1. High-intensity, high-diversity trace fossil assemblage with high levels of overprinting. Ro – *Rosselia*, Pa – *Palaeophycus*, Th – *Thalassinoides* and Sk* – possible *Skolithos*; b) FA6 from Meda 1, core 1. Interbedded Hxs and Sfx, hummocky–swaley beds (Sfx beds in red boxes); c) Hxs from PND 1 displaying the high-abundance, high-diversity trace-fossil assemblage, and overprinting of larger traces by *Chondrites* (Ch); d) FA6 Gmc bed from PND 1 with well-rounded sandstone pebbles (Sc) in a mixed quartz sand, mud, and fragmented bioclast matrix (Sf).**

traces by suspension feeding traces, e.g. *Palaeophycus*, suggests transition to fair-weather conditions after initial colonization. Abundant Sfx sandstones interbedded with highly bioturbated sandstones, dominated by the burrows of suspension feeding organisms, indicate high-energy settings and frequent storm reworking, and suggest deposition in a shoreface environment (Buatios et al., 2002; Lever, 2002; Rygel et al., 2008). Very high to extreme bioturbation is not usually observed in upper shoreface environments and siltstone interbeds indicate lower energy episodes suggesting a middle to lower shoreface setting (Buatios et al., 2002).

## Facies association 6 (FA6) – offshore transition

### *Description*

FA6 is dominated by thinly bedded, extensively bioturbated, heterolithic, very fine-grained sandstone and siltstone (*Hxs*) (Fig. 16b,c). Sandstones in Hxs are sharp-based massive beds or planar-laminated beds that grade up to ripple cross-laminated sandstones or siltstones. Brachiopod shells are only sparsely distributed throughout Hxs, but are seen in thin horizons along

bedding planes. Lenticular-bedded siltstone (*Ml*) and hummocky–swaley cross-laminated sandstones (*Sfx*) are interbedded with Hxs (Fig. 16b). Sfx sandstones are commonly present as beds about 5 cm thick, with sharp bed contacts; however, amalgamated beds up to 20 cm thick are locally present (Fig. 16b). Thin, sharp-based, calcareous pebble conglomerates (*Gmc*) are locally present (Fig. 16d). Bioturbation is absent in Sfx and Gmc and low in Ml. High levels of bioturbation characterize Hxs facies, although bioturbation is reduced and even absent in places. *Zoophycos*, *Chondrites* and *Phycosiphon* are most abundant, with *Teichichnus*, *Thalassinoides* and *Nereites* common in highly bioturbated beds. *Asterosoma* is locally present.

### Interpretation

Siltstones interbedded with thin, erosionally based, planar-laminated beds and lenses (Ml) and hummocky–swaley cross-laminated sandstone (Sfx) facies indicate low-energy settings with episodic higher energy currents and storm activity (Hart and Plint, 1993; Martinius et al., 2001; Dumas and Arnott, 2006; Buatois et al., 2012). Alternation of low-energy suspension fallout and thin storm beds are characteristic of offshore environments. *Teichichnus* and *Asterosoma* indicate marine settings consistent with an offshore environment (Buatois and Mángano, 2011). Intense bioturbation and high levels of overprinting are common in lower offshore environments, and when siltstone facies interbedded with Sfx sandstone facies are highly bioturbated by trace-fossil assemblages including *Zoophycos*, *Chondrites*, *Phycosiphon*, *Teichichnus*, and *Planolites*, offshore transitional environments are commonly inferred (Posamentier and Chamberlain, 1993; Buatios et al., 2002, 2012; Di Celma et al., 2010). Local, fragmented bioclastic lags have also been associated with these deposits (Buatios et al., 2002). Episodes of reduced bioturbation suggest biological stress that may be attributed to turbidity or nutrient fluctuations.

## Facies association 7 (FA7) – offshore

### Description

FA7 comprises interbedded lenticular-bedded siltstone (*Ml*) and planar-laminated mudstone (*M*). Lenticular-bedded siltstone facies also contain thin, fine-grained sandstone beds with gradational contacts. Sharp-based, hummocky–swaley cross-bedded facies (*Sfx*) are rare and interbedded with Ml. Thin, sharp-based, pebble conglomerates (*Gmc*) are locally present. Bioturbation is absent in facies M and Sfx but is typically present in low levels in Ml (BI 1–2). Trace fossils include small *Planolites* and *Teichichnus* and abundance increases locally (BI 3–4), although most traces are indistinct and unidentifiable.

### Interpretation

The dominance of mudstone facies indicates very low-energy conditions and deposition mainly by suspension settling. Thin sandstone laminae and lenses indicate weak traction currents. Hummocky bedding and localized conglomeratic facies (*Gmc*, *Sfx*) indicate episodic high-energy events, possibly related to storms. Suspension deposits punctuated by rare storm events suggest offshore deposition above storm wave base. The presence of *Teichichnus* indicates marine conditions and beds with low levels of bioturbation further suggest episodes of biological stress possibly related to fluctuating oxygen-poor conditions.

## Facies association 8 (FA8) – muddy tidal flats

### Description

FA8 is dominated by laminated mudstones (M) which commonly overlie, and are gradational with, sharp-based, ripple cross-laminated sandstone lenses. Bioturbation is low to moderate (BI 0–1), but commonly higher in lenticular-bedded facies (BI 3). Observed trace fossils are restricted to small *Planolites* and *Teichichnus*. Small synaeresis cracks are present throughout.

### Interpretation

Thick mudstone beds and lenticular bedding indicate the predominance of low-energy, suspension settling deposition and fluctuation between this and lower-flow regime conditions in settings with high suspended loads (Ponten and Plink-Björklund, 2007; Dalrymple, 2010). *Teichichnus* indicates marine influence, and low to moderate bioturbation dominated by small trace fossils suggests a biologically stressed setting (Buatois and Mángano, 2011). Syneresis cracks indicate salinity fluctuations consistent with biological stress, as is typically attributed to such conditions (Burst, 1965).

## Facies association 9 (FA9) – shallow marine carbonate setting

### Description

FA9 consists of thinly to thickly interbedded skeletal grainstone (*Lgs*) and skeletal packstone (*Lps*) facies. Both facies comprise fragmented, abraded bioclasts including abundant brachiopods, bryozoans and crinoids, some gastropods, ostracods and bivalves, with rare sponge fragments (Fig. 17). Large, well-rounded limestone clasts are locally present. An upward transition from grainstone dominated to packstone dominated is apparent (Fig. 17a). There are no trace fossils.

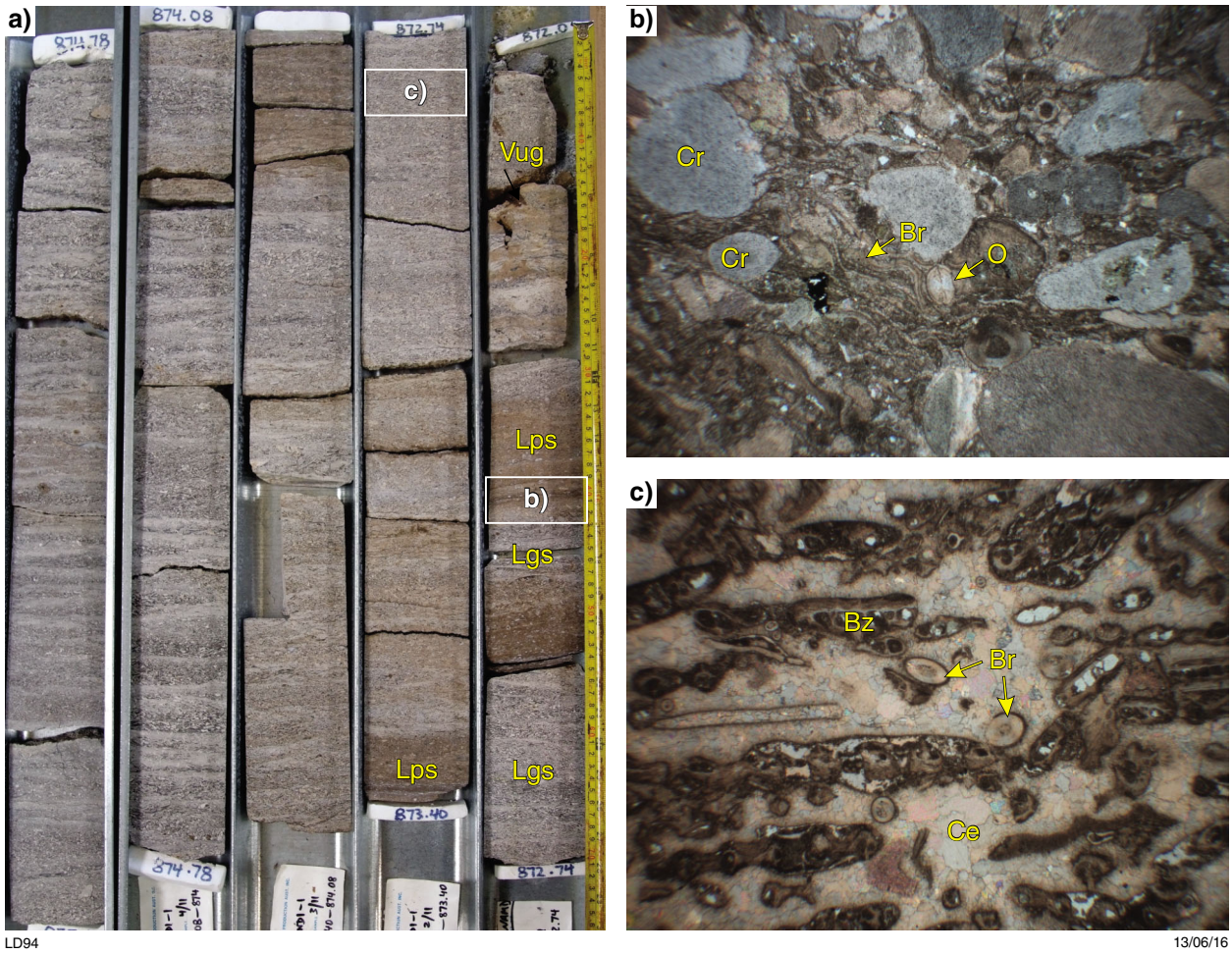


**Figure 17. FA9 in core section from Perindi 1, 872.04 – 875.5 m: a) interbedded grainstone (Lgs) and packstone (Lps) facies showing where samples for thin sections shown in (b) and (c) were taken from; b) photomicrograph of packstone facies at 872.4 m displaying a crinoid-dominated fabric. Br – brachiopod, Cr – crinoid, O – ostracod; FOV 11 mm; c) photomicrograph of grainstone facies at 872.8 m dominated by highly fragmented, well-rounded bryozoan fragments (Bz) with common brachiopod spines (Br) supported by equant carbonate cement (Ce), FOV 11 mm.**

### *Interpretation*

Bryozoans and crinoids indicate a well-oxygenated marine setting and the abundance of bioclasts indicates high carbonate productivity (Brigaud et al., 2009). A high-energy setting with reworking of sediment most likely by wave action is inferred from the coarse, highly fragmented and abraded grains. Interbedded packstone and grainstone fabrics suggest alternating fair weather and higher energy conditions respectively. High-energy, high carbonate productivity settings with regular reworking and storm influences suggest a shallow marine carbonate ramp setting above fair-weather wave base (Flügel, 2004). This is supported by the packstone and grainstone facies composed of highly abraded and fragmented bioclasts (e.g. Gramigna et al., 2011; Bassi and Nebelsick, 2010).

## Petrographic analysis

Key facies from drillcore sections were sampled for petrographic examination to describe detrital composition and authigenic modification, and to interpret diagenetic processes and their influences on porosity and permeability. This section describes the characteristics of six major siliciclastic facies and two major carbonate facies, and discusses significant trends and diagenetic character across the study area. Detailed descriptions of each sample are presented in Appendix 3. Detrital components are described as a percentage of the framework based on optical estimates. Porosity and authigenic products are described as a percentage of the whole rock.

## Siliciclastic facies

### *Detrital composition*

The framework in the siliciclastic facies is dominated by monocrystalline quartz (>60%) with minor plagioclase feldspar and microcline (Appendix 3). Fine-grained sandstones commonly contain minor biotite, up to 10%. Traces of carbonaceous material are common and lithic fragments are rare, except in some conglomerates. Of those lithic fragments seen, most have fine-grained clastic textures, although some are highly altered to kaolinite and chlorite and primary composition is not preserved. Fossil debris is locally present. The primary matrix is composed of brown clays and is a minor component in most samples but locally constitutes up to 25% of some sandstones. Well-sorted, subrounded to rounded grains, and planar contacts characterize all facies except conglomerates (*Gmc*), which have subangular grains. Compositionally, the sandstone facies are mainly quartz arenites and subfeldsarenites based on the QRF classification of Folk et al. (1970).

### *Authigenic phases*

Quartz overgrowth cement is common whereas kaolinite and carbonate cements are minor and are patchily distributed (Fig. 18a). Initial development of quartz overgrowths was followed by occlusion of pore space by kaolinite and carbonate cements. In Gmc, fibrous carbonate cements and quartz overgrowths are overprinted by carbonate veins (Fig. 18d). As could be expected, quartz overgrowths are best developed in clean sandstones or where detrital clay is minimal (<5%). Dissolution of plagioclase feldspar is common with grains replaced by carbonate cements and kaolinite (Fig. 18 a,b). Chlorite is present mainly as an alteration product after biotite but also locally occludes intergranular porosity. Extensive chlorite is present in all sandstone facies in Scarpia 1 due to the abundance of biotite in these facies (Fig. 18c). Fine-grained iron oxide is present in one sample, PND 1, overprinting all other cement types in this sample (Fig. 18a). Deformation of biotite by surrounding grains is common (Fig. 18b).

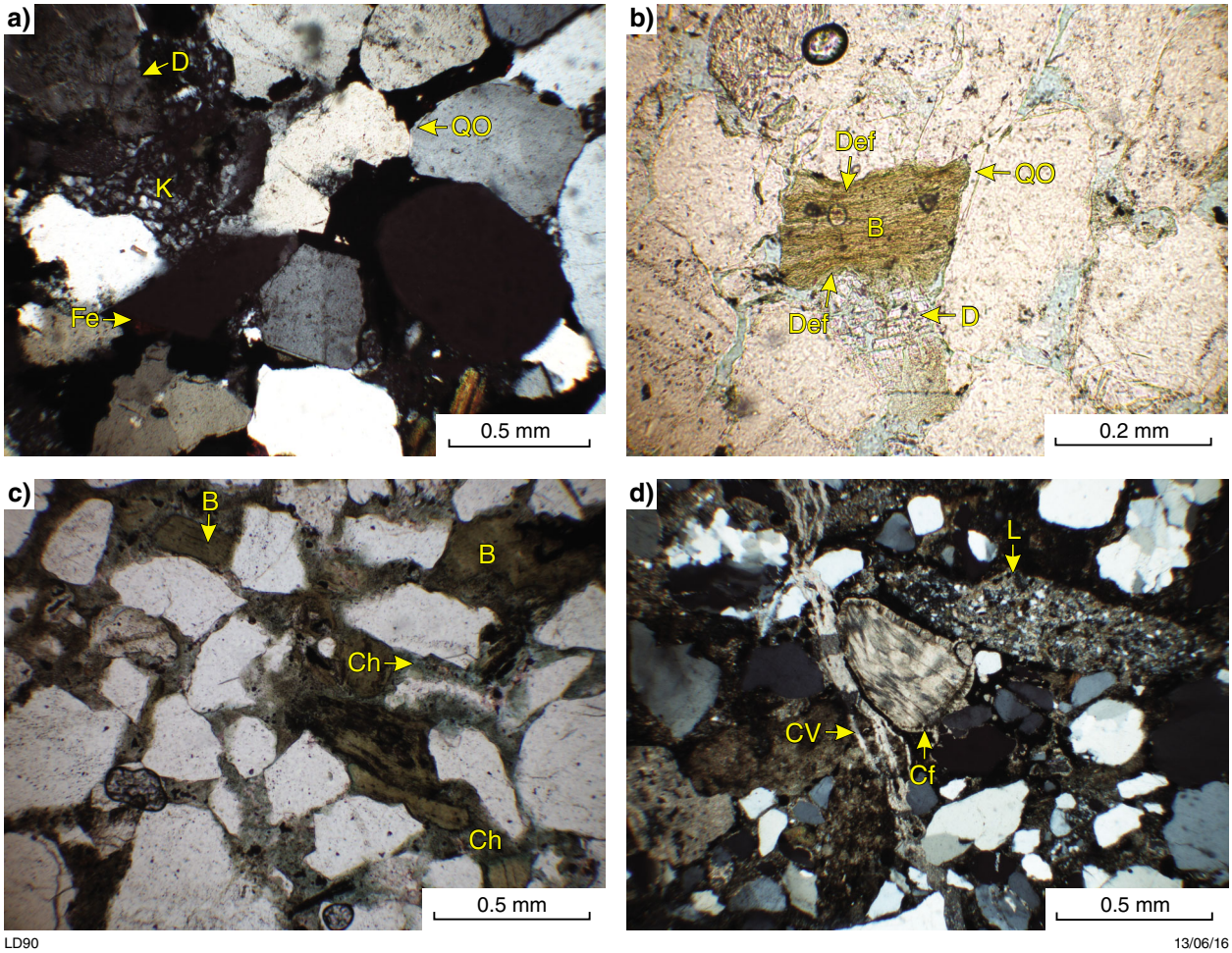


**Figure 18. Detrital composition and diagenetic features of siliciclastic facies: a) PND1 307.5 m, illustrating quartzose composition and cement history; quartz overgrowths (QO) followed by by kaolinite (K) filling intergranular pore space, both phases overprinted by iron-oxide cements (Fe). Dissolution of quartz (D) is also observed; b) PND1 317 m, deformation (Def) of biotite (B) by surrounding quartz and plagioclase feldspar. Quartz overgrowth cement is developed on some grains (QO) and dissolution of plagioclase feldspar is observed (D), post-biotite deformation; c) Scarpia 1, extensive chlorite formation in replacement of biotite grains (B), extending into intergranular spaces (Ch); d) PND1 300 m, Gmc facies, very poorly sorted with abundant lithic clasts (L), carbonate skeletal fragments rimmed by fibrous cement (Cf), and overprinted by carbonate veins (CV).**

## Carbonate facies

### *Detrital composition*

Fragmented bioclasts are abundant (>70%), composed mainly of brachiopods, crinoids and bryozoans, with minor gastropods, ostracods and coral debris. Crinoid bioclasts are distinctly more abundant in packstone facies than in grainstone facies. Carbonate facies may contain up to 30% very fine-grained, subangular quartz grains (Fig. 19a). Glauconite may be present in bioclast cavities and rare, well-rounded, limestone clasts are locally present. Bioclasts in grainstone facies are highly fragmented, mostly granule sized, abraded and very well rounded (Fig. 19a–c), compared to bioclasts in packstones which are generally less fragmented. (Fig. 19d).

### *Authigenic phases*

Fibrous to columnar calcite cement commonly forms a thin rim around bioclasts and quartz in grainstones and packstones (Fig. 19b,d). Calcite overgrowths are well developed on some bioclasts, particularly crinoid fragments, in Lgs and Lps (Fig. 19b). Equant carbonate cement is extensive in all samples, occluding intergranular pores and some internal skeletal cavities (Fig. 19a–c). Crystal size varies with both large and small calcite crystals observed. Partial to total replacement of bioclasts by equant calcite is seen in both facies (Fig. 19c). Blue staining indicates the equant carbonate is ferroan in some samples. Calcite-filled veins are common and overprint equant calcite (Fig. 19c).

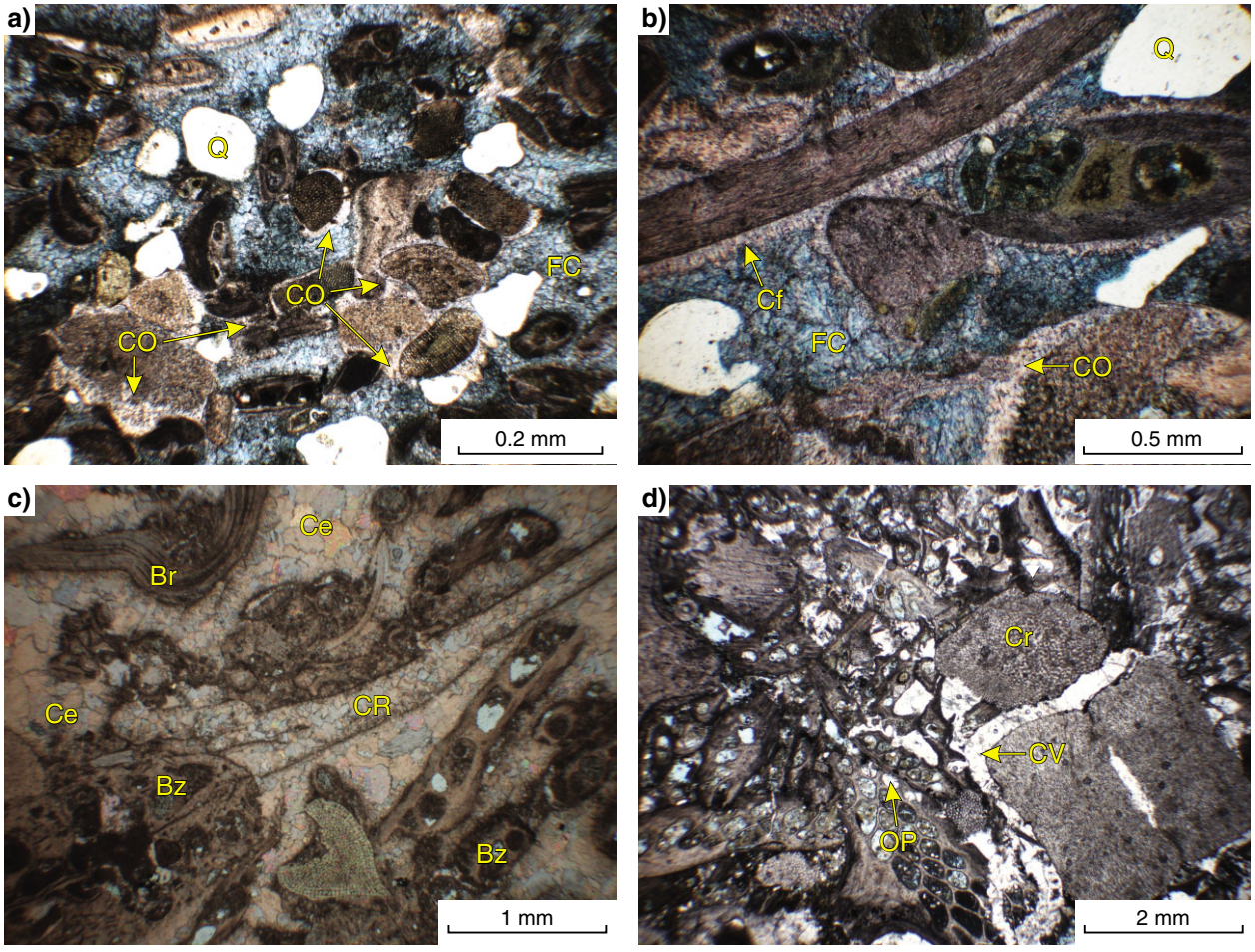


**Figure 19. Detrital composition and diagenetic features of carbonate facies: a) Langoora 1 Lgs facies, detrital composition dominated by fossil fragments with some quartz (Q). Pervasive ferroan calcite cement (FC) with some calcite overgrowths on crinoid fragments (CO) stained pink; b) Langoora 1 Lgs facies, bioclasts surrounded by fibrous calcite cement (Cf) and calcite grain overgrowths on crinoid fragments (CO). Intergranular space is extensively filled with equant ferroan carbonate cement (FC) stained blue; c) Perindi 1 Lgs facies, pervasive equant calcite cement occluding intergranular space (Ce) and supporting skeletal fragments including brachiopods (Br) and bryozoans (Bz); some clasts are totally recrystallized (CR); d) Roebuck Bay 1 Lps, Crinoid-dominated (Cr) packstone fabric with calcite cement occluding intergranular and intragranular spaces (OP) and as veins (CV).**

## Diagenetic history

Some mechanical compaction of the clastic rocks has taken place, as indicated by the presence locally of predominantly planar contacts and deformation of more ductile components such as biotite and carbonaceous material. Features associated with deep burial, such as grain fracturing and pressure dissolution, are notably absent, and there is good preservation of primary porosity. Taken together, these features indicate that compaction was limited. The development of quartz overgrowth cement indicates temperatures of at least 70–80 °C were achieved during burial (Worden and Burley, 2003). Overgrowths are absent or poorly developed where detrital clay and authigenic chlorite envelop grains (Worden and Morad, 2000; Worden and Burley, 2003).

Chlorite replaces biotite, and its abundance is controlled by the amount of primary biotite content originally in the rock. The extent of transformation from biotite to oxychlorite is variable, suggesting gradual and continuous formation, consistent with chlorite forming during both early and late diagenesis (Milliken, 2004). The common diagenetic dissolution of plagioclase feldspars observed is likely due to their chemical instability in comparison to the more stable quartz grains. This process is the main factor in the development of secondary porosity in siliciclastic facies (Milliken, 2004). The presence of iron-oxide cement in PND 1 is consistent with iron staining observed in core sections. Late formation of this cement indicates iron-rich formation fluid affected these areas during burial.

Overprinting relationships in carbonate facies indicate four main phases of cement precipitation. Fibrous calcite is commonly associated with carbonate facies deposited in open-marine settings, and is interpreted to have formed shortly after marine deposition before burial and compaction (Fig. 19b; Flügel, 2004). Point to planar grain contacts in Lgs and some Lps facies suggest early formation of equant carbonate, preventing grain rearrangement and closer packing associated with burial compaction. Grain overgrowth cements formed on crinoid fragments are enclosed by ferroan calcite (Fig. 19b). Both cements are commonly associated with burial diagenesis (Flügel, 2004). Ferroan carbonate cements comprise large and small equant crystals suggesting at least two phases of cementation. Partial to total replacement of bioclasts by equant carbonate indicates continued development of calcite after the initial cementation phase. This is a common feature of carbonate cements and is consistent with variation in crystal size in ferroan cements (Milliken, 2004).

Paragenetic sequences for both siliciclastic and carbonate facies based on the overprinting relationships of authigenic features are summarized in Figures 20 and 21. Diagenetic history is consistent across the study region for sandstones in the Poole Sandstone and Noonkanbah Formation, and is similar to that recorded from previous studies of the Grant Group (Dentith et al., 2015). The composition of Grant Group samples is similar to Sx facies which display the same quartz overgrowth, kaolinite, and calcite development history. Grain and grain-rim fracturing and contact suturing are seen in the deepest samples, consistent with their lower stratigraphic position and deeper burial.

Continuous burial of sediments between deposition of the Grant Group to the Noonkanbah Formation is consistent with accommodation generated by regional extension and subsidence at this time (early Permian; Shaw et al., 1994; Parra-Garcia et al., 2014). Transpression during the Early Triassic caused significant uplift and folding of sediments, preventing deep burial and the formation of related diagenetic fabrics (Shaw et al., 1994; Parra-Garcia et al., 2014).

# Stratigraphic characterization and correlation

## Grant Group (G1)

To date, the Grant Group has been considered stratigraphically distinct from the Poole Sandstone, classified as part of a separate, preceding second-order supersequence, Supersequence H (Fig. 2). Classically, the boundary between the Grant Group and the Poole Sandstone is marked by the end of glacial conditions and the *P. confluens – P. pseudoreticulata* zone boundary (Fig. 5). There are distinct variations in the well-log character of the uppermost Grant Group, designated here G1, which have implications for both the Poole Sandstone and Grant Group in the existing stratigraphic framework. These variations and their implications are explored in the following sections.

### Distribution of facies associations

In the Sundown 3H well, muddy tidal flat (FA8) and tidal-channel (FA4) associations are present at the base of G1 overlying a fluvial facies association (FA1; Fig. 22). A fluvial association is also present in the same stratigraphic position in the neighbouring Whitewell 1.

Palynological samples from the base of G1 indicate brackish conditions or settings with a strong freshwater influence based on the presence of the algae *Botryococcus* sp. in wells neighbouring Sundown 3H (e.g. Sundown 2, Terrace 1, Janpam 1; Plate 2). In the study areas to the northwest, limestone is recorded throughout G1, with glauconite at its base in some wells (e.g. Perindi 1, Minjin 1, Jum Jum 1, Curringa 1; Plate 2).

### Wireline characteristics and distribution

Blocky motifs on well logs indicate that the majority of the Grant Group is composed of thick, amalgamated sandstone packages with aggradational stacking patterns. An abrupt increase in gamma ray log values occurs above these aggradational trends, followed by a gradual decline of values, resulting in funnel-shaped motifs interpreted as coarsening-up cycles (e.g. Terrace 1, Whitewell 1, Hangover 1; Plate 1). The basal incursion and coarsening-up character are laterally continuous and are correlated across the northwest and central regions of the study area, but become difficult to distinguish in the southeast, and on the

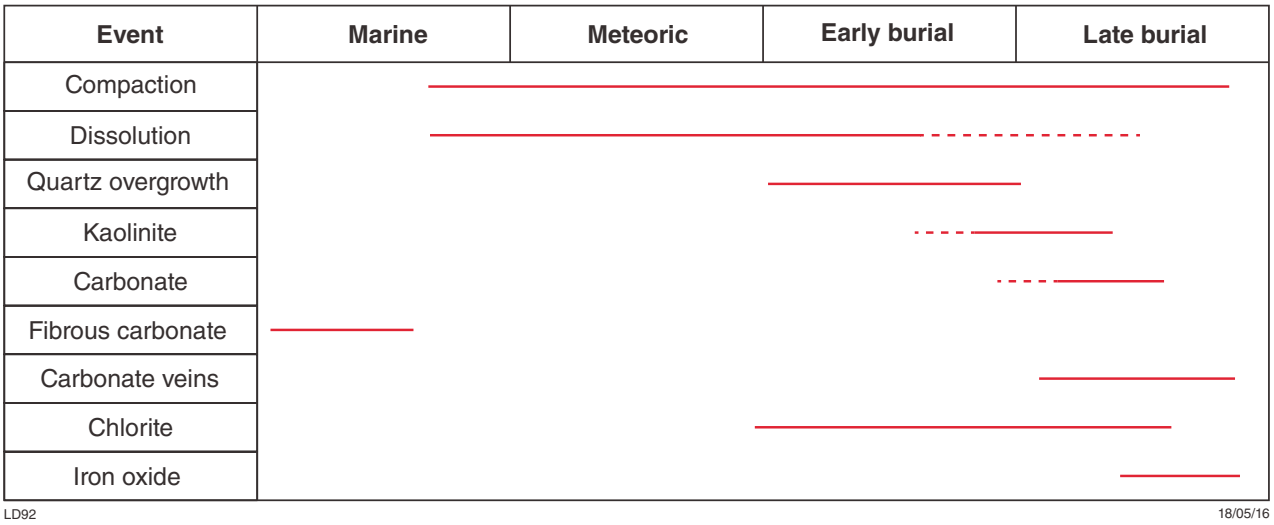


**Figure 20. Paragenetic sequence of authigenic minerals in siliciclastic facies in the uppermost Grant Group, Poole Sandstone and Noonkanbah Formation**

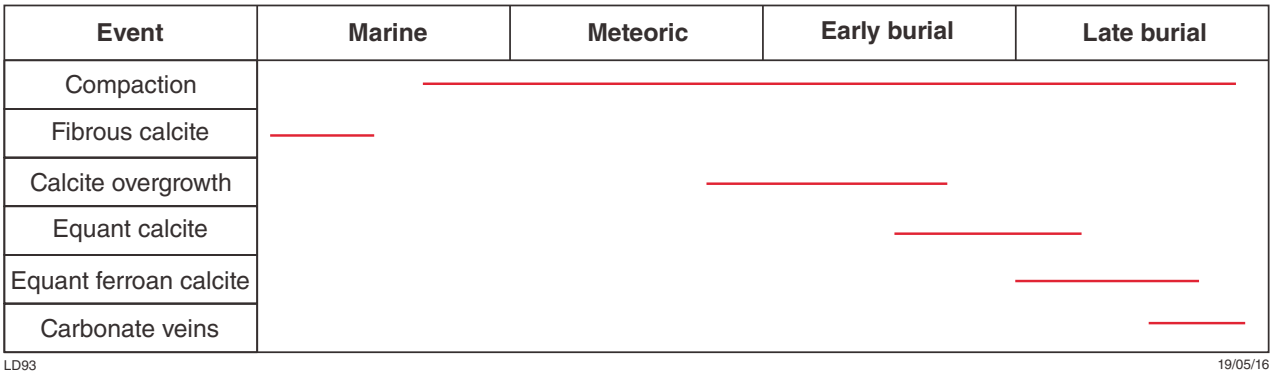


**Figure 21. Paragenetic sequence of authigenic minerals in carbonate facies in the Poole Sandstone and Noonkanbah Formation sampled in this study**

Jurgurra Terrace and Broome Platform (e.g. Kilang Kilang 1, Point Moody 1; Plate 1). The basal incursion becomes less distinct in the northwest of the study area where G1 is not directly underlain by an aggradational sandstone sequence (e.g. Curringa 1 and Puratte 1; Plate 1).

## Depositional model

Fluvial deposition is inferred for the Grant Group below G1 based on cored sections from Whitewell 1 and Sundown 3H, cylindrical log motifs known from such deposits (Martinius et al., 2001; Catuneanu, 2006), and previous work in the Canning Basin (Redfern and Millward, 1994; O'Brien et al., 1998; Eyles et al., 2001; Redfern and Williams, 2002; Al-Hinaai and Redfern, 2013; Dentith et al., 2015). The abrupt increase in the gamma ray log signature for rocks overlying these deposits, and associated deepening-up trend from fluvial (FA1) to tidal (FA3) associations in Sundown 3H, mark the presence of an extensive flooding surface. The presence of limestone and glauconite indicate marine conditions in the northwest. Marine influence extends southeast to Janpam 1 and Sundown 3H, but given the distinct coarsening-up trend in these wells, it is likely that this influence is limited to the base of G1 in the southeast.

## Grant Group – Poole Sandstone boundary

The uppermost Grant Group (G1) and Poole Sandstone (P1) have a similar facies and prograding architecture. There has previously been confusion in locating the boundary because of the uncertainty as to whether the Poole Sandstone consisted of one, two or three coarsening-up packages. Dentith et al. (2015) re-assessed the boundary between the two units based on regional well-

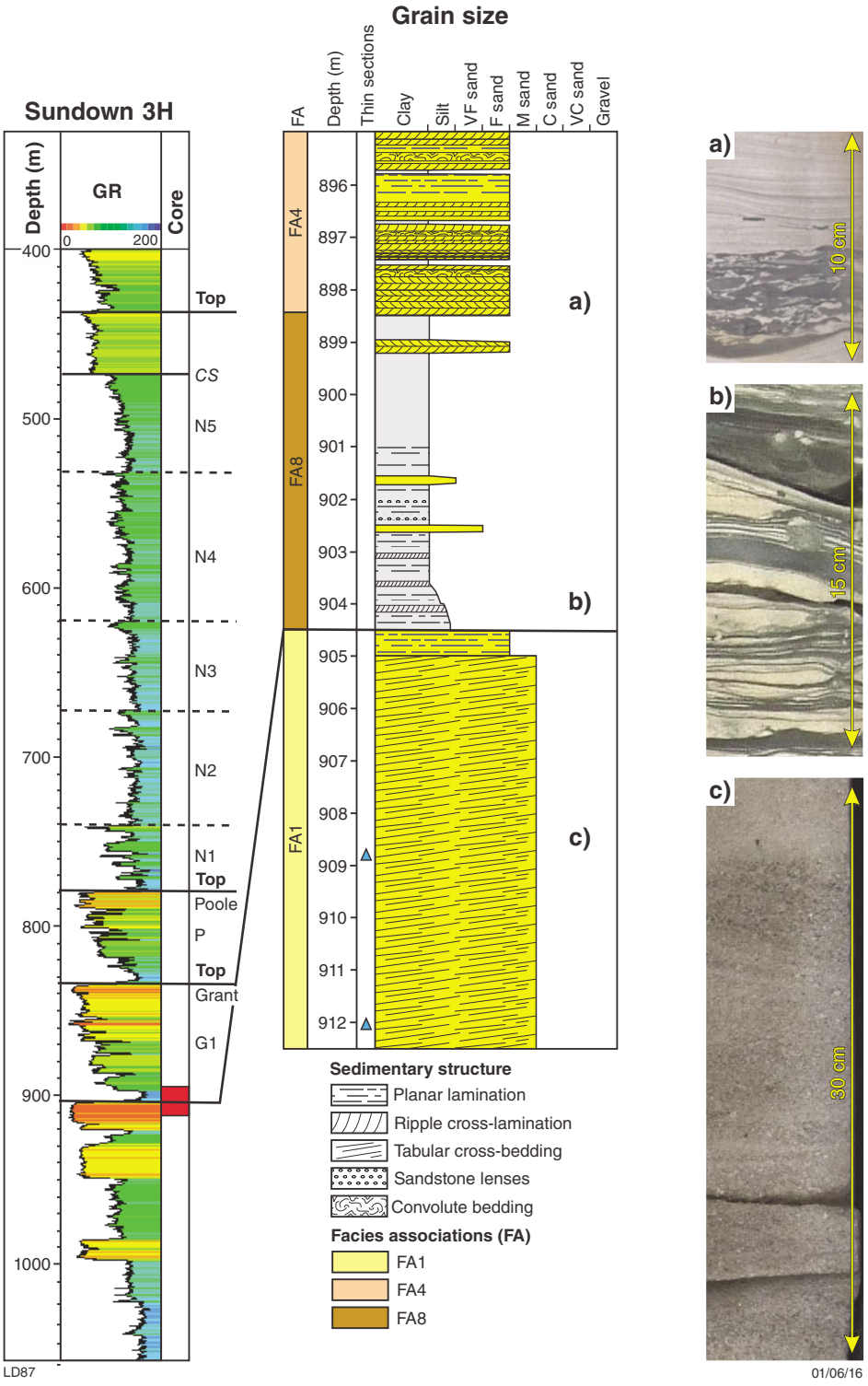


**Figure 22. Major flooding surface at the base of G1 (Grant Group) observed in the gamma ray log, and corresponding shift from fluvial (FA1) to tidal (FA8) facies associations identified in core section. *CS* – position of the casing shoe. P is Poole Sandstone; N1–5 is Noonkanbah Formation; red rectangle adjacent to gamma ray log is interval of interpreted core section. Core photographs correspond to sections a), b) and c) on core log.**

log correlation, and concluded that the Poole Sandstone contains only a single coarsening-up cycle. Many previous well completion reports have assigned two coarsening-up packages in the Poole Sandstone, thus including what is now considered to be the uppermost Grant Group (G1).

Palynology from 29 wells, including 27 existing reports and two new samples, indicates the presence of the *P. confluens* or equivalent palynological zones in G1 (e.g. Sundown 3H, Whitewell 1, Terrace 1, and Curringa 1; Plate 1; Appendix 5). This distinguishes it from the Poole Sandstone according to the *P. confluen*s – *P. pseudoreticulata* boundary (Eyles et al., 2002) and supports the model of the Poole Sandstone as a single coarsening-up package.

# Poole Sandstone

## Nura Nura Member

The Nura Nura Member is easily defined in the northwest where a distinct carbonate lithofacies is present (e.g. Perindi 1 and Jum Jum 1; Plate 3). This definition is hindered towards the southwest as the member becomes increasingly siliciclastic and identification varies from well to well. In some places it is identified as a thin fossil-rich unit (e.g. Meda 2; Plate 4), in others as a thick siliciclastic section (e.g. Janpam 1, Sundown 1; Plate 4), or as entire cycles that are predominantly siliciclastic (e.g. Sundown 3H; Plate 4).

In the following, the character and lateral correlation of the Nura Nura Member in the study area are described using available core material and well logs in combination with supporting well information (Appendix 6).

### *Distribution of facies associations*

A shallow marine carbonate ramp association (FA9) in Perindi 1 overlies a thick mudstone facies (M; Appendix 2). The packstone facies (Lps) identified in this association is also recorded in Roebuck Bay 1; however, paucity of core in this well prevents further interpretation. A sandy limestone facies is present at Nura Nura Ridge, in which bioclasts are typically whole and moderately to highly abundant.

### *Wireline characteristics*

FA9 identified in Perindi 1 corresponds to a distinct decrease in gamma ray (GR), sonic log (DT) and neutron log porosity (NPIH) values, and an increase in the formation density log values (RHOB) (Fig. 23). The same gamma ray log response is observed at the position of the packstone (Lps) sample in Roebuck Bay 1 (Fig. 23).

The decreased gamma, sonic and neutron trends, and increased density trend, are consistent across 15 wells in the northwest of the study area, corresponding to records of limestone facies in the Nura Nura Member (e.g. Moogana 1, Jum Jum 1, Booran 1; Plate 3; Appendix 6). For simplicity, only the gamma, sonic and density logs are illustrated. These log trends are observed in wells farther to the southeast which record sandstone and siltstone facies; however, responses are typically of lower amplitude (e.g. Canegrass 1, Janpam 1, Meda 2, Yarrada 1; Plate 3).

An abrupt upward decrease in gamma ray log values is observed in 21 wells, is common in both carbonate and siliciclastic rocks, and is interpreted as a coarsening-up trend (e.g. Booran 1, Thompson 1; Plate 3). In Perindi 1 this corresponds to the change from mudstone to grainstone facies (Fig. 23). The base of this trend is distinguished by an abrupt increase in gamma ray log values above the G1 coarsening-up trend. The top of the member is distinguished by an abrupt increase in gamma values at the base of cycle P1 that can be correlated across the study area.

### *Thickness and distribution*

The Nura Nura Member is represented by limestone facies in 17 wells, fossiliferous sandstone and siltstone in 10 wells, and non-fossiliferous sandstone and siltstone in three wells (Fig. 24; Appendix 6). A distinct facies trend is observed from carbonate facies in the northwest to clastic-dominated facies in the southeast (Fig. 24). The member extends farthest to the southeast in the Fitzroy Trough, with sandy limestone facies at Nura Nura Ridge and fossiliferous sandstone and siltstone facies recorded by Crowe and Towner (1976a) in the St George Ranges (Fig. 24).

In the northwest, the Nura Nura Member is intersected in all wells but one, where the Poole Sandstone is recorded; however, farther southeast the member cannot be identified in a number of wells (e.g. Sundown 1, Lloyd 2; Plate 3). The member averages 8 m thick with a maximum of ~13.5 m in Meda 2 and minimum of 2.5 m in Hangover 1. No relationship between thickness and facies or structural position is observed.

### *Depositional setting*

Distribution of the Nura Nura Member indicates widespread marine conditions, inundation from the northwest, and development of a shallow epicontinental sea, consistent with interpretations by Forman and Wales (1981) and Dickins (1996). Grainstone and packstone facies associations indicate a carbonate depositional setting was present in the northwest. Open-marine conditions are supported by the biological assemblage and fibrous (early marine) calcite cement in grainstone facies. Limestone distribution suggests clastic starvation in the northwest of the study area and the transition to onshore, siliciclastic dominated facies suggest the influence of clastic sources from the southeast, consistent with the interpretation of deltaic to lagoonal settings (Crowe and Towner, 1976a; Forman and Wales, 1981). Nura Nura Ridge and St George Ranges facies indicate that marine conditions extended farther inland in the Fitzroy Trough than on adjacent shelves and terraces (Fig. 1).

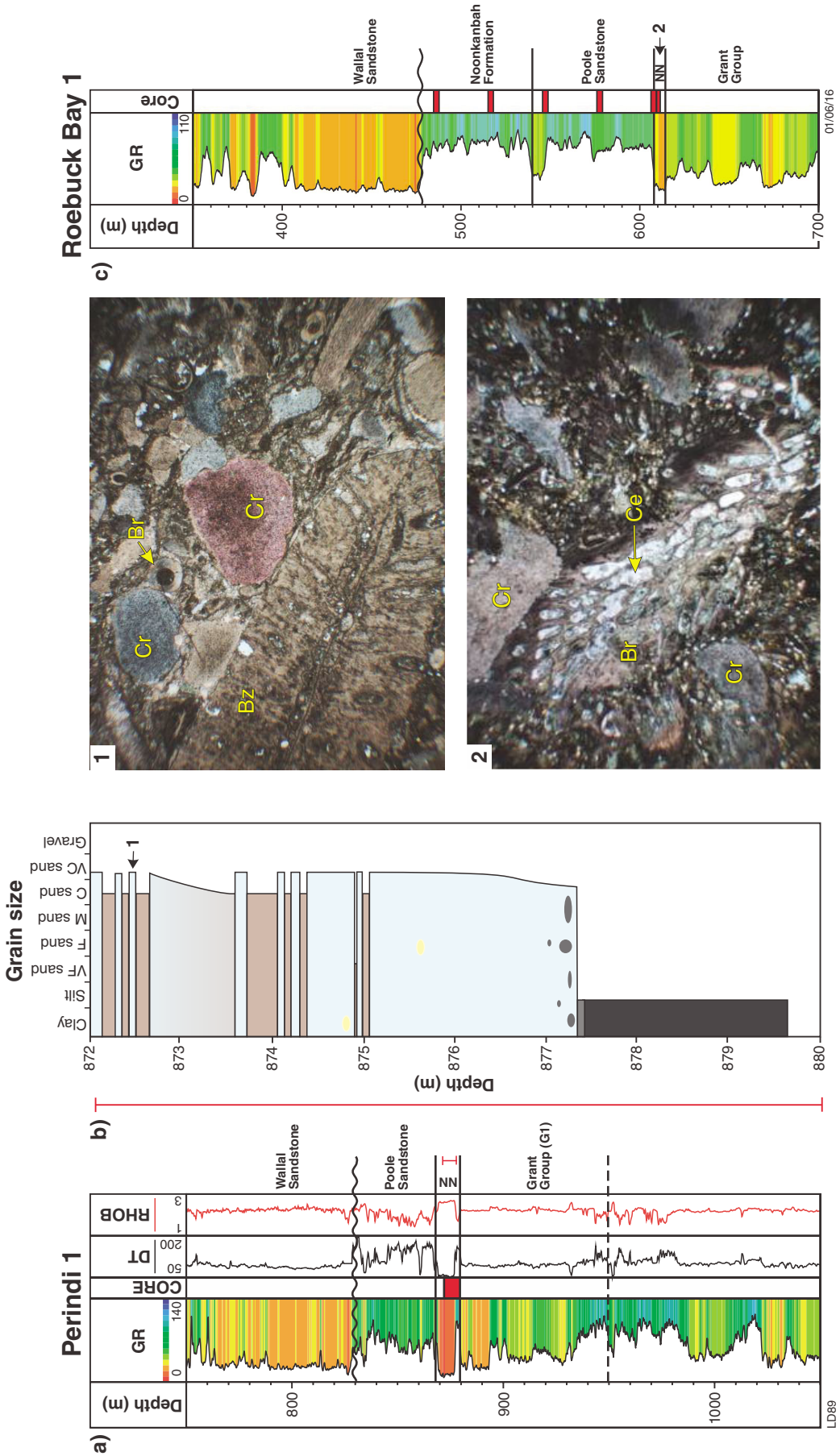


**Figure 23. Petrophysical log and petrographic features of Nura Nura Member carbonate facies: a), b) petrophysical and core logs, respectively, of Perindi 1 displaying decreased gamma ray (GR) and sonic (DT) log values, and increased density (RHOB) signatures. The corresponding core log illustrates a change from mudstone to grainstone facies that correlates with the shift in well log signatures; c) gamma ray log of Roebuck Bay 1 with similar low in gamma ray log values corresponding to samples of packstone facies (Lps) similar to those found in Perindi 1. Red rectangles adjacent to gamma ray logs are intervals of interpreted core sections. Arrows numbered 1 and 2 in gamma ray logs are locations of thin section micrographs from Perindi 1 and Roebuck Bay 1, which show packstone facies (Lps) of similar composition. Components include: Cr – crinoid fragments, Bz – bryozoan fragments, Br – brachiopod spines and Ce – calcite cement.**

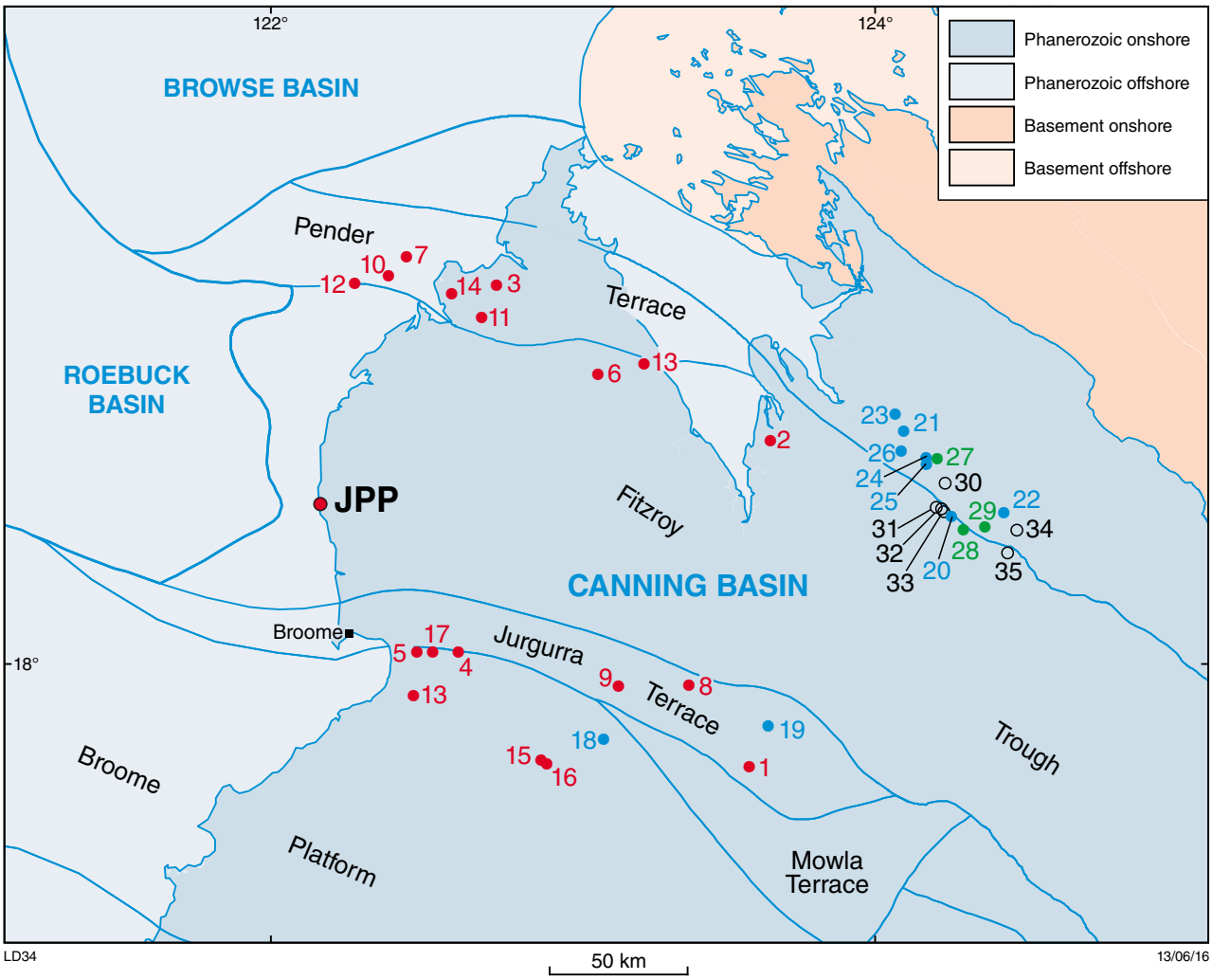


| | |
|---|---|
| •13 | Limestone |
| •18 | Fossiliferous sandstone and siltstone |
| •27 | Sandstone and Siltstone |
| ○27 | Nura Nura Member not distinguished |
| JPP | James Price Point |

1 Babrongan
2 Booran 1
3 Curringa 1
4 East Crab Creek 1
5 Freney 1
6 Jum Jum 1
7 Kambara 1
8 Logue 1
9 Mahe 1
10 Minjin 1
11 Moogana 1
12 Perindi 1
13 Roebuck Bay 1
14 Tappers Inlet 1
15 Thangoo 1
16 Whistler 1
17 Crab Creek 1
18 Dampier Downs 1
19 Frome Rocks 2
20 Hangover 1
21 Langoora 1
22 Mariana 1
23 May River 1
24 Meda 1
25 Meda 2
26 Yarrada 1
27 Canegrass 1
28 Sunup 1
29 Thompsons 1
30 Lloyd 2
31 Sundown 1
32 Sundown 2
33 Sundown 3H
34 Blina 7
35 Hakea 1

**Figure 24. Wells that intersect the Nura Nura Member. Wells are classified based on the dominant lithology of the Nura Nura Member found in each.**

### Discussion

Based on well-log responses, the upper and lower contacts of the Nura Nura Member are interpreted as flooding surfaces. The member is identified as a discrete cycle, possibly fifth order, of limestone or siliciclastic composition commonly characterized by a small-scale coarsening-up trend. The prevalence of limestone facies in far northwestern wells favours continuity of the member in this area. These carbonate facies have previously been described as lenticular in outcrop (Mory and Hocking, 2011), but more data are required to determine the extent of this lenticular character to the northwest. Where siliciclastic facies are present, the member cannot be consistently identified in well logs, suggesting patchy distribution and possibly nondeposition locally in these areas. Sandstone-dominated facies in the Nura Nura Member, for example meandering- to braided-style river deposit as interpreted by Crowe and Towner (1976a), may be indistinguishable from G1 in well logs, and thus misinterpreted as absent rather than a facies transition. Consequently, the extent of the member in the southeast is unclear. Crowe and Towner (1976a) recorded the Nura Nura Member at Mount Hutton, but no distinct differentiation of the Nura Nura Member from P1 sedimentary units could be made at the outcrop site or at the Poole Range and east St George Ranges localities, suggesting either patchy distribution or absence.

## P1

### Distribution of facies associations

Fluvial (FA1), sandy tidal flat (FA2), shoreface (FA5), and offshore (FA7) facies associations were identified in core and outcrop sections of P1. Two distinct facies trends were observed: a northwest to southeast facies shift, and an up-section facies shift (Fig. 25). Fluvial (FA1) and sandy tidal flat (FA2) associations are extensive in the southeast of the study area (Appendix 2). Fine- to medium-grained sandstones dominate these associations and are typically present throughout the section. Coarse- to very coarse-grained sandstone is locally present at section tops. Marginal marine to nearshore brackish environments are interpreted farther northwest based on the presence of spinose acritarchs and freshwater algae *Botryococcus* sp. in sidewall core sections (e.g. Janpam 1 and Terrace 1; Plate 2). A transition to lower shoreface (FA5) and offshore marine associations (FA7) is observed in core sections Meda 1 and Frome Rocks 2 (Appendix 2). North of Meda 1, core and outcrop sections are absent; however, limestone and glauconite have been recorded in well reports and these suggest marine conditions persisted in the northwest (Plate 2).

An up-section facies transition is observed from distal fluvial to proximal fluvial associations at Mount Bannerman (Fig. 26a), and from sandy tidal flat to fluvial associations at Poole Range and Mount Hutton (Fig. 26b). At Mount Bannerman, the transition is indicated by a distinct increase in the size of channel scours and channel-fill elements, which display coarser, poorly sorted facies in comparison to very well-sorted, well-rounded channel-fill elements of similar bedform size in distal associations. An overall increase in average grain size and bedform size is observed and interpreted as recording a more proximal position.

The basal contact with the Grant Group is generally abrupt (e.g. Mount Hutton; Fig. 26) where the Nura Nura Member is absent, but its character varies. At Mount Bannerman, a highly ferruginized distorted layer less than 1 m thick is present, a subtle angular relationship is seen at Poole Range, and thin quartz-pebble lags mark the contact at west St George Ranges, and in PND 1 core section.

### Wireline characteristics

Distinct upper and lower contacts enable confident correlation of P1 across the study area (Plate 1). The upper contact with the Noonkanbah Formation is defined by a sharp increase in values on the gamma ray log, and these increased values persist up-section over the next few hundred metres.

The base of P1 is identified by an abrupt increase in gamma ray log values followed by a gradual decline in values up-section. The basal inflection typically corresponds to a lithological change from sandstone or limestone to siltstone or siltstone-rich facies. Above this basal inflection, P1 takes on one of three well-log characters (Fig. 27): 1) a weak funnel-shaped character is defined by retention of high gamma values up-section, and reduces gradually at the top (e.g. Kambara 1 and Minjin 1; Plate 2); 2) a classic funnel-shaped character shows temporary retention of high gamma values followed by a steady overall decrease (e.g. Meda 2 and Hangover 1; Plate 2); 3) a cylindrical response is defined by a rapid return to low gamma values, which remain consistently low up-section (e.g. Olios 1 and Kilang Kilang 1; Plate 2).

Well-log character has a distinct relationship to location in the study area. Funnel-shaped responses are interpreted as coarsening-up trends (Martinius et al., 2001; Chow et al., 2005; Amigun et al., 2014) correlated to demonstrable increases in sandstone content. These signatures dominate the central and northwest of the study area with a transition to weak funnel signatures seen to the far northwest (e.g. Moogana 1 and Jum Jum 1; Plate 3). On the Jurgurra Terrace, Broome Platform and Crossland Platform, these weak funnel signatures are abrupt with a sharp decrease in gamma values mid-P1 (Plate 5). Cylindrical log responses are interpreted as aggradational packages and correspond to records of sandstone dominance from base to top (e.g. Olios 1 and Kilang Kilang 1; Plate 2). This trend is common in southeastern wells and is consistent with thick sandstone packages observed in outcrop sections and in core from PND 1.

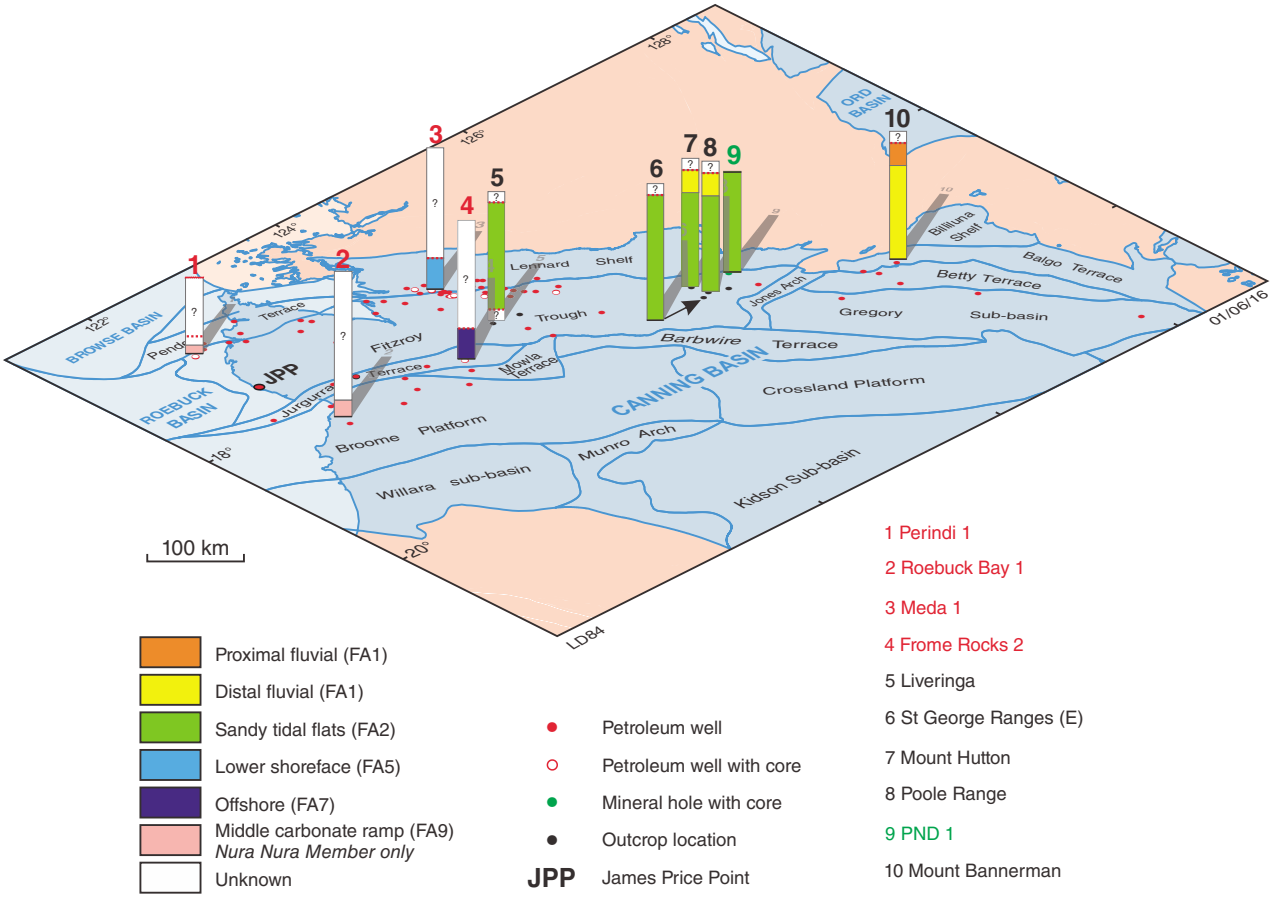


**Figure 25. Distribution of facies associations recorded in the Poole Sandstone (Nura Nura Member and P1) across the study area from outcrop and core sections. Heights of columns represent relative proportions of various facies associations within each well (not true thicknesses).**

### *Thickness and distribution*

P1 is distributed across the study area and crops out in the southeast, but is locally incomplete or absent in subsurface sections. On the western Broome Platform and northwestern Pender Terrace, partial sections of P1 (e.g. Thangoo 1 and Perindi 1; Fig. 6, Plate 3) or Grant Group (e.g. Hedonia 1; Fig. 6) are unconformably overlain by the Middle to Upper Jurassic Wallal Sandstone. Mesozoic sedimentary rocks unconformably overlying the Grant Group are also recorded on anticlines in the Fitzroy Trough (e.g. Fraser River 1 and Yulleroo 1; Fig. 6).

The average thickness of P1 is 57.7 m, maximum thickness is 122.5 m in Petaluma 1, Fitzroy Trough, and minimum thickness is 29 m in PND 1. Thicknesses were calculated from complete P1 intervals only; the overall minimum thickness recorded in the study area is 24.4 m from the partial section in Thangoo 1. Two main trends are observed; thickening into the Fitzroy Trough, and thickening towards the southeast on the Lennard Shelf.

### *Depositional model*

Facies associations indicate shallow, open-marine, conditions in the northwest of the study area through to marine-influenced, tidal to fluvial settings in the southeast (Fig. 25). The distribution of limestone and glauconite suggests that marine conditions prevailed across a large area to the northwest. The diverse facies associations support previous interpretations of the Poole Sandstone as recording fluvio-deltaic deposition (e.g. Mory, 2010 and references therein; Dentith et al., 2015). The sharp basal incursion of the gamma ray logs and the abrupt facies shift from sandstone to siltstone records a widespread flooding event and transgression from the northwest. Landward transitions in lithofacies up-sequence and coarsening-up log profiles reflect progradation across the study area following flooding. Rare aggradational to retrogradational trends may represent deltaic channel or distributary facies (Selley and Sonnenberg, 2015).

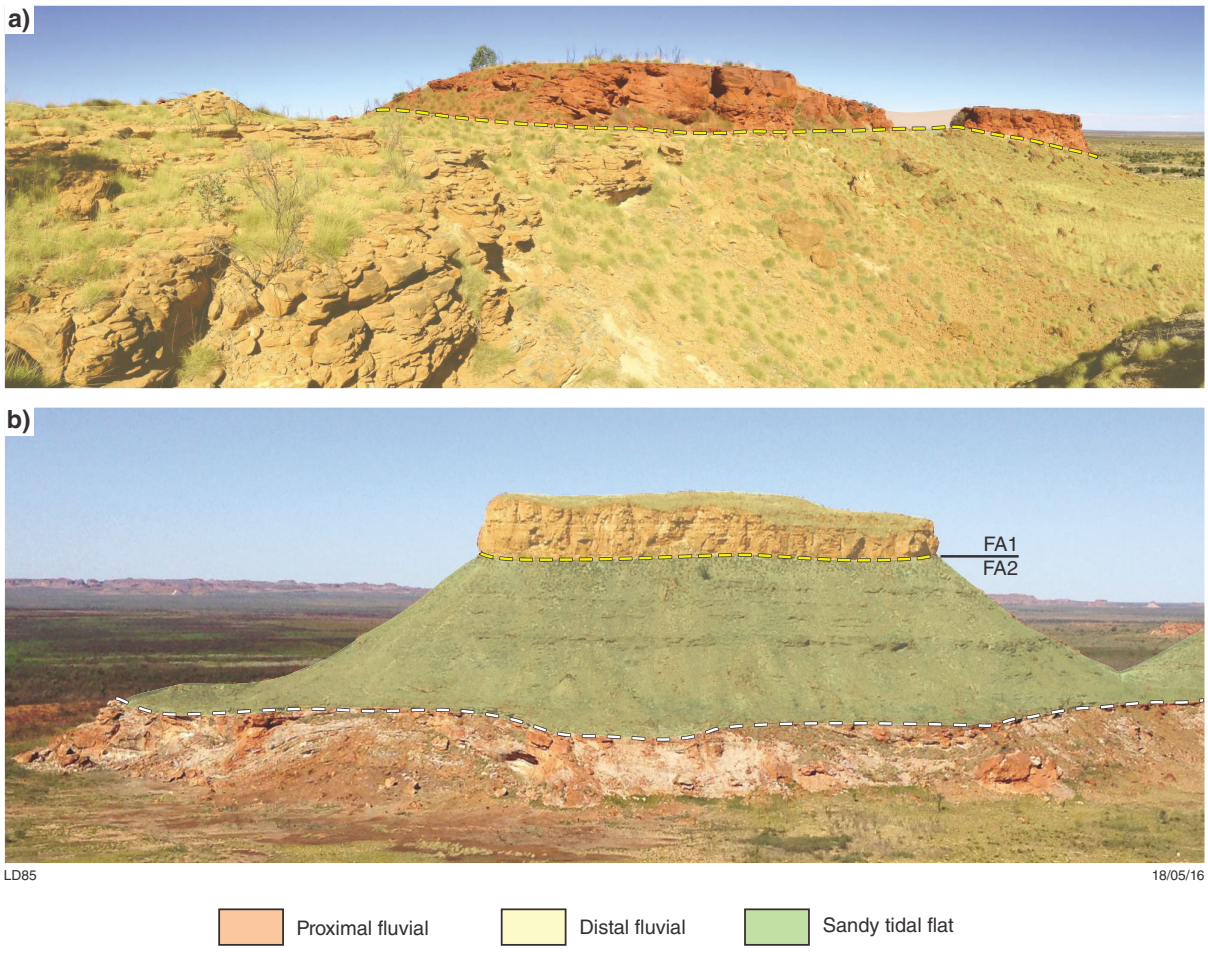


**Figure 26. Up-section facies transitions observed in outcrop exposures of P1: a) transition within FA1, from distal fluvial facies to proximal fluvial facies (separated by dashed line) up-section at Mount Bannerman; b) transition from sandy tidal-flat associations (FA2) to distal fluvial associations (FA1) at Mount Hutton**

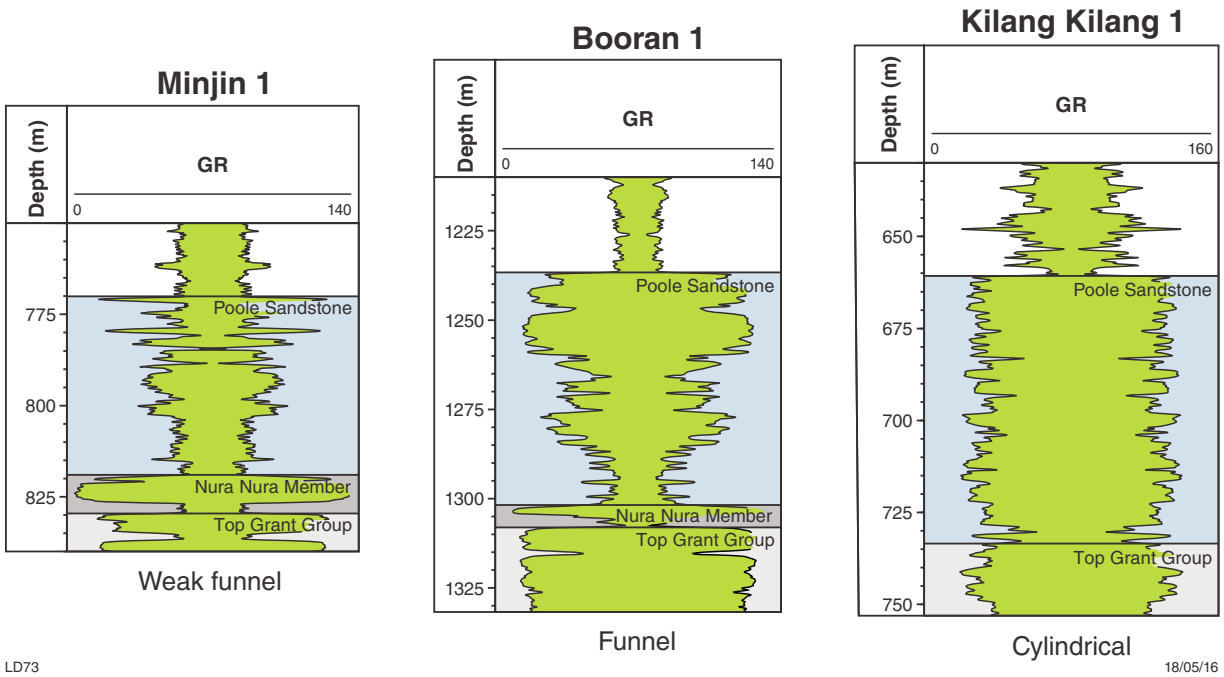


**Figure 27. Gamma ray log signature shapes — weak funnel, funnel, and cylindrical — observed in log sections through the Poole Sandstone**

Thickening of P1 to the southeast may be attributed to higher rates of deposition in more proximal areas of deltaic systems, consistent with classic deltaic profiles (Dalrymple and Choi, 2007). Thick, widely distributed, sandy tidal flat facies associations (Fig. 25) suggest the presence of complex and extensive intertidal areas that probably were part of vast delta-plain environments consistent with the more landward position of these associations (FA2; Dashtgard, 2011). Shoreface associations found farther to the northwest probably formed in delta-front settings (Fielding, 2010), and offshore associations may represent the prodelta area (Buatois et al., 2012). Facies distributions suggest very large deltaic systems, on a scale akin to modern deltaic systems such as the Irriwaddy, Mekong and Mississippi deltas (Woodroffe, 2000; Meselhe et al., 2012).

#### *Discussion*

The facies profiles, abundance of limestone in the northwest, dominance of sandstone in the southeast, and a dominant paleocurrent direction towards the west-southwest together indicate the development of large deltaic systems fed by a southeastern sediment source. Progradational profiles are most prominent on the Lennard Shelf, and are attributed to lower levels of accommodation resulting in more rapid reduction of available accommodation space. The dominance of aggradational trends to the southeast are attributed to proximity to the source area. Similarly, the less distinct progradational character in the northwest is attributed to a higher proportion of muddier facies due to distal position from the source region and greater accommodation space.

The extensive basal flooding surface is consistent with the interpretations of regional transgression at the time of deposition (Middleton, 1990; Kennard et al., 1994). The regressive shoreline model proposed by Warris (1993) and Adkins (2003) records regression as sediment supply outpaced the rate at which accommodation space was produced (Catuneanu, 2002). This temporarily regressive character is common during early transgression due to initial low rates of relative sea-level rise (Catuneanu, 2002; Cattaneo and Steel, 2003).

# Noonkanbah Formation

## Distribution of facies associations

Mixed tidal flats (FA3), lower shoreface (FA5), offshore transition (FA6), and offshore (FA7) facies associations are recognized in the Noonkanbah Formation. The stratigraphic position and succession of facies associations is consistent among the studied wells (Fig. 28). Mixed tidal flat associations are recorded at the base of the formation and are abruptly overlain by lower shoreface associations (e.g. PND 1 and Scarpia 1; Fig. 28), with a transition to offshore associations in PND 1. Offshore (FA7) associations are overlain by offshore transition (FA6) associations (e.g. PND 1, The Sisters 1, Frome Rocks 2; Fig. 28). In PND 1, there is an up-section return to offshore associations, and offshore transitional settings are observed in the uppermost part of the formation in Meda 1 (Fig. 28).

In the northwest, glauconite and shell fragments are abundant throughout the formation, and limestone is commonly interbedded with siliciclastic facies. These features decrease in abundance towards the southeast and limestone is absent in PND 1, although marine trace fossils, and shell fragments are still common.

## Wireline characteristics

Typically, the entire Noonkanbah Formation is characterized by consistently high gamma ray log responses. The upper contact with the Liveringa Group is identified by a sharp increase in gamma ray log values, which is distinct across the study area (Plate 6). Variations in this log indicate two overarching trends and six nested subtrends (N1–N6) in the formation (Fig. 29). The general increase in values in the lower half of the formation is interpreted as a retrogradational trend overlain by a progradational trend shown by an overall decrease in values upward.

Superimposed on these two large trends are six smaller trends N1–N6. N1 is a funnel-shaped gamma ray response, interpreted as a progradational trend, and N2–N5 are cylindrical signatures interpreted as aggradational trends (Fig. 29). N6 is variable, either funnel-shaped (e.g. Langoora 1 and May River 1) or cylindrical (e.g. Blackstone 1). Boundaries between N1–N6 are defined by abrupt increases in gamma ray log values, most distinct at the base of N2 and N5 (Fig. 29). These incursions are laterally consistent and are correlated across the study area (Plate 6).

In the far northwest of the study area, N1 and N2 are indistinguishable in well logs and the funnel-shaped signatures observed elsewhere are difficult to distinguish (e.g. Padilpa 1 and Puratte 1; Plate 6). The distinction between N5 and N6 is unclear in some wells, and as such, they are shown as a conjoined unit in Plate 6. However, the clarity of N6 in a significant number of wells warrants distinction from N5. Correlation of trends at all scales is hindered towards the southwest by the absence of the uppermost parts of the Noonkanbah Formation.

D-INPEFA revealed two distinct trends in the Noonkanbah Formation. Whole-log D-INPEFA displayed an overall positive log trend, interpreted as an overall fining-up of the formation (Fig. 29). The partial D-INPEFA illustrates two positive–negative trends, the first constituting N1–N4 and the second N5–N6, with a positive turning point (PTP) separating the two at the base of N5 (Fig. 29). This signature shows local variability (e.g. Meda 1 and PND 1; Plate 6) and is inconsistent in the Gregory Sub-basin and on the Betty Terrace (e.g. Bindi 1; Plate 6).

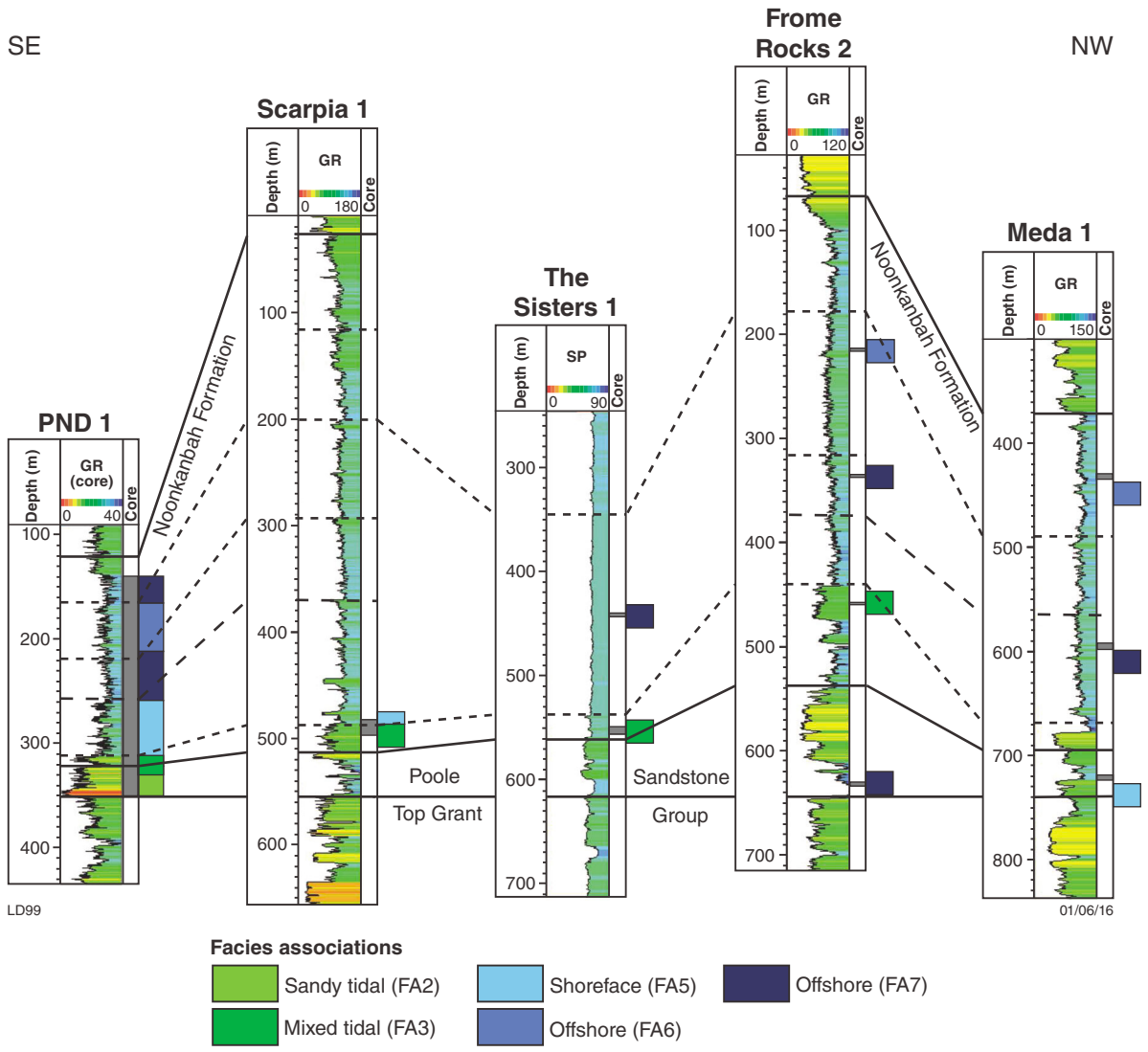


**Figure 28. Stratigraphic position of cored sections interpreted from facies associations. In the Noonkanbah Formation, tidal (FA2/3) and shoreface (FA5) associations correspond to the basal coarsening-up trend and, above this, offshore facies (FA7) are consistently present in the second and third trends, stratigraphically overlain by offshore transitional associations (FA6). The order of facies associations in the Noonkanbah Formation—tidal, shoreface, offshore, offshore transitional — is consistent in all wells.**

## Thickness and distribution

The Noonkanbah Formation was deposited across the study area, and outcrops in the southeast. On the Pender Terrace, Jurgurra Terrace, Broome Platform and Crossland Platform, partial sections of the formation are present in the subsurface, unconformably overlain by Jurassic sediments (e.g. Roebuck Bay 1, Freney 1, and Crab Creek 1; Plate 5). In the Fitzroy Trough, the formation is locally absent, removed from the cores of some anticlines (e.g. Fraser River 1; Fig. 6).

Average thickness, calculated from complete sections, is 343.1 m but varies widely. Minimum thickness is 202 m in PND 1, maximum thickness is 640.8 m in Petaluma 1. Partial sections are 25–310 m thick. Two trends are observed: thickening from the Lennard Shelf into the Fitzroy Trough, and thickening from southeast to northwest along the Lennard Shelf.

## Depositional history

The facies associations recognized in the Noonkanbah Formation indicate the dominance of widespread, low-energy, open-marine conditions during deposition.

Cycles N1–N6 record changes in the depositional environment, and are closely related to facies associations. The sections with the highest gamma ray log readings, N3 and N5, correlate with records of thick mudstone-dominated lithologies and N3 hosts the most distal facies association (FA7, offshore). The excellent lateral continuity of these cycles suggests a low-gradient paleoslope.

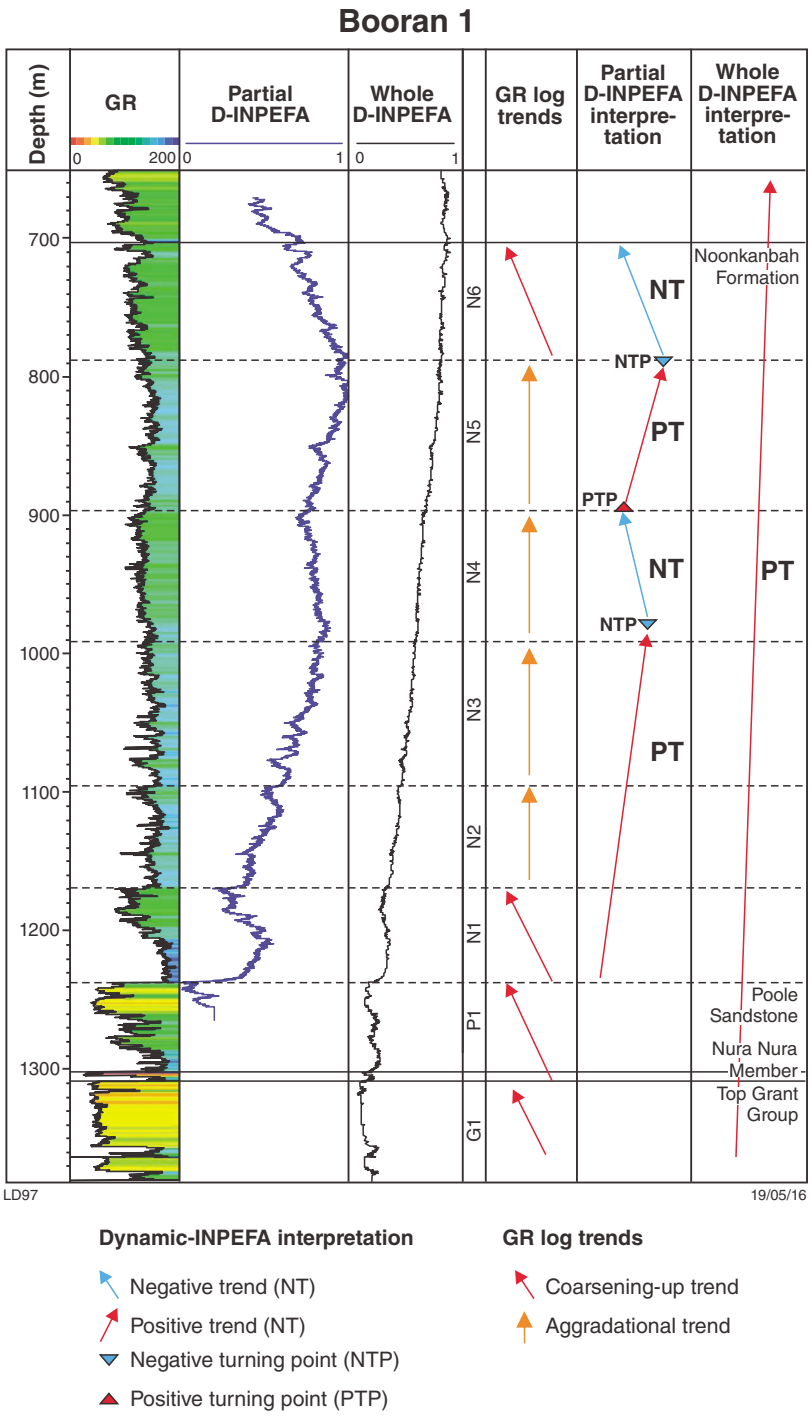


**Figure 29. Representative log section and interpretation of eight gamma ray log trends G1, P1 and N1–N6, and whole and partial D-INPEFA curves run on the gamma ray log, with interpreted positive and negative trends and turning points**

The abrupt shift in the gamma ray log at the base of the formation, recorded across the study area, indicates a regional flooding surface. This was followed by successive, regional transgressive–regressive packages, S1 and S2. Above the basal flooding surface, the increase in muddier facies above the basal flooding surface and deepening-up trends from mixed tidal flats to offshore associations indicate a long phase of deepening marine conditions (e.g. PND 1, The Sisters 1, Scarpia 1; Fig. 28). This was followed by regional shallowing-up, indicated by decreasing gamma ray log values and a transition to offshore transitional associations (FA6; e.g. PND1 and Frome Rocks 2; Fig. 28).

A second phase of deepening is indicated by a second abrupt incursion in the gamma ray log at the base of N5, accompanied by deepening-up from offshore transitional to offshore facies associations (FA6–FA7). Gamma ray log profiles indicate large-scale shallowing-up following this flooding event.

## Discussion

The Noonkanbah Formation represents major flooding and quiescent open-marine facies overlying the fluvial and fluvio-deltaic Grant Group and Poole Sandstone, consistent with interpretations from previous work (Wade, 1936; Yeates et al., 1975; Forman and Wales, 1981; Mory and Hocking, 2011), and with models of glacio-eustatic sea-level rise (Wopfner, 1999) and regional transgression (Middleton, 1990; Warris, 1993; Kennard et al., 1994).

The landward limit of marine incursion is difficult to establish. The facies associations and presence of fossiliferous carbonate lags with fibrous calcite cement indicates open-marine conditions were present as far southeast as PND1. This is consistent with previously interpreted open-marine conditions based on the presence of goniatites as far southeast as the Balgo Hills, which is located over 200 km southeast of PND 1 (Casey and Wells, 1960; Yeates et al., 1975).

# Porosity

Porosity data were compiled from existing well reports for all wells within a 200 km radius of James Price Point (Appendix 7), although data for the Noonkanbah Formation were only available for one well. Porosity measurements are based on well-log predictions and the following section presents a summary of these data. Permeability measurements were not available for most wells.

## Poole Sandstone

### *Nura Nura Member*

Porosity measurements for the Nura Nura Member were available from three wells (Appendix 7). Average porosity per well was low, 0 – 4.6 %, and individual measurements are in the range 0–13 %. Porosity of the member in Perindi 1 is predominantly intragranular, preserved in bioclast cavities with dissolution producing minor secondary porosity (Fig. 31a; Appendix 7). Visual porosity estimates were higher for the Roebuck Bay 1 sample with a mix of primary inter- and intragranular porosity (Appendix 7). Large vugs in packstone facies as in Perindi 1 may cause significant increase in porosity locally.

### *P1*

Porosity measurements for P1 were available for 14 wells (Appendix 7). Average porosity per well is 1.3 – 28%, and individual measurements are in the range 0–32%. No clear relationship between depth and porosity was observed. Visual porosity estimates from thin-section analysis are consistent with the range recorded from well reports. Bioturbated heterolithic facies (*Hxs*) show selective porosity enhancement within trace fossils (Fig. 31b,c).

## Noonkanbah Formation

In the 200 km radius around James Price Point porosity measurements were retrieved from short intervals in one well, West Kora 1, in the range 15.5 – 17.7%. Enhanced porosity within trace fossils in Hxs facies was observed in thin section (Fig. 31d; Appendix 3).

The Scarpia 1 well sits well beyond the 200 km radius; however, it is noteworthy that very high porosities were recorded from core plugs taken in shoreface and mixed tidal flat facies associations from this well. Porosities averaged 29.5% with a range of 25.8 – 33.1%. Visual porosity estimates indicate similar high porosity in mixed tidal flat associations in the Noonkanbah Formation from PND 1 (Appendix 3).

# Stratigraphic implications

The Poole Sandstone, Noonkanbah Formation and Liveringa Group represent a second-order transgressive–regressive package identified by Kennard et al. (1994) as Supersequence I. Supersequence I is the third of four supersequences that constitute a Late Carboniferous – Triassic first-order megasequence (Fig. 2). Further to this, the Noonkanbah Formation can be divided into two third-order trends (S1 and S2) and eight fourth-order trends (G1, P, and N1–N6). Fourth and higher order sequences are composed of stacked high-frequency transgressive cycles.

# First order

First-order transgressive conditions are represented by the large-scale positive trend recorded by the whole formation D-INPEFA (Fig. 29). The trend is not distinct in the gamma ray log, which best represents the second-order sequence, but is consistent with basinwide subsidence of the Canning Basin from the late Carboniferous to Early Triassic, related to the breakup of Australia's northwestern margin (Parra-Garcia et al., 2014).

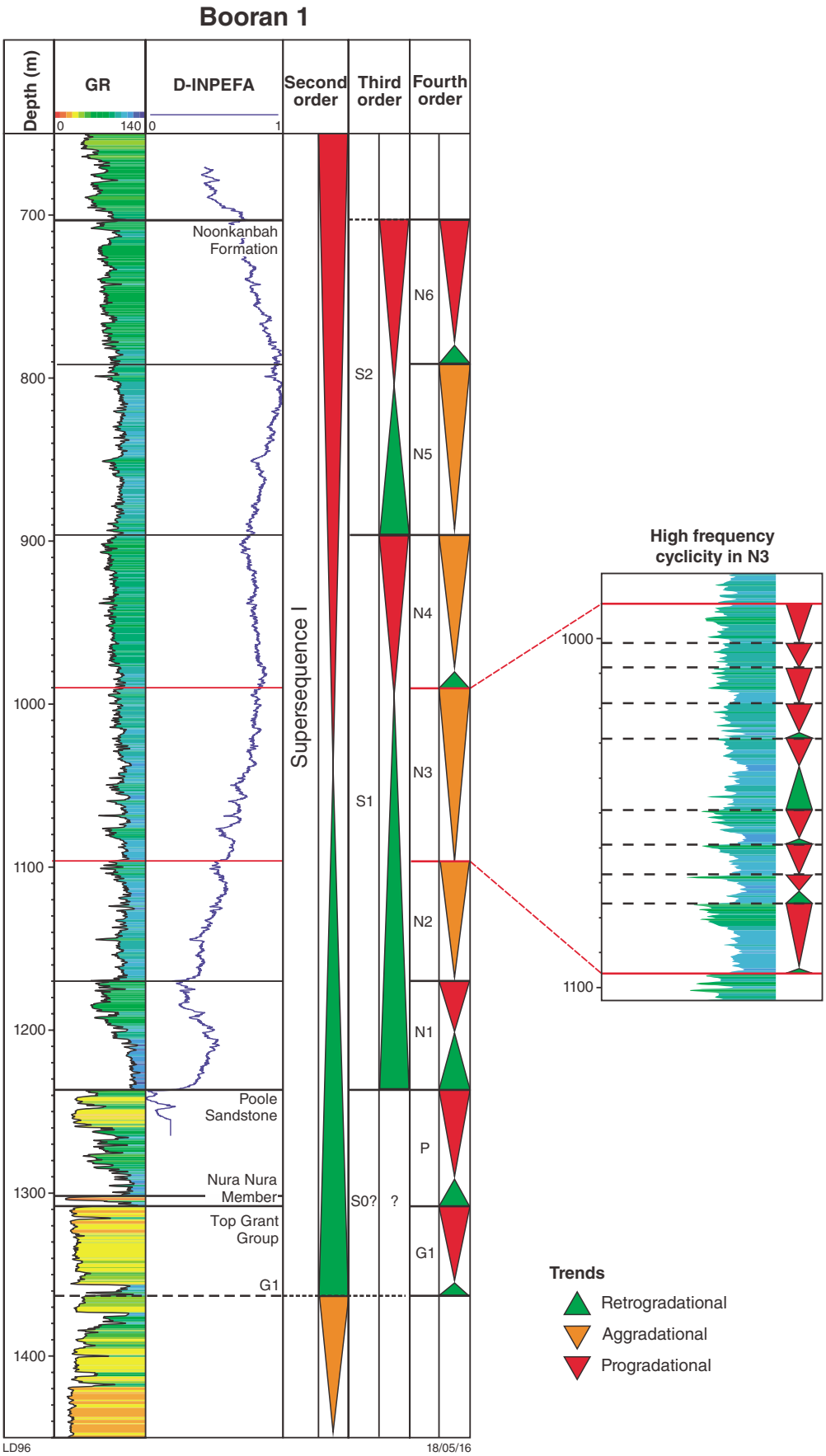


**Figure 30. Position and character of second-, third- and fourth-order sequences between the uppermost Grant Group and the top of the Noonkanbah Formation. High-frequency sequences identified in the Noonkanbah Formation are identified for the fourth-order cycle N3.**

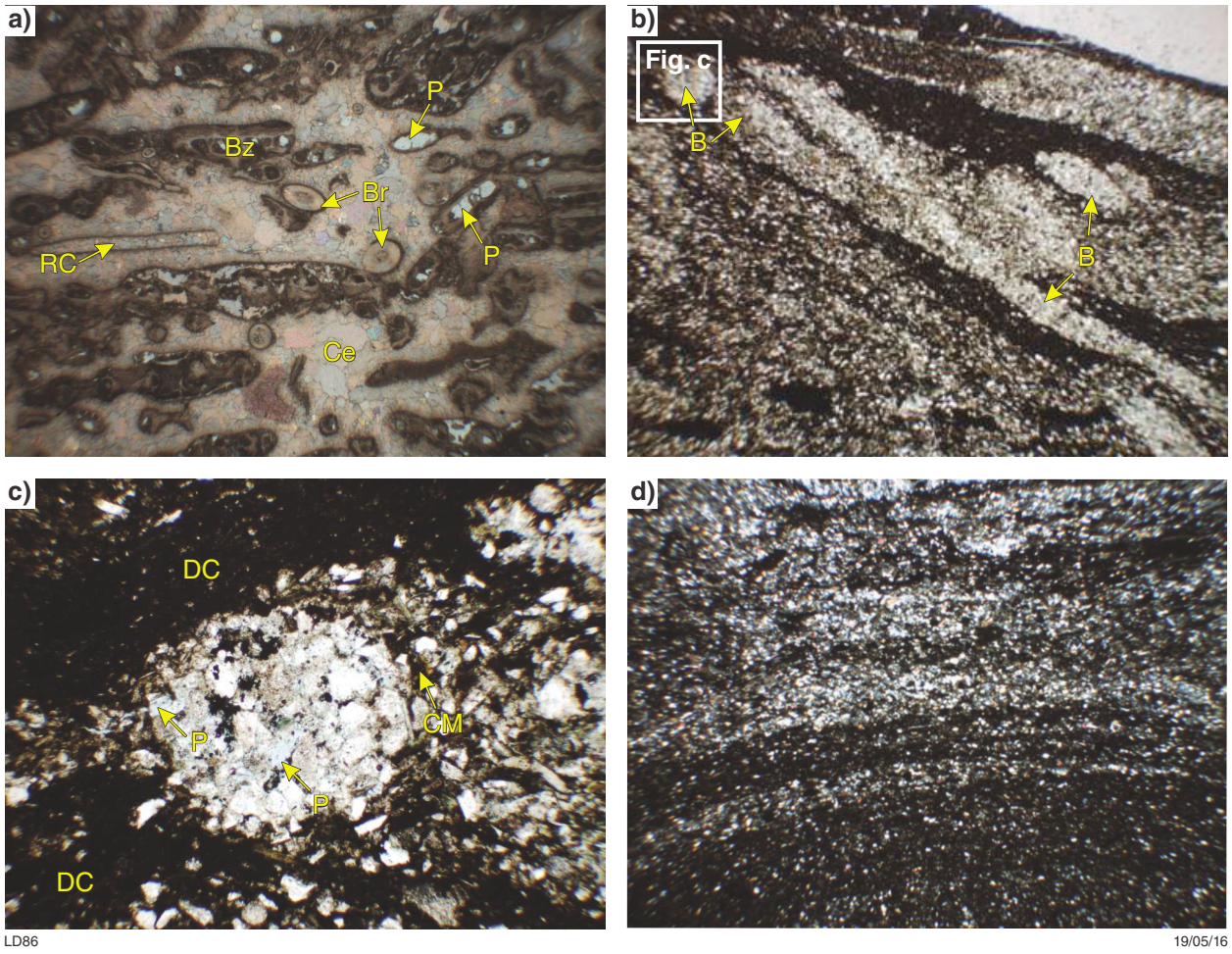


**Figure 31. Style and structure of porosity in carbonate and siliciclastic facies: a) primary intragranular porosity preserved in bioclast cavities in grainstone facies from the Nura Nura Member in Perindi 1; b) biologically enhanced porosity at the base of the Poole Sandstone in offshore facies association (FA7), Frome Rocks 2; B – burrows; c) scaled-up burrow in b) showing reduced carbonaceous matter (CM) and detrital clay (DC), and increased porosity (P) within the burrow; d) biologically enhanced porosity, lighter coloured bands, in the Noonkanbah Formation in offshore transitional (FA6) facies association, Frome Rocks 2.**

## Second order

The transgressive–regressive character of Supersequence I is represented by a thick retrogradational trend overlain by an aggradational to progradational trend that is distinct on well logs (Fig. 30). The maximum flooding zone is interpreted at the base of this aggradational trend, in the lower half of the Noonkanbah Formation, and is represented by the thickest section of high gamma ray log values in the sequence. This log signature is laterally extensive and correlates to records of siltstone–claystone dominated facies and the most distal facies in Supersequence I, offshore associations (FA7; e.g. PND1 and Frome Rocks 2; Fig. 28).

Kennard et al. (1994) interpreted the base of the Poole Sandstone as the base of Supersequence I, which appears to coincide with the *P. confluens – P. pseudoreticulata* boundary, and has been interpreted to mark the end of glacial conditions (Eyles et al., 2002). Typically, the transgressive surface and beginning of transgressive conditions are interpreted on the basis of first evidence of deepening and switch in shoreline trajectory (Cattaneo and Steel, 2003). A transition from aggradational to retrogradational stacking pattern is observed at the base of G1. The base of this cycle is also marked by the presence of a laterally extensive siltstone-dominated layer representing an abrupt deepening-up of facies from fluvial to tidal in Sundown 3H (Fig. 22). These features, and marine indicators in G1, suggest widespread flooding prior to deposition of the Poole Sandstone. Further assessment of the uppermost Grant Group and characterization of the contact between G1 and underlying sediments is required to verify this interpretation.

Second-order cyclicity is consistent with eustatic sea-level rise and equivalent second-order transgressive deposits are found in Gondwanan basins globally, preserving evidence of the link between glaciation and transgression intensity (Wopfner, 1999; Izart et al., 2003; Veevers,

2006). Examples of such deposits are recorded in the South Oman Basin, Peninsular India, and Tibet (Wopfner and Jin, 2009). In the Carnarvon Basin, Western Australia, glacio-eustatic sea-level rise has been interpreted during deposition of the Callytharra Formation (Hocking et al., 1987; Crostella and Iasky, 1997), which, based on foraminiferal evidence (Kempin, 1956), is considered to be an equivalent of the Nura Nura Member of the Poole Sandstone.

## Third order

The Noonkanbah Formation consists of two third-order transgressive–regressive cycles (S1 and S2) bounded by distinct, laterally persistent flooding surfaces. Flooding surfaces are indicated by sharp shifts in the gamma ray log and can be correlated across the study region (Fig. 30; Plate 5). The transgressive–regressive character of cycles is reflected in the successive positive–negative trends displayed by the partial D-INPEFA logs and deepening-up to shallowing-up facies transitions (Fig. 29). Sequence division is based on the identification of flooding surfaces rather than subaerial unconformities as the sequence boundaries (Catuneanu, 2006) due to the prevalence of shallow marine conditions.

Crude estimates of cycle duration were achieved using existing palynological data. The base of S1 records both *P. pseudoreticulata* and *S. fusus* zones. The base of S2 correlates weakly to the beginning of the *P. sinuosus* zone, which is constrained between this surface and the top of S2. The *D. villosa* zone is also recorded locally at the top of S2. These constraints indicate cycle duration of 8–11 Ma, using the Gradstein et al. (2012) timescale to calibrate palynological zones.

The duration of cyclicity suggests that their development is probably tectonically controlled (Isbell et al., 2012). The current tectonic model for the Canning Basin suggests a single extensional phase, the Point Moody Extension, that included uplift, extension and volcanic events (Parra-Garcia et al., 2014). Locally, extension involved reactivation of half-graben structures in the Fitzroy Trough in the Permian and activity along the trough's major south-bounding fault, the Fenton Fault (Parra-Garcia et al., 2014). Tectonic influence is suggested by the nesting of these third-order sequences in a glacio-eustatic controlled, second-order trend, in tectonically active settings. In addition, third-order cycles do not display a distinct correlation with global eustatic events (Haq and Schutter, 2008; Wopfner and Jin, 2009). This interpretation is consistent with a large-scale study of cyclicity in Gondwanan basins, which found that third- and fourth-order cyclicity was tectonically controlled in all Permian strata assessed (Izart et al., 2003).

Cycles of 8–10 Ma duration have been attributed to glacio-eustatic processes in eastern Australia, related to remnant glaciers (Fielding et al., 2008). However, glaciers in Western Australia and central northern Australia are inferred to have been absent at this time (Fielding et al., 2008; Isbell et al., 2012). Furthermore, these eastern Australian deposits display alternation between glacial and nonglacial deposits not observed in the Poole Sandstone or Noonkanbah Formation. Long-duration glacio-eustatic cycles, up to 8.3 Ma were initially proposed for deposits of similar age in the Karoo and Kalahari Basins in South Africa (Visser, 1997); however, later revisions proposed tectonic control (Isbell et al., 2012).

Tectonic influence on third-order cyclicity may be assessed by examining variations of facies within structural domains (Holz et al., 2006; Grader et al., 2008). Some variation is apparent from the variability of the D-INPEFA signatures in the Gregory Sub-basin and Betty Terrace wells; however, currently analysis is hindered by lack of well data in these regions and erosion of the upper sections of the Noonkanbah Formation on the Jurgurra Terrace and Crossland Platform. The lack of distinct third-order cyclicity below S1 may be due to a masking effect produced by the strong progradational character of fourth-order cyclicity.

## Fourth order

Eight fourth-order cycles are identified: G1, P1 and, N1–N6, each bounded by extensive flooding surfaces. P1, G1 and N1 have a distinct transgressive–regressive character (Fig. 30) in which the regressive phase is dominant. The character of these cycles appears to depend on the influence of the second- and third-order sequences. Temporal variations in character are most obvious during early second-order transgression. For example, the absence of clear coarsening-up trends in the most northwestern N1 deposits is likely a function of distal conditions related to overall transgression. Similarly, the aggradational character of P1 in the southeast is attributed to the proximal position of the deposits relative to their likely source.

## Fifth order

Stacked high-frequency transgressive–regressive cycles are the building blocks of higher order sequences and are observed in well logs across the Canning Basin. Cycles are dominated by coarsening-up trends, and in many cycles a transgressive section is absent (Fig. 30). The transgressive phase is best preserved in the Fitzroy Trough where cycles are thickest. In the Noonkanbah Formation, cycles are defined by variations in the gamma ray log responses and distinct lithological variation in core section (Fig. 30). In Poole Sandstone outcrop sections, distinct banding is observed where prominent blocky benches alternate with crumbly layers that have been eroded to a greater extent. A detailed study by Adkins (2003) indicated thicknesses of approximately <5–10 m for these bands, similar to those in the Noonkanbah Formation. Banding is not distinct in well-log representations of the Poole Sandstone, probably due to its overriding progradational character.

The spatial extent of these cycles suggests a large-scale depositional control. The character is similar to high-frequency cycles that have been extensively documented in both siliciclastic and carbonate Pennsylvanian – early Permian deglaciation deposits worldwide (Haq and

Schutter, 2008), including mid-continent North America (Heckel, 1986); Horquilla Limestone, Southeast Arizona (Connolly and Stanton, 1992); the Karoo and Kalahari Basins, South Africa (Visser, 1997); eastern Australia (Fielding et al., 2008), and Western Australia, in the Kennedy Group, Southern Carnarvon Basin (Lever, 2004). In these systems, high-frequency cyclicity was attributed to Milankovitch processes, which Lever (2004) further divided into precession, obliquity, and eccentricity-forced cycles based on the cycle hierarchy observed. It was suggested these orbital processes were the likely driving mechanism for the fifth-order cyclicity observed in the Poole Sandstone and Noonkanbah Formation. The Nura Nura Member may represent one such cycle. Thicknesses and coarsening-up character are consistent with this interpretation. Similar, laterally extensive, high-frequency cycles comprising mudstone overlain by grainstone have been recorded in early Mississippian deposits in Wyoming, North America (Westphal et al., 2004).

# Implications for $CO_2$ sequestration

Core material from the Poole Sandstone and Noonkanbah Formation in the 200 km radius around James Price Point is scarce (Fig. 32). Lateral and vertical facies trends, and large-scale correlation for sequences, provide a basis for the prediction of depositional settings and lithofacies likely to be present within this radius. The stratigraphic model and porosity data available within this 200 km radius provide an insight into the role of the Poole Sandstone and the suitability of the Noonkanbah Formation as a sealing unit in a potential $CO_2$ sequestration system. Similar to hydrocarbon reservoirs, high porosity and permeability are key features of $CO_2$ reservoirs (Bachu et al., 2007; Xie and Economides, 2009), while caprocks are typically laterally extensive, low-permeability lithologies such as claystones (Chadwick et al., 2004; Solomon et al., 2008; Shulka et al., 2010).

## Role of the Poole Sandstone

The Poole Sandstone has characteristics suitable for both trapping and storing $CO_2$. The likelihood of low-porosity and low-permeability lithologies such as siltstones and mudstones, which are potential sealing layers and baffles in the lower formation, suggest it is suitable for retention of $CO_2$ and has the ability to stall the vertical migration of $CO_2$ out of the potential Grant Group reservoir to the surface. Lithological variation up-sequence suggests that upper sections of this formation may be better suited to storage of $CO_2$, lacking the trapping potential of lower sections.

The basal Nura Nura Member is dominated by limestone facies within the 200 km radius around James Price Point, transitioning to sandstone and siltstone facies towards the southeastern boundary of this radius. The interaction of carbonates and $CO_2$ can serve to both increase and decrease porosity and permeability (Lagneau et al., 2005; Izgec et al., 2008). In some conditions, limestone will dissolve on contact with $CO_2$ presenting potential migration pathways (Snippe et al., 2013). Low-porosity, low-permeability limestones may also provide a barrier to $CO_2$ migration, and have been assessed as potential sealing units for $CO_2$ sequestration sites (Harrisson et al., 2009). The reaction between the two is highly complex, governed by numerous factors including salinity, pH, temperature and pressure (Lagneau et al., 2005; Izgec et al., 2008), and requires detailed studies to evaluate. Available porosity data for the Nura Nura Member suggest very low porosities so it may have potential to act as a preliminary stratigraphic barrier or baffle to $CO_2$ migration. Its effectiveness in this regard may be limited by its potentially lenticular character (Hocking et al., 2008; Mory and Hocking, 2011), limited thickness, and unknown distribution of the vuggy porosity observed in Perindi 1. This baffle effect will be limited towards the southeast by the transition to more siliciclastic facies.

Marine conditions are inferred for the lower part of P1 in a 200 km radius from James Price Point, based on facies associations in neighbouring wells and the presence of limestone and glauconite. Lateral facies transitions indicate that the depositional setting is more distal to the northwest where offshore, offshore transitional, and possible shoreface deposits are present. This is consistent with the abundance of claystone and siltstones; however, sandstone and limestone beds are also commonly recorded and porosity is highly variable, suggesting heterogeneity. Heterogeneity in $CO_2$ reservoirs can both increase and decrease storage capacity (Chadwick et al., 2004; Ambrose et al., 2008; Kuuskraa et al., 2009). Heterogeneity on the lithofacies scale, as well as on the scale of porosity and permeability, affects connectivity and the migration pathway of the $CO_2$ plume (Torp and Gale, 2004; Deng et al., 2012; Lu et al., 2013; Sundal et al., 2013). The abundance of claystone–siltstone lithologies suggests the laterally extensive claystone–siltstone interval at the base of P1 may provide an initial stratigraphic barrier and may have limited capacity as a reservoir (Ambrose et al., 2008). These layers could act as intraformational baffles hindering vertical $CO_2$ migration, while sandstone interbeds could serve as the main $CO_2$ conduits (Deng et al., 2012). On a microscale, heterogeneity can also be developed by burrowing organisms. Selectively enhanced porosity in trace fossils (Fig. 31d) may increase overall porosity and permeability, particularly in intensely bioturbated beds. This may increase heterogeneity and produce flow pathways for $CO_2$ (Gingras et al., 2012a; La Croix et al., 2013).

The uppermost sections of P1 and deposits towards the southeastern limit of the 200 km radius are more suitable $CO_2$ reservoirs due to increasingly sandstone-dominated successions towards the southeast and its widespread coarsening-up character. In addition, very high porosities of 26–32% are recorded in these upper sandstone sections (e.g. East Crab Creek1, Freney 1, West Terrace 1; Appendix 7).

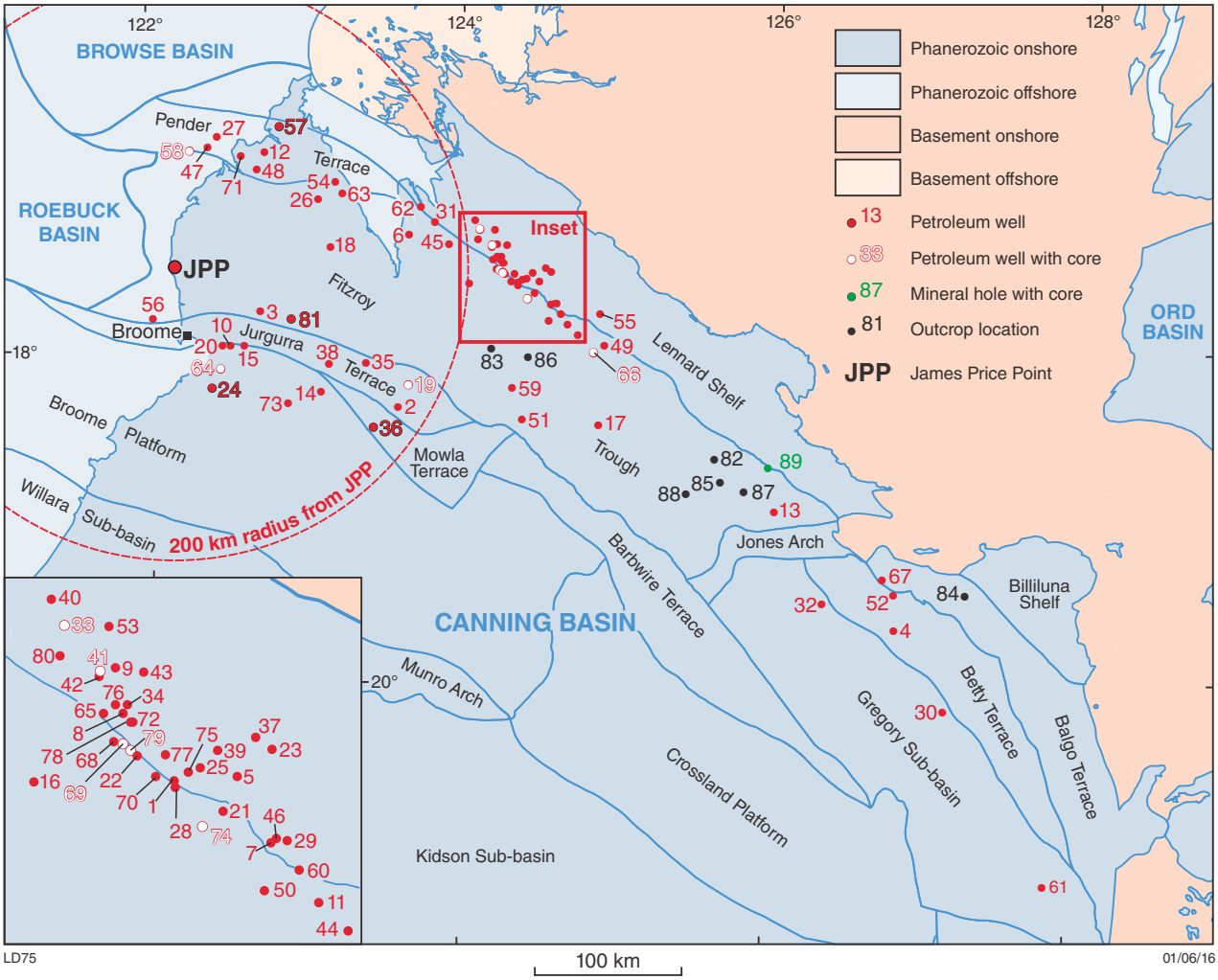


1 Aquanita 1
2 Babrongan 1
3 Barlee 1
4 Bindi 1
5 Blina 1,2,3,4,5,6,7,8
6 Booran 1
7 Boronia 1
8 Boundary 1
9 Canegrass 1
10 Crab Creek 1
11 Crimson Lake 1
12 Curringa 1
13 Cycas 1
14 Dampier Downs 1
15 East Crab Creek 1
16 East Yeeda 1
17 Fitzroy River 1
18 Fraser River 1
19 Frome Rocks 2
20 Freney 1
21 Hakea 1
22 Hangover 1
23 Harold 1
24 Hedonia 1
25 Janpam 1
26 Jum Jum 1
27 Kambara 1
28 Katy 1
29 Kennedia 1
30 Kilang Kilang 1
31 Kora 1
32 Lake Betty 1
33 Langoora 1
34 Lloyd 2
35 Logue 1
36 Lovells Pocket 1
37 Lukins 1
38 Mahe 1
39 Mariana 1
40 May River 1
41 Meda 1
42 Meda 2
43 Mellany 1
44 Metters 1
45 Millard 1
46 Mimosa 1
47 Minjin 1
48 Moogana 1
49 Mt Hardman 1
50 Nemile 1
51 Nerrima 1
52 Olios 1
53 Orange Pool
54 Padilpa 1
55 Palm Spring 1
56 Pearl 1
57 Pender 1
58 Perindi 1
59 Petaluma 1
60 Philydrum 1
61 Point Moody 1
62 Point Torment 1
63 Puratte 1
64 Roebuck Bay 1
65 Runthrough 1
66 Scarpia 1
67 Selenops 1
68 Sundown 1,2,3,4,5
69 Sundown 3H
70 Sunup 1
71 Tappers Inlet 1
72 Terrace 1
73 Thangoo 1
74 The Sisters 1
75 Thompsons 1
76 Wattle 1
77 West Blackstone 1
78 West Terrace 1
79 Whitewell 1
80 Yarrada 1
81 Yulleroo 1
82 Brutens Yard
83 Liveringa
84 Mount Bannerman
85 Mount Hutton
86 Nura Nura Ridge
87 Pool Range
88 St George Ranges (E)
89 PND 1

**Figure 32. The 200 km radius around James Price Point, within which $CO_2$ sequestration would take place. Petroleum wells and mineral drillholes, and other features, are described as for Figure 6.**

## Sealing ability of the Noonkanbah Formation

The spatial extent, thickness and dominance of claystone–siltstone facies in the Noonkanbah Formation make it a potentially excellent sealing unit (Holloway, 1997; Metz et al., 2005; Shulka et al., 2010; Buttinelli et al., 2011). The Noonkanbah Formation contains two thick, laterally extensive, claystone-rich packages; the maximum flooding zone in the lower formation and the base of the S2 third-order cycle in the upper formation. These packages comprise the most distal facies associations in the formation, offshore (FA7; e.g. PND1 and Frome Rocks 2; Fig. 28), which are continuous across the study area (Plate 5) and likely host the lowest porosity and permeability lithofacies in the formation. These claystone-rich lithofacies have potential as barriers to $CO_2$ migration. The most proximal facies associations, mixed tidal flat (FA3) and shoreface (FA5), are recorded at the base of the formation and are associated with fourth-order cycles N1 and N2. In drillcore, these associations have a high sandstone component, and high porosity and permeability values are recorded in Scarpia 1 (Appendix 7). N1 is not distinct in the far northwest of the study region near James Price Point; however, more sandy, higher porosity deposits at the base of the formation, and the potential of these to compromise the sealing ability of the formation's base, should be considered for southeastern areas within the 200 km radius.

Heterogeneity in sealing units can result in zones more prone to leakage and can significantly affect seal integrity (Deng et al., 2012; Kano and Ishido, 2013). Heterogeneity is present on several levels in the Noonkanbah Formation; large- or formation-scale heterogeneity related to second- and third-order cyclicity is observed in facies transitions. High-frequency cyclicity produces heterogeneity on the scale of tens of metres, evidenced in gamma ray log signatures (Fig. 30) and siltstone–sandstone coarsening-up packages in PND 1 core sections. Intensely bioturbated facies (Smb and Hmb) show selective porosity enhancement (Fig. 31d), leading to heterogeneity on a centimetre to millimetre scale. The distribution of clay minerals and cements, particularly chlorite and quartz can also have a large influence on the distribution of porosity and permeability (Armitage et al., 2010, 2011; Lu et al., 2013). Both of these have variable distribution in the formation and may produce microscale heterogeneity.

In summary, lithologically, the Noonkanbah Formation has good potential as a sealing unit, but heterogeneity is high due to cyclic facies arrangements, bioturbation, and clay mineral distribution. These features may compromise seal integrity. Generally, the thickness of the formation makes it desirable as a sealing unit, but the removal of large portions of the formation on the Jurgurra Terrace and Broome Platform and its absence in some anticlines in the Fitzroy Trough are potential threats to suitability for retaining $CO_2$. Furthermore, strata overlying these eroded, partial sections are sandstone rich and unlikely to behave as a secondary sealing layer.

# Conclusions

The depositional setting of the Poole Sandstone ranges from open marine in the northwest to fluvial in the southeast. The basal Nura Nura Member is most distinct in the northwest of the study area and displays a northwest to southeast facies trend from carbonate to predominantly siliciclastic facies. Offshore (FA7), shoreface (FA5), tidal flat (FA2) and fluvial (FA1) associations are recorded by overlying siliciclastic sedimentary rocks, P1, which were probably deposited in large deltaic systems. A widespread flooding event marks the base of the Noonkanbah Formation and subsequent drowning resulted in marine conditions across the study area. Marginal marine tidal flat (FA3) to offshore (FA7) associations are recorded in cored sections. Vertical facies progressions between these tidal flat and offshore associations and well-log trends indicate two widespread deepening events during deposition of the Noonkanbah Formation.

The Poole Sandstone and Noonkanbah Formation record a regional transgression followed by regional regression which together form a second-order supersequence, the base of which may be lower than originally defined. Two third-order and eight fourth-order sequences are identified nested within this second-order trend. These lower-order trends are bounded by flooding surfaces, and show good lateral continuity across the study area. Stacked high-frequency cycles form the base unit for all larger cycles. Second-order cyclicity is attributed to global eustatic rise, tectonic processes are suggested as the main control on the formation of third- and fourth-order sequences, and Milankovitch forcing is suggested as the main forcing on high-frequency cycle development.

Lateral and vertical facies variations in the Poole Sandstone give it a bimodal character with regard to $CO_2$ storage suitability. In the vicinity of James Price Point, the prevalence of siltstone and mudstone lithologies and the presence of a basal carbonate layer in the lower Poole Sandstone suggest limited potential for this formation as a reservoir, but that it could act as a barrier to $CO_2$ migration. The southeastern and uppermost sections of the sandstone present better reservoir potential.

Within the Noonkanbah Formation, cyclicity, clay and cement distribution, and bioturbation have resulted in heterogeneity on a variety of scales. This heterogeneity and variable formation thickness due to basin structure and local structural features within the 200 km radius may have a significant negative impact on the suitability of the formation as a regional $CO_2$ sequestration sealing unit.

# References


Adkins, RM 2003, Regressive systems tract cyclicity in shore-zone deposits: sedimentology and stratigraphy of the Lower Permian Tuckfield Member (Poole Sandstone), onshore Canning Basin, Western Australia: Australian Journal of Earth Sciences, v. 50, p. 365–376.

Al-Hinaai, J and Redfern, J 2013, Permo-Carboniferous glacial channel systems on the margin of the Lennard Shelf, Canning Basin, Western Australia: implication for ice sheet dynamics, *in* The sedimentary basins of Western Australia IV *edited by* M Keep and SJ Moss: Petrolem Exploration Society of Australia, WA Branch, Perth, Western Australia, p. 1–12.

Ambrose, WA, Lakshminarasimhan, S, Holtz, MH, Núñez-López, V and Hovorka, SD 2008, Geologic factors controlling $CO_2$ storage capacity and permanence; case studies based on experience with heterogeneity in oil and gas reservoirs applied to $CO_2$ storage: Environmental Geology, v. 54, p. 1619–1633.

Amigun, JO, Adewoye, O, Olowolafe, T and Okwoli, E 2014, Well logs — 3D seismic sequence stratigraphy evaluation of "Holu" field, Niger delta, Nigeria: International Journal of Science and Technology, v. 4, no. 2, p. 26–36.

Amorosi, A and Milli, S 2001, Late Quaternary depositional architecture of Po and Tevere river deltas (Italy) and worldwide comparison with coeval deltaic successions: Sedimentary Geology, v. 144, p. 357–375.

Apak, SN 1996, Depositional history of the Lower Permian Carolyn Formation and Poole Sandstone in the northern Canning Basin: Implications for hydrocarbon potential: Geological Survey of Western Australia, Record 1996/8, 29p.

Archbold, NW 1982, Correlation of the Early Permian faunas of Gondwana: Implications for the Gondwanan Carboniferous–Permian boundary: Journal of the Geological Society of Australia, v. 29, no. 3–4, p. 267–276.

Archbold, NW 1998, Marine biostratigraphy and correlation of the West Australian Permian basins, *in* The sedimentary basins of Western Australia 2 *edited by* PG Purcell and RR Purcell: Petroleum Exploration Society of Australia; Petroleum Exploration Society of Australia Symposium, Perth, Western Australia, p. 141–151.

Archbold, NW 1999, Permian Gondwanan correlations: the significance of the Western Australian marine Permian: Journal of African Earth Sciences, v. 29, no. 1, p. 63–75.

Archbold, NW 2002, Peri-Gondwanan Permian correlations: The meso-Tethyan margins, *in* The sedimentary basins of Western Australia 3 *edited by* M Keep and SJ Moss: Petroleum Exploration Society of Australia; Petroleum Exploration Society of Australia Symposium, Perth, Western Australia, 20 October 2002, p. 223–236.

Armitage, PJ, Faulkner, DR, Worden, RH, Alpin, AC, Butcher, AR and Iliffe, J 2011, Experimental measurement of, and controls on, permeability and permeability anisotropy of caprocks from the $CO_2$ storage project at the Krechba Field, Algeria: Journal of Geophysical Research, v. 116, p. 1–18.

Armitage, PJ, Worden, RH, Faulkner, DR, Alpin, AC, Butcher, AR and Iliffe, J 2010, Diagenetic and sedimentary controls on porosity in Lower Carboniferous fine-grained lithologies, Krechba Field, Algeria: A petrological study of a caprock to a carbon capture site: Marine and Petroleum Geology, v. 27, p. 1395–1410.

Arrhenius, S 1896, On the influence of carbonic acid in the air upon the temperature of the ground: Philosophical Magazine and Journal of Science, v. 41, p. 237–276.

Bachu, S 2008, $CO_2$ storage in geological media: Role, means, status and barriers to deployment: Progress in Energy and Combustion Science, v. 34, no. 2, p. 254–273.

Bachu, S, Bonijoly, D, Bradshaw, J, Burruss, R, Holloway, S, Christensen, NP and Mathiassen, OM 2007, $CO_2$ storage capacity estimation: methodology and gaps: International Journal of Greenhouse Gas Control, v. 1, p. 430–443.

Backhouse, J 1993, Palynology and correlation of Permian sediments in the Perth, Collie, and Officer Basins, Western Australia, *in* Professional papers: Geological Survey of Western Australia, Report 34, p. 111–128.

Bassi, D and Nebelsick, JH 2010, Components, facies and ramps: redefining Upper Oligocene shallow water carbonates using coralline red algae and larger foraminifera (Venetian area, northeast Italy): Palaeogeography, Palaeoclimatology, Palaeoecology, v. 295, p. 258–280.

Blatchford, T 1927, The geology of portions of the Kimberley Division, with special reference to the Fitzroy Basin and the possibilities of the occurrence of mineral oil: Geological Survey of Western Australia, Bulletin 93, 56p.

Brigaud, B, Durlet, C, Deconinck, J-F, Vincent, B, Pucéat, E, Thierry, J and Trouiller, A 2009, Facies and climate/environmental changes recorded on a carbonate ramp: a sedimentological and geochemical approach on Middle Jurassic carbonates (Paris Basin, France): Sedimentary Geology, v. 222, p. 181–206.

Buatios, LA, Mángano, MG, Alissa, A and Carr, TR 2002, Sequence stratigraphic and sedimentologic significance of biogenic structures from a late Paleozoic marginal- to open-marine reservoir, Morrow Sandstone, subsurface of southwest Kansas, USA: Sedimentary Geology, v. 152, p. 99–132.

Buatois, LA and Mángano, MG 2011, Ichnology: Organism–substrate interactions in space and time: Cambridge University Press, Cambridge, UK, 358p.

Buatois, LA, Santiago, N, Herrera, M, Plink-Björklund, P, Steel, R, Espin, M and Parra, K 2012, Sedimentological and ichnological signatures of changes in wave, river and tidal influence along a Neogene tropical deltaic shoreline: Sedimentology, v. 59, p. 1568–1612.

Burst, JF 1965, Subaqueously formed shrinkage cracks in clay: Journal of Sedimentary Petrology, v. 35, p. 348–353.

Buttinelli, M, Procesi, M, Caucci, F, Quattrocchi, F and Boschi, E 2011, The geo-database of caprock quality and deep saline aquifers distribution for geological storage of $CO_2$ in Italy: Energy, v. 36, p. 2968–2983.

Casey, JN and Wells, AT 1960, Cornish, WA Sheet SF52-1: Geological Survey of Western Australia, 1:250 000 Geological Series.

Casey, JN and Wells, AT 1964, The geology of the north-east Canning Basin, Western Australia: Australian Bureau of Mineral Resources, Report 49, 61p.

Cattaneo, A and Steel, RJ 2003, Transgressive deposits: a review of their variability: Earth Science Reviews, v. 62, p. 187–228.

Catuneanu, O 2002, Sequence stratigraphy of clastic systems: concepts, merits, and pitfalls: Journal of African Earth Sciences, v. 35, p. 1–43.

Catuneanu, O 2006, Principles of sequence Stratigraphy: Elsevier Science, Amsterdam, 386p.

Chadwick, RA, Zweigel, P, Gregersen, U, Kirby, GA, Holloway, S and Johanessen, PN 2004, Geological reservoir characterization of a $CO_2$ storage site: the Utsira Sand, Sleipner, northern North Sea: Energy, v. 29, p. 1371–1381.

Chakrabarti, A 2005, Sedimentary structures of tidal flats: A journey from coast to inner estuarine region of eastern India: Journal of Earth Systems and Science, v. 114, p. 353–368.

Chow, JC, Li, M-C and Fuh, S-C 2005, Geophysical well log study on the paleoenvironment of the hydrocarbon producing zones in the Erchungchi Formation, Hsinyin, SW Taiwan: Terrestrial, Atmospheric, and Oceanic Studies, v. 16, no. 3, p. 531–545.

Cohen, KM, Finney, SC, Gibbard, PL and Fan, J-X 2013, The ICS International Chronostratigraphic Chart, v2015/01 (upated): Episodes, v. 36, p. 199–204

Connolly, WM and Stanton, RJ 1992, Interbasinal cyclostratigraphic correlation of Milankovich band transgressive–regressive cycles: Correlation of Desmoinesian–Missourian strata between southeastern Arizona and the midcontinent of North America: Geology, v. 20, p. 999–1002.

Cook, P 2006, Carbon dioxide capture and geological storage: research, development and application in Australia: International Journal of Environmental Studies, v. 63, p. 731–749.

Crostella, A 1998, A review of oil occurrences within the Lennard Shelf, Canning Basin, Western Australia: Geological Survey of Western Australia, Report 56, 40p.

Crostella, A and Iasky, RP 1997, Structural interpretation and hydrocarbon potential of the Giralia area, Carnarvon Basin: Geological Survey of Western Australia, Report 52, 38p.

Crowe, RWA and Towner, RR 1975, Permian stratigraphic nomenclature, Noonkanbah 1:250 000 sheet, in Annual Report for the year 1975: Geological Survey of Western Australia, Perth, Western Australia, p. 56–58.

Crowe, RWA and Towner, RR 1976a, Environmental interpretation of the Permian Nura Nura Member of the Poole Sandstone, Noonkanbah sheet area, Canning Basin: a gradation between fluviate and shallow-water marine facies, *in* Annual report for the year 1975: Geological Survey of Western Australia, Perth, Western Australia, p. 59–62.

Crowe, RWA and Towner, RR 1976b, Definitions of some new and revised rock units in the Canning Basin: Geological Survey of Western Australia, Record 1976/24, 22p.

Dalrymple, RW 2010, Tidal depositional systems, *in* Facies models 4 *edited by* NP James and RW Dalrymple: Geological Association of Canada, p. 201–232.

Dalrymple, RW and Choi, K 2007, Morphologic and facies trends through the fluvial-mairne transition in tide-dominated depositional systems: A schematic framework for environmental and sequence-stratigraphic interpretation: Earth Science Reviews, v. 81, p. 135–174.

Dalrymple, RW, Knight, RJ, Zaitlin, RJ and Middleton, GV 1990, Dynamics and facies model of a macrotidal sand-bar complex, Cobequid Bay–Salmon River Estuary (Bay of Fundy): Sedimentology, v. 37, p. 577–612.

Dalrymple, RW, Mackay, DA, Ichaso, AA and Choi, KS 2012, Processes, morphodynamics, and facies of tide-dominated estuaries, *in* Principles of tidal sedimentology *edited by* RA Davis and RW Dalrymple: Springer, Dordrecht, Netherlands, p. 79–107.

Dashtgard, SE 2011, Neoichnology of the lower delta plain: Fraser River Delta, British Columbia, Canada: Implications for the ichnology of deltas: Palaeogeography, Palaeoclimatology, Palaeoecology, v. 307, p. 98–108.

Deng, H, Stauffer, PH, Dai, Z, Jiao, Z and Surdam, RC 2012, Simulation of industrial-scale $CO_2$ storage: multi-scale heterogeneity and its impacts on storage capacity, injectivity and leakage: International Journal of Greenhouse Gas Control, v. 10, p. 397–418.

Dentith, MC, Dent, LM, George, AD, Langhi, L, Sanchez, G, Seyedmehdi, Z, Strand, J, Vaslin, A and Zaheer, R 2015, Geosequestration potential of the Carboniferous–Permian Grant Group and Permian Poole Sandstone, northwest Canning Basin, Western Australia: Geological Survey of Western Australia, Report 139, 101p.

Desjardins, PR, Buatois, LA and Mángano, MG 2012, Tidal flats and subtidal sand bodies, *in* Trace fossils as Indicators of Sedimentary Environments *edited by* D Knaust and RG Bromley *compiled by* AJ Van Loon: Elsevier, Developments in Sedimentology 64, p. 529–561.

Di Celma, C, Cantalamessa, G, Landini, W and Ragaini, L 2010, Stratigraphic evolution from shoreface to shelf-indenting channel depositional systems during transgression: Insights from the lower Pliocene Sua Member of the basal Upper Onzole Formation, Borbon Basin, northwest Ecuador: Sedimentary Geology, v. 223, p. 162–179.

Dickins, JM 1996, Problems of a Late Palaeozoic glaciation in Australia and subsequent climate in the Permian: Palaeogeography, Palaeoclimatology, Palaeoecology, v. 125, p. 185–197.

Donselaar, ME and Geel, CR 2007, Facies architecture of heterolithic tidal deposits; the Holocene Holland Tidal Basin: Netherlands Journal of Geosciences, v. 86, p. 389–402.

Dreyer, T 1994, Architecture of an unconformity-based tidal sandstone unit in the Ametlla Formation, Spanish Pyrenees: Sedimentary Geology, v. 94, p. 21–48.

Drummond, BJ, Sexton, MJ, Barton, TJ and Shaw, RD 1991, The nature of faulting along the margins of the Fitzroy Trough, Canning Basin, and implications for the tectonic development of the trough: Exploration Geophysics, v. 22, p. 111–116.

Dumas, S and Arnott, RWC 2006, Origin of hummocky and swaley cross-stratification — The controlling influence of unidirectional current strength and aggradation rate: Geology, v. 34, no. 12, p. 1073–1076.

Dunham, RJ 1962, Classification of carbonate rocks according to depositional texture, in Classification of carbonate rocks *edited by* WE Hamm: American Association of Petroleum Geologists, p. 108–121.

Eyles, N, Eyles, CH, Apak, SN and Carlsen, GM 2001, Permian–Carboniferous tectono-stratigraphic evolution and petroleum potential of the northern Canning Basin, Western Australia: AAPG Bulletin, v. 85, p. 989–1006.

Eyles, N, Mory, AJ and Backhouse, J 2002, Carboniferous–Permian palynostratigraphy of west Australian marine rift basins: resolving tectonic and eustatic controls during Gondwanan glaciations: Palaeogeography, Palaeoclimatology, Palaeoecology, v. 184, p. 305–319.

Eyles, N, Mory, AJ and Eyles, CH 2003, Carboniferous–Permian facies and tectono-stratigraphic successions of the glacially influenced and rifted Carnarvon Basin, Western Australia: Sedimentary Geology, v. 155, p. 63–86.

Fenies, H and Faugeres, JC 1998, Facies and geometry of tidal channel-fill deposits (Arcachon Lagoon, SW France): Marine Geology, v. 150, p. 131–148.

Fielding, CR 2010, Planform and facies variability in asymmetric deltas: facies analysis and depositional architecture of the Turonian Ferron Sandstone in the Western Henry Mountains, south-central Utah, USA: Journal of Sedimentary Research, v. 80, p. 455–479.

Fielding, CR, Frank, TD, Birgenheier, LP, Rygel, MC, Jones, AT and Roberts, J 2008, Stratigraphic imprint of the Late Palaeozoic Ice Age in eastern Australia: a record of alternating glacial and nonglacial climate regime: Journal of the Geological Society, London, v. 165, p. 129–140.

Flügel, E 2004, Microfacies of carbonate rocks: analysis, interpretation and application: Springer-Verlag, New York, US, 984p.

Folk, RL, Andrews, PB and Lewis, DW 1970, Detrital sedimentary rock classification nomenclature for use in New Zealand: New Zealand Journal of Geology and Geophysics, v. 13, p. 937–968.

Forman, DJ and Wales, DW 1981, Geological evolution of the Canning Basin, Western Australia: Bureau of Mineral Resources, Geology and Geophysics, Bulletin 210, 91p.

George, AD, Seyedmehdi, Z and Chow, N 2013, Late Devonian – Early Carboniferous tectonostratigraphic framework for northern Canning Basin carbonate platform evolution, *in* The sedimentary basins of Western Australia IV: proceedings of the Petroleum Exploration Society of Australia Symposium *edited by* M Keep and SJ Moss: Petroleum Exploration Society of Australia Symposium Western Australia Branch, Perth, Western Australia, p. 1–16.

Ghommem, M, Hajj, MR and Puri, IK 2012, Influence of natural and anthropogenic carbon dioxide sequestration on global warming: Ecological Modelling, v. 1–7, p. 235–236.

Gingras, MK, Baniak, GM, Gordon, J, Hovikoski, J, Konhauser, KO, La Croix, A, Lamiski, R, Mendoza, C, Pemberton, G, Polo, C and Zonneveld, J-P 2012a, Porosity and permeability in bioturbated sediments, *in* Trace fossils as indicators of sedimentary environments *edited by* D Knaust and R Bromley: Elsevier, Developments in sedimentology 64, p. 837–868.

Gingras, MK, MacEachern, JA and Dashtgard, SE 2012b, The potential of trace fossils as tidal indicators in bays and estuaries: Sedimentary Geology, v. 279, p. 97–106.

Glenister, BF, Rogers, FS and Skwarko, SK 1993, Ammonoids, in Palaeontology of the Permian of Western Australia *edited by* SK Skwaro: Geological Survey of Western Australia, Bulletin 136, p. 54–63.

Grader, GW, Isaacson, PE, Díaz-Martínez, E and Pope, MC 2008, Pennsylvanian and Permian sequences in Bolivia: direct responses to Gondwana glaciation: The Geological Society of America Special Paper, v. 441, p. 1–17.

Gradstein, FM, Ogg, JG, Schmitz, MD and Ogg, GM 2012, The geological time scale (Volume 1): Elsevier, Boston, US, 1176p.

Gramigna, P, Bassi, D and Russo, F 2011, An Upper Miocene siliciclastic-carbonate ramp: depositional architecture, facies distribution, and diagenetic history (Capo Vaticano area, southern Italy): Facies, v. 58, no. 2, p. 191–215.

Guppy, DJ, Linder, AW, Rattigan, JH and Casey, JN 1951, The stratigraphy of the Mesozoic and Permian sediments of the Desert Basin, Western Australia: Bureau of Mineral Resources Geology and Geophysics, Record 1951/60, 16p.

Guppy, DJ, Lindner, AW, Rattigan, JH and Casey, JN 1958, The geology of the Fitzroy Basin, Western Australia: Bulletin of the Bureau of Mineral Resources, Australia, no. 36.

Haines, PW, Wingate, MTD and Kirkland, CL 2013, Detrital zircon U–Pb ages from the Paleozoic of the Canning and Officer Basins, Western Australia: implications for provenance and interbasin connections, *in* The sedimentary basins of Western Australia IV *edited by* M Keep and SJ Moss: Petroleum Exploration Society of Australia; West Australian Basins Symposium, Perth, Western Australia, 18 August 2013, 19p.

Haq, BU and Schutter, SR 2008, A chronology of Paleozoic sea-level changes: Science, v. 322, p. 64–68.

Harrisson III, WB, Grammer, GM and Barnes, DA 2009, Reservoir characteristics of the Bass Islands dolomite in Otsego Country, Michigan: results for a saline reservoir $CO_2$ sequestration demonstration: Environmental Geosciences, v. 16, no. 3, p. 139–151.

Hart, BS and Plint, AG 1993, Origin of an erosion surface in shoreface sandstones of the Kakwa Member (Upper Cretaceous Cardium Formation, Canada): importance for reconstruction of stratal geometry and depositional history, *in* Sequence stratigraphy and facies associations *edited by* HW Posamentier, CP Summerhayes, BU Haq and GP Allen: Blackwell Scientific Publications, Oxford, UK, p. 449–467.

Heckel, PH 1986, Sea-level curve for Pennsylvanian eustatic marine transgressive–regressive depositional cycles along midcontinent outcrop belt, North America: Geology, v. 14, p. 330–334.

Hocking, RM 1994, Subdivisions of Western Australian Neoproterozoic and Phanerozoic sedimentary basins: Geological Survey of Western Australia, Record 1994/4, 85p.

Hocking, RM, Moors, HT and Van De Graaff, WJE 1987, Geology of the Carnarvon Basin, Western Australia: Geological Survey of Western Australia, Bulletin 133, 289p.

Hocking, RM, Playford, PE, Haines, PW and Mory, AJ 2008, Paleozoic geology of the Canning Basin — a field guide: Geological Survey of Western Australia, Record 2008/18, 40p.

Holloway, S 1997, An overview of the underground disposal of carbon dioxide: Energy Conversion and Management, v. 38, p. 193–198.

Holz, M, Küchle, J, Philipp, RP, Bischoff, AP and Arima, N 2006, Hierarchy of tectonic control on stratigraphic signatures: Base-level changes during the Early Permian in the Paraná Basin, southernmost Brazil: Journal of South American Earth Sciences, v. 22, p. 185–204.

Houghton, JT, Jenkins, GJ and Ephraums, JJ (editors) 1990, Climate change: The IPCC scientific assessment, *in* Report prepared for Intergovernmental Panel on Climate Change by Working Group I: Cambridge University Press, Cambridge, UK, 410p.

Isbell, JL, Henry, LC, Gulbranson, EL, Limarion, CO, Fraiser, ML, Koch, ZJ, Ciccioli, PL and Dineen, AA 2012, Glacial paradoxes during the late Paleozoic ice age: Evaluation the equilibrium line altitude as a control on glaciation: Gondwana Research, v. 22, p. 1–19.

Izart, A, Stephenson, R, Battista Vai, G, Vachard, D, Nindre, YL, Vaslet, D, Fauvel, PJ, Suss, P, Kossovaya, O, Chen, Z, Maslo, A and Stovba, S 2003, Sequence stratigraphy and correlation of late Carboniferous and Permian in the CIS, Eurpoe, Tethyan area, North Africa, Arabia, China, Gondwanaland and the USA: Palaeogeography, Palaeoclimatology, Palaeoecology, v. 196, no. 1–2, p. 59–84.

Izgec, O, Demiral, B, Bertin, H and Akin, S 2008, $CO_2$ injection into saline carbonate aquifer formations I: laboratory investigation: Transport in Porous Media, v. 72, no. 1, p. 1–24.

Jenkins, CR, Cook, PJ, Ennis-King, J, Underschultz, J, Boreham, C, Dance, T, de Caritat, P, Etheridge, DM, Freifeld, BM, Hortle, A, Kirste, D, Paterson, L, Pevzner, R, Schacht, U, Sharma, S, Stalker, L and Urosevic, M 2012, Safe storage and effective monitoring of $CO_2$ in depleted gas fields: Proceedings of the National Academy of Sciences, v. 109, no. 2, p. E35–E41.

Kano, Y and Ishido, T 2013, Effects of heterogeneous seal layer property on the long-term behaviour of $CO_2$ injected into deep saline aquifers: Energy Procedia, v. 37, p. 3800–3807.

Kempin, ET 1956, Roebuck Bay No. 1; West Australian Petroleum Pty Limited: Geological Survey of Western Australia, Statutory petroleum exploration report, W000066 (open file).

Kennard, JM, Jackson, MJ, Romine, KK, Shaw, RD and Southgate, PN 1994, Depositional sequences and associated petroleum systems of the Canning Basin, WA, *in* The sedimentary basins of Western Australia *edited by* PG Purcell and RR Purcell: Petroleum Exploration Society of Australia, Western Australian Branch, Perth, Western Australia, p. 657–676.

Kingsley, D and Streitberg, E 2013, The exploration history of the Laurel Basin-centered gas system Canning Basin, Western Australia, *in* WABS 2013 — Proceedings *edited by* M Keep and SJ Moss: West Australian Basins Symposium 2013, Perth, Western Australia, 18 August 2013, p. 1–13.

Kuuskraa, VA, Koperna, GJ, Riestenberg, D and Esposito, R 2009, Using reservoir architecture to maximize $CO_2$ storage capacity: Energy Procedia, v. 1, p. 3063–3070.

La Croix, A, Gingras, MK, Pemberton, SG, Mendoza, CA and Maceachern, LRT 2013, Biogenically enhanced reservoir properties in the Medicine Hat gas field, Alberta, Canada: Marine and Petroleum Geology, v. 43, p. 464–477.

Lagneau, V, Pipart, A and Catalette, H 2005, Reactive Transport Modelling of $CO_2$ Sequestration in Deep Saline Aquifers: Oil & Gas Science and Technology, v. 60, no. 2, p. 231–247.

Lever, H 2002, Stratigraphy of the Upper Permian Kennedy Group of the onshore Carnarvon Basin (Merlinleigh Sub-basin) Western Australia: Australian Journal of Earth Sciences, v. 49, p. 539–550.

Lever, H 2004, Cyclic sedimentation in the shallow marine Upper Permian Kennedy Group, Carnarvon Basin, Western Australia: Sedimentary Geology, v. 172, p. 187–209.

Lu, J, Kordi, M, Hovorka, SD, Meckel, TA and Christopher, CA 2013, Reservoir characterisation and complications for trapping mechanisms at Cranfield $CO_2$ injection site: International Journal of Greenhouse Gas Controls, v. 18, p. 361–374.

Mángano, MG and Buatois, LA 2004, Ichnology of Carboniferous tide-influenced environments and tidal-flat variability in the North American Midcontinent, *in* The Application of Ichnology to Palaeoenvironmental and Stratigraphic Analysis *edited by* D McIlroy: Geological Society of London, Special Publication 228, p. 157–178.

Martin, DM, Hocking, RM, Riganti, A and Tyler, IM 2015, 1:500 000 tectonic units of Western Australia, 2015: Geological Survey of Western Australia, <www.dmp.wa.gov.au/geoview>.

Martinius, AW, Kaas, I, Naess, A, Helgesen, G, Kjaerefjord, JM and Leith, DA 2001, Sedimentology of the heterolithic and tide-dominated Tilje Formation (Early Jurassic, Halten Terrace, offshore mid-Norway), *in* Sedimentary Environments Offshore Norway — Palaeozoic to Recent *edited by* OJ Martinsen and T Dreyer: Elsevier Science, Amsterdam, The Netherlands, Norwegian Petroleum Society Special Publications 10, p. 103–144.

McWhae, JRH, Playford, PE, Lindner, AW, Glenister, BF and Balme, BE 1956, The stratigraphy of Western Australia: Australian Journal of Earth Sciences, v. 4, no. 2, p. 1–153, doi:10.1080/00167615608728471.

Meselhe, EA, Georgiou, I, Allison, MA and McCorquodale, JA 2012, Numerical modelling of hydrodynamics and sediment transport in lower Mississippi at a proposed delta building diversion: Journal of Hydrogeology, v. 472–473, p. 340–354.

Metz, B, Davidson, O, de Coninck, H, Loos, M and Meyer, L (editors) 2005, IPCC special report on carbon dioxide capture and storage, *in* Report prepared for Intergovernmental Panel on Climate Change by Working Group III: Cambridge University Press, Cambridge, UK, 431p.

Miall, A 2010, Alluvial deposits, *in* Facies models 4 *edited by* NP James and RW Dalrymple: Geological Association of Canada, St. Johns, Newfoundland, Canada, p. 105–137.

Middleton, MF 1990, Canning Basin, *in* Geology and mineral resources of Western Australia: Geological Survey of Western Australia, Memoir 3, p. 425–457.

Midtkandal, I, Nystuen, JP and Nagy, J 2007, Paralic sedimentation on an epicontinental ramp shelf during a full cycle of relative sea-level fluctuation; the Helvetiafjellet Formation in Nordenskiöld Land, Spitsbergen: Norwegian Journal of Geology, v. 87, p. 343–359.

Milliken, KL 2004, Late diagenesis and mass transfer in sandstone–shale sequences, *in* Treatise on Geochemistry, Volume 7: Sediments, diagenesis and sedimentary rocks *edited by* FT MacKenzie: Elsevier-Pergamon, Oxford, p. 159–190.

Mory, AJ 2010, A review of mid-Carboniferous to Triassic stratigraphy, Canning Basin, Western Australia: Geological Survey of Western Australia, Report 107, 130p.

Mory, AJ and Hocking, RM 2011, Permian, Carboniferous and Upper Devonian geology of the northern Canning Basin — a field guide: Geological Survey of Western Australia, Record 2011/16, 36p.

Nio, SD, Böhm, AR, Brouwer, JH, De Jong, MGG and Smith, DG 2006, Climate stratigraphy, principals and applications in subsurface correlation: European Association of Geoscientists and Engineers, Short Course Series 1, 130p.

O'Brien, PE, Lindsay, JF, Knauer, K and Sexton, MJ 1998, Sequence stratigraphy of a sandstone-rich Permian glacial succession, Fitzroy Trough, Canning Basin, Western Australia: Australian Journal of Earth Sciences, v. 45, p. 533–545.

Owen, G and Moretti, M 2011, Identifying triggers for liquefaction-induced soft-sediment deformation in sands: Sedimentary Geology, v. 235, p. 141–147.

Parra-Garcia, M, Sanchez, G, Dentith, MC and George, AD 2014, Regional structural and stratigraphic study of the Canning Basin, Western Australia: Geological Survey of Western Australia, Report 140, 215p.

Playford, PE 2001, The Permo-Carboniferous glaciation of Gondwana: its legacy in Western Australia, *in* GSWA 2001 extended abstracts: New geological data for WA explorers: Geological Survey of Western Australia, Record 2001/5, p. 15–16.

Playford, PE 2002, Palaeokarst, pseudokarst, and sequence stratigraphy in Devonian reef complexes of the Canning Basin, Western Australia, *in* The sedimentary basins of Western Australia 3 *edited by* M Keep and SJ Moss: Proceedings of the Petrolem Exploration Society of Australia Symposium, Perth, Western Australia, p. 763–793.

Plink-Bjorklund, P 2012, Effects of tides on deltaic deposition: Causes and responses: Sedimentary Geology, v. 279, p. 107–133.

Ponten, A and Plink-Bjorklund, P 2007, Depositional environments in an extensive tide-influenced delta plain, Middle Devonian Gauja Formation, Devonian Baltic Basin: Sedimentology, v. 54, p. 969–1006.

Posamentier, HW and Chamberlain, CJ 1993, Sequence-stratigraphic analysis of Viking Formation lowstand beach deposits at Joarcam Field, Alberta, Canada, *in* Sequence stratigraphy and facies associations *edited by* HW Posamentier, CP Summerhayes, BU Haq and GP Allen: Blackwell Publishing Ltd, Oxford, UK, International Association of Sedimentologists, Special Publication 18, p. 469–485.

Powell, CM and Veevers, JJ 1987, Namurian uplift in Australia and South America triggered the main Gondwanan glaciation: Nature, v. 326, p. 177–179.

Rebata Hernani, LA, Gingras, MK, Räsänen, ME and Barberi, M 2006, Tidal-channel deposits on a delta plain from the Upper Miocene Nauta Formation, Marañón Foreland Sub-basin, Peru: Sedimentology, v. 53, p. 971–1013.

Redfern, J and Millward, E 1994, A review of the sedimentology and stratigraphy of the Permian–Carboniferous Grant Group, Canning Basin, *in* The sedimentary basins of Western Australia *edited by* PP Purcell and RR Purcell: Petroleum Exploration Society of Australia, WA Branch, Perth, Western Australia, p. 753–756.

Redfern, J and Williams, BPJ 2002, Canning Basin Grant Group glaciogenic sediments: part of the Gondwanan Permo-Carboniferous hydrocarbon province, *in* The sedimentary basins of Western Australia 3 *edited by* M Keep and SJ Moss: Petroleum Exploration Society of Australia; Western Australian Basins Symposium, Perth, Western Australia, 20 October 2002; Proceedings, p. 851–871.

Romine, KK, Southgate, PN, Kennard, JM and Jackson, MJ 1994, The Ordovician to Silurian phase of the Canning Basin WA, *in* The sedimentary basins of Western Australia *edited by* PG Purcell and RR Purcell: Petroleum Exploration Society of Australia, Western Australian Branch; West Australian Basins Symposium, Perth, Western Australia, 1994, p. 677–696.

Rygel, MC, Fielding, CR, Bann, KL, Frank, TD, Birgenheier, LP and Tye, SC 2008, The Lower Permian Wasp Head Formation, Sydney Basin: high-latitude, shallow marine sedimentation following the late Asselian to early Sakmarian glacial event in eastern Australia: Sedimentology, v. 55, p. 1517–1540.

Santos, AEA and Rossetti, DF 2006, Depositional model of the Ipixuna Formation (Late Cretaceous-?Early Tertiary), Rio Capim Area, Northern Brazil: Latin American Journal of Sedimentology and Basin Analysis, v. 13, p. 101–117.

Shaw, RD, Sexton, M and Zeilinger, I 1994, The tectonic framework of the Canning Basin, WA, including 1:2 million structural elements map of the Canning Basin: Australian Geological Survey Organisation, Record 1994/48, 89p.

Shulka, R, Ranjith, P, Haque, A and Choi, X 2010, A review of studies on $CO_2$ sequestration and caprock integrity: Fuel, v. 89, p. 2651–2664.

Snippe, J, Wei, L and Tucker, O 2013, Containment inpact of calcite pathways in the primary caprock of $CO_2$ storage in a depleted North Sea gas field: Energy Procedia, no. 37, p. 5528–5538.

Solomon, S, Carpenter, M and Flach, TA 2008, Intermediate storage of carbon dioxide in geological formations: a technical perspective: International Journal of Greenhouse Gas Control, p. 502–510.

Southgate, PN, Kennard, JM, Jackson, MJ, O'Brien, PE and Sexton, MJ 1993, Reciprocal lowstand clastic and highstand carbonate sedimentation, subsurface Devonian reef complex, Canning Basin, Western Australia, *in* Carbonate sequence stratigraphy, recent developments and applications *edited by* RG Loucks and JF Sarg: American Association of Petroleum Geologists, Memoir, p. 157–179.

Sundal, A, Nystuen, JP, Dypvik, H, Miri, R and Aagaard, P 2013, Effects of geological heterogeneity on $CO_2$ distribution and migration – a case study from the Johansen Formation, Norway: Energy Procedia, v. 37, p. 5946–5054.

Taylor, A, Goldring, R and Gowland, S 2003, Analysis and application of ichnofabrics: Earth Science Reviews, v. 60, p. 227–259.

Taylor, AM and Goldring, R 1993, Description and analysis of bioturbation and ichnofabric: Journal of the Geological Society, v. 150, no. 1, p. 141–148.

Tedesco, A, Ciccioli, P, Suriano, J and Limarino, CO 2010, Changes in the architecture of fluvial deposits in the Paganzo Basin (Upper Paleozoic of San Juan province): an example of sea level and climatic controls on the development of coastal fluvial environments: Geologica Acta, v. 8, no. 4, p. 463–482.

Torp, TA and Gale, J 2004, Demonstrating storage of $CO_2$ in geological reservoirs: The Sleipner and SACS projects: Energy, v. 29, p. 1361–1369.

Towner, RR, Crowe, RWA and Yeates, AN 1976, Notes on the geology of the southern part of the Canning Basin: Bureau of Mineral Resources, Geology and Geophysics, Record 1976/95, 166p.

Towner, RR and Gibson, DL 1980, Geology of Late Carboniferous and younger rocks of the onshore western Canning Basin, Western Australia: Bureau of Mineral Resources, Geology and Geophysics, Record 1980/3, 67p.

Towner, RR and Gibson, DL 1983, Geology of the onshore Canning Basin, Western Australia: Bureau of Mineral Resources, Geology and Geophysics, Bulletin 215, 51p.

Traves, DM, Casey, JN and Wells, AT 1956, The geology of the south-western Canning Basin, Western Australia: Bureau of Mineral Resources, Geology and Geophysics, Report 29, 76p.

Varma, S, Hodgkinson, J, Langhi, L, Ciftci, B, Harris, B and Underschultz, J 2011, Basin resource management for carbon storage: a literature review: CSIRO, Report No. EP 116370, 71p.

Veevers, JJ 2006, Updated Gondwana (Permian–Cretaceous) Earth history of Australia: Gondwana Research, v. 9, p. 231–260.

Veevers, JJ and Wells, AT 1961, The geology of the Canning Basin: Bureau of Mineral Resources, Geology and Geophysics, Bulletin 60, 323p.

Vesely, FF and Assine, ML 2006, Deglaciation sequences in the Permo-Carboniferous Itarare Group, Paraná Basin, southern Brazil: Journal of South American Earth Sciences, v. 22, p. 156–168.

Visser, JN 1997, Deglaciation sequences in the Permo-Carboniferous Karoo and Kalahari basins of southern Africa; a tool in the analysis of cyclic glaciomarine basin fills: Sedimentology, v. 44, p. 507–521.

Wade, A 1936, The geology of the West Kimberley District of Western Australia: 82p. (unpublished).

Warris, BJ 1993, The hydrocarbon potential of the Palaeozoic basins of Western Australia: APEA Journal, v. 33, p. 123–137.

Westphal, H, Eberli, GP, Smith, LB, Grammer, GM and Kislak, J 2004, Reservoir characterization of the Mississippian Madison Formation, Wind River basin, Wyoming: The American Association of Petroleum Geologists, v. 88, no. 4, p. 405–432.

White, ME and Yeates, AN 1976, Plant fossils from the northeastern part of the Canning Basin, Western Australia: Bureau of Mineral Resources, Geology and Geophysics, Record 1976/18, 60p.

Woodroffe, CD 2000, Deltaic and estuarine environments and their Late Quaternary dynamics on the Sunda and Sahul shelves: Journal of Asian Earth Sciences, v. 18, p. 393–413.

Wopfner, H 1999, The early Permian deglaciation event between East Africa and northwestern Australia: Journal of African Earth Sciences, v. 29, p. 77–90.

Wopfner, H and Jin, XC 2009, Pangea Megasequences of Tethyan Gondwana-margin reflect global changes of climate and tectonism in Late Palaeozoic and Early Triassic times – a review: Palaeoworld, v. 18, p. 169–192.

Worden, RH and Burley, SD 2003, Sandstone diagenesis: the evolution of sand to stone, *in* Sandstone Diagenesis: Recent and Ancient *edited by* SD Burley and RH Worden: International Association of Sedimentologists, Reprint Series vol. 4, p. 1–44.

Worden, RH and Morad, S 2000, Quartz cementation in oil field sandstones: a review of key controversies, *in* Quartz cementation in Sandstones *edited by* R Worden and S Morad: International Association of Sedimentologists, Special Publication 29, p. 1–20.

Xie, X and Economides, MJ 2009, The impact of carbon geological sequestration: Journal of Natural Gas Science and Engineering, v. 1, p. 103–111.

Yeates, AN, Crowe, RWA, Towner, RR, Wyborn, AI and Passmore, VL 1975, Notes on the geology of the Gregory Sub-basin and adjacent areas of the Canning Basin, Western Australia: Bureau of Mineral Resources, Geology and Geophysics, Record 1975/77, 268p.

Yeates, AN, Gibson, DL, Towner, RR and Crowe, RWA 1984, Regional geology of the onshore Canning Basin, WA, *in* The Canning Basin, W.A. *edited by* PG Purcell: Geological Society of Australia and Petroleum Exploration Society of Australia; Canning Basin Symposium, Perth, Western Australia, Proceedings, p. 24–55.

Zhan, Y and Mory, AJ 2013, Structural interpretation of the northern Canning Basin, Western Australia, *in* The sedimentary basins of Western Australia IV *edited by* M Keep and SJ Moss: West Australian Basins Symposium, Perth, WA, 18 August 2013, 18p.

# Appendix 1

## Summary of core and outcrop sections and samples

**Table 1.1. Summary of core sections assessed and samples taken for this study**

| *Ref. No.* | *Well* | *Location* | *Basin subdivision* | *Core* | *Top (m)* | *Base (m)* | *Lithostratigraphic unit* | *Samples* |
|---|---|---|---|---|---|---|---|---|
| 19 | Frome Rocks 2 | 123°39'29.951"E 18°15'15.417"S | Jurgurra Terrace | 1 | 212.15 | 215.2 | Noonkanbah Fm.. | |
| | | | | 2 | 334.35 | 337.4 | Noonkanbah Fm. | |
| | | | | 3 | 456.6 | 459.65 | Noonkanbah Fm. | |
| | | | | 4 | 631.55 | 635 | Poole Sandstone | |
| 33 | Langoora 1 | 124°6'32.187"E 17°17'57.283"S | Lennard Shelf | 1 | 577.6 | 581.55 | Poole Sandstone | TS |
| 41 | Meda 1 | 124°11'20.472"E 17°23'46.847"S | Lennard Shelf | 1 | 429.75 | 435.85 | Noonkanbah Fm. | |
| | | | | 2 | 592.25 | 598.3 | Noonkanbah Fm. | |
| | | | | 3 | 719.65 | 723.9 | Poole Sandstone | TS |
| 58 | Perindi 1 | 122°15'54.25"E 16°49'33.116"S | Fitzroy Sub-basin | 1 | 872 | 881 | Nura Nura Member | |
| 87 | PND1* | 125°57'14.988"E 18°44'15.875"S | Lennard Shelf | 3 | 136.54 | 299.52 | Noonkanbah Fm. | TS |
| | | | | 4 | 299.52 | 330.88 | Noonkanbah Fm. | TS |
| | | | | 5 | 330.88 | 354.31 | Poole Sandstone / Grant Group | TS |
| 64 | Roebuck Bay 1 | 122°27'42.882"E 18°9'32.487"S | Broome Platform | 19 | 484.65 | 487.7 | Noonkanbah Fm. | |
| | | | | 20 | 515.1 | 518.15 | Noonkanbah Fm. | |
| | | | | 21 | 545.6 | 548.65 | Poole Sandstone | |
| | | | | 22 | 576.05 | 579.1 | Poole Sandstone | |
| | | | | 23 | 606.25 | 609.3 | Nura Nura Member | |
| | | | | 24 | 609.3 | 611.45 | Nura Nura Member | TS |
| 66 | Scarpia 1 | 124°50'29.499"E 18°3'10.68"S | Fitzroy Trough | 1 | 483 | 501 | Noonkanbah Fm. | TS, P |
| 69 | Sundown 3H | 124°14'47.853"E 17°33'20.383"S | Lennard Shelf | 1 | 895 | 913 | Grant Group | TS, P |
| 74 | The Sisters 1 | 124°25'25.082"E 17°43'8.761"S | Fitzroy Trough | 1 | 443.8 | 446.85 | Noonkanbah Fm. | |
| | | | | 2 | 555.05 | 561.15 | Noonkanbah Fm. | |
| 79 | Whitewell 1 | | Lennard Shelf | 1 | 862 | 871 | Grant Group | TS, P |

**NOTES**: TS – thin section sample, for details see Appendix 3; P – palynological sample collected, for details see Appendix 4; Ref. No. – reference number of each well as listed in Figure 6; * – mineral drillhole

**Table 1.2. Summary of outcrop localities and formations assessed**

| *Ref. No.* | *Site ID* | *Location* | *Basin subdivision* | *Outcrop style* | *Thickness (m)* | *Lithostratigraphic unit* |
|---|---|---|---|---|---|---|
| 87 | Poole Range | 125°47’12”E 18°53’40”S | Fitzroy Trough | Measured section | 50 | Poole Sandstone |
| 85 | Mount Hutton | 125°38’4.01”E 18°49’58.70”S | Fitzroy Trough | Measured section | 51 | Poole Sandstone |
| 83 | Liveringa | 124°10’53.37”E 18° 2’22.36”S | Fitzroy Trough | Measured section | 72 | Poole Sandstone |
| 83 | Liveringa | 124°10’42.15”E 18° 2’13.32”S | Fitzroy Trough | Low outcrop | – | Poole Sandstone |
| 88 | Eastern St George Ranges | 125°23’34.88”E 18°49’20.11”S | Fitzroy Trough | Measured section | 75 | Poole Sandstone |
| 84 | Mount Bannerman | 127° 8'49.84"E 19°28'23.52"S | Balgo Terrace | Outcrop | – | Poole Sandstone |
| 86 | Nura Nura Ridge | 124°24'37.50"E 18° 5'10.46"S | Fitzroy Trough | Low outcrop | – | Nura Nura Member |

**NOTE:** Ref. No. – number of outcrop site as listed in Figure 6

# Appendix 2

# Facies descriptions, core log and outcrop records

**Table 2.1. Summary of core and outcrop data used to compile drillcore log analyses and list of facies associations identified in drillcore or outcrop sections**

| *Site* | *Well or outcrop name* | *Core No.* | *Top depth (m)* | *Base depth (m)* | *Formation* | *FA* |
|---|---|---|---|---|---|---|
| Well | Frome Rocks 2 (Fig. 2.1) | 1 | 212.15 | 215.2 | Noonkanbah Formation | 6 |
| | | 2 | 334.35 | 337.4 | Noonkanbah Formation | 7 |
| | | 3 | 456.6 | 459.65 | Noonkanbah Formation | 3 |
| | | 4 | 631.55 | 635 | Poole Sandstone | 7 |
| | Meda 1 (Fig. 2.2) | 1 | 429.75 | 435.85 | Noonkanbah Formation | 6 |
| | | 2 | 592.25 | 598.3 | Noonkanbah Formation | 7 |
| | | 3 | 719.65 | 723.9 | Poole Sandstone | 5 |
| | Perindi 1 (Fig. 2.3) | 1 | 872 | 881 | Nura Nura Member | 9 |
| | PND 1 (Fig. 2.4) | 3 | 136.54 | 299.52 | Noonkanbah Formation | 5,6,7 |
| | | 4 | 299.54 | 330.88 | Noonkanbah / Poole Sandstone | 2,3,5 |
| | | 5 | 330.88 | 354.31 | Poole Sandstone / Grant Group | 2 |
| | Scarpia 1 (Fig. 2.5) | 1 | 483 | 501 | Noonkanbah Formation | 3,5 |
| | Sundown 3H (Fig. 2.6) | 1 | 895 | 913 | Grant Group | 1,4,8 |
| | The Sisters 1 (Fig. 2.7) | 1 | 443.8 | 446.85 | Noonkanbah Formation | 7 |
| | | 2 | 555.05 | 561.15 | Noonkanbah Formation | 3 |
| | Whitewell 1 (Fig. 2.8) | 1 | 862 | 871 | Grant Group | 1 |
| Outcrop | Poole Range (Fig. 2.9) | - | 50 | 0 | Poole Sandstone | 2 |
| | Liveringa (Fig. 2.10) | - | 72 | Unknown | Poole Sandstone | 2 |

**NOTES**: Facies associations (FA): 1 – fluvial; 2 – sandy tidal flats; 3 – mixed tidal flats; 4 – tidal channels; 5 – lower shoreface; 6 – offshore transitional; 7 – offshore; 8 – muddy tidal flats; 9 – middle carbonate ramp

**Table 2.2. Lithofacies of the Noonkanbah Formation, Poole Sandstone and Grant Group, and interpretation of depositional processes. Bioturbation index (BI) after Taylor and Goldring (1993)**

| *Facies* | *Lithology* | *Geometry and sedimentary structures* | *Biogenic structures* | *Depositional processes* |
|---|---|---|---|---|
| **Gm**<br>*Pebble conglomerate* | Well-rounded quartz sandstone and elongate black mudstone clasts in a very fine- to coarse-grained quartz sandstone matrix | Medium bedding, up to 40 cm thick, with sharp bed contacts. Clast supported, poorly sorted and massive to locally normally graded | Absent | High to very high energy deposition indicated by clast size<br>Waning flow velocity indicated by normally graded profile |
| **Gmc**<br>*Pebble conglomerate with a calcareous sandstone matrix* | Well-rounded quartz sandstone pebbles in a medium-grained sandstone matrix composed of quartz grains and fragmented bioclasts | Conglomerate beds up to 10 cm thick with sharp contacts<br>Matrix supported, very poorly sorted conglomerate, dominantly massive with bioclasts locally concentrated in thin lags | Bioclast lags composed of shell fragments including brachiopods and bryozoans with some gastropods and possible coral fragments | High to very high energy marine deposition indicated by clast size, fragmentation of shell debris and sharp-based beds |
| **Bm**<br>*Pebble breccia with sandstone matrix* | Angular quartz sandstone pebbles with a medium-grained quartz sandstone matrix | Thinly bedded breccia beds with erosive basal contacts and abrupt upper contacts<br>Massive and matrix supported | Absent | High current energy deposition indicated by clast size and erosional basal contacts |
| **Bmr**<br>*Mud rip-up clast breccia* | Elongate, sub-rounded, black mudstone clasts in a medium-grained quartz sandstone matrix | Thinly bedded, ~ 5 cm, matrix supported with weak alignment of clasts to bedding plane | Absent | High energy flows indicated by the presence of rip-up clasts |
| **Sx**<br>*Tabular cross-bedded sandstone* | Well-sorted, medium- to coarse-grained, quartz sandstone with abundant fragments of carbonaceous material | Cross-beds are 30–40 cm thick<br>Carbonaceous material is concentrated along bedding planes and in 5 cm thick horizons | Absent | Lower flow regime, 2D bedform migration (Miall, 2010). Close proximity to a terrestrial setting |
| **St**<br>*Trough cross-bedded sandstone* | Well-sorted, fine- to very coarse-grained quartz sandstone with scattered, angular, quartz granules | Individual foresets 3–15 cm thick. Single set or amalgamated sections are thinly to thickly bedded, 10–50 cm thick. Lower contacts are sharp and rip-up impressions are locally present on the soles of sandstone beds. Upper contacts are sharp to gradational | Absent | Lower flow regime, 3D bedform migration (Miall, 2010) |
| **Smb**<br>*Bioturbated sandstone* | Well-sorted, fine- to medium-grained quartz sandstone with subordinate siltstone | Thin- to medium-bedded sandstones ~10–40 cm, in which primary sedimentary structure obliterated by high-intensity, high-diversity bioturbation | BI 4–6<br>Traces are dominantly vertical, silt lined and sad filled. Overprinting generations of trace fossils is common. *Diplocraterion*, *Rosselia*, *Thalassinoides* and possible *Skolithos*, *Ophiomorpha* and *Palaeophycus* traces are present | Shallow marine conditions are indicated by the presence of *Rosselia*. Moderate energy, oxygenated conditions are suggested by the abundance of filter feeding traces, and siltstone burrow linings (Buatois and Mángano, 2011) |
| **Sfx**<br>*Swaley to hummocky cross-bedded sandstone* | Fine-grained quartz sandstone | Thinly bedded swaley–hummocky cross-stratification which occurs as single beds and amalgamated sections; sets up to 20 cm high | Absent | Deposition at or above storm wave base (Hart and Plint, 1993) |

**Table 2.2. continued**

| *Facies* | *Lithology* | *Geometry and sedimentary structures* | *Biogenic structures* | *Depositional processes* |
|---|---|---|---|---|
| **Sr**<br>*Ripple cross-laminated sandstone* | Very fine- to fine-grained quartz sandstone | Ripple cross-lamination, single ripple trains or thick amalgamated sections. Sigmoidal and climbing ripples, ladder-back and interference ripples are locally present | BI 0–2<br>Small, sparsely distributed *Planolites* and *Teichichnus*<br>Abundant large wood fragments | Lower flow regime, shallow water settings (Miall, 2010)<br>High suspended sediment load where climbing ripples are present (Ponten and Plink-Bjorklund, 2007)<br>Low-diversity trace fossil assemblages suggest stressed bottom water conditions (Buatois and Mángano, 2011) |
| **Sp**<br>*Planar-laminated sandstone* | Fine-grained, well-sorted, quartz sandstone | Thinly planar-bedded, 1–3 cm, parallel laminated sandstone. Bedsets may be >1 m thick | Absent | Upper-flow regime conditions (Miall, 2010) |
| **Sfc**<br>*Convolute-laminated sandstone* | Fine- to very fine-grained quartz sandstone and minor siltstone | Beds are 5–15 cm thick, with sharp-scoured bases<br>Soft sediment deformation structures include convolute laminations, load clasts, ball and pillow structures and possible flame structures | Absent | Rapid deposition of overlying sediments resulting in loading and dewatering indicated by soft sediment deformation |
| **Sff**<br>*Flaser-bedded sandstone and mudstone* | Dominantly fine- to medium-grained quartz sandstone with mudstone partings | Thick flaser-bedded sandstone with singular to bifurcated drapes, commonly mudstone but locally comprising carbonaceous fragments. Siderite bands and rip-up clasts are locally present | BI 1<br>*Planolites* traces are small and sparse | Alternating low current energy and slackwater conditions indicated by flaser bedding<br>Small burrow dimensions and low-diversity trace fossil assemblages indicate stressed settings, probably due to fluctuations in salinity and oxygen levels (Buatois and Mángano, 2011) |
| **Sfw**<br>*Wavy-bedded sandstone and siltstone* | Dominantly fine-grained quartz sandstone with thin to thick siltstone laminations | Thick wavy-bedded sandstone with bi-directional ripple cross-lamination and reactivation surfaces | Absent | Alternating low energy and slackwater conditions indicated by wavy-bedded structure<br>Tidal settings suggested from bi-directional ripples and alternating energy conditions |
| **Sxs**<br>*Interbeddded sandstone and siltstone* | Very fine- to fine-grained sandstone with interbedded siltstone | Thin beds, 10–20 cm, of ripple to swaley cross-laminated sandstone interbedded with thin to moderate thickness, 3–15 cm siltstone beds and thin, 1–2 cm thick, interlaminated sandstone–siltstone beds. Typically arranged into successions of fining-up profiles | BI 1–2<br>*Planolites* and *Phycosiphon* are present in siltstone and interlaminated beds | Repetitive high-energy events followed by waning flow conditions are indicated by the succession of fining-up profiles |

**Table 2.2. continued**

| *Facies* | *Lithology* | *Geometry and sedimentary structures* | *Biogenic structures* | *Depositional processes* |
|---|---|---|---|---|
| **Hxs**<br>*Bioturbated heterolithics* | Interbedded fine- to very fine-grained sandstone and siltstone | Thin erosive beds or lenses of sandstone. Sandstone beds are massive, planar or ripple cross laminated and fine upwards to siltstone<br>Intense bioturbation has removed primary sedimentary structures in places. Sandstone beds with very low levels of bioturbation are present at irregular intervals throughout the facies | BI 0–6<br>Assemblage is diverse and strongly overprinted. *Chondrites*, *Phycosiphon*, *Zoophycos* and *Teichichnus* are common, with some *Asterosoma* and *Nereites*<br>Brachiopod shells concentrated along bedding planes are sparsely distributed throughout. Rare ostracods | Very low energy, suspension settling with episodic higher energy currents. Marine conditions are suggested by ichnofauna present, with episodes of biological stress indicated by intervals of trace fossil paucity |
| **Hm**<br>*Planar to ripple cross-laminated heterolithics* | Siltstone with interbedded fine- to very fine-grained sandstone | Thin-bedded siltstone interbedded with planar-laminated to ripple cross-laminated sandstone. Sandstone beds are sharp based and normally grade to siltstone | BI 0–2<br>Dominated by horizontal traces including *Planolites*, *Phycosiphon*, *Thalassinoides* and *Teichichnus*<br>Indistinct mottling is locally present | Suspension settling with intermittent low-energy currents<br>Marine conditions or influence, periodically stressed |
| **Ml**<br>*Lenticular-bedded mudstone* | Mudstone with very fine- to fine-grained sandstone lenses that constitute 5–30% of composition | Very thin beds and lenses of planar or ripple cross-laminated sandstone in mudstone | BI 0–3<br>Small, sparse, *Planolites* and rare *Teichichnus*<br>Indistinct mottling is locally present | Suspension settling with intermittent low-energy currents<br>Stressed marine conditions are suggested by low trace fossil diversity |
| **M**<br>*Planar-laminated mudstone* | Mudstone with fine-grained sandstone laminations | Sparse, fine, planar laminations and lenses of sandstone | BI 0–1<br>Rare *Planolites* | Low-energy suspension settling occasionally influenced by weak currents (Ponten and Plink-Bjorklund, 2007). Biologically stressful conditions resulting from nutrient or oxygen depletion is indicated by the impoverished trace fossil assemblage |
| **Lgs**<br>*Skeletal grainstone* | Well-cemented bioclasts, 0.5 – 5 mm, equant carbonate cement, and minor fine-grained quartz sandstone | Thinly to thickly bedded<br>Bioclasts are fragmented and rounded. Recrystallization of clasts to equant carbonate is common. Grains are weakly aligned parallel to bedding surfaces | Bioclast assemblage is dominated by fragments of brachiopods, bryozoans and crinoids. Gastropods and ostracods are present in minor amounts | Crinoid and bryozoan bioclasts indicate marine deposition (Brigaud et al., 2009)<br>High-energy setting and reworking is indicated by the abrasion of bioclast fragments and the absence of a fine-grained matrix |
| **Lps**<br>*Skeletal packstone* | Bioclasts, 0.5 – 10 mm, are well cemented with equant carbonate cement. Minor detrital clay is present | Thinly to thickly bedded with highly fragmented bioclasts that are weakly aligned to bedding surfaces | The bioclast assemblage is dominated by crinoids with some brachiopods and bryozoans | Crinoid and bryozoan bioclasts indicate marine deposition (Brigaud et al., 2009) |

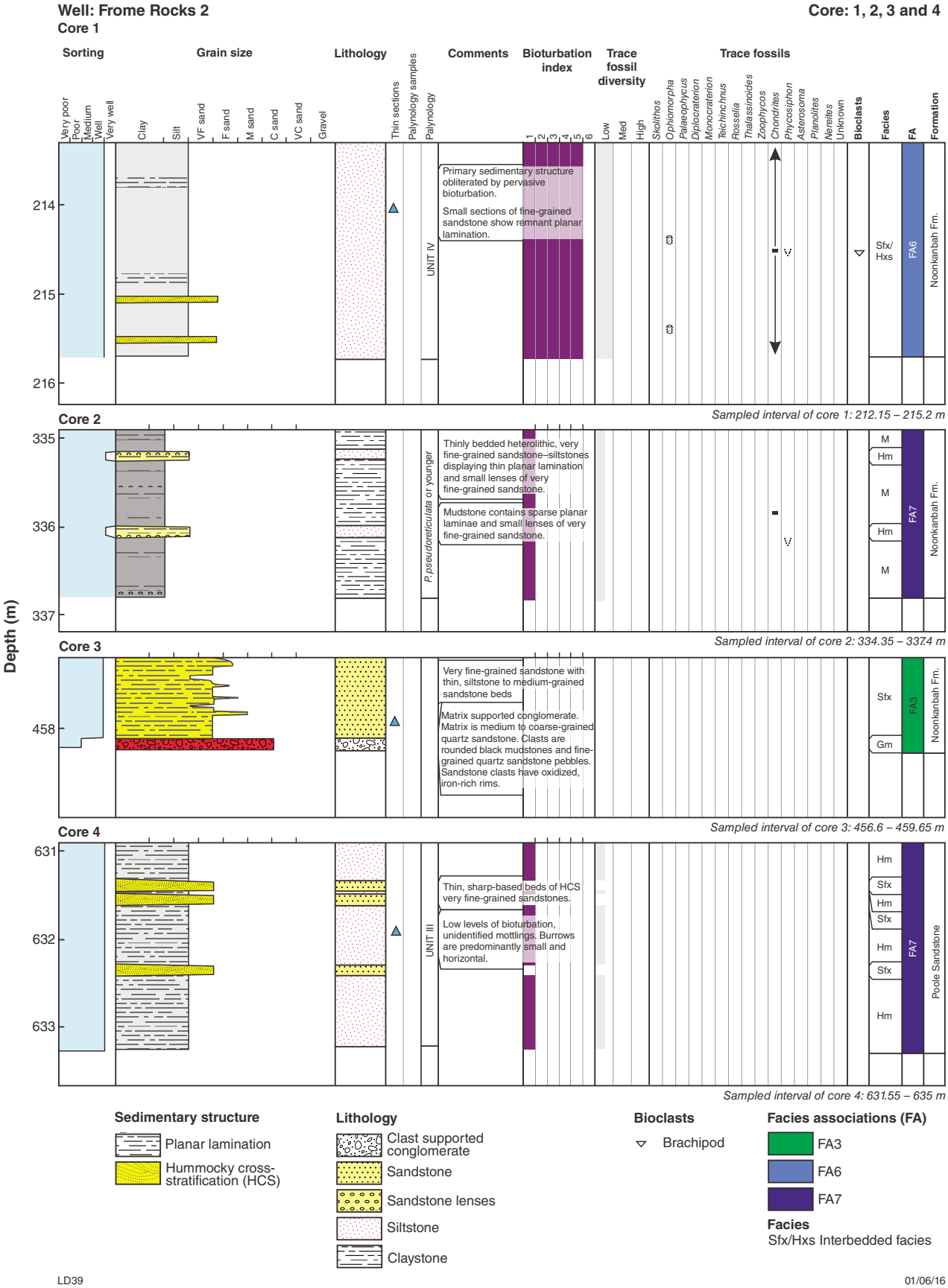
Well: Frome Rocks 2
Core: 1, 2, 3 and 4
Core 1
Sorting
Grain size
Lithology
Comments
Bioturbation index
Trace fossil diversity
Trace fossils
Very poor
Poor
Medium
Well
Very well
Clay
Silt
VF sand
F sand
M sand
C sand
VC sand
Gravel
Thin sections
Palynology samples
Palynology
Low
Med
High
Skolithos
Ophiomorpha
Palaeophycus
Diplocraterion
Monocraterion
Teichichnus
Rossella
Thalassinoides
Zoophycos
Chondrites
Phycosiphon
Asterosoma
Planolites
Nereites
Unknown
Bioclasts
Facies
FA
Formation
Depth (m)
214
215
216
UNIT IV
Primary sedimentary structure obliterated by pervasive bioturbation.
Small sections of fine-grained sandstone show remnant planar lamination.
Sfx/Hxs
FA6
Noonkanbah Fm.
Sampled interval of core 1: 212.15 – 215.2 m
Core 2
335
336
337
P. pseudoreticulata or younger
Thinly bedded heterolithic, very fine-grained sandstone–siltstones displaying thin planar lamination and small lenses of very fine-grained sandstone.
Mudstone contains sparse planar laminae and small lenses of very fine-grained sandstone.
M
Hm
M
Hm
M
FA7
Noonkanbah Fm.
Sampled interval of core 2: 334.35 – 337.4 m
Core 3
458
Very fine-grained sandstone with thin, siltstone to medium-grained sandstone beds
Matrix supported conglomerate. Matrix is medium to coarse-grained quartz sandstone. Clasts are rounded black mudstones and fine-grained quartz sandstone pebbles. Sandstone clasts have oxidized, iron-rich rims.
Sfx
Gm
FA3
Noonkanbah Fm.
Sampled interval of core 3: 456.6 – 459.65 m
Core 4
631
632
633
UNIT III
Thin, sharp-based beds of HCS very fine-grained sandstones.
Low levels of bioturbation, unidentified mottlings. Burrows are predominantly small and horizontal.
Hm
Sfx
Hm
Sfx
Hm
Sfx
Hm
FA7
Poole Sandstone
Sampled interval of core 4: 631.55 – 635 m
Sedimentary structure
Planar lamination
Hummocky cross-stratification (HCS)
Lithology
Clast supported conglomerate
Sandstone
Sandstone lenses
Siltstone
Claystone
Bioclasts
Brachipod
Facies associations (FA)
FA3
FA6
FA7
Facies
Sfx/Hxs Interbedded facies
LD39
01/06/16

**Figure 2.1.**

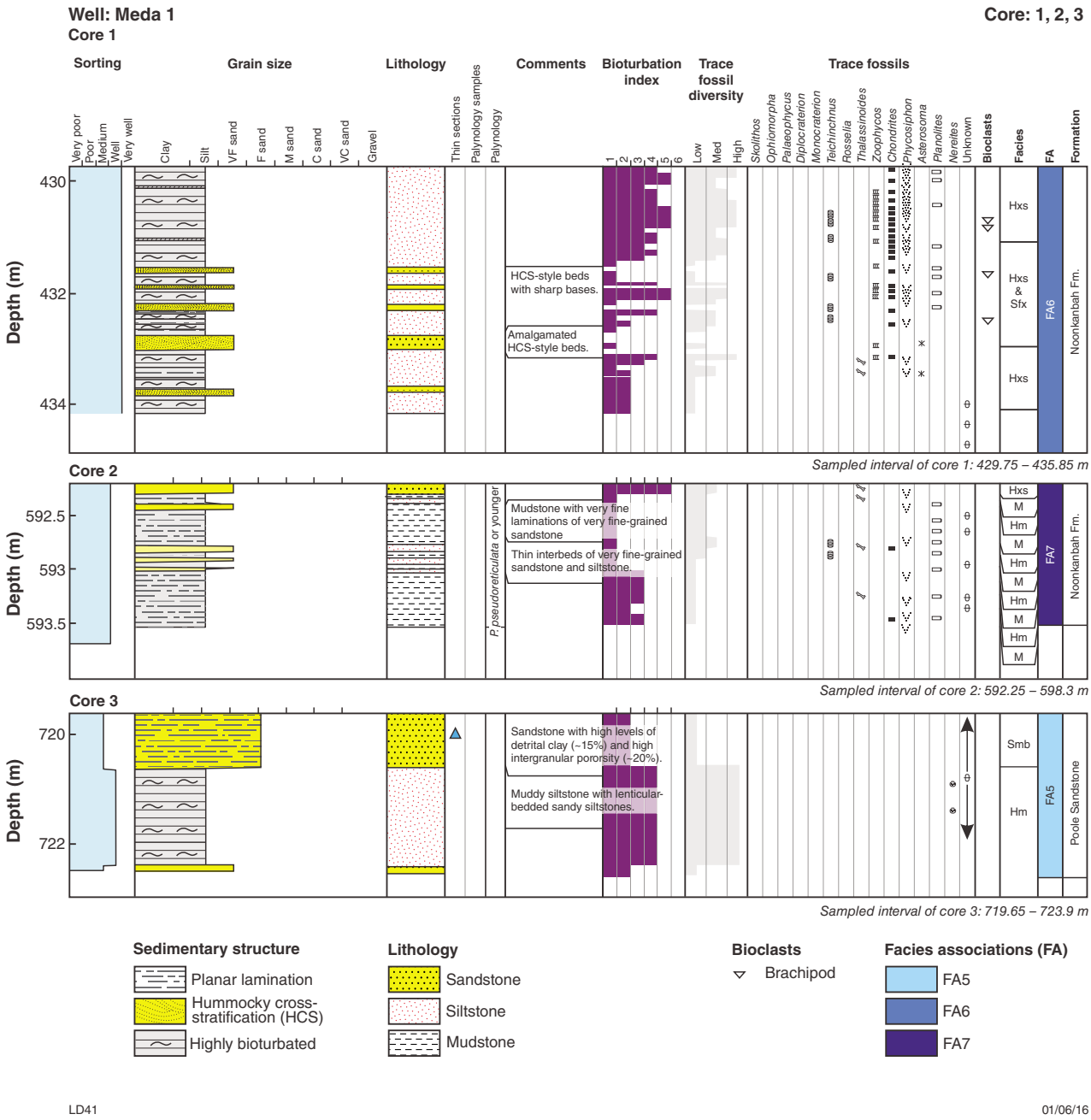
Well: Meda 1
Core: 1, 2, 3
Core 1
Sorting
Grain size
Lithology
Comments
Bioturbation index
Trace fossil diversity
Trace fossils
Very poor
Poor
Medium
Well
Very well
Clay
Silt
VF sand
F sand
M sand
C sand
VC sand
Gravel
Thin sections
Palynology samples
Palynology
Low
Med
High
Skolithos
Ophiomorpha
Palaeophycus
Diplocraterion
Monocraterion
Teichichnus
Rosselia
Thalassinoides
Zoophycos
Chondrites
Phycosiphon
Asterosoma
Planolites
Nereites
Unknown
Bioclasts
Facies
FA
Formation
Depth (m)
430
432
434
HCS-style beds with sharp bases.
Amalgamated HCS-style beds.
Hxs
Hxs & Sfx
Hxs
FA6
Noonkanbah Fm.
Sampled interval of core 1: 429.75 – 435.85 m
Core 2
592.5
593
593.5
P. pseudoreticulata or younger
Mudstone with very fine laminations of very fine-grained sandstone
Thin interbeds of very fine-grained sandstone and siltstone.
Hxs
M
Hm
FA7
Noonkanbah Fm.
Sampled interval of core 2: 592.25 – 598.3 m
Core 3
720
722
Sandstone with high levels of detrital clay (~15%) and high intergranular porosity (~20%).
Muddy siltstone with lenticular-bedded sandy siltstones.
Smb
Hm
FA5
Poole Sandstone
Sampled interval of core 3: 719.65 – 723.9 m
Sedimentary structure
Planar lamination
Hummocky cross-stratification (HCS)
Highly bioturbated
Lithology
Sandstone
Siltstone
Mudstone
Bioclasts
Brachipod
Facies associations (FA)
FA5
FA6
FA7
LD41
01/06/16

**Figure 2.2.**

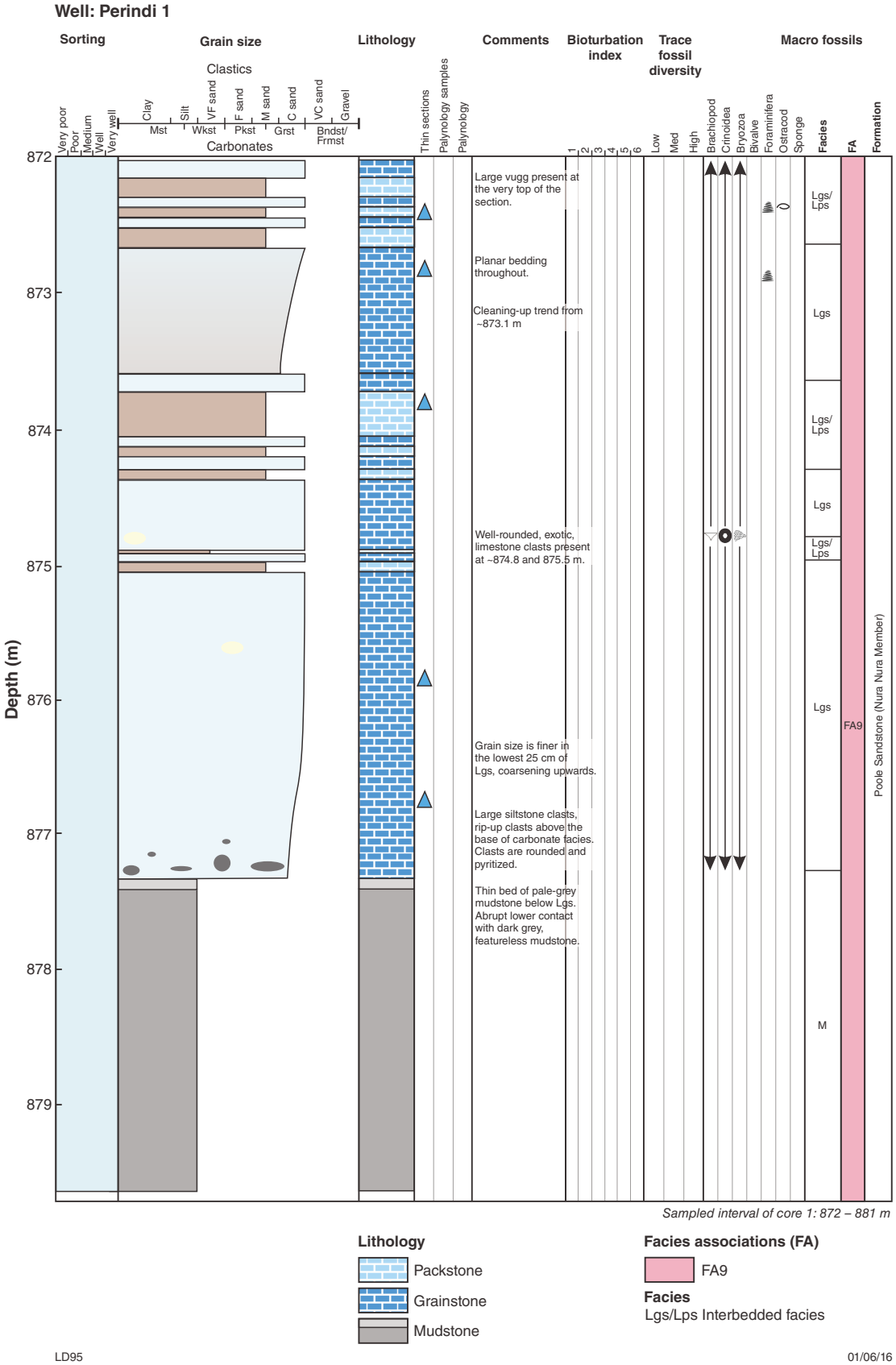
Well: Perindi 1
Sorting
Very poor
Poor
Medium
Well
Very well
Grain size
Clastics
Clay
Silt
VF sand
F sand
M sand
C sand
VC sand
Gravel
Mst
Wkst
Pkst
Grst
Bndst/ Frmst
Carbonates
Lithology
Thin sections
Palynology samples
Palynology
Comments
Bioturbation index
1
2
3
4
5
6
Trace fossil diversity
Low
Med
High
Macro fossils
Brachiopod
Crinoidea
Bryozoa
Bivalve
Foraminifera
Ostracod
Sponge
Facies
FA
Formation
Depth (m)
872
873
874
875
876
877
878
879
Large vugg present at the very top of the section.
Planar bedding throughout.
Cleaning-up trend from ~873.1 m
Well-rounded, exotic, limestone clasts present at ~874.8 and 875.5 m.
Grain size is finer in the lowest 25 cm of Lgs, coarsening upwards.
Large siltstone clasts, rip-up clasts above the base of carbonate facies. Clasts are rounded and pyritized.
Thin bed of pale-grey mudstone below Lgs. Abrupt lower contact with dark grey, featureless mudstone.
Lgs/ Lps
Lgs
Lgs/ Lps
Lgs
Lgs/ Lps
Lgs
M
FA9
Poole Sandstone (Nura Nura Member)
Sampled interval of core 1: 872 – 881 m
Lithology
Packstone
Grainstone
Mudstone
Facies associations (FA)
FA9
Facies
Lgs/Lps Interbedded facies
LD95
01/06/16

**Figure 2.3.**

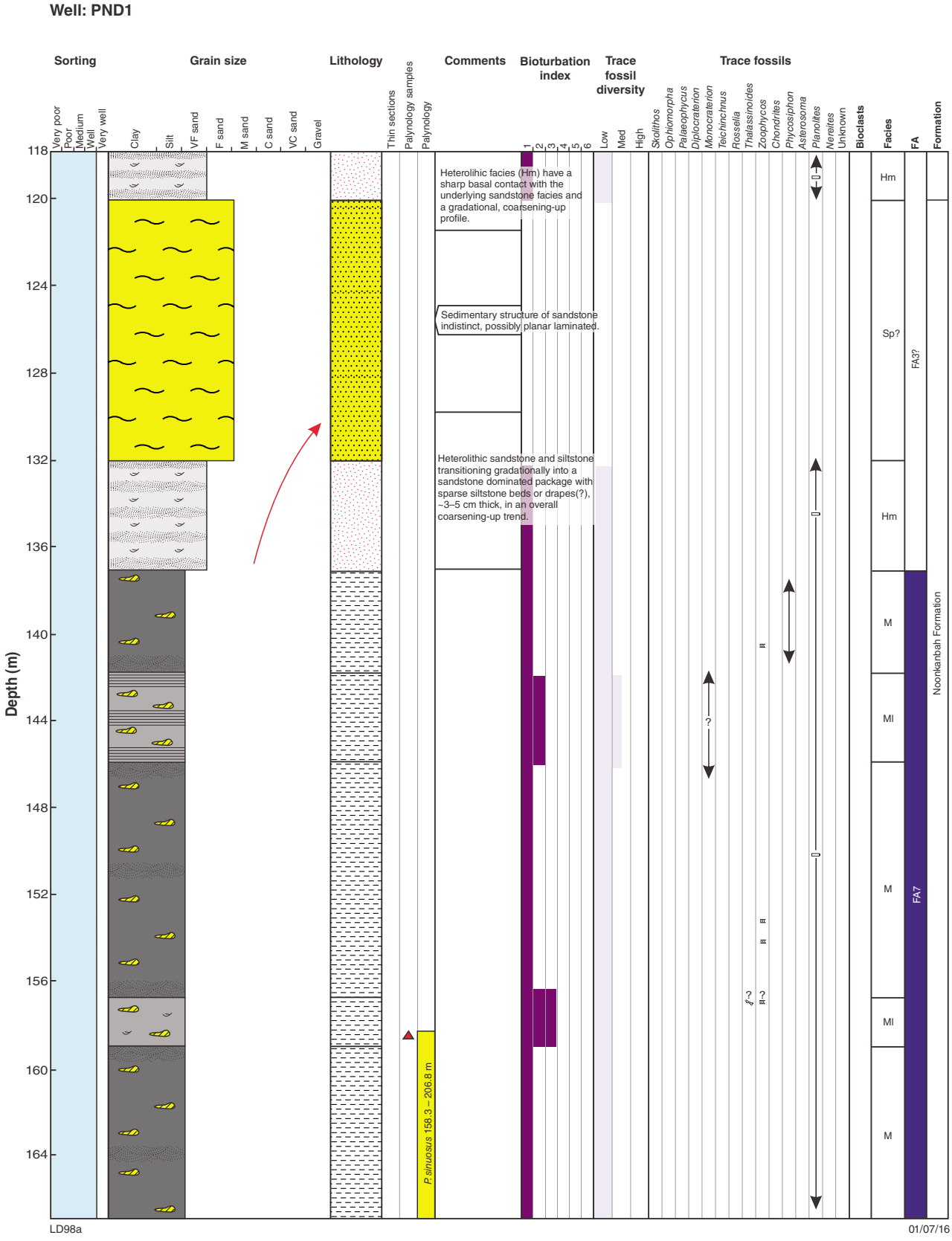


**Figure 2.4. Refer to p. 62 for legend.**

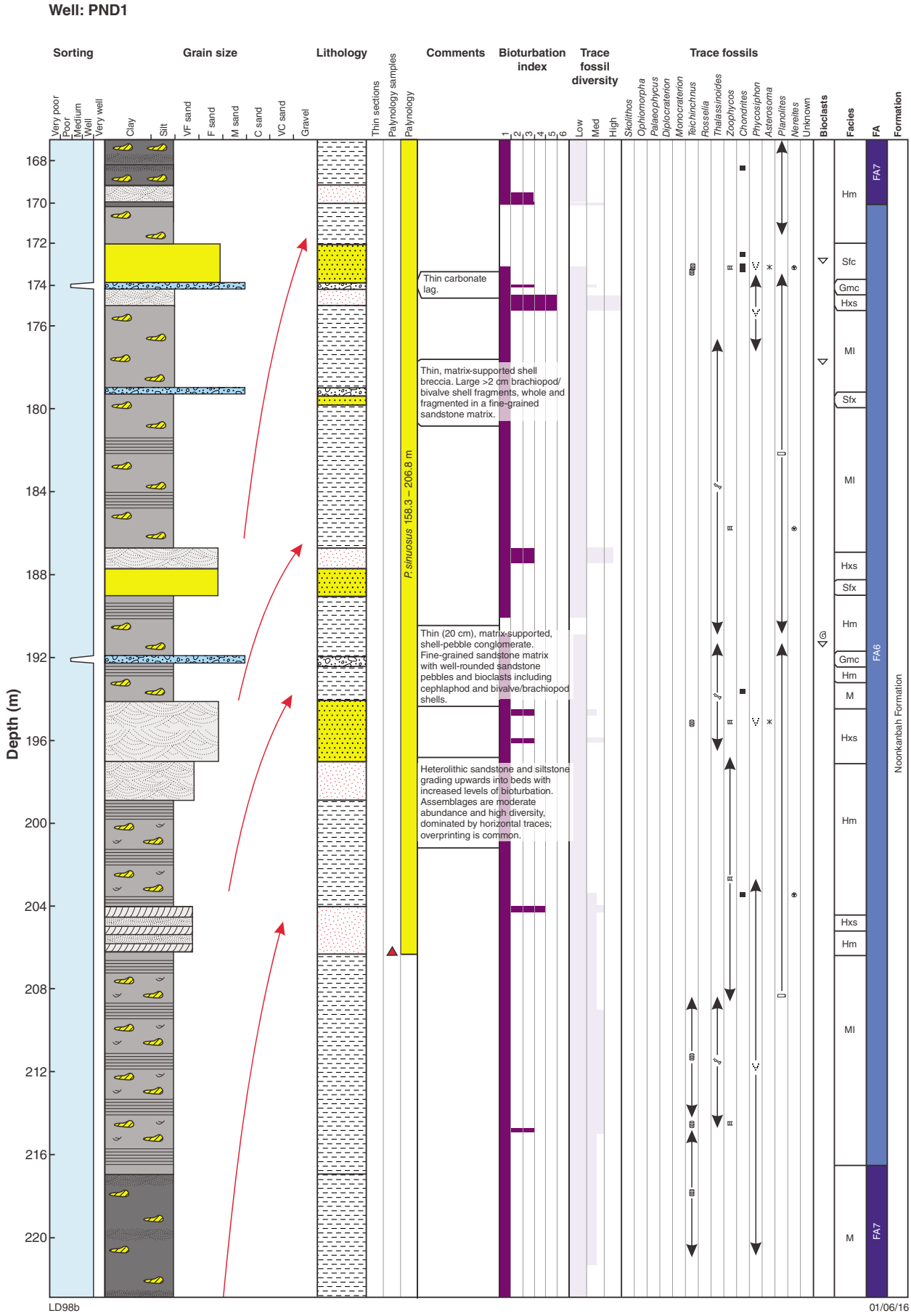


**Figure 2.4. continued**

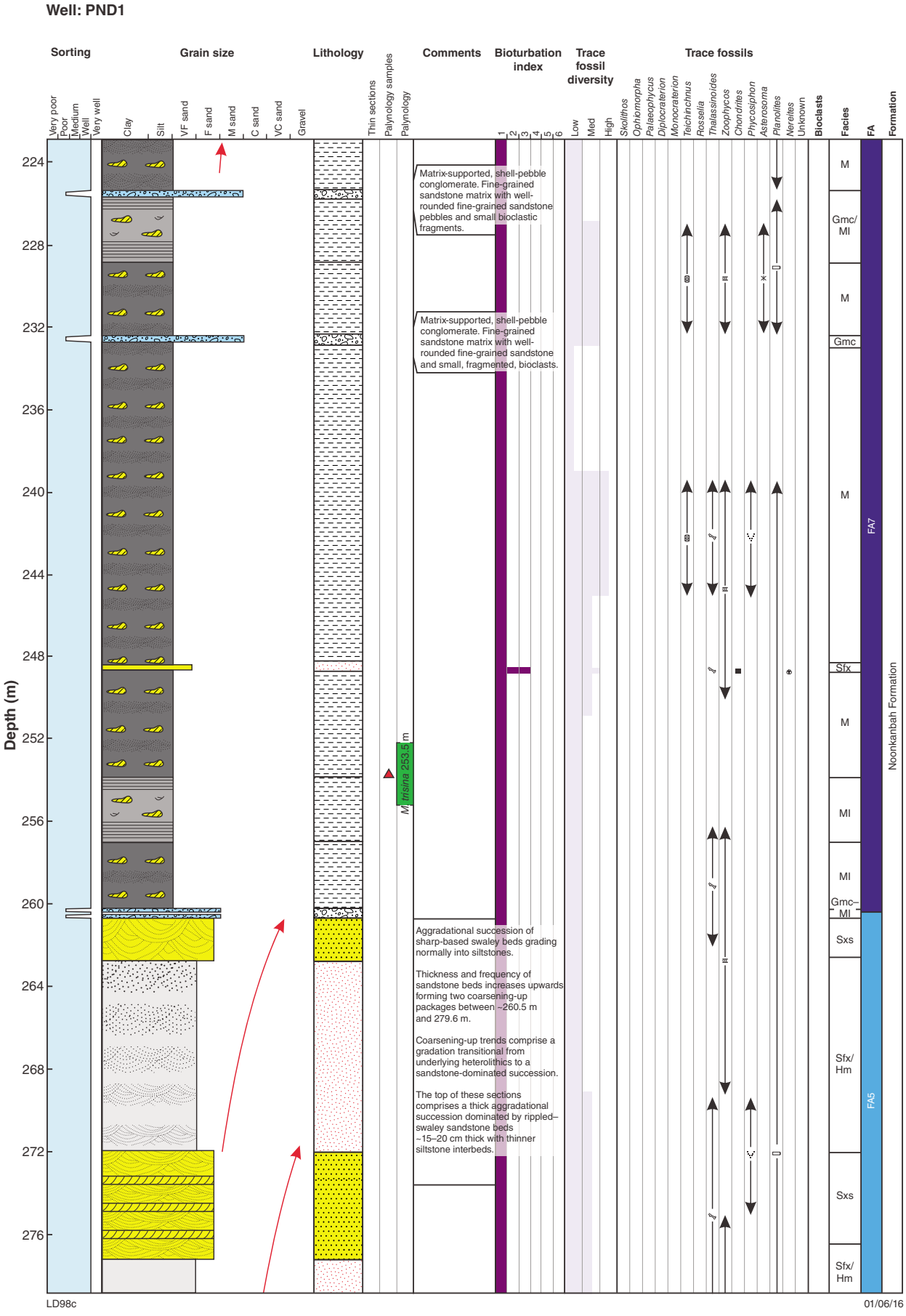


**Figure 2.4. continued**

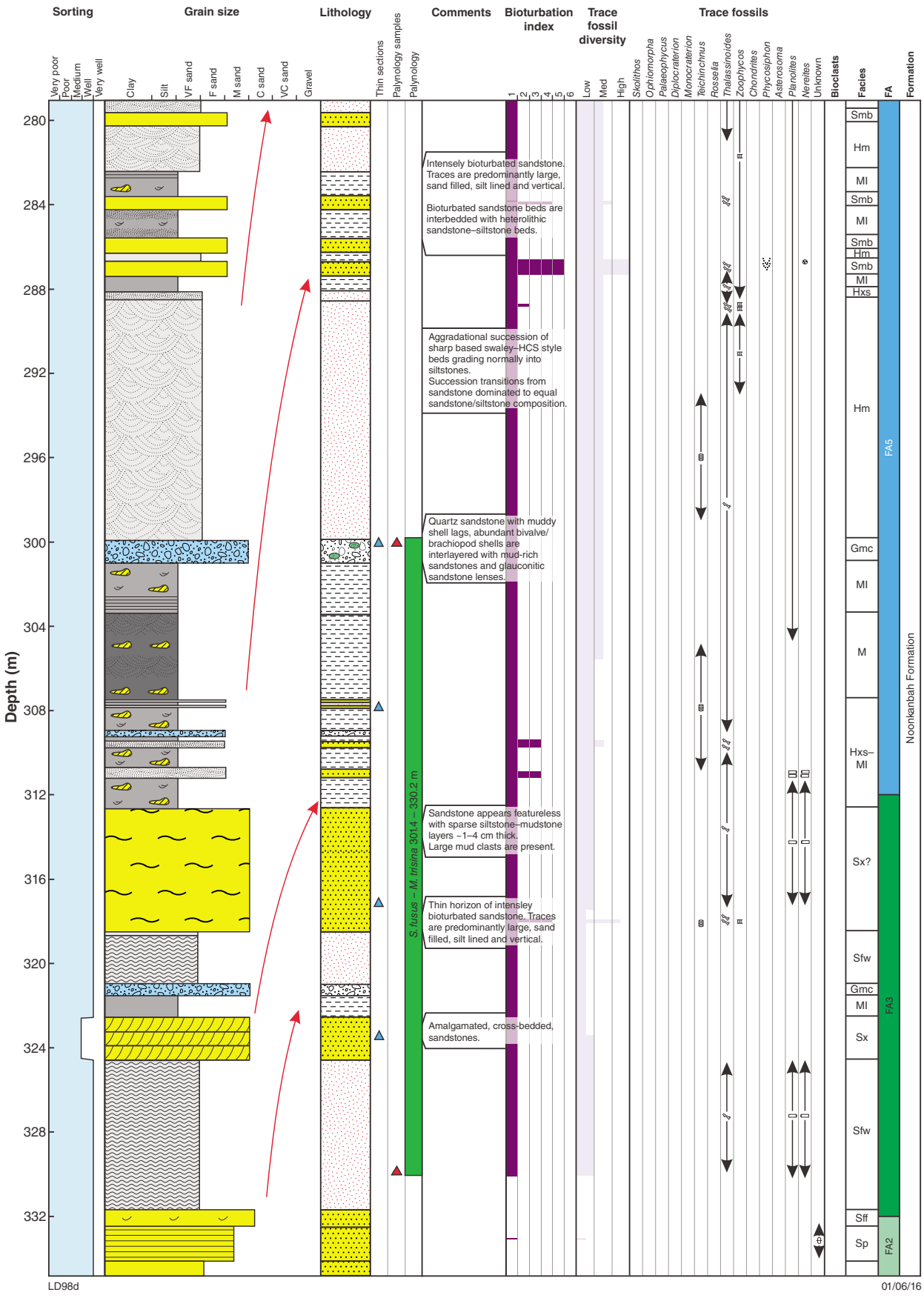


**Figure 2.4. continued**

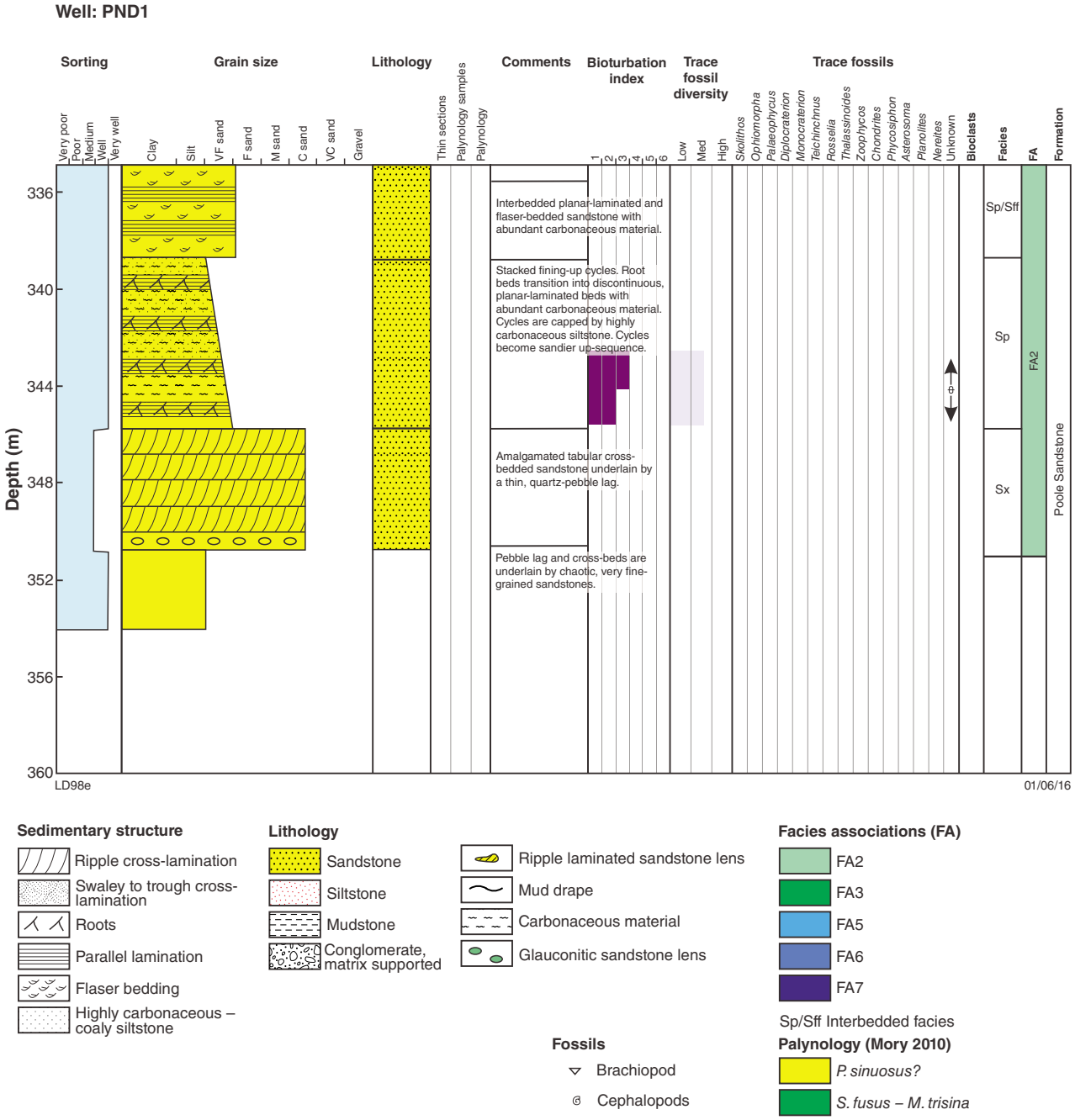


**Figure 2.4. contined**

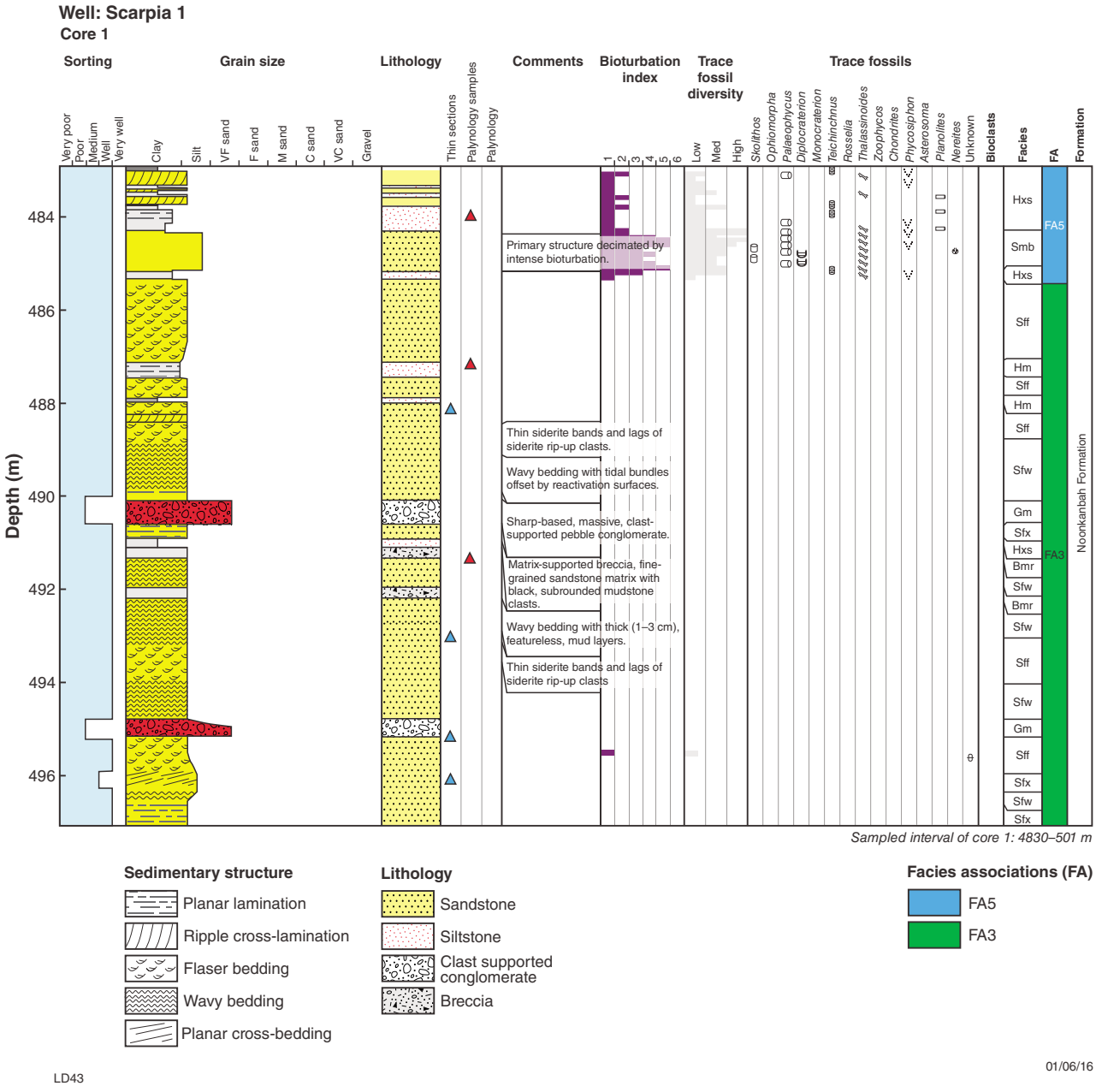
Well: Scarpia 1
Core 1
Sorting
Very poor
Poor
Medium
Well
Very well
Grain size
Clay
Silt
VF sand
F sand
M sand
C sand
VC sand
Gravel
Lithology
Thin sections
Palynology samples
Palynology
Comments
Bioturbation index
1
2
3
4
5
6
Trace fossil diversity
Low
Med
High
Trace fossils
Skolithos
Ophiomorpha
Palaeophycus
Diplocraterion
Monocraterion
Teichichnus
Rossella
Thalassinoides
Zoophycos
Chondrites
Phycosiphon
Asterosoma
Planolites
Nereites
Unknown
Bioclasts
Facies
FA
Formation
Depth (m)
484
486
488
490
492
494
496
Primary structure decimated by intense bioturbation.
Thin siderite bands and lags of siderite rip-up clasts.
Wavy bedding with tidal bundles offset by reactivation surfaces.
Sharp-based, massive, clast-supported pebble conglomerate.
Matrix-supported breccia, fine-grained sandstone matrix with black, subrounded mudstone clasts.
Wavy bedding with thick (1–3 cm), featureless, mud layers.
Thin siderite bands and lags of siderite rip-up clasts
Hxs
Smb
Hxs
Sff
Hm
Sff
Hm
Sff
Sfw
Gm
Sfx
Hxs
Bmr
Sfw
Bmr
Sfw
Sff
Sfw
Gm
Sff
Sfx
Sfw
Sfx
FA5
FA3
Noonkanbah Formation
Sampled interval of core 1: 4830–501 m
Sedimentary structure
Planar lamination
Ripple cross-lamination
Flaser bedding
Wavy bedding
Planar cross-bedding
Lithology
Sandstone
Siltstone
Clast supported conglomerate
Breccia
Facies associations (FA)
FA5
FA3
LD43
01/06/16

**Figure 2.5.**

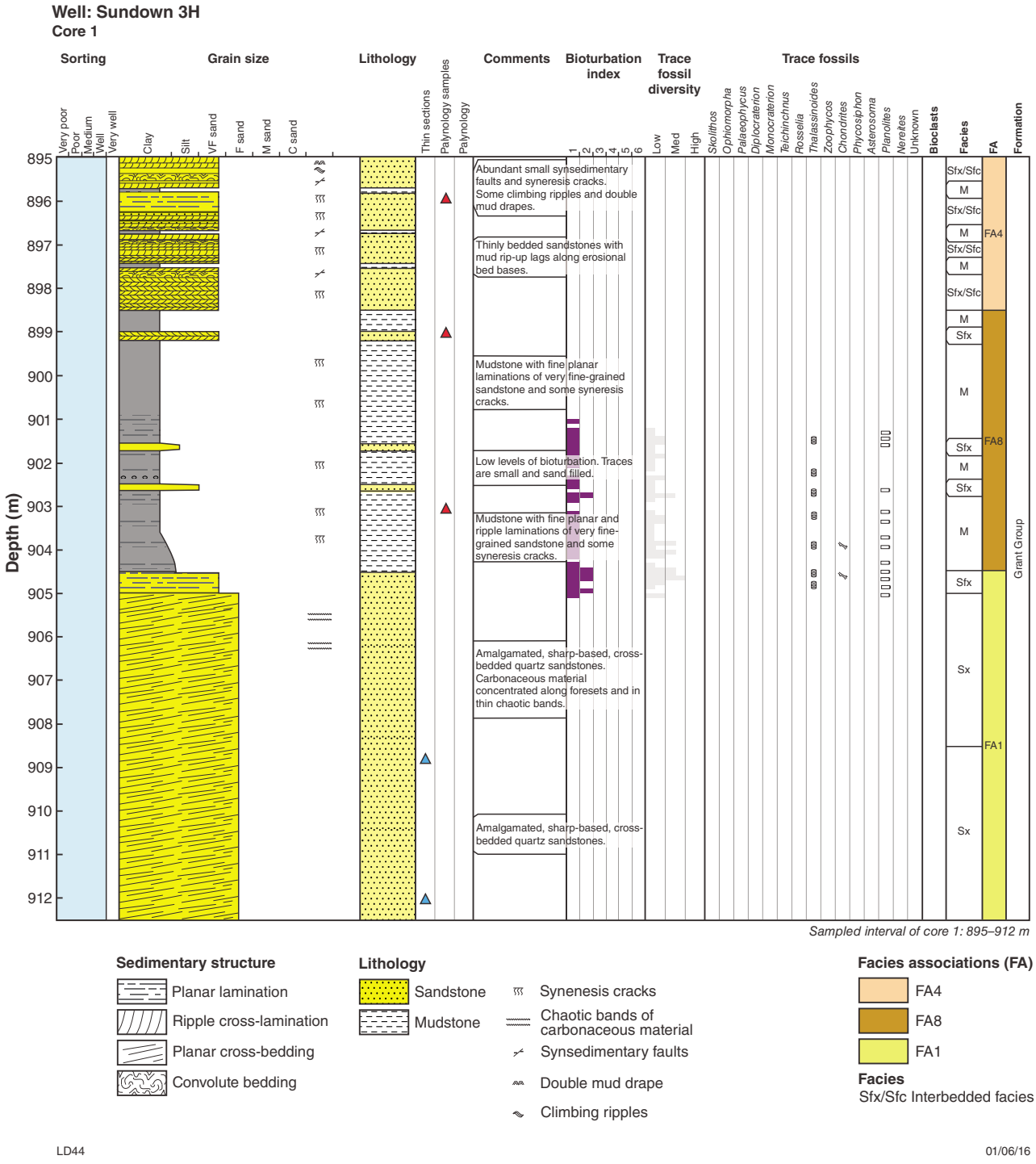
Well: Sundown 3H
Core 1
Sorting
Grain size
Lithology
Comments
Bioturbation index
Trace fossil diversity
Trace fossils
Very poor
Poor
Medium
Well
Very well
Clay
Silt
VF sand
F sand
M sand
C sand
Thin sections
Palynology samples
Palynology
Low
Med
High
Skolithos
Ophiomorpha
Palaeophycus
Diplocraterion
Monocraterion
Teichichnus
Rosselia
Thalassinoides
Zoophycos
Chondrites
Phycosiphon
Asterosoma
Planolites
Nereites
Unknown
Bioclasts
Facies
FA
Formation
Depth (m)
Abundant small synsedimentary faults and syneresis cracks. Some climbing ripples and double mud drapes.
Thinly bedded sandstones with mud rip-up lags along erosional bed bases.
Mudstone with fine planar laminations of very fine-grained sandstone and some syneresis cracks.
Low levels of bioturbation. Traces are small and sand filled.
Mudstone with fine planar and ripple laminations of very fine-grained sandstone and some syneresis cracks.
Amalgamated, sharp-based, cross-bedded quartz sandstones. Carbonaceous material concentrated along foresets and in thin chaotic bands.
Amalgamated, sharp-based, cross-bedded quartz sandstones.
Grant Group
Sampled interval of core 1: 895–912 m
Sedimentary structure
Planar lamination
Ripple cross-lamination
Planar cross-bedding
Convolute bedding
Lithology
Sandstone
Mudstone
Synenesis cracks
Chaotic bands of carbonaceous material
Synsedimentary faults
Double mud drape
Climbing ripples
Facies associations (FA)
FA4
FA8
FA1
Facies
Sfx/Sfc Interbedded facies
LD44
01/06/16

**Figure 2.6.**

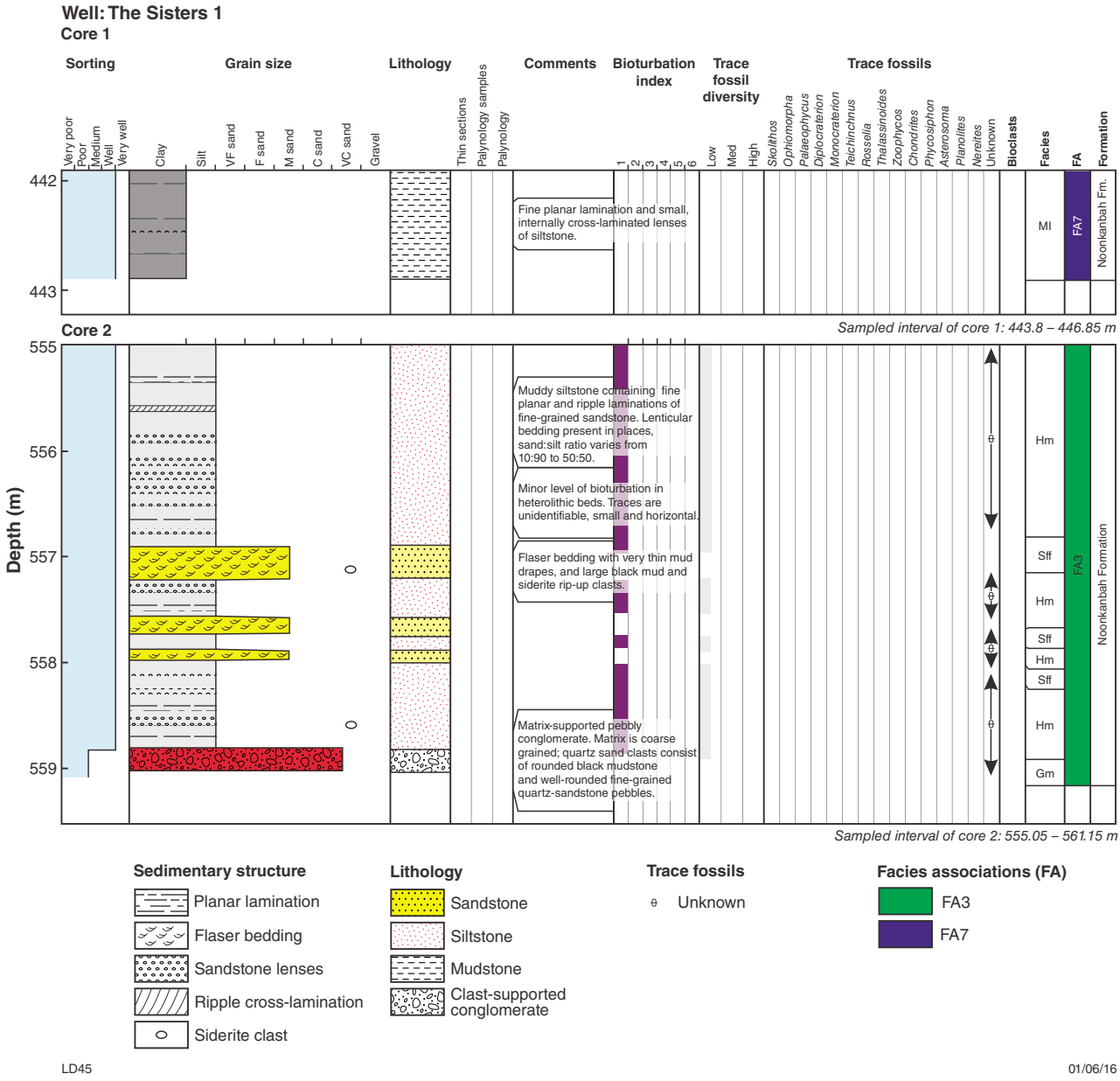
Well: The Sisters 1
Core 1
Sorting
Grain size
Lithology
Comments
Bioturbation index
Trace fossil diversity
Trace fossils
Very poor
Poor
Medium
Well
Very well
Clay
Silt
VF sand
F sand
M sand
C sand
VC sand
Gravel
Thin sections
Palynology samples
Palynology
Low
Med
High
Skolithos
Ophiomorpha
Palaeophycus
Diplocraterion
Monocraterion
Teichinchnus
Rosselia
Thalassinoides
Zoophycos
Chondrites
Phycosiphon
Asterosoma
Planolites
Nereites
Unknown
Bioclasts
Facies
FA
Formation
442
443
Fine planar lamination and small, internally cross-laminated lenses of siltstone.
MI
FA7
Noonkanbah Fm.
Core 2
Sampled interval of core 1: 443.8 – 446.85 m
555
556
557
558
559
Depth (m)
Muddy siltstone containing fine planar and ripple laminations of fine-grained sandstone. Lenticular bedding present in places, sand:silt ratio varies from 10:90 to 50:50.
Minor level of bioturbation in heterolithic beds. Traces are unidentifiable, small and horizontal.
Flaser bedding with very thin mud drapes, and large black mud and siderite rip-up clasts.
Matrix-supported pebbly conglomerate. Matrix is coarse grained; quartz sand clasts consist of rounded black mudstone and well-rounded fine-grained quartz-sandstone pebbles.
Hm
Sff
Hm
Sff
Hm
Sff
Hm
Gm
FA3
Noonkanbah Formation
Sampled interval of core 2: 555.05 – 561.15 m
Sedimentary structure
Planar lamination
Flaser bedding
Sandstone lenses
Ripple cross-lamination
Siderite clast
Lithology
Sandstone
Siltstone
Mudstone
Clast-supported conglomerate
Trace fossils
Unknown
Facies associations (FA)
FA3
FA7
LD45
01/06/16

**Figure 2.7.**

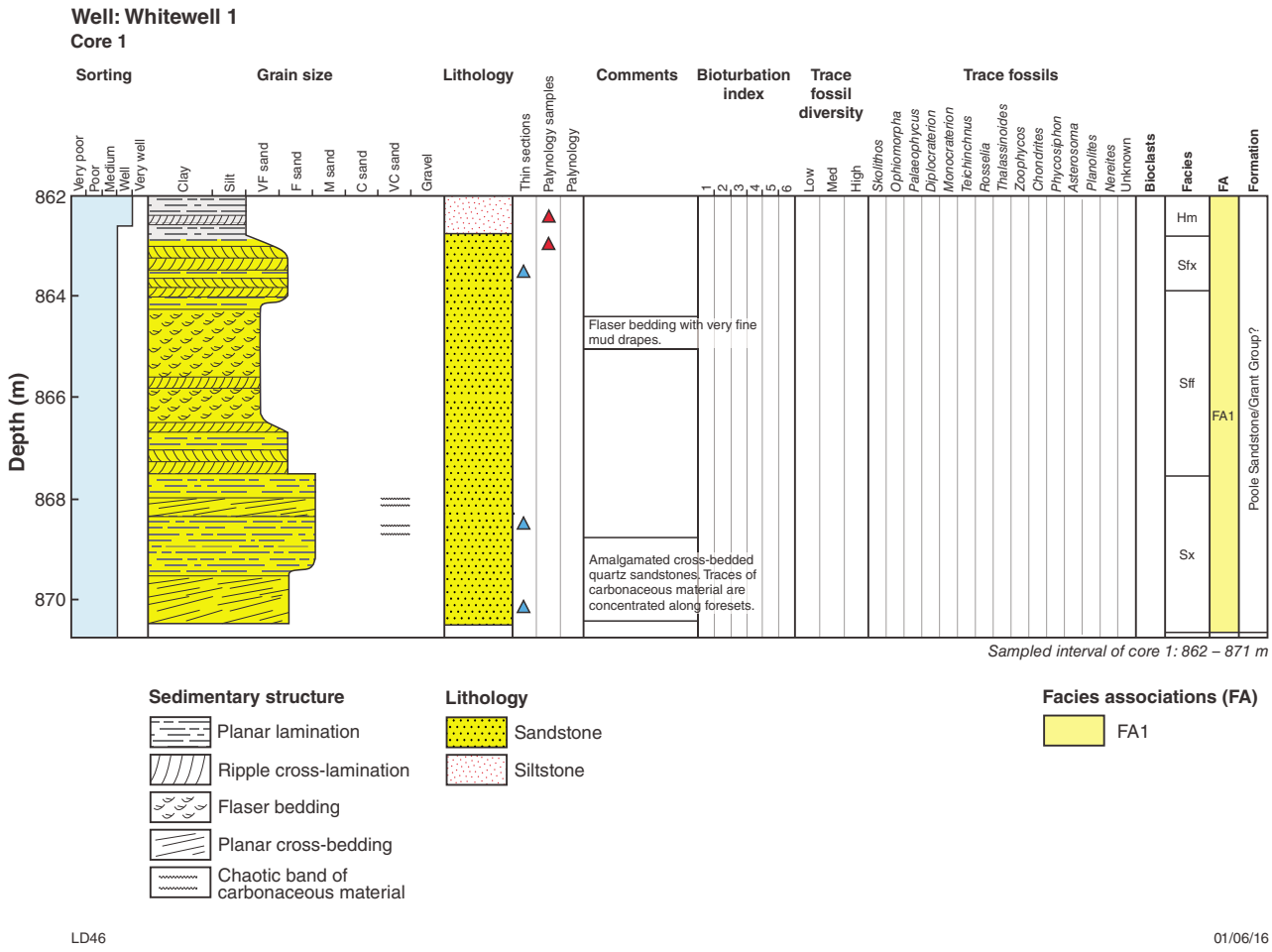
Well: Whitewell 1
Core 1
Sorting
Very poor
Poor
Medium
Well
Very well
Grain size
Clay
Silt
VF sand
F sand
M sand
C sand
VC sand
Gravel
Lithology
Thin sections
Palynology samples
Palynology
Comments
Bioturbation index
1
2
3
4
5
6
Trace fossil diversity
Low
Med
High
Trace fossils
Skolithos
Ophiomorpha
Palaeophycus
Diplocraterion
Monocraterion
Teichichnus
Rosselia
Thalassinoides
Zoophycos
Chondrites
Phycosiphon
Asterosoma
Planolites
Nereites
Unknown
Bioclasts
Facies
FA
Formation
Depth (m)
862
864
866
868
870
Flaser bedding with very fine mud drapes.
Amalgamated cross-bedded quartz sandstones. Traces of carbonaceous material are concentrated along foresets.
Hm
Sfx
Sff
Sx
FA1
Poole Sandstone/Grant Group?
Sampled interval of core 1: 862 – 871 m
Sedimentary structure
Planar lamination
Ripple cross-lamination
Flaser bedding
Planar cross-bedding
Chaotic band of carbonaceous material
Lithology
Sandstone
Siltstone
Facies associations (FA)
FA1
LD46
01/06/16

**Figure 2.8.**

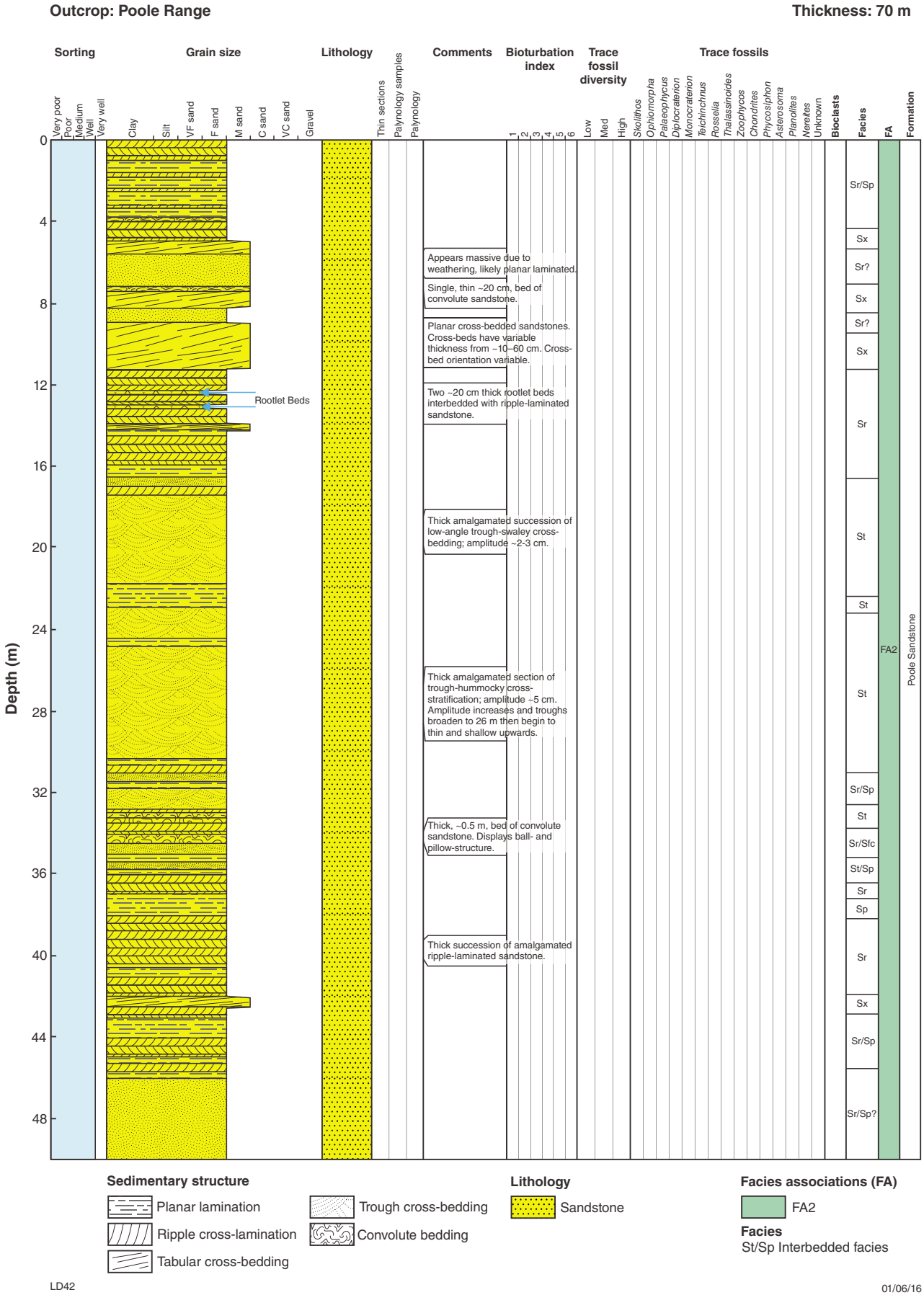
Outcrop: Poole Range
Thickness: 70 m
Sorting
Very poor
Poor
Medium
Well
Very well
Grain size
Clay
Silt
VF sand
F sand
M sand
C sand
VC sand
Gravel
Lithology
Thin sections
Palynology samples
Palynology
Comments
Bioturbation index
1
2
3
4
5
6
Trace fossil diversity
Low
Med
High
Trace fossils
Skolithos
Ophiomorpha
Palaeophycus
Diplocraterion
Monocraterion
Teichichnus
Rosselia
Thalassinoides
Zoophycos
Chondrites
Phycosiphon
Asterosoma
Planolites
Nereites
Unknown
Bioclasts
Facies
FA
Formation
Depth (m)
0
4
8
12
16
20
24
28
32
36
40
44
48
Rootlet Beds
Appears massive due to weathering, likely planar laminated.
Single, thin ~20 cm, bed of convolute sandstone.
Planar cross-bedded sandstones. Cross-beds have variable thickness from ~10–60 cm. Cross-bed orientation variable.
Two ~20 cm thick rootlet beds interbedded with ripple-laminated sandstone.
Thick amalgamated succession of low-angle trough-swaley cross-bedding; amplitude ~2-3 cm.
Thick amalgamated section of trough-hummocky cross-stratification; amplitude ~5 cm. Amplitude increases and troughs broaden to 26 m then begin to thin and shallow upwards.
Thick, ~0.5 m, bed of convolute sandstone. Displays ball- and pillow-structure.
Thick succession of amalgamated ripple-laminated sandstone.
Sr/Sp
Sx
Sr?
Sx
Sr?
Sx
Sr
St
St
St
Sr/Sp
St
Sr/Sfc
St/Sp
Sr
Sp
Sr
Sx
Sr/Sp
Sr/Sp?
FA2
Poole Sandstone
Sedimentary structure
Planar lamination
Ripple cross-lamination
Tabular cross-bedding
Trough cross-bedding
Convolute bedding
Lithology
Sandstone
Facies associations (FA)
FA2
Facies
St/Sp Interbedded facies
LD42
01/06/16

**Figure 2.9.**

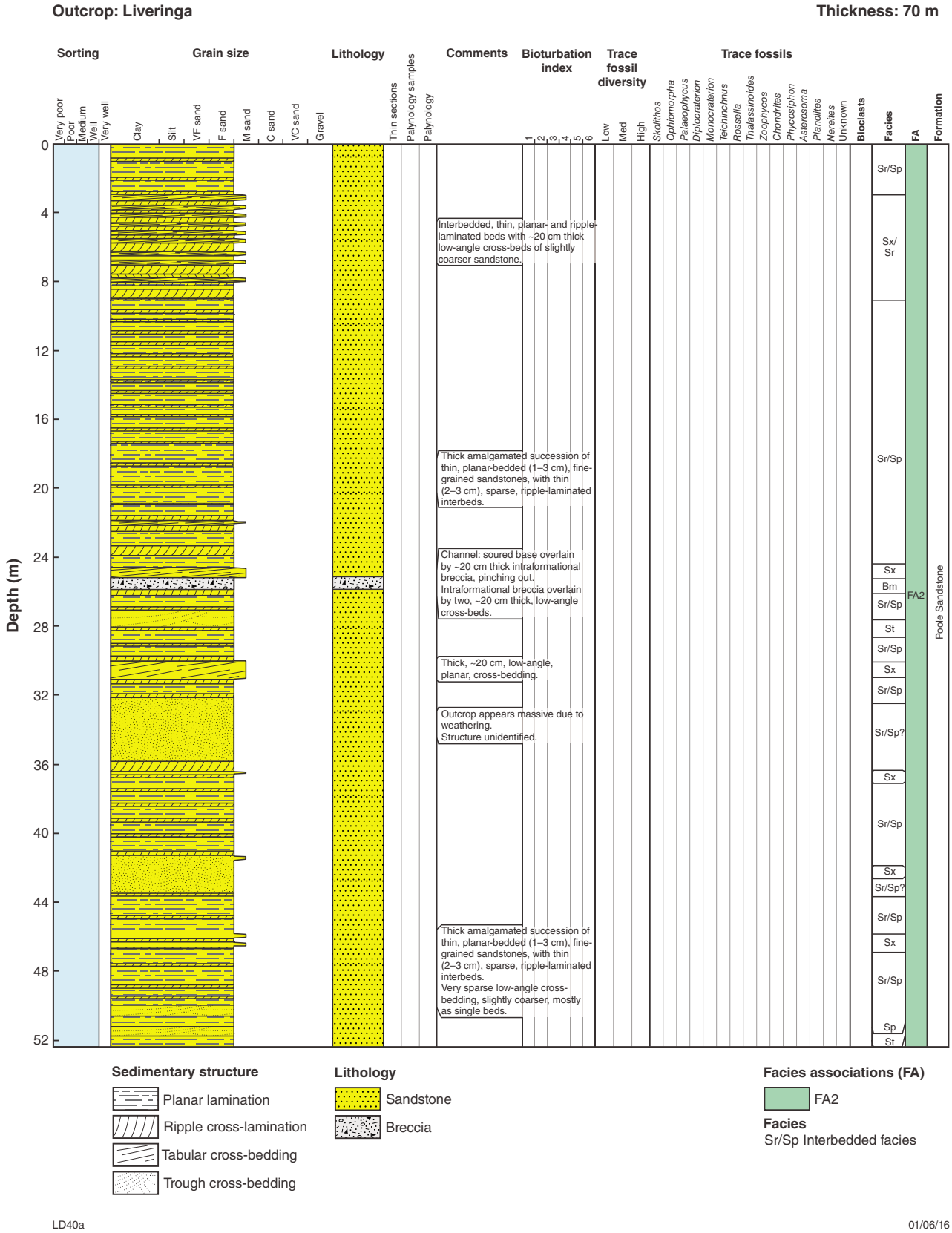
Outcrop: Liveringa
Thickness: 70 m
Sorting
Very poor
Poor
Medium
Well
Very well
Grain size
Clay
Silt
VF sand
F sand
M sand
C sand
VC sand
Gravel
Lithology
Thin sections
Palynology samples
Palynology
Comments
Bioturbation index
1
2
3
4
5
6
Trace fossil diversity
Low
Med
High
Trace fossils
Skolithos
Ophiomorpha
Palaeophycus
Diplocraterion
Monocraterion
Teichichnus
Rosselia
Thalassinoides
Zoophycos
Chondrites
Phycosiphon
Asterosoma
Planolites
Nereites
Unknown
Bioclasts
Facies
FA
Formation
Depth (m)
0
4
8
12
16
20
24
28
32
36
40
44
48
52
Interbedded, thin, planar- and ripple-laminated beds with ~20 cm thick low-angle cross-beds of slightly coarser sandstone.
Thick amalgamated succession of thin, planar-bedded (1–3 cm), fine-grained sandstones, with thin (2–3 cm), sparse, ripple-laminated interbeds.
Channel: soured base overlain by ~20 cm thick intraformational breccia, pinching out.
Intraformational breccia overlain by two, ~20 cm thick, low-angle cross-beds.
Thick, ~20 cm, low-angle, planar, cross-bedding.
Outcrop appears massive due to weathering.
Structure unidentified.
Thick amalgamated succession of thin, planar-bedded (1–3 cm), fine-grained sandstones, with thin (2–3 cm), sparse, ripple-laminated interbeds.
Very sparse low-angle cross-bedding, slightly coarser, mostly as single beds.
Sr/Sp
Sx/ Sr
Sr/Sp
Sx
Bm
Sr/Sp
St
Sr/Sp
Sx
Sr/Sp
Sr/Sp?
Sx
Sr/Sp
Sx
Sr/Sp?
Sr/Sp
Sx
Sr/Sp
Sp
St
FA2
Poole Sandstone
Sedimentary structure
Planar lamination
Ripple cross-lamination
Tabular cross-bedding
Trough cross-bedding
Lithology
Sandstone
Breccia
Facies associations (FA)
FA2
Facies
Sr/Sp Interbedded facies
LD40a
01/06/16

**Figure 2.10.**

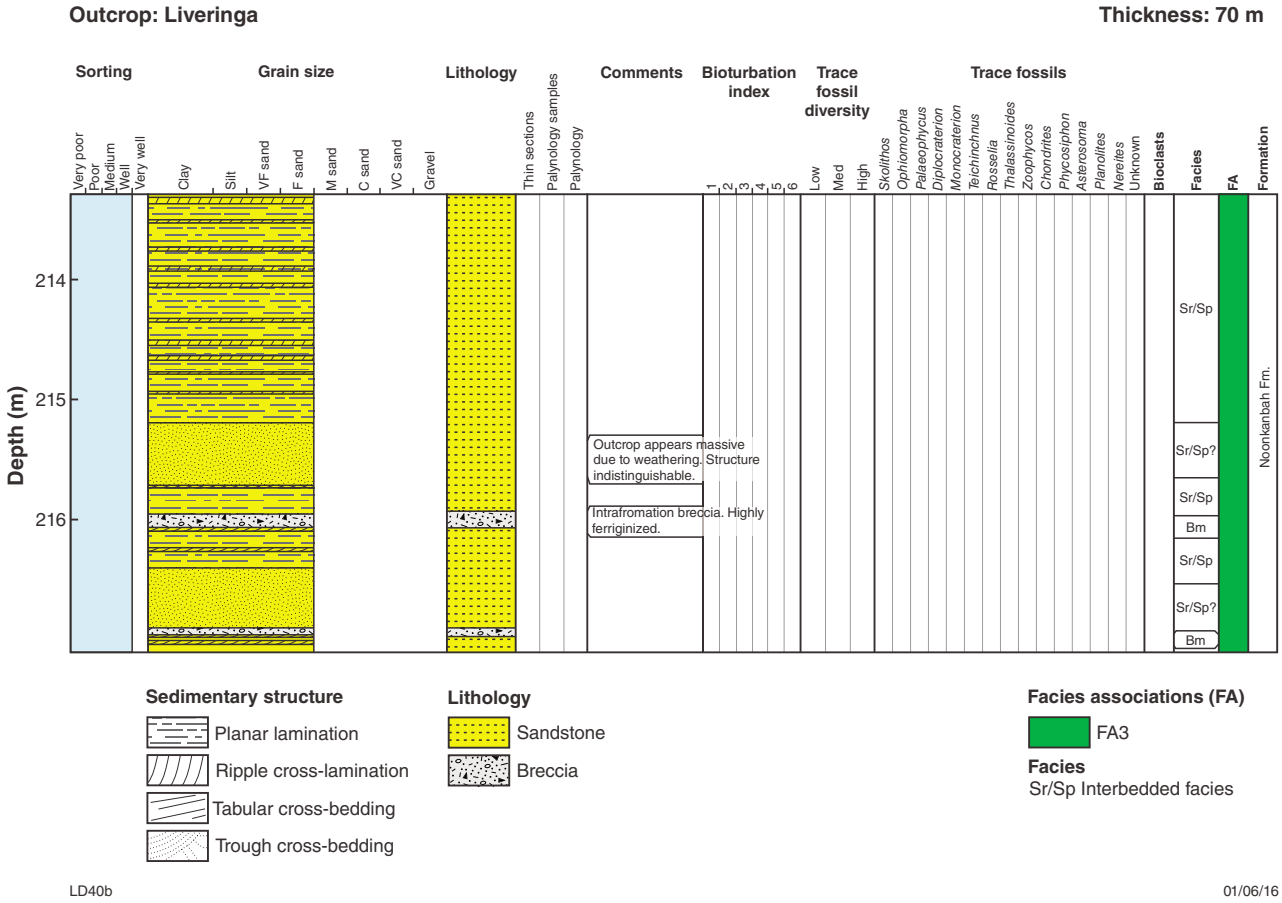


**Figure 2.10. continued**

# Appendix 3

# Petrographic sample descriptions

**Table 3.1. Summary of authigenic diagenetic features of samples for which petrographic descriptions are provided**

| *Authigenic characteristics* | | | | *Porosity* | |
|---|---|---|---|---|---|
| *Facies* | *Order of cements* | *Dissolution and replacement textures* | *Compaction features* | *%* | *Type* |
| Sx | QO, K | Plagioclase dissolution (common) and rare quartz dissolution | | 20–25 | Primary intergranular |
| | | | | <1 | Secondary via dissolution |
| Sfx | QO, K, Chl | Plagioclase dissolution | | 5 | Primary intergranular |
| | | | | <5 | Secondary via dissolution |
| Sfx | Cp, Chl | Plagioclase dissolution, replacement by carbonate | Warped biotite and carbonaceous material | <10–20 | Primary intergranular |
| | | Replacement of biotite by chlorite | | <5 | Secondary via dissolution |
| Sff | | Plagioclase dissolution, replacement by chlorite | | 5 | Primary intergranular |
| | | Replacement of biotite by chlorite | | <1 | Secondary via dissolution |
| Smb | QO, K, C, Chl | Quartz dissolution around grain edges and replacement with kaolinite | Warped biotite | <5–20 | Primary intergranular |
| | | Chlorite replacing biotite | | <1 | Secondary via dissolution |
| Gm | QO, K, Chl | Chlorite replacing biotite | | 15 | Primary intergranular |
| | | | | <5 | Secondary via dissolution |
| Gmc | Cf,QO, CV | Plagioclase and microcline dissolution | | <5 | Secondary via dissolution |
| | | Carbonate replacing plagioclase and microcline | | | |
| Lps | Ce, K | Partial to total replacement of skeletal fragments by equant carbonate cement | | 10 | Primary intergranular and intragranular |
| Lgs | Cf, Ce | Partial to total replacement of skeletal fragments by equant carbonate cement | | <5 | Primary intragranular |

**NOTES:** QO – quartz overgrowth; K – kaolinite; Cl – chlorite; Ce – equant calcite; Cf – fibrous calcite; Cp – patchy carbonate; CV – carbonate-filled veins

**Table 3.2. List of of drillcore samples and depth of samples in wells for which petrographic descriptions are given**

| *Well* | *Depth of sample (m)* | *Formation* |
|---|---|---|
| Frome Rocks 2 | 213.3 – 216 | Noonkanbah Formation |
| Frome Rocks 2 | 457.2 – 460 | Noonkanbah Formation |
| Frome Rocks 2 | 630.9 – 633 | Poole Sandstone |
| Langoora 1 | 519.4 – 581 | Poole Sandstone |
| Langoora 1 | 579.4 – 581 | Poole Sandstone |
| Meda 1 | 719.6 – 723.9 | Poole Sandstone |
| Perindi 1 | 872.4 | Nura Nura Member |
| Perindi1 | 872.8 | Nura Nura Member |
| Perindi 1 | 873.85 | Nura Nura Member |
| Perindi1 | 875.88 | Nura Nura Member |
| Perindi 1 | 976.78 | Nura Nura Member |
| PND 1 | 300 | Noonkanbah Formation |
| PND 1 | 307 | Noonkanbah Formation |
| PND 1 | 317 | Noonkanbah Formation |
| PND 1 | 323.4 | Poole Sandstone |
| Roebuck Bay 1 | 609.3 – 611.4 | Nura Nura Member |
| Scarpia 1 | 488 | Noonkanbah Formation |
| Scarpia 1 | 493 | Noonkanbah Formation |
| Scarpia 1 | 495 | Noonkanbah Formation |
| Scarpia 1 | 496 | Noonkanbah Formation |
| Sundown 3H | 908 | Grant Group |
| Sundown 3H | 912.3 | Grant Group |
| Whitewell 1 | 863.5 | Grant Group |
| Whitewell 1 | 868 | Grant Group |
| Whitewell 1 | 870 | Grant Group |

**Table 3.3. Summary of detrital composition and grain characteristics for samples in detailed petrographic descriptions**

| *Fabric and texture* | | | | *Detrital composition (%)* | | | | | | | | | |
|---|---|---|---|---|---|---|---|---|---|---|---|---|---|
| *Facies* | *Grain size* | *Grain contacts* | *Sorting* | *Q* | *Mx* | *PF* | *AF* | *Bt* | *M* | *L* | *CM* | *G* | *BC* |
| Sx | f–m sand | Planar | Well | 70–95 | <5 | 5–10 | <5 | | | | Tr | | |
| Sfx 1 | f–m sand | Planar | Well | 90–95 | <5* | <5 | | <1 | <1 | | | | |
| Sfx 2 | f–c sand | Planar | Well | 60–75 | <5–25 | | | | | | <5* | | |
| Sff | f sand | Point-planar | Well | 85 | | <5 | <5 | 10 | <1 | | | | |
| Smb | m sand | Planar | Well | 70–80 | | <5 | <5 | <1 | | | | | |
| Gm | c–vf matrix sand | Planar | Poor | 80 | 10 | <5 | <5 | | 1–2 | 5–10 | | | |
| Gmc | f–vf matrix sand | Point | Very Poor | 70 | 10–15 | <5 | <5 | | | 10 | | | 5 |
| Lps | granule | Point-planar | Poor | <1 | 30 | | | | | | | | 70 |
| Lgs | granule | Point | Well | 1–30 | | | | | | | | 1–2 | 70–98 |

**NOTES:** Q – quartz, Mx – matrix, PF – plagioclase feldspar, AF – alkalic feldspar (microcline), Bt – biotite, M – microcline, L – lithic fragments, CM – carbonaceous material, G – glauconitic material and BC – bioclasts. Facies codes correlate to the facies table in Appendix 2.

# Frome Rocks 2

**Depth**: 213.3 – 216.4 m **Formation**: Noonkanbah Formation **Facies**: Hxs

## SILTSTONE

## Texture and fabric

**Grain size**: average 0.025 mm

**Shape**: subangular **Sorting**: moderate **Contacts**: point–elongate

## Detrital composition

This sample is dominated by quartz (70%) with abundant dark brown-grey clay (20–25%), minor muscovite (5%) and some organic material (<5%).

## Diagenetic features

Organic material and muscovite flakes show minor ductile deformation. Minor amounts of calcite cement fill intergranular space.

## Diagenetic sequence

Compaction is indicated by the deformation of organic material and muscovite flakes.

## Porosity

**Proportion of sample**: <5%

**Style**: Porosity is primary and intergranular

**Infill**: Very minor fill with calcite cement

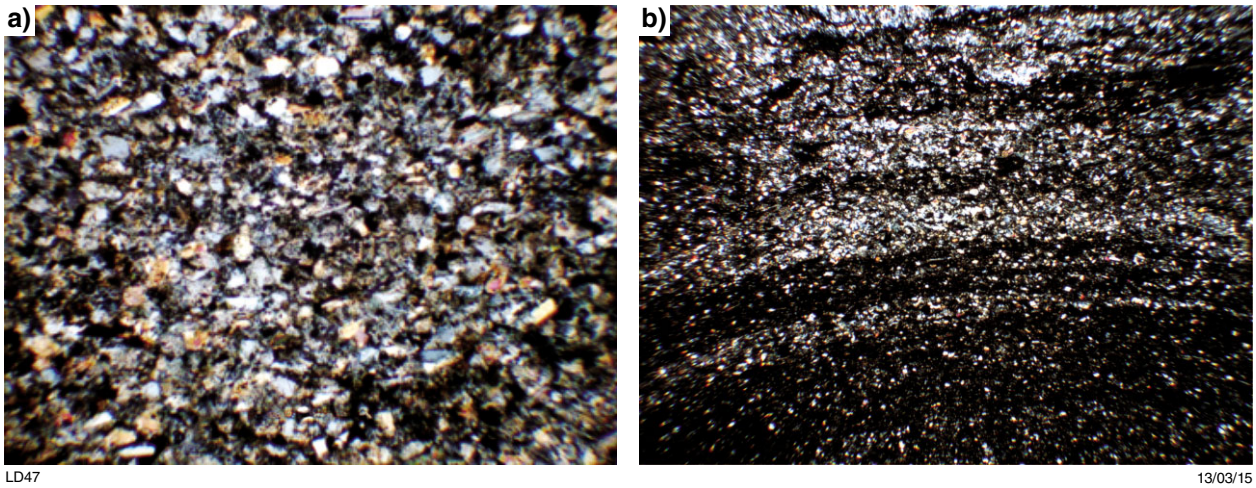


**Figure 3.1. a) Grain composition and distribution showing the abundance of quartz and detrital clay, FOV: 1 mm; b) bioturbated sediment, thin alternating bands of clay-rich and quartz-rich sediments that result from the backfill of the burrow, FOV: 11 mm**

# Frome Rocks 2

**Depth**: 457.2 – 460.2 m **Formation**: Noonkanbah Formation **Facies**: Sfx

## QUARTZARENITE (Q:97 F:3 R:0)

### Texture and fabric

**Grain size**: average 0.1 mm; range 0.05 – 0.2 mm

**Shape**: subangular **Sorting**: moderate **Contacts**: point–elongate

### Detrital composition

This sample is dominated by quartz (75%) with minor biotite (5–10%), brown detrital clay (5%), muscovite (1–2%) and plagioclase feldspar (1–2%), and trace microcline (<1%).

### Diagenetic features

Trace carbonate cement is present in pores and replacing plagioclase grains. Minor chlorite is present as an alteration product of biotite.

### Porosity

**Proportion of sample**: 15%

**Style**: Porosity is primary and intergranular

**Infill**: Fill mainly by chlorite, with very minor infill by patchy carbonate cement

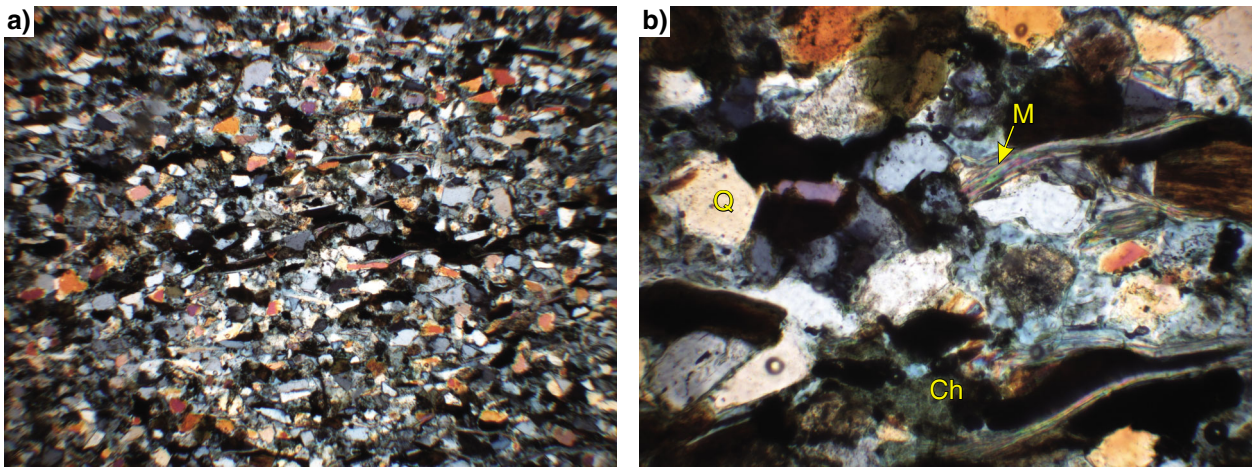


**Figure 3.2.** **a) Grain composition and distribution showing the dominance of quartz, FOV: 5.5 mm; b) detailed view of grain composition and authigenic features showing quartz, muscovite, and chlorite, FOV: 1 mm. Detrital quartz (Q), muscovite (M) and chlorite (Ch)**

# Frome Rocks 2

**Depth**: 630.9 – 633.9 m **Formation**: Poole Sandstone **Facies**: Hxs

## BIOTURBATED SILTSTONE

### Texture and fabric

**Grain size**: average 0.05 mm; range 0.05 – 0.1 mm

**Shape**: subangular **Sorting**: moderate **Contacts**: elongate

### Detrital composition

This sample is dominated by quartz (65%), mainly monocrystalline with high levels of detrital clay (20–25%) and minor plagioclase feldspar (5%), biotite (2%), muscovite (2%) and carbonaceous material (2%). Detrital composition is strongly affected by bioturbation. Burrowed sections are cleaner, devoid of detrital clay and carbonaceous material, and richer in quartz.

### Porosity

**Proportion of sample**: <5%

**Style**: Low levels of primary intergranular porosity are preserved. However, the majority of the porosity is secondary, created by burrowing organisms due to the selective removal of carbonaceous material

**Infill**: Very minor infill by patchy carbonate cement

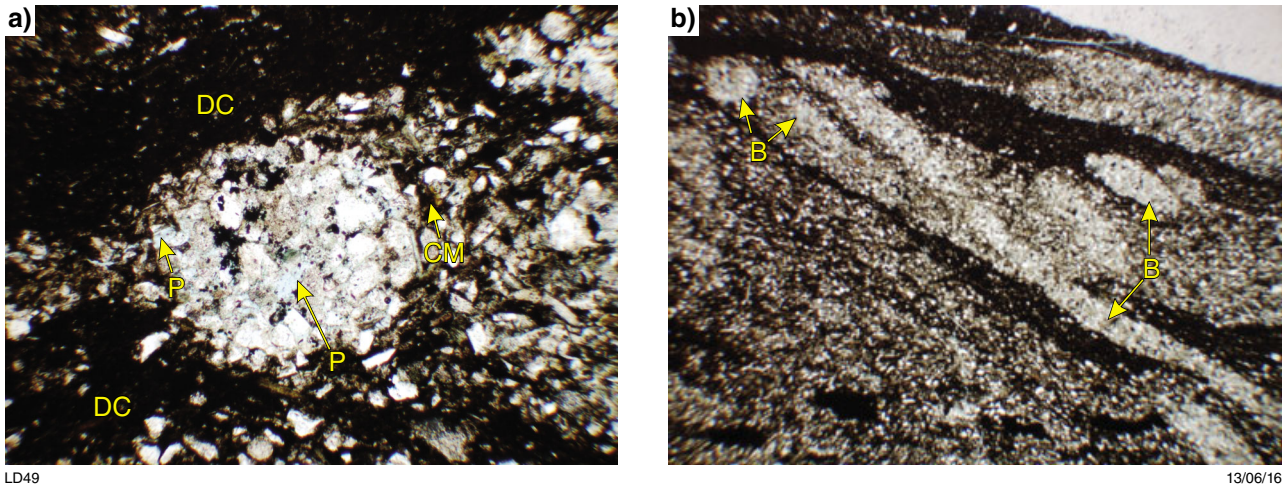


**Figure 3.3.** **a) Bioturbation, *Planolites* burrow. Compared to the surrounding sediment the burrow is quartz rich with higher intergranular porosity, FOV: 2 mm; b) multiple burrows showing the contrast of burrow fill and clay-rich surrounding sediments, FOV: 11 mm. Detrital clay (DC), pore space (P), carbonaceous material (CM) and burrows (B)**

# Langoora 1

**Depth**: 519.4 – 581.2 m **Formation**: Poole Sandstone (Nura Nura Member) **Facies**: Lgs

## SKELETAL GRAINSTONE

### Texture and fabric

**Grain size**: average 0.6 mm; range 0.2 – 1 mm

**Shape**: rounded **Sorting**: moderate **Contacts**: point

### Detrital composition

Well-rounded skeletal fragments comprise 85% of this sample's detrital composition; whole skeletons are rare. These skeletal fragments are most commonly bryozoans and planktonic foraminifera with minor gastropods and crinoids. Quartz is present (10–15%), dominantly monocrystalline with a few well-rounded polycrystalline grains, with minor microcline (1–2%), plagioclase feldspar (1–2%) and trace quantities (<1%) of muscovite and sedimentary lithic fragments.

### Diagenetic features

Equant, ferroan calcite cement is pervasive throughout the sample. Fibrous calcite cement forms rims around some bioclasts and equant calcite overgrowths are well developed on some grains. Dissolution of plagioclase feldspars, microcline and bioclasts, and replacement with calcite cement, is extensive. The intensity and extent of dissolution and replacement varies from minor around grain rims, to extensive with total recrystallization of skeletal grains and their internal cavities.

### Diagenetic sequence

Staining indicates that fibrous calcite and calcite overgrowths are not ferroan but the pervasive equant calcite indicates the fibrous rims and overgrowths formed prior to the equant calcite cement.

### Porosity

**Proportion of sample**: <5%

**Style**: Primary, intragranular porosity preserved in some bioclasts

**Infill:** Extensive infill of primary intergranular, and some intragranular, pore space with calcite cement

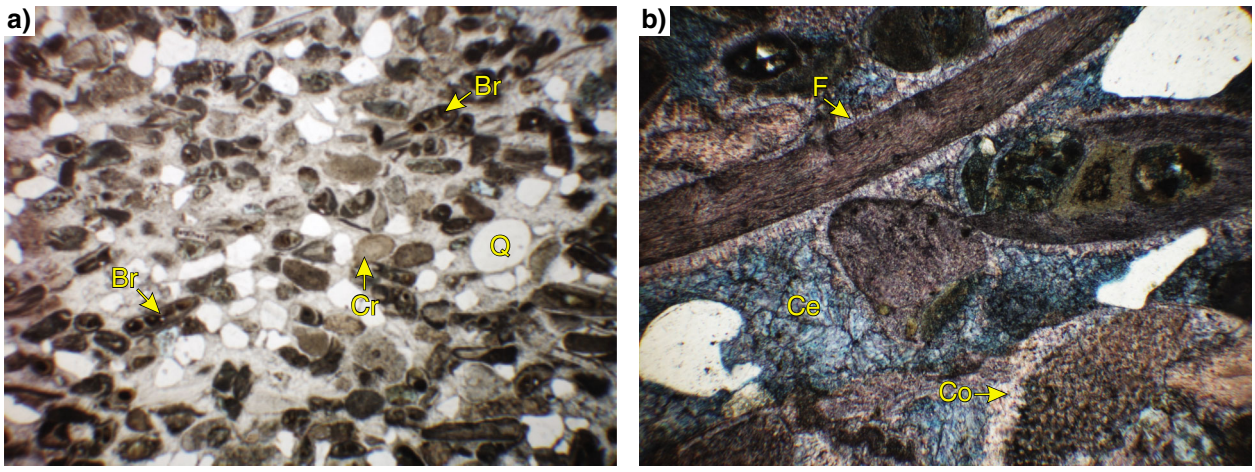


**Figure 3.4. a) Detrital characteristics showing detrital composition dominated by well-rounded skeletal fragments with some detrital quartz, FOV: 11 mm; b) carbonate cement phases showing fibrous calcite and calcite overgrowth on crinoid fragment surrounded by ferroan calcite indicated by blue staining, FOV: 2 mm. Detrital quartz (Q), crinoid (Cr), bryozoan (Br), fibrous calcite (F), calcite overgrowth (Co) and ferroan equant calcite (Ce)**

# Langoora 1

**Depth**: 579.4 – 581.2 m **Formation**: Poole Sandstone **Facies**: Smb

## SILTSTONE

### Texture and fabric

**Grain size**: average 0.05 mm; range 0.025 – 0.1 mm

**Shape**: subangular **Sorting**: poor **Contacts**: point–elongate

### Detrital composition

The sample is dominated by monocrystalline quartz (70–75%) with abundant detrital clay (~20%) and minor carbonaceous material, microcline (1–2%), plagioclase feldspar (1–2%) and trace amounts of zircon (<1%). Detrital clay and carbonaceous material are concentrated along thin, planar laminae.

### Diagenetic features

Compaction is indicated by close grain packing and ductile deformation of muscovite.

### Porosity

**Proportion of sample**: <5%

**Style**: Primary, intergranular porosity

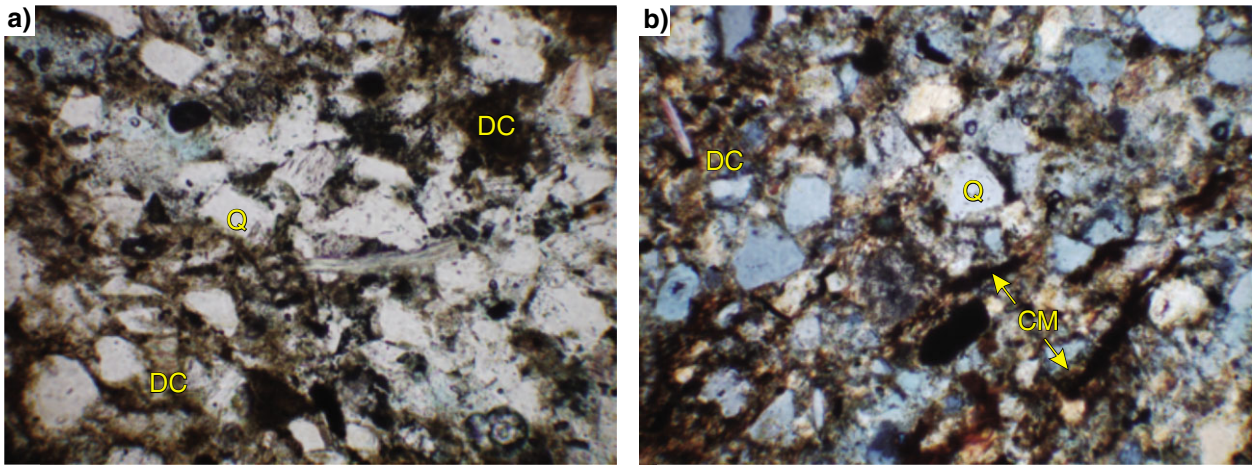


**Figure 3.5. a) Grain composition and characteristics showing dominance of quartz grains and abundant detrital clay, FOV: 2 mm; b) showing traces of carbonaceous material, FOV: 2 mm. Detrital quartz (Q), detrital clay (DC) and carbonaceous material (CM)**

# Meda 1

**Depth**: 719.6 – 723.9 m **Formation**: Poole Sandstone **Facies**: Smb

## SUBFELDSARENITE (Q:94 F:6 R:0)

### Texture and fabric

**Grain size**: average 0.3 mm; range 0.1 – 0.5 mm

**Shape**: subrounded **Sorting**: moderate **Contacts**: elongate

### Detrital composition

This sample is dominated by quartz (75%) with ~15% brown clay, minor microcline (1–2%), plagioclase feldspar (1–2%), and trace zircon (<1%). Remnants of alkali feldspars are observed, but the majority of these grains have been dissolved.

### Diagenetic features

Quartz overgrowths are present but minor; these are overlain by patchy kaolinite and patchy carbonate cement. Dissolution of plagioclase feldspars and partial replacement by kaolinite is observed.

### Diagenetic sequence

Quartz overgrowths were the first cement to form, followed by kaolinite and carbonate cements.

### Porosity

**Proportion of sample**: 20%

**Style**: Porosity is mainly primary, intergranular, with minor secondary porosity created from the dissolution of potassium feldspars

**Infill**: Minor infill by kaolinite and carbonate cement

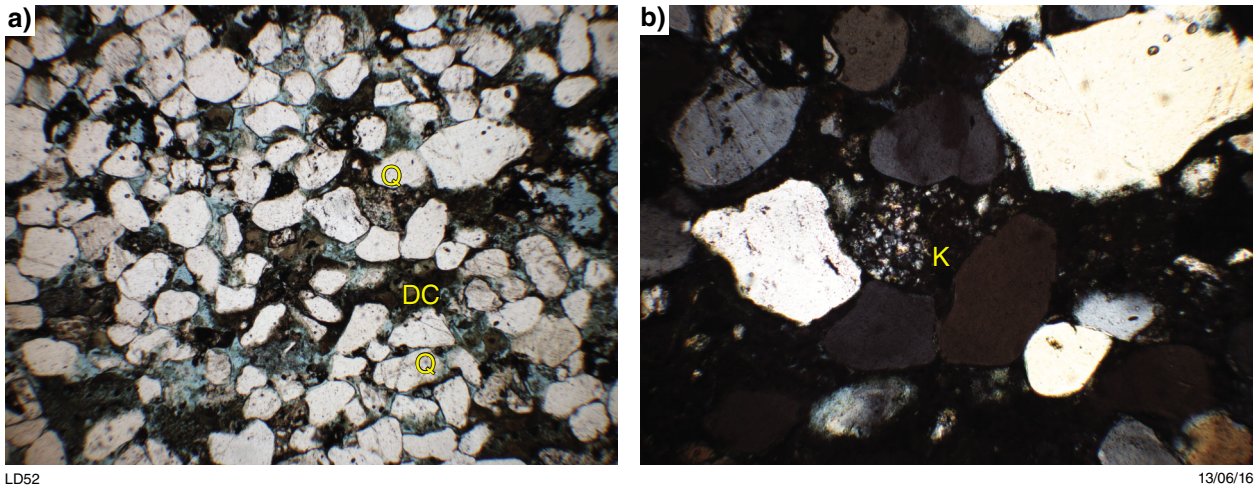


**Figure 3.6. a) Grain composition and characteristics displaying high intergranular porosity and abundant detrital quartz and clay material, FOV: 11 mm; b) diagenetic features, kaolinite infilling intergranular spaces, FOV: 1 mm. Detrital quartz (Q), detrital clay (DC) and kaolinite (K)**

# Perindi 1

**Depth**: 872.4 m **Formation**: Nura Nura Member **Facies**: Lps

## SKELETAL PACKSTONE

### Texture and fabric

**Grain size**: average 2 mm; range 1–10 mm

**Shape**: subrounded **Sorting**: well **Contacts**: point–elongate

### Detrital composition

The main constituents of this sample are carbonate bioclasts (60%) and detrital clay (40%). Bioclasts are highly fragmented, have rounded ends and consist of ~70% crinoids, ~10% bryozoans, ~10% brachiopods and ~1–2% each of foraminifera, ostracods, cephlapods and possible bivalves.

### Diagenetic features

Pervasive, equant, calcite cement constitutes ~20–30% of the overall sample. The cement forms in internal skeletal cavities and in intergranular spaces. There is low to moderate (5–30%) dissolution of bioclasts and some replacement of bioclasts with equant calcite.

### Diagenetic sequence

Elongate grain contacts indicate that equant carbonate cement formed post-compaction. Dissolution was a continual process, as indicated by occurrence in different levels in different grains.

### Porosity

**Proportion of sample**: <5%

**Style**: Primary porosity, intergranular and intragranular, occurring in the skeletal cavities of bioclasts. Minor secondary porosity has been created by grain dissolution

**Infill**: Extensive infill with equant carbonate cement; minor infill with micrite

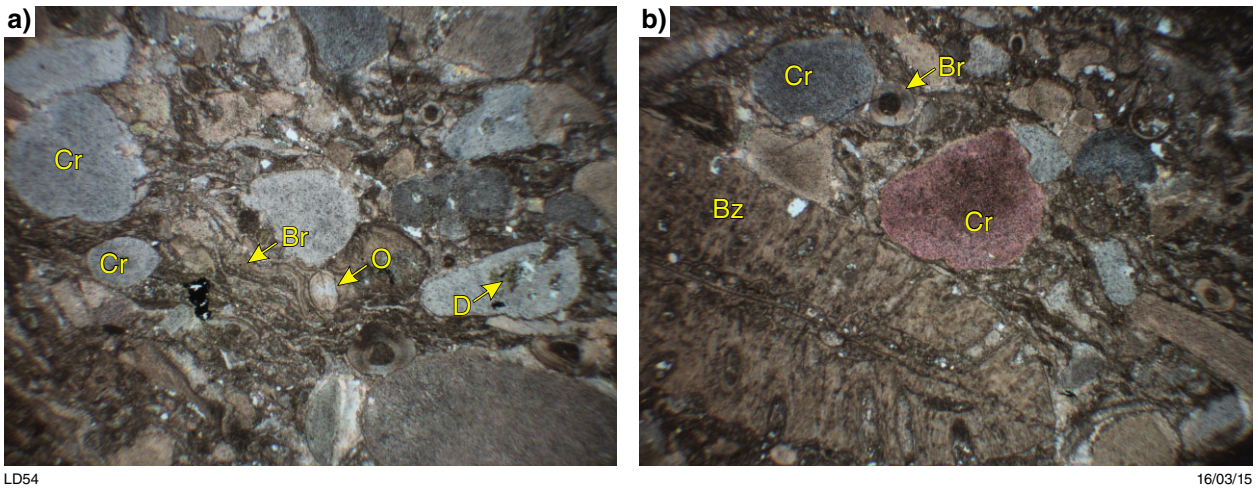


**Figure 3.7.** **a) Grain composition and characteristics showing dominance of crinoid fragments, dissolution of crinoid plate, infill of an ostracod skeletal cavity, and brachiopod fragments, FOV: 11 mm; b) bryozoan fragments, crinoid plates and brachiopod spines, FOV: 11 mm. Crinoid (Cr), ostracod, (O), brachiopod (Br), bryozoan (Bz) and dissolution (D)**

# Perindi 1

**Depth**: 872.8 m **Formation**: Nura Nura Member **Facies**: Lgs

## SKELETAL GRAINSTONE

### Texture and fabric

**Grain size**: average 2 mm; range 1–5 mm

**Shape**: subrounded **Sorting**: well **Contacts**: point

### Detrital composition

This sample is composed of highly fragmented, well-rounded, skeletal bioclasts dominantly bryozoans (~45%) and brachiopods (~40%) with some crinoid fragments (~10%). Planktonic foraminifera, gastropods, ostracods and a few unidentified clasts constitute the remainder of the assemblage.

### Diagenetic features

Pervasive, equant, calcite cement constitutes ~40–50 % of the overall sample. The cement forms in internal skeletal cavities and in intergranular spaces. Some bioclasts are totally recrystallized to equant calcite and dissolution of crinoid fragments is observed. Poorly defined columnar calcite rims are present on many grains.

### Diagenetic sequence

Point contacts and cement-supported grains indicate formation of equant calcite during deposition. Columnar calcite enclosing grains indicates two main phases of cementation.

### Porosity

**Proportion of sample**: <5%

**Style**: Primary porosity, intergranular and intragranular, in the skeletal cavities of bioclasts. Minor secondary porosity has been created by grain dissolution

**Infill**: Extensive infill with equant carbonate cement

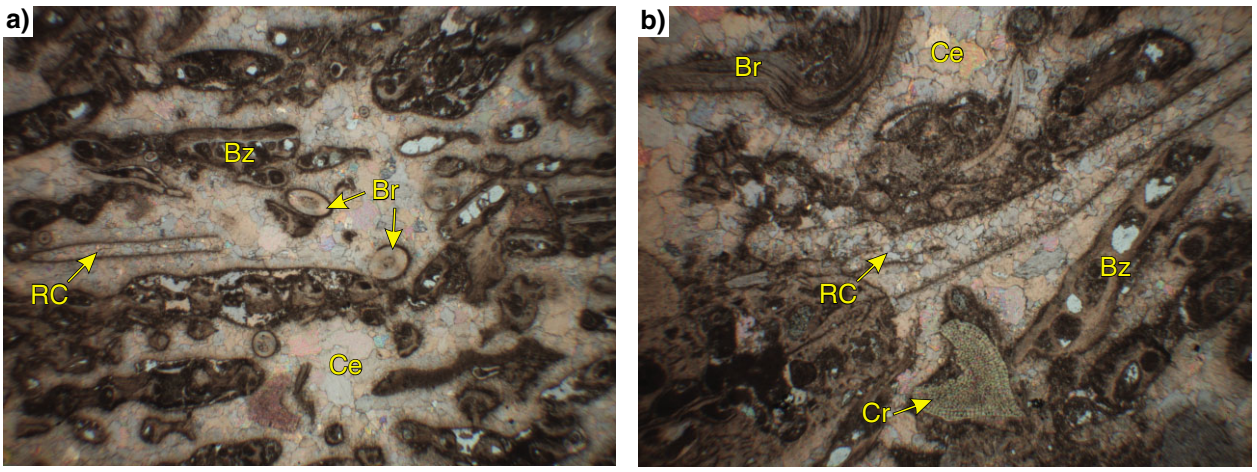


**Figure 3.8.** **a) Grain composition and characteristics showing dominance of bryozoans and brachiopods supported by equant carbonate cement; some grains show total replacement with cement, FOV:11 mm; b) grain replacement by carbonate cements, FOV: 5.5 mm. Crinoid (Cr), bryozoan (Bz), brachiopod (Br), equant carbonate cement (Ce), replacement cement (RC)**

# Perindi 1

**Depth**: 873.85 m **Formation**: Nura Nura Member **Facies**: Lps

## SKELETAL PACKSTONE

### Texture and fabric

**Grain size**: average 2 mm; range 0.5 – 3 mm

**Shape**: rounded **Sorting**: poor **Contacts**: point

### Detrital composition

This sample is composed of highly fragmented, well-rounded, skeletal bioclasts, dominantly bryozoans (~80%) with minor crinoid fragments (~5%) and brachiopods (~5%), and lesser planktonic foraminifera and ostracods. Unidentified clasts constitute the remainder of the assemblage.

### Diagenetic features

Pervasive, equant, calcite cement constitutes ~30% of the overall sample, and micrite ~20%. Both form in internal skeletal cavities and in intergranular spaces. Fibrous calcite encloses some grains and dissolution of crinoid fragments is observed.

### Diagenetic sequence

Point contacts and cement-supported grains indicate formation of equant calcite during deposition. Fibrous calcite enclosing grains indicates two main phases of cementation.

### Porosity

**Proportion of sample**: <5%

**Style**: Primary porosity, intergranular and intragranular, in the skeletal cavities of bioclasts

**Infill**: Extensive infill with equant carbonate cement

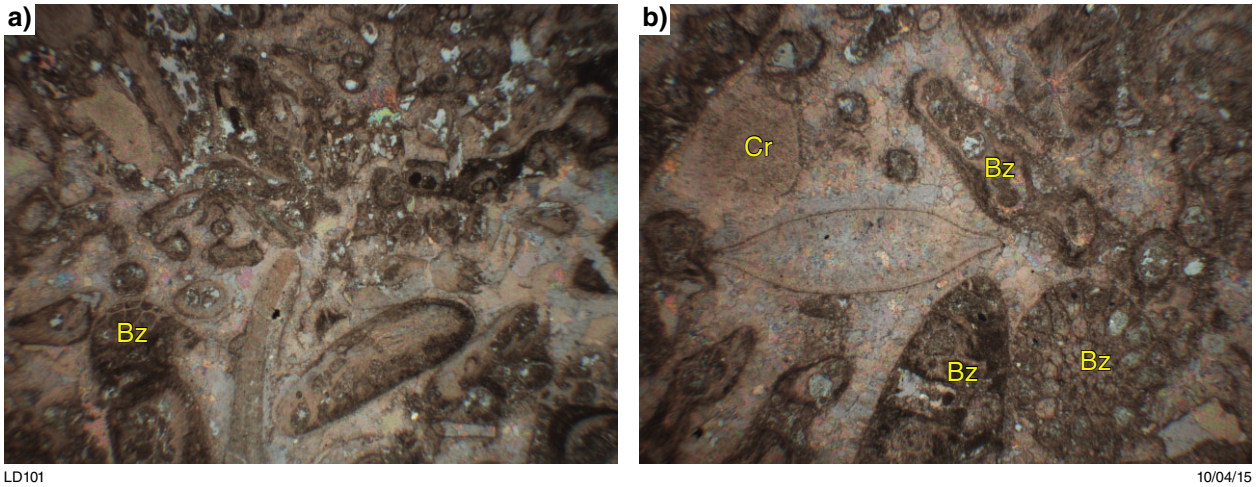


**Figure 3.9.** **a) Grain composition and characteristics showing bioclasts supported by equant carbonate cement, FOV: 11 mm; b) showing the dominance of bryozoan bioclasts, crinoid fragments and grain replacement by carbonate cements, FOV: 5.5 mm. Bryozoans (Bz) and crinoids (Cr)**

# Perindi 1

**Depth**: 875.88 m **Formation**: Nura Nura Member **Facies**: Lps

## SKELETAL PACKSTONE

### Texture and fabric

**Grain size**: average 2 mm; range 0.5 – 3 mm

**Shape**: rounded **Sorting**: poor **Contacts**: point

### Detrital composition

This sample is composed of highly fragmented, well-rounded, skeletal bioclasts dominantly bryozoans (~70%) with minor crinoid fragments (~10%) and brachiopods (~10%). Small, angular quartz grains form thin lags (~1%). Unidentified clasts constitute the remainder of the assemblage.

### Diagenetic features

Pervasive, equant, calcite cement constitutes ~30 % of the overall sample, and micrite ~20%. Both form in internal skeletal cavities and in intergranular spaces. Fibrous calcite encloses some grains and dissolution and recrystallization of crinoid fragments is observed.

### Diagenetic sequence

Point contacts and cement-supported grains indicate formation of equant calcite during deposition. Fibrous calcite enclosing grains indicates two main phases of cementation.

### Porosity

**Proportion of sample**: <5%

**Style**: Primary porosity, intergranular and intragranular, occurring in the skeletal cavities of bioclasts

**Infill**: Extensive infill with equant carbonate cement and micrite

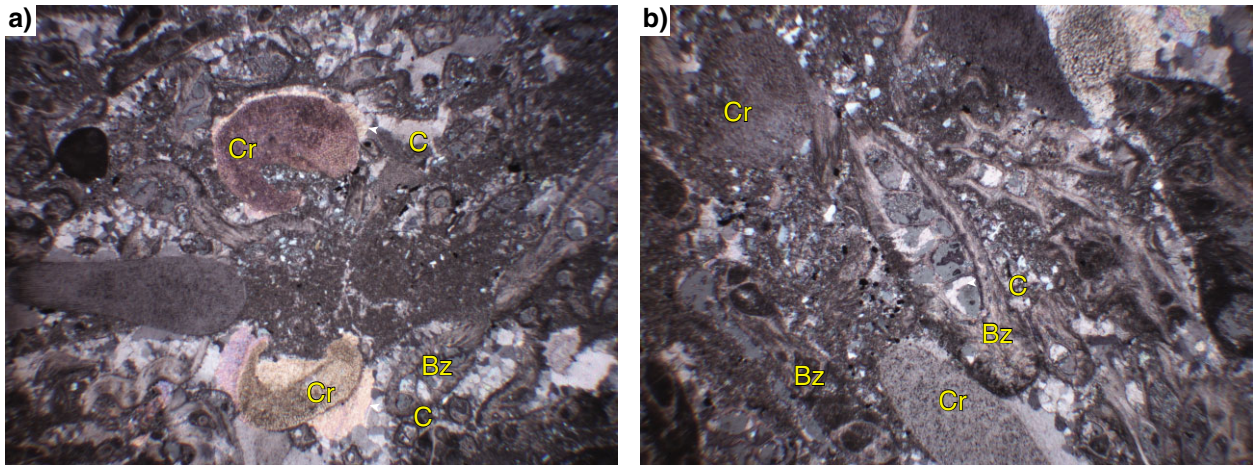


**Figure 3.10. a) Grain characteristics showing crinoid fragments with cemented rims, FOV: 11 mm; b) grain composition showing the dominance of bryozoan bioclasts, some crinoid fragments and the infill of skeletal cavities by carbonate cements, FOV 5.5 mm. Crinoids (Cr), bryozoans (Bz) and carbonate cements (C)**

# Perindi 1

**Depth**: 876.78 m **Formation**: Nura Nura Member **Facies**: Lgs

## SKELETAL GRAINSTONE

### Texture and fabric

**Grain size**: average 0.1 mm; range 0.2 – 0.5 mm

**Shape**: rounded **Sorting**: poor **Contacts**: point

### Detrital composition

This sample is composed of highly fragmented, well-rounded, skeletal bioclasts dominantly bryozoans (~75%) with some crinoid fragments (~10%) and brachiopods (~5–10%). Planktonic foraminifera, bivalves and a few unidentified clasts constitute the remainder of the assemblage.

### Diagenetic features

Pervasive, equant, calcite cement constitutes ~40–50% of the overall sample. The cement forms in internal skeletal cavities and in intergranular spaces. Dissolution and replacement of some bioclasts with equant carbonate cement is observed. Poorly defined fibrous calcite rims are present on many grains.

### Diagenetic sequence

Point contacts and cement-supported grains indicate formation of equant calcite during deposition. Fibrous calcite enclosing grains indicates two main phases of cementation.

### Porosity

**Proportion of sample**: <5%

**Style**: Primary porosity, intergranular and intragranular, in the skeletal cavities of bioclasts

**Infill**: Extensive infill with equant carbonate cement

# PND 1

**Depth**: 259.8 m **Formation**: Noonkanbah Formation **Facies**: Smc

## CONGLOMERATE

### Texture and fabric

**Grain size**: average 0.1 mm (matrix); 0.5 – 1 cm range in clast size

**Shape**: subangular – angular **Sorting**: poor **Contacts**: point

### Detrital composition

The sample consists of 80% quartz (dominantly monocrystalline, with a few polycrystalline grains) with ~12% carbonate grains constituting ~10% bioclasts and 1–2% ooids. Bioclasts are mostly whole bivalves or brachiopods and gastropods, but there are also rare fragments of bryozoans and coralst. Minor microcline (<5%), biotite (<5%) and sedimentary lithic clasts (2%) are also present.

### Diagenetic features

Quartz overgrowths and kaolinite are minor, <5% of the sample each. Equant carbonate cement is pervasive (~30–40% of the sample) and occupies intergranular space and the skeletal cavities of bioclasts. Dissolution of quartz and feldspar is extensive and grain replacement by carbonate cement is common.

### Diagenetic sequence

Crosscutting relationships indicate that quartz overgrowths formed first, followed by kaolinite, and carbonate cement formed last. Dissolution ranges from minor dissolution of the grain rims to whole grain consumption, indicating a continual process.

### Porosity

**Proportion of sample**: <5%

**Style**: Primary, intragranular and intragranular, in the skeletal cavities of bioclasts. Minor secondary porosity has been created by grain dissolution

**Infill**: Major infill by carbonate cement with minor infill by quartz overgrowths

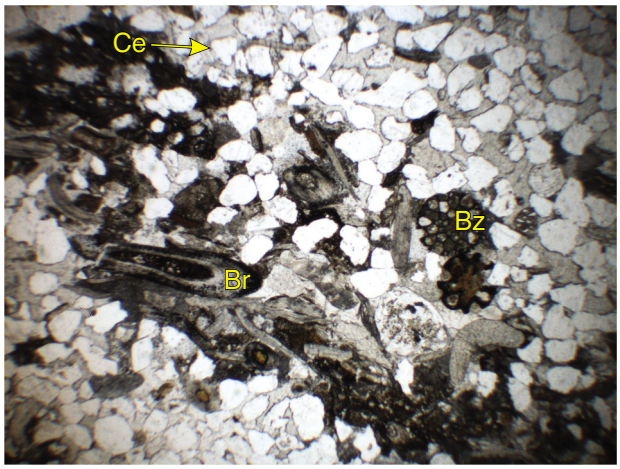


LD55 13/06/16

**Figure 3.11. Grain composition and characteristics showing bioclasts and intergranular carbonate cement, FOV: 5.5 mm. Brachiopod (Br), bryozoan (Bz) and equant carbonate (Ce)**

# PND 1

**Depth**: 300 m **Formation**: Noonkanbah Formation **Facies**: Gmc

## CONGLOMERATE

### Texture and fabric

**Grain size**: average 0.1 mm (matrix); 0.5 – 1 cm range in clast size

**Shape**: subangular – angular **Sorting**: poor **Contacts**: point

### Detrital composition

The sample consists of 50% quartz (dominantly monocrystalline, with a few polycrystalline grains) and detrital clay (30%), plus ~10% subround, quartz-rich, lithic sedimentary clasts, and minor microcline (1–2%) and trace alkali feldspars (<1%). Carbonate grains, including ooids (1–2%) and unidentified bioclasts (2–3%), form the remainder of the detrital assemblage.

### Diagenetic features

Fibrous carbonate cement (5%) partially to fully encloses all carbonate grains, and some quartz and plagioclase grains. Patchy carbonate cement is abundant (20%). Dissolution of plagioclase feldspars and replacement with patchy carbonate cements is common. Detrital clays show minor alteration to kaolinite (<1%). Vertical, carbonate-filled veins cut across grains and cements.

### Diagenetic sequence

Fibrous carbonates formed first followed by patchy carbonate with vertical carbonate veins formed last cutting across all other diagenetic products.

### Porosity

**Proportion of sample**: <5%

**Style**: Primary, intragranular, within sedimentary lithic clasts

**Infill**: Minor infill by patchy carbonate cement, with minor influence from fibrous and carbonate veins

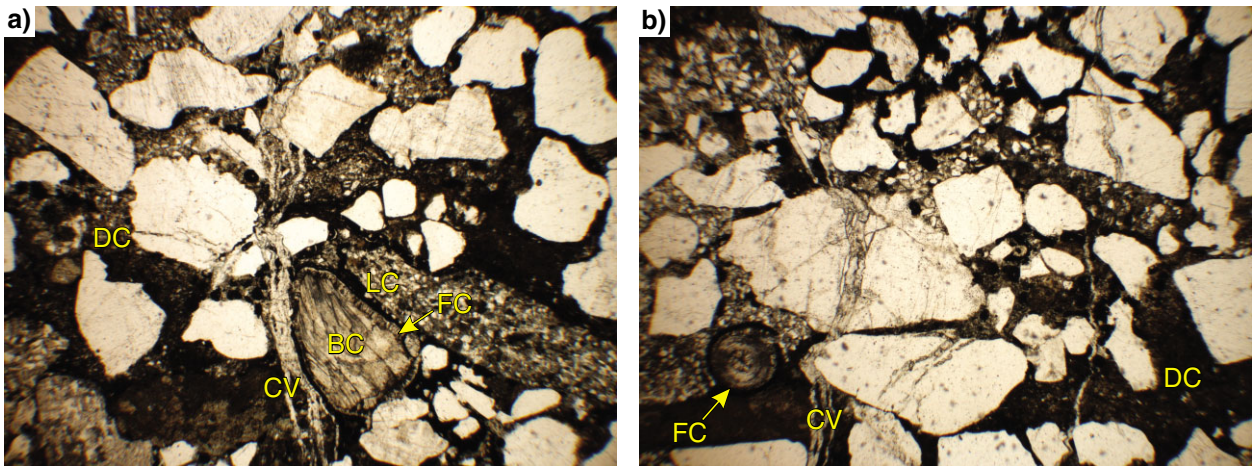


**Figure 3.12. a) Grain composition and characteristics showing subangular to angular quartz grains and abundant detrital clay, FOV: 11 mm; b) fibrous carbonate cement surrounding bioclasts and carbonate filled grains crosscutting detrital quartz, FOV: 5.5 mm. Detrital clay (DC), lithic sedimentary clasts (LC), carbonate bioclast (BC), fibrous carbonate cement (FC) and carbonate veins (CV)**

# PND 1

**Depth**: 307.8 m **Formation**: Noonkanbah Formation **Facies**: Smb

## QUARTZARENITE (Q:98 F:2 R:0)

### Texture and fabric

**Grain size**: average 0.3 mm; range 0.25 – 0.5 mm

**Shape**: rounded **Sorting**: very well **Contacts**: elongate

### Detrital composition

The sample is composed predominantly of quartz (~85%), mostly monocrystalline quartz, with a few polycrystalline grains. Detrital clays (10%) are present as thin to thick laminae or drapes. Small amounts of plagioclase feldspar (<5%), microcline (<5%) and biotite (1–2%) are present, along with trace amounts of muscovite (<1%).

### Diagenetic features

Quartz cement forms rims around detrital quartz grains (5%), and rims are well developed on most grains. Patchy kaolinite (<5%) and very minor patchy carbonate cement (<1%) occupy intergranular spaces. Chlorite is also present in very small quantities (<1%). Siderite is common (10%).

### Diagenetic sequence

Quartz overgrowth rims were the first to form, overprinted by kaolinite then carbonate, and finally iron-oxide cements.

### Porosity

**Proportion of sample**: <5%

**Style**: Primary, intergranular; within sedimentary lithic clasts

**Infill**: Major infill by siderite; minor infill by quartz overgrowths, kaolinite and patchy carbonate cement

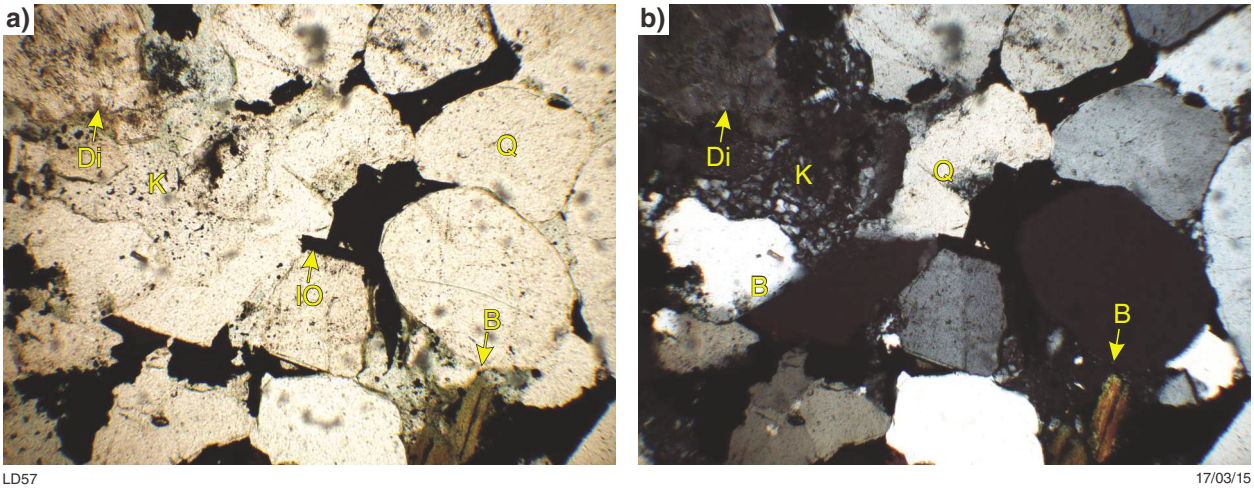


**Figure 3.13. a) Grain composition and characteristics viewed in plane-polarized light showing abundance of rounded detrital quartz grains and the infill of intergranular space by clay and cement phases, FOV: 2 mm; b) same as view in a) under cross-polarized light. Detrital quartz (Q), kaolinite (K), biotite (B), iron oxide (IO) and dissolution (Di)**

# PND 1

**Depth**: 317 m **Formation**: Noonkanbah Formation **Facies**: Sfx

## QUARTZARENITE (Q:99 F:1 R:0)

### Texture and fabric

**Grain size**: average 0.3 mm; range 0.1 – 0.4 mm

**Shape**: subangular to angular **Sorting**: very well **Contacts**: elongate

### Detrital composition

The sample consists of ~95% quartz (dominantly monocrystalline with a few polycrystalline grains). Detrital clays (5%) are present as clasts and as thin rims around grains. Plagioclase feldspar, microcline, biotite, muscovite and carbonaceous material are all present in trace quantities (<1%).

### Diagenetic features

Formation of quartz rims is minor (<5%) and does not occur on all grains. Patchy kaolinite is also present forming in small quantities (<5%) in intergranular space. Alteration to kaolinite is observed on many plagioclase grains.

### Diagenetic sequence

Quartz rims were the first to form, followed by kaolinite, indicated by their crosscutting relationships.

### Porosity

**Proportion of sample**: 20%

**Style**: Porosity is predominantly primary, intergranular, with minor secondary porosity created by the dissolution of feldspars

**Infill**: Minor infill with quartz cement and kaolinite

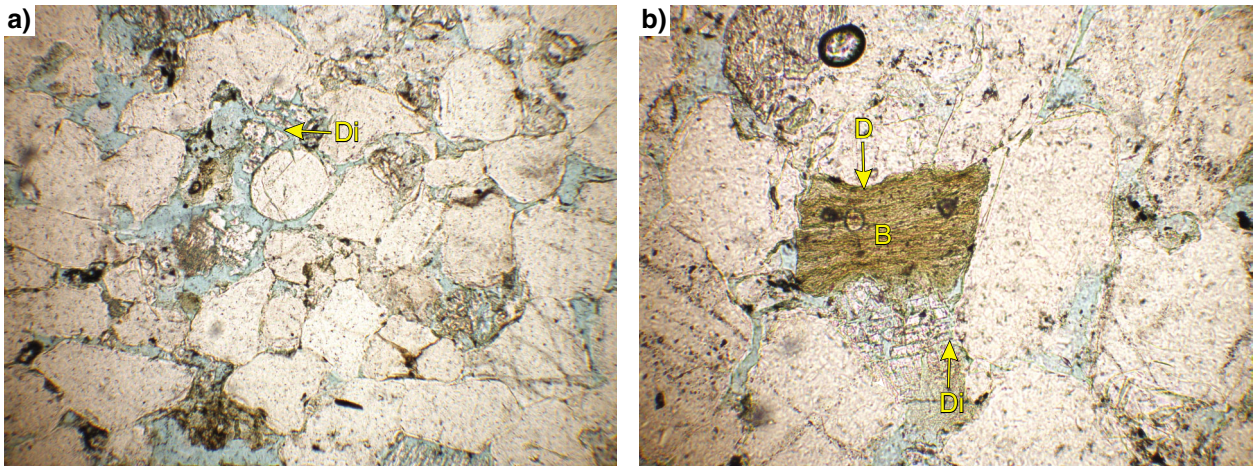


**Figure 3.14. a) Grain composition and characteristics illustrating high level of intergranular porosity (blue) and the development of secondary porosity by grain dissolution, FOV: 5.5 mm; b) deformation of biotite grain and dissolution of plagioclase, FOV: 2mm. Biotite (B), deformation (D) and dissolution (Di)**

# PND 1

**Depth**: 323.4 m **Formation**: Poole Sandstone **Facies**: Sx

## QUARTZARENITE

### Texture and fabric

**Grain size**: average 1 mm; range 0.25 – 1.4 mm

**Shape**: subrounded **Sorting**: moderate **Contacts**: elongate

### Detrital composition

This sample is composed predominantly of monocrystalline quartz (~70%) and polycrystalline quartz (~15%) with some plagioclase feldspar (~5–10%) and quartz-rich lithic sedimentary grains (~5%). Trace amounts (<1%) of microcline, chert, biotite and muscovite were present, and a single grain of zebraic chalcedony was observed.

### Diagenetic features

Quartz rims are present on most grains and constitute ~5% of the sample. Kaolinite is present and has a patchy distribution in intergranular spaces (<5%). Plagioclase feldspars are extensively dissolved.

### Diagenetic sequence

Quartz rims were the first to form, followed by kaolinite, indicated by their crosscutting relationships.

### Porosity

**Proportion of sample**: 25%

**Style**: Porosity is predominantly primary, intergranular, with minor secondary porosity created by the dissolution of feldspars

**Infill**: Minor infill with quartz cement and kaolinite

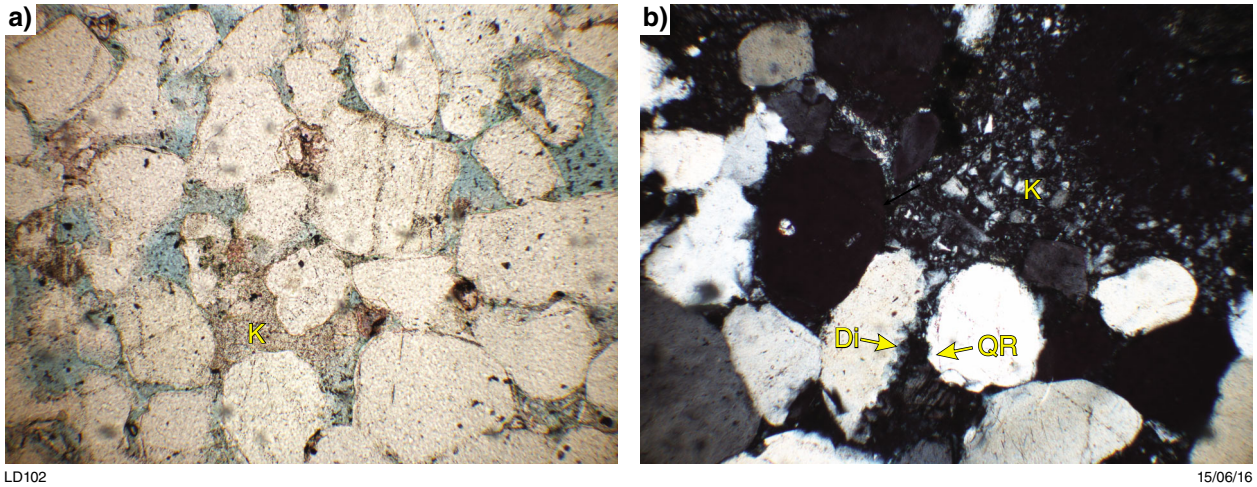


**Figure 3.15. a) Grain composition and characteristics showing high levels of intergranular porosity, FOV: 11 mm; b) authigenic composition showing quartz rims and kaolinite infilling pore spaces, and dissolution of microcline grain, FOV: 2 mm. Quartz rim (QR), kaolinite (K) and dissolution (Di)**

# PND 1

**Depth**: 323.4 m **Formation**: Poole Sandstone **Facies**: Sx

## QUARTZARENITE

### Texture and fabric

**Grain size**: average 1 mm; range 0.25 – 1.4 mm

**Shape**: subrounded **Sorting**: moderate **Contacts**: elongate

### Detrital composition

This sample is composed predominantly of monocrystalline quartz (~70%) and polycrystalline quartz (~15%) with some plagioclase feldspar (~5–10%) and quartz-rich lithic sedimentary grains (~5%). Trace amounts (<1%) of microcline, chert, biotite and muscovite were present, and a single grain of zebraic chalcedony was observed.

### Diagenetic features

Quartz rims are present on most grains and constitute ~5% of the sample. Kaolinite is present and has a patchy distribution in intergranular spaces (<5%). Plagioclase feldspars are extensively dissolved.

### Diagenetic sequence

Quartz rims were the first to form, followed by kaolinite, indicated by their crosscutting relationships.

### Porosity

**Proportion of sample**: 25%

**Style**: Porosity is predominantly primary, intergranular, with minor secondary porosity created by the dissolution of feldspars

**Infill**: Minor infill with quartz cement and kaolinite

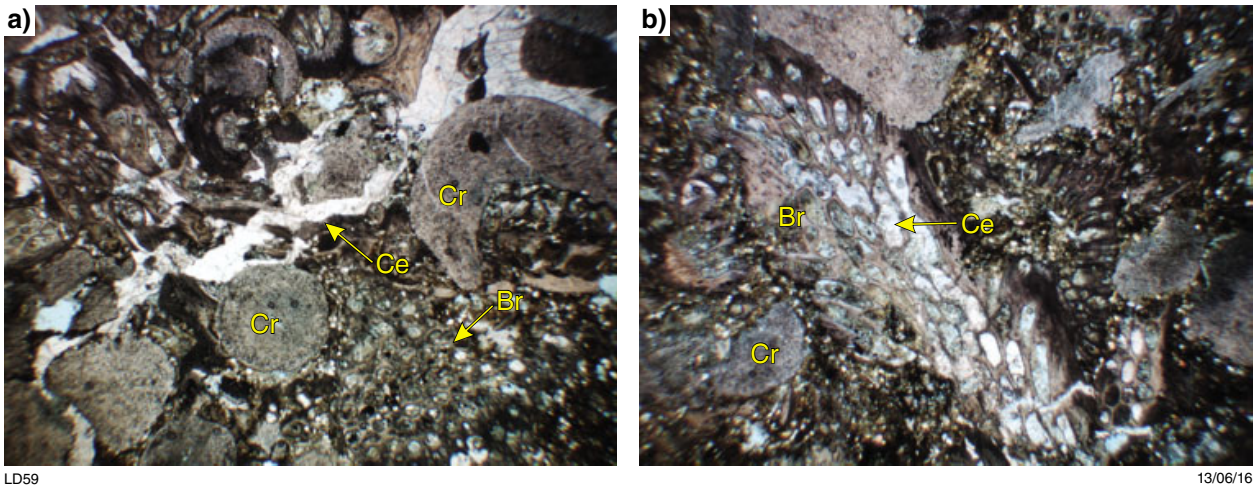


**Figure 3.16. a) Grain composition and distribution of packstone; crinoids are the most abundant bioclast with some bryozoans; carbonate-filled vein also shown, FOV: 11 mm; b) bryozoan fragment with intragranular space both filled and not filled by carbonate cement, FOV: 5.5 mm. Crinoid fragment (Cr), bryozoan fragment (Br) and carbonate cement (Ce)**

# Scarpia 1

**Depth**: 488.1 m **Formation**: Poole Sandstone **Facies**: Hm

## SILTSTONE

### Texture and fabric

**Grain size**: average 0.2 mm; range 0.05 – 0.25 mm

**Shape**: subangular **Sorting**: well **Contacts**: elongate

### Detrital composition

This sample is dominated by quartz (~55%) with abundant carbonaceous material (~30%), minor biotite (5–10%), plagioclase feldspar (5%), detrital clay (5%) and muscovite (1–2%), and trace microcline (<1%). Carbonaceous material is concentrated in thin laminae; muscovite is also more common along these laminae.

### Diagenetic features

Chlorite is abundant (10%), mainly derived from the alteration of biotite. Kaolinite is also abundant (10%), present in intergranular spaces and replacing both quartz and feldspar.

### Diagenetic sequence

Chlorite overprints kaolinite indicating that kaolinite was the first clay to form.

### Porosity

**Proportion of sample**: 5–10 %

**Style**: Primary, intergranular with some secondary porosity created by the dissolution of quartz and feldspars

**Infill**: Infill mainly by kaolinite; chlorite has a minor contribution to porosity reduction

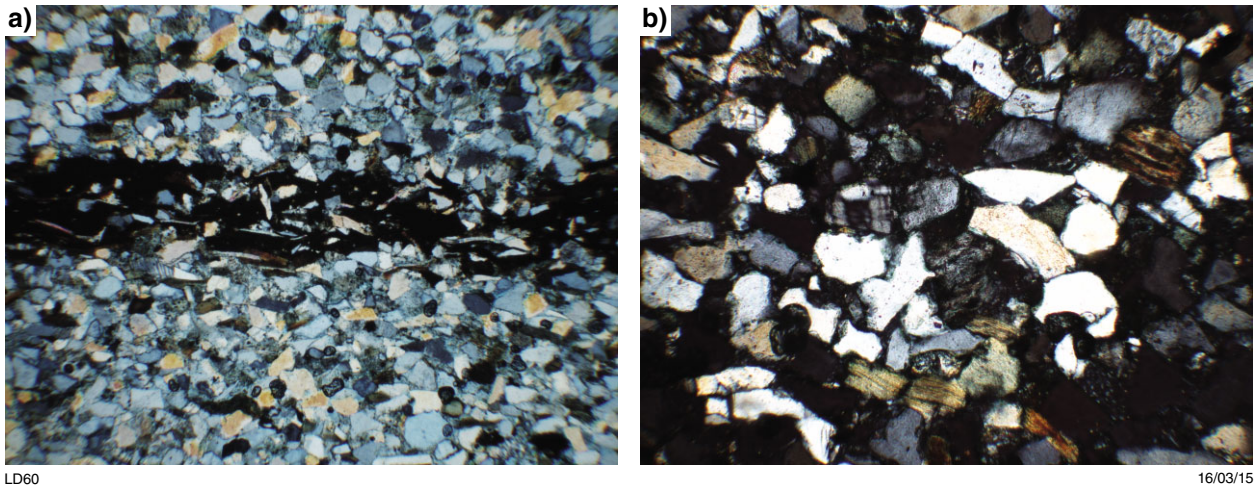


**Figure 3.17. a) Grain composition and characteristics showing abundant carbonaceous material concentrated into laminae, FOV: 5.5 mm; b) quartz and common biotite grains, FOV: 2 mm**

# Scarpia 1

**Depth**: 493 m **Formation**: Noonkanbah Formation **Facies**: Sff

## QUARTZARENITE

### Texture and fabric

**Grain size**: average 0.15 mm; range 0.05 – 0.2 mm

**Shape**: subangular **Sorting**: well **Contacts**: point–elongate

### Detrital composition

This sample is dominated by quartz (~85%) with biotite (5–10%), minor plagioclase feldspar (2%) and microcline (2%), and trace muscovite (<1%).

### Diagenetic features

Chlorite (10%) forms in intergranular spaces and replaces biotite forming orthochlorite; degree of replacement varies. Dissolution of plagioclase and replacement by chlorite is also observed. Biotite grains show evidence of ductile deformation.

### Diagenetic sequence

Chlorite is not deformed with biotite grains indicating that compaction occurred before chlorite formation.

### Porosity

**Proportion of sample**: 5%

**Style**: Primary, intergranular

**Infill**: Minor infill by chlorite

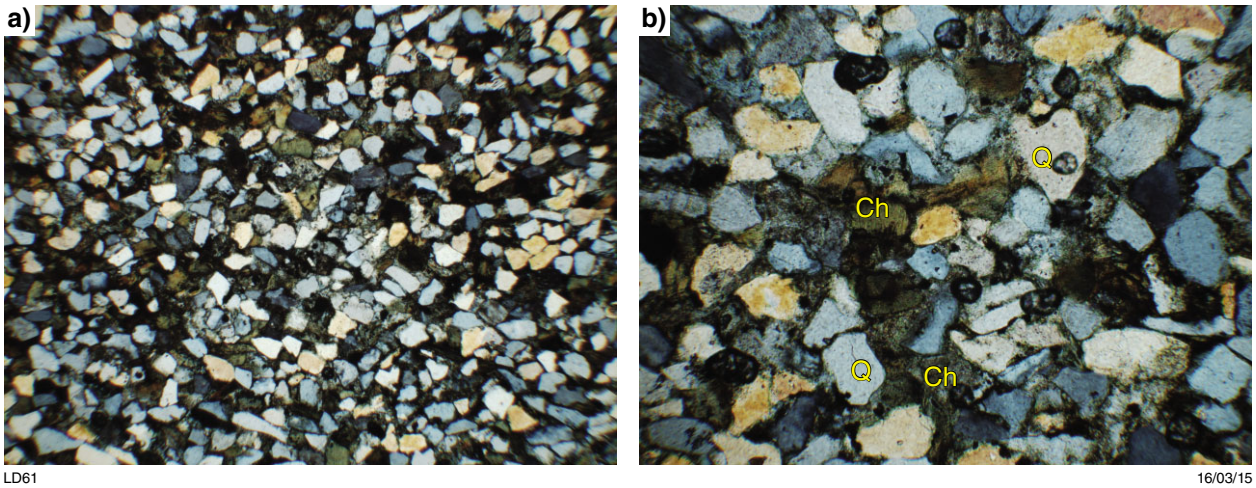


**Figure 3.18. a) Grain composition and characteristics showing abundance of quartz and biotite, FOV: 5.5 mm; b) showing replacement of biotite to chlorite, FOV: 1 mm. Detrital quartz (Q) and chlorite (Ch)**

# Scarpia 1

**Depth**: 495.1 m **Formation**: Noonkanbah Formation **Facies**: Gm

## SUBLITHARENITE

### Texture and fabric

**Grain size**: average 0.1 mm (matrix); 0.5 – 2 mm range in clast size

**Shape**: rounded to subangular **Sorting**: poor **Contacts**: point–elongate

### Detrital composition

This sample is dominated by quartz (~75%); smaller grains are subangular and larger grains are rounded. Detrital clay comprises ~10% of the sample as angular–rounded clasts, and quartz-dominated, sedimentary, lithic clasts also constitute ~10%. Plagioclase feldspar, microcline and biotite are minor at ~2% of the sample each.

### Diagenetic features

Quartz overgrowths are present on some grains (~5% of the total sample); chlorite also constitutes ~5% of the sample and forms as a replacement of biotite and some plagioclase and quartz grains. Different stages of alteration are present and orthobiotite is common. Kaolinite is minor, replacing detrital clay (<5%).

### Diagenetic sequence

Quartz overgrowths formed first followed by kaolinite then chlorite, as indicated by overprinting relationships.

### Porosity

**Proportion of sample**: 15%

**Style**: Primary, intergranular, small amounts of secondary porosity are created by the dissolution of plagioclase grains

**Infill**: Major fill by chlorite, minor fill by quartz overgrowths and kaolinite

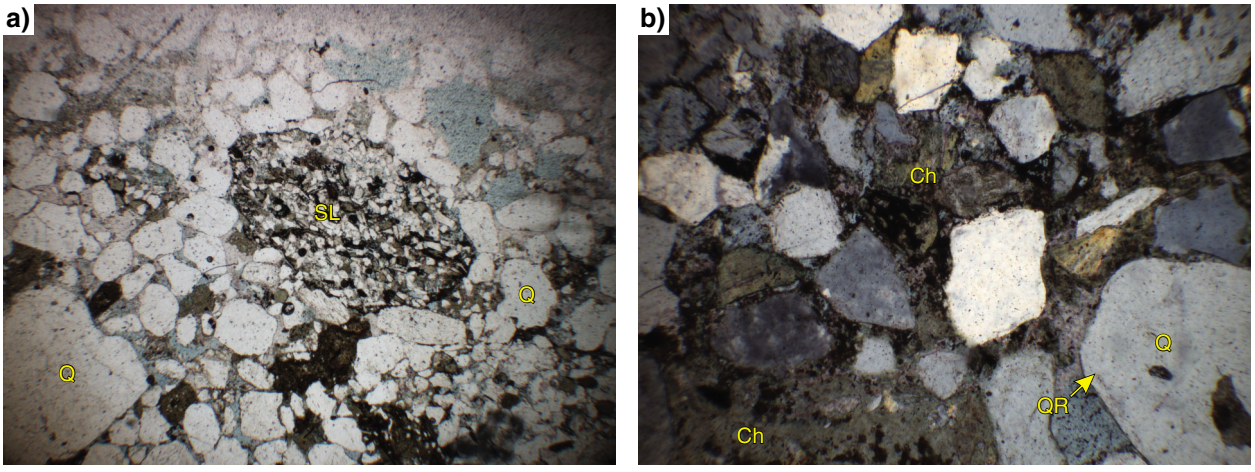


**Figure 3.19. a) Grain composition and characteristics showing sedimentary lithic fragment and detrital quartz, FOV: 11 mm; b) diagenetic features, quartz rims and extensive replacement of biotite by chlorite, FOV: 5.5 mm. Detrital quartz (Q), sedimentary lithic fragment (SL), quartz rim (QR) and chlorite (Ch)**

# Scarpia 1

**Depth**: 496 m **Formation**: Noonkanbah Formation **Facies**: Sfx

## SUBFELDSARENITE

### Texture and fabric

**Grain size**: average 0.5 mm; range 0.1 – 0.7 mm

**Shape**: subrounded **Sorting**: moderate to poor **Contacts**: elongate

### Detrital composition

This sample is dominated by quartz (~65%) with detrital clay (~20%) and plagioclase feldspar (~15%). Detrital clay occurs as both thin laminae and rims around other detrital grains. Trace quantities (<1%) of microcline, biotite and carbonaceous material are present.

### Diagenetic features

Kaolinite is abundant, filling intergranular space (~10%), quartz overgrowths are present on some grains (~5% of the total sample), and minor chlorite is also present (<5%). Chlorite forms as an alteration product of biotite and as a replacement when plagioclase feldspars have been dissolved. Patchy calcite cement is present in very minor amounts.

### Diagenetic sequence

Quartz overgrowths formed first followed by kaolinite, indicated by their crosscutting relationship. Chlorite formation followed kaolinite and calcite formed last.

### Porosity

**Proportion of sample**: 25%

**Style**: Primary, intergranular, small amounts of secondary porosity created by the dissolution of plagioclase grains

**Infill**: Kaolinite is the main pore-filling clay with minor fill by quartz overgrowths, chlorite and carbonate cement

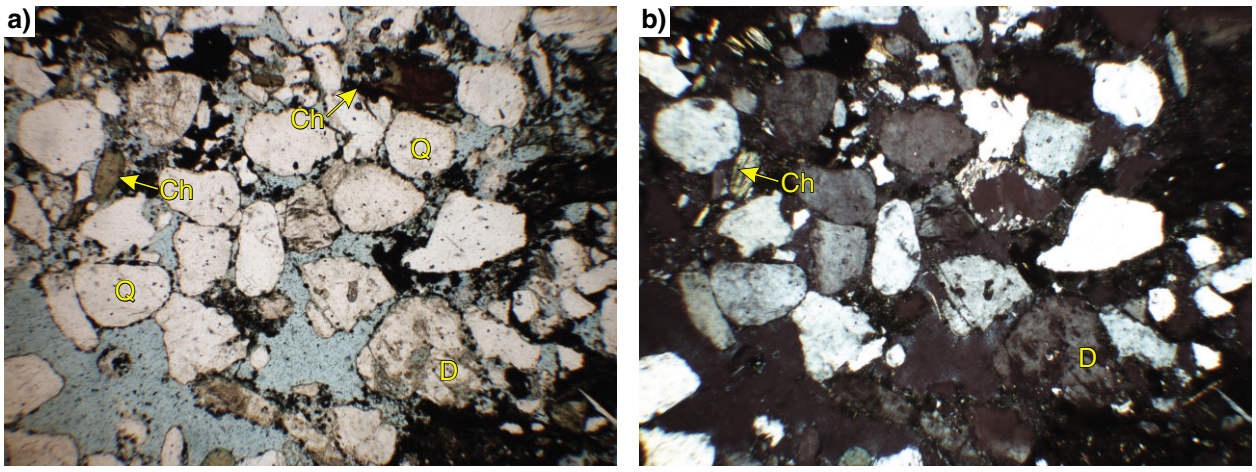


**Figure 3.20. a) Grain composition and characteristics showing abundance of quartz, alteration of biotite to chlorite, and dissolution of plagioclase feldspars; plane-polarized light, FOV: 4 mm; b) same view as in (a) in cross-polarized light, FOV: 4 mm. Detrital quartz (Q), chlorite (Ch) and dissolution feature (D)**

# Sundown 3H 1

**Depth**: 908.8 m **Formation**: Grant Group **Facies**: Sx

## SUBFELSARENITE

### Texture and fabric

**Grain size**: average 0.4 mm; range 0.2 – 0.5 mm

**Shape**: rounded **Sorting**: well **Contacts**: elongate–sutured

### Detrital composition

This sample is dominated by quartz (~90%) with minor plagioclase feldspar (~5%), microcline (~2%), and trace detrital clay and chert (<1%).

### Diagenetic features

Quartz overgrowths are well developed, sutured in places, and constitute 5% of the whole sample. Fracturing of quartz grains and suturing of contacts is observed but not common. Kaolinite is present in intergranular space (<5%). Minor dissolution of quartz and plagioclase grains is observed.

### Diagenetic sequence

Quartz overgrowths formed first followed by kaolinite as indicated by their crosscutting relationships.

### Porosity

**Proportion of sample**: 25%

**Style**: Primary, intergranular with minor secondary porosity created by the dissolution of grains

**Infill**: Infill by quartz overgrowths with minor intergranular occlusion by kaolinite

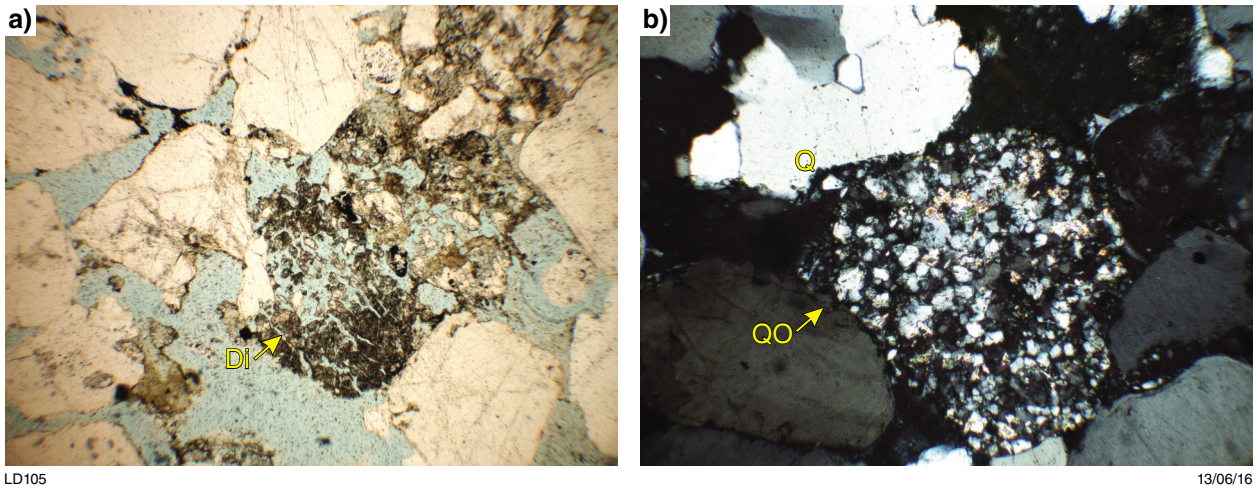


**Figure 3.21. a) Grain composition and characteristics showing abundance of quartz and high intergranular porosity, FOV: 5.5 mm; b) authigenic characteristics, quartz overgrowths filling intergranular spaces, and feldspar dissolution creating secondary porosity, FOV: 2 mm. Detrital quartz (Q), quartz overgrowths (QO) and dissolution (Di)**

# Sundown 3H 1

**Depth**: 912.3 m **Formation**: Grant Group **Facies**: Sx

## SUBFELSARENITE

## Texture and fabric

**Grain size**: average 0.3 mm; range 0.1 – 0.4 mm

**Shape**: rounded **Sorting**: well **Contacts**: elongate–sutured

## Detrital composition

This sample is dominated by quartz (90–95%) with minor plagioclase feldspar (5%) and trace microcline (<1%).

## Diagenetic features

Quartz overgrowths are well developed and constitute 10% of the whole sample. Edges of quartz grains show minor fracturing. Kaolinite is present in intergranular space (10%). Minor dissolution of quartz and plagioclase grains is observed, some replacement of dissolved plagioclase grains by kaolinite is observed.

## Diagenetic sequence

Quartz overgrowths formed first followed by kaolinite, as indicated by their crosscutting relationships. Dissolution ranges from minor dissolution of grain rims to whole-grain consumption, indicating that it is a continuous process.

## Porosity

**Proportion of sample**: 15%

**Style**: Primary, intergranular with minor secondary porosity created by the dissolution of grains

**Infill**: Infill by quartz overgrowths and kaolinite

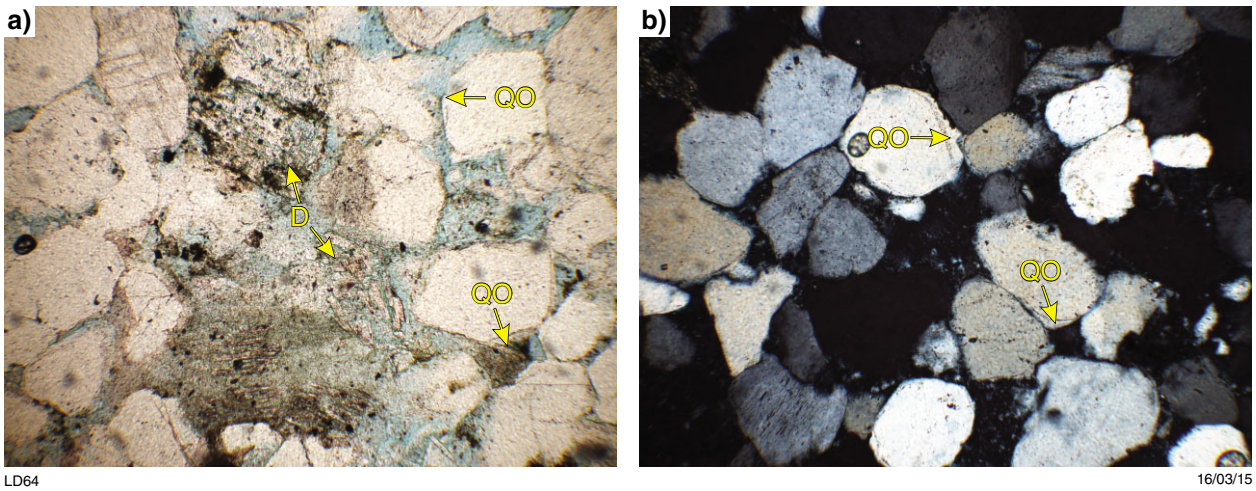


**Figure 3.22. a) Grain composition and characteristics showing quartz overgrowths and dissolution of plagioclase feldspar, FOV: 2 mm; b) authigenic characteristics in cross-polarized light, showing well-developed quartz overgrowths and kaolinite occluding intergranular space, FOV: 2 mm. Quartz overgrowths (QO), dissolution feature (D)**

# Whitewell 1

**Depth**: 863.5 m **Formation**: Grant Group **Facies**: Sfx

## SUBFELDSARENITE (Q:98 F:2 R:0)

### Texture and fabric

**Grain size**: average 0.25 mm; range 0.1 – 0.3 mm

**Shape**: subrounded **Sorting**: moderate **Contacts**: elongate–sutured

### Detrital composition

This sample is dominated by quartz (90%) with minor plagioclase feldspars (<5%) and detrital clay (<5%), and trace muscovite sedimentary lithic fragments and zircon (each <1%).

### Diagenetic features

Moderate to well-developed quartz overgrowths, patchy kaolinite filling intergranular space, and minor patchy carbonate cement are also present in intergranular space.

### Diagenetic sequence

Quartz overgrowths formed first followed by kaolinite, indicated by their crosscutting relationship. Carbonate cement overprints kaolinite, indicating that it formed last.

### Porosity

**Proportion of sample**: <5%

**Style**: Primary, intergranular, with minor secondary porosity created by grain dissolution

**Infill**: Significant infill by kaolinite; less significant infill by quartz overgrowths and calcite cement

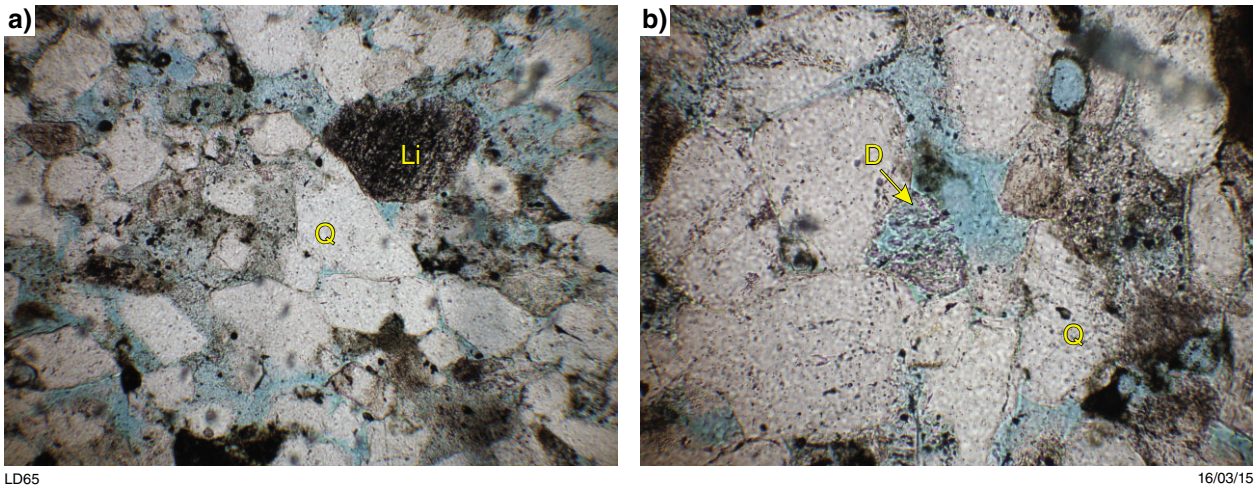


**Figure 3.23. a) Grain composition and characteristics showing dominance of quartz and presence of sedimentary lithic fragment, FOV: 2 mm; b) authigenic features, dissolution of plagioclase feldspar creating secondary porosity, FOV: 1 mm. Detrital quartz (Q), lithic fragment (Li) and dissolution feature (D)**

# Whitewell 1

**Depth**: 868.5 m **Formation**: Grant Group **Facies**: Sx

## SUBFELDSARENITE (Q:80 F:10 R:10)

### Texture and fabric

**Grain size**: average 0.5 mm; range 0.1 – 1 mm

**Shape**: subrounded **Sorting**: moderate **Contacts**: elongate

### Detrital composition

This sample is dominated by quartz (80%) with minor plagioclase feldspars (5–10%) and lithic grains (10%), minor brown detrital clays (2%), and trace chert (<1%). Lithic fragments are metamorphic and have a textured appearance.

### Diagenetic features

Kaolinite forms in patches filling intergranular space (10–15% of the sample). Quartz overgrowths are well developed and constitute 5–10% of the sample. Grain rims are fractured; however, fractures are not seen in overgrowths, possibly due to annealing. Alteration of plagioclase grains to muscovite is observed.

### Diagenetic sequence

Quartz overgrowths formed first followed by kaolinite, indicated by their crosscutting relationship.

### Porosity

**Proportion of sample**: 20%

**Style**: Primary, intergranular

**Infill**: Infill by both kaolinite and quartz overgrowths

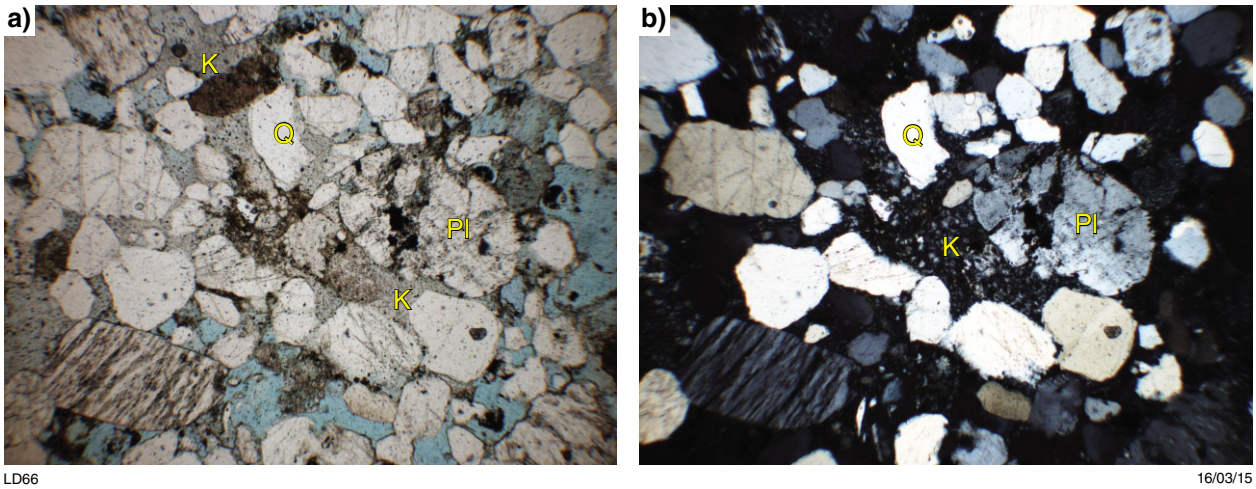


**Figure 3.24. a) Grain composition and characteristics showing extensive intergranular porosity (blue stain) and reduction of this pore space by kaolinite, FOV: 11 mm; b) authigenic features, dissolution of plagioclase feldspar and distribution of kaolinite, FOV: 1 mm. Detrital quartz (Q), plagioclase feldspar (Pl) and kaolinite (K)**

# Whitewell 1

**Depth**: 870.16 m **Formation**: Grant Group **Facies**: Sx

## SUBFELDSARENITE (Q:85 F:15 R:0)

### Texture and fabric

**Grain size**: average 0.25 mm; range 0.1 – 0.5 mm

**Shape**: subangular **Sorting**: moderate **Contacts**: elongate

### Detrital composition

This sample is dominated by quartz (~80%) with minor plagioclase feldspar (~10%), microcline (~5%), brown detrital clays (5%) and carbonaceous material (2%), which is concentrated in fine planar laminae.

### Diagenetic features

Moderate to well-developed quartz overgrowths. Grain rims are fractured; however, fracturing is not observed in overgrowths possibly due to annealing. Kaolinite is common, present in intergranular space. Ductile deformation of muscovite grains and dissolution of quartz grain rims is also observed.

### Diagenetic sequence

Quartz overgrowths formed first followed by kaolinite, indicated by their crosscutting relationship.

### Porosity

**Proportion of sample**: 20%

**Style**: Primary, intergranular

**Infill**: Infill by both kaolinite and quartz overgrowths

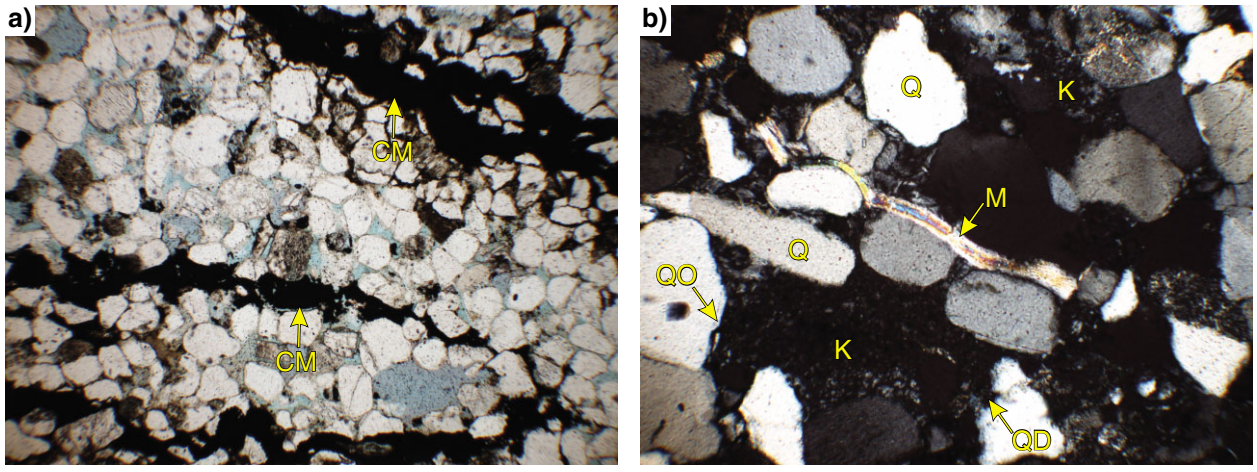


**Figure 3.25. a) Grain composition and characteristics showing laminae of concentrated carbonaceous material, FOV: 5.5 mm; b) authigenic features, quartz overgrowths and kaolinite filling intergranular spaces, FOV: 1 mm. Carbonaceous material (CM), detrital quartz (Q), quartz overgrowth (QO), quartz dissolution (QD), muscovite (M) and kaolinite (K)**

# Appendix 4

## Summary of well log formation picks, and Poole Sandstone and Noonkanbah Formation thicknesses by well

**Table 4.1. Summary of formation picks on well logs and formation thicknesses for the Poole Sandstone and Noonkanbah Formation. All depth and thickness values in metres.**

| *Well* | *Top Noonkanbah Fm.* | *Top Poole Ss.* | *Top Nura Nura Mbr* | *Top Grant* | *Base G1* | *Noonkanbah Fm. thickness* | *Poole Ss. thickness* | *Nura Nura Mbr thickness* | *Casing shoe* | *Palynology available* |
|---|---|---|---|---|---|---|---|---|---|---|
| Aquantia 1 | 545 | 797.4 | – | 867.5 | 927.0 | 252.4 | 70.1 | – | 538.66 | Y |
| Babrongan 1 | 110* | 184.8 | 260.9 | 273 | – | 74.8 | 76.1 | 12.1 | 80.77 | – |
| Bindi 1 | 475.6 | 909.47 | – | 990.2 | – | 433.97 | 80.73 | – | 223 & 849.5 | Y |
| Blackstone 1 | 500 | 780 | – | 834 | 884.97 | 280 | 54 | – | – | Y |
| Blina 1 | 325.27 | 586.5 | – | 632.5 | 680 | 261.23 | 46 | – | – | – |
| Blina 3 | 330 | 591 | – | 638.8 | 685 | 261 | 47.8 | – | 403 | – |
| Blina 4 | 318.3 | 581 | – | 627.7 | 672.95 | 262.7 | 46.7 | – | 363.5 | – |
| Blina 5 | 327.7 | 589.5 | – | 638 | 685 | 261.8 | 48.5 | – | 368.17 | – |
| Blina 7 | 337.9 | 601.5 | – | 651.5 | 699.14 | 263.6 | 50 | – | – | – |
| Blina 8 | 345.1 | 612.4 | – | 659.4 | 699.91 | 267.3 | 47 | – | – | – |
| Booran 1 | 703.2 | 1236.7 | 1301.8 | 1308 | 1363 | 533.5 | 65.1 | 6.2 | – | Y |
| Boronia 1 | 348 | 644 | – | 697 | 755 | 296 | 53 | – | – | – |
| Boundary 1 | 547.5 | 845 | – | 892 | 950 | 297.5 | 47 | – | – | – |
| Boundary Southeast 1 | 542.7 | 841 | – | 889 | 942.9 | 298.3 | 48 | – | – | – |
| Canegrass 1 | 275.9 | 555 | 598 | 602.9 | 643.13 | 279.1 | 43 | 4.9 | 367.2 | – |
| Crab Creek 1 | 486* | 716 | 784.5 | 792 | 832? | 74.8 | 68.44 | 7.5 | 658 | Y |
| Crimson Lake 1 | 277 | 712 | – | 780 | – | 435 | 68 | – | 463 | – |
| Curringa 1 | 583 | 882.7 | 915 | 923 | 978.94 | 299.7 | 32.3 | 8 | 735 | Y |
| Cycas 1 | 0* | 443.3 | – | 536.9 | – | 443.3 | 93.6 | – | 246 | Y |
| Dampier Downs 1 | 316* | 389 | 469 | 482 | – | 73 | 80 | 13 | – | Y |
| East Crab Creek 1 | 447* | 676 | 750 | 758.5 | – | 229 | 74 | 8.5 | 550 | Y |
| East Yeeda 1 | 661.7 | 1148 | – | 1217 | 1302.88 | 486.3 | 69 | – | – | Y |
| Fitzroy River 1 | 4 | 396.6 | – | 498.2 | – | 392.6 | 101.6 | – | – | – |
| Freney 1 | 500* | 745 | 814 | 822 | – | 245 | 69 | 8 | 284 | Y |
| Frome Rocks 2 | 63 | 541.3 | 635.2 | 644.5 | – | 478.3 | 93.9 | 9.3 | – | Y |
| Hakea 1 | 166 | 549.8 | – | 603.5 | – | 383.8 | 53.7 | – | | Y |
| Hangover 1 | 432.5 | 770 | 825.5 | 828 | 892.8 | 337.5 | 55.5 | 2.5 | 488.5 | Y |
| Harold 1 | 6* | 221.8 | – | 260 | 315 | 215.8 | 38.2 | – | 21.3 and 183 | – |
| Janpam 1 | 509.4 | 785 | 837.2 | 841.2 | 888 | 275.6 | 52.2 | 4 | 544 | Y |

**Table 4.1. continued**

| *Well* | *Top Noonkanbah Fm.* | *Top Poole Ss.* | *Top Nura Nura Mbr* | *Top Grant* | *Base G1* | *Noonkanbah Fm. thickness* | *Poole Ss. thickness* | *Nura Nura Mbr thickness* | *Casing shoe* | *Palynology available* |
|---|---|---|---|---|---|---|---|---|---|---|
| Jum Jum 1 | 1110 | 1545 | 1595.9 | 1605 | 1656 | 435 | 50.9 | 10 | – | Y |
| Kambara 1 | 655* | 808 | 843.6 | 854.5 | 894.6 | 153 | 35.6 | 10.9 | 724 | Y |
| Katy 1 | 330 | 704 | – | 760.1 | 833.1 | 374 | 56.1 | – | 458.13 | Y |
| Kennedia 1 | 303 | 600.5 | – | 656.9 | – | 297.5 | 56.4 | – | – | Y |
| Kilang Kilang 1 | 354 | 660.7 | – | 733.4 | 792* | 306.7 | 72.7 | – | 569 | Y |
| Kora 1 | 615.8 | 998 | – | 1047 | 1090* | 382.2 | 49 | – | – | Y |
| Lake Betty 1 | 257.7 | 678 | – | 764 | – | 420.3 | 86 | – | 457.2 | Y |
| Langoora 1 | 245.1 | 539.7 | 579 | 587 | 620.67 | 294.6 | 39.3 | 8 | 580 | Y |
| Lloyd 2 | 528.2 | 822 | – | 868.1 | 921.3 | 293.8 | 46.1 | – | – | – |
| Logue 1 | 164.6* | 448.7 | 505 | 512 | 542? | 284.1 | 56.3 | 7 | 320 | Y |
| Lukins 1 | 49.5 | 306 | – | 351 | 389.0 | 256.5 | 45 | – | 302 | – |
| Mahe 1 | 244.3* | 516 | 607.5 | 615.3 | – | 271.7 | 91.5 | 7.8 | 324 | – |
| Mariana 1 | – | 630 | 678 | 691 | – | – | 48 | 13 | 430.05 | – |
| Meda 1 | 357.1 | 678 | 723 | 730.9 | 759.4 | 320.9 | 45 | 7.9 | 126.5 | Y |
| Meda 2 | 420.5 | 724.5 | 770.5 | 783.8 | 813.4 | 304 | 46 | 13.3 | – | Y |
| Mellany 1 | 173 | 436 | – | 478 | 515 | 263 | 42 | – | 399 | – |
| Metters 1 | 182.25 | 647.2 | – | 730 | 776.9 | 464.95 | 82.8 | – | 495.7 | – |
| Millard 1 | 751.4 | 1178 | – | 1235 | –* | 426.6 | 57 | – | 229 | Y |
| Mimosa 1 | 336.4 | 617 | – | 675 | 755? | 280.6 | 58 | – | – | Y |
| Minjin 1 | 745* | 770 | 819 | 829.6 | | 25 | 49 | 10.6 | 746 | Y |
| Moogana 1 | 820 | 1117.9 | 1159 | 1165.2 | 1197 | 297.9 | 41.1 | 6.2 | 918 | Y |
| Mt Hardman 1 | 14 | 368.2 | – | 413 | 453 | 354.2 | 44.8 | – | 130 | Y |
| Nemelie 1 | 261.8 | 770 | – | 832 | 885? | 508.2 | 62 | – | 304 | – |
| Nerrima 1 | 0* | 485 | – | 597 | 658? | 485 | 112 | – | 347* | – |
| Nollamara 1 | 50* | 122 | – | 232 | 275? | 72 | 110 | – | 83 | Y |
| Notabilis 1 | 138* | 340 | – | 436 | ? | 202 | 96 | – | – | Y |
| Olios 1 | 61 | 270 | – | 305 | – | 209 | 35 | – | 213 | Y |
| Orange Pool 1 | 75 | 320 | – | 359.6 | 415 | 245 | 39.6 | – | 159.7 | – |
| Padilpa 1 | 669.7 | 1041 | – | 1081 | 1150? | 371.3 | 40 | – | 688 | Y |
| Palm Spring 1 | 0* | 485 | – | 597 | 261.7? | 171.6 | 41 | – | 79.85 | Y |

**Table 4.1. continued**

| *Well* | *Top Noonkanbah Fm.* | *Top Poole Ss.* | *Top Nura Nura Mbr* | *Top Grant* | *Base G1* | *Noonkanbah Fm. thickness* | *Poole Ss. thickness* | *Nura Nura Mbr thickness* | *Casing shoe* | *Palynology available* |
|---|---|---|---|---|---|---|---|---|---|---|
| Perindi 1 | – | 828* | 869 | 879.5 | 949.6 | – | 41 | 10.5 | 831.3 | Y |
| Petaluma 1 | 274 | 914.8 | – | 1037.3 | 1070 | 640 | 122.5 | – | 309 | Y |
| Philydrum 1 | 208.6 | 582 | – | 645 | – | 373.4 | 63 | – | 460 | Y |
| PND 1 | 120 | 322 | – | 351 | – | 202 | 29 | – | – | Y |
| Point Moody 1 | 18 | 404 | – | 488.6 | – | 386 | 84.6 | – | 112.26 | Y |
| Point Torment 1 (3 cycyles) | 525 | 894 | – | 944.9 | 992? | 369 | 50.9 | – | 290 | – |
| Puratte 1 | 935.1 | 1435.7 | 1497.5 | 1504 | 1537.5 | 500.6 | 61.8 | 6.5 | – | Y |
| Roebuck Bay 1 | 478* | 538 | 607.9 | 614.2 | 668? | 60 | 69.9 | 6.3 | 163 | Y |
| Runthrough 1 | 646.1 | 981.2 | – | 1031 | 1094.3 | 335.1 | 49.8 | – | 341.3 | – |
| Scarpia 1 | 24 | 514.5 | – | 552 | 606? | 490.5 | 49.8 | – | 448.1 | Y (New) |
| Selenops 1 | 28* | 55 | – | 92 | 160 | 27 | 37 | – | 29 | Y |
| Sundown 1 | 440.5 | 777 | – | 831.5 | 896.7 | 336.5 | 54.5 | – | 484 | Y |
| Sundown 2 | 444 | 785 | – | 840 | 908.4 | 341 | 55 | – | 483.88 | Y |
| Sundown 3H | 437 | 779 | – | 835 | 905 | 342 | 56 | – | 476.6 | Y (New) |
| Sundown 4 | 441.8 | 783 | – | 836.4 | 903.8 | 341.2 | 53.4 | – | 489.7 | – |
| Sundown 5 | 441 | 784.7 | – | 840.3 | 905 | 343.7 | 55.6 | – | – | – |
| Sunup 1 | 319.4 | 756 | 812 | 816 | – | 436.6 | 56 | 4 | 389 | – |
| Tappers Inlet 1* | 618.9 | 929 | 967 | 973.3 | | 310.1 | 38 | 6.3 | 535.2 | Y |
| Terrace 1 | 538 | 827 | – | 879.3 | 933.56 | 289 | 52.3 | – | 537 | Y |
| Thangoo 1 | – | 420* | 444.2 | 456.8 | – | – | 24.2 | 12.6 | 451 | – |
| The Sisters 1 | 159 | 560 | – | 617 | ? | 401 | 57 | – | 243.84 | – |
| Thompsons 1 | 539 | 815 | 868 | 877 | 920 | 276 | 53 | 9 | – | – |
| Wattle 1 | 578 | 901.2 | – | 953 | 1021.75 | 323.2 | 51.8 | – | 613 | – |
| West Blackstone 1 | 483.1 | 766 | – | 812 | 866.3 | 282.9 | 46 | – | 521.27 | – |
| West Kora 1 | 598.9 | 977 | – | 1024 | 1088.8 | 378.1 | 47 | – | 976 | Y |
| West Philydrum 1 | 235 | 579 | | 344 | 700 | 344 | 58 | – | 292 | Y |
| West Terrace 1 | 541 | 824.7 | – | 875 | 930 | 283.7 | 50.3 | – | 539 | – |
| Whitewell 1 | 418.9 | 748.5 | – | 805 | 865 | 329.6 | 56.5 | – | 464.4 | Y (New) |
| Yarrada 1 | 478.5 | 799 | 843 | 848 | 886.45 | 329.6 | 56.5 | 5 | – | – |

**NOTE:** * Indicates where the thickness is eroded; – indicates where a formation or member, or other information, is absent, unidentified or unavailable; (New) indicates the first presentation of palynology results.

# Appendix 5

# Summary of palynological sampling

## Palynological characterization carried out by J Backhouse (Backhouse Biostrat Pty Ltd; written comm., November 2015)

**Table 5.1. Summary of results from Sundown 3H**

| *Depth (m)* | *Palynological zone* | *Age* |
|---|---|---|
| 895.95 | *Pseudoreticulatispora confluens* | Tastubian–Asselian |
| 899 | *Pseudoreticulatispora confluens* | Tastubian–Asselian |
| 903.5 | *Pseudoreticulatispora confluens* | Tastubian–Asselian |

**Table 5.2. Summary of results from Whitewell 1**

| *Depth (m)* | *Palynological zone* | *Age* |
|---|---|---|
| 862.45 | *Pseudoreticulatispora confluens* | Tastubian–Asselian |
| 862.95 | *Pseudoreticulatispora confluens* | Tastubian–Asselian |

# Appendix 6

## Summary descriptions of the Nura Nura Member from well completion records

**Table 6.1. Summary of Nura Nura Member descriptions recorded in well completion records of petroleum wells in the study area**

| *Well* | *Top (m)* | *Base (m)* | *Thickness (m)* | *Lithology* | *Notes* | *Fossils* |
|---|---|---|---|---|---|---|
| Babrongan 1 | 260.9 | 266.4 | 5.5 | Siltstone | Slightly calcareous, thin streaks of fossiliferous calcarenite and calcilutite | Br |
| Booran 1 | 1301 | 1308 | 7 | Limestone | White, very hard, with silt-sized quartz and fossil fragments | Bz, C |
| Canegrass 1 | 598 | 601 | 3 | Shale | Black, with thin, planar sandstone laminae | |
| Crab Creek 1 | 784.5 | 792 | 7.5 | Limestone | Massive, hard-brittle, microcrystalline with occasional sparry fossil remnants | Sp, Si |
| Curringa 1 | No WCR Record | | | | | |
| Dampier Downs 1 | 468.8 | 482.2 | 13.4 | Sandstone and siltstone | Interbedded with calcarenite, abundant fossil fragments | Bz |
| East Crab Creek 1 | 750 | 758.5 | 8.5 | Limestone | White, wackestone–packstone texture, sparry calcite and micrite matrix | Bv, Cr (fragments) |
| East Yeeda 1 | 1200 | 1217 | 17 | Limestone | White-orange, slightly sandy, soft, thin calcilutite beds, maximum bed thickness ~1 m | |
| Feney 1 | 814 | 822 | 8 | Limestone | White, buff, hard, microcrystalline, silty in parts with rare fossil fragments | |
| Frome Rocks 2 | 635.2 | 642.8 | 7.6 | Sandy siltstone | Minor calcilutite and possible limestone? | Bz |
| Hangover 1 | 825.5 | 828 | 2.5 | – | Bryozoans locally abundant from 825.5 – 830 m | Bz |
| Janpam 1 | 838 | 855 | 17 | Sandstone and siltstone | Interbedded | |
| Jum Jum 1 | 1595 | 1605 | 10 | Limestone | Medium to coarse wackestone, occasional thin calcite veins and slightly calcareous siltstone | |
| Kambara 1 | 844 | 852 | 8 | Limestone | | |
| Kora 1 | 1025? | 1047 | 22? | – | | |
| Langoora 1 | 579.1 | 594.3 | 15.2 | – | Rare fossils and traces of calcareous cement | |
| Logue 1 | 500 | 512 | 12 | Limestone | Fossiliferous siltstone grades to fossiliferous limestone | |
| Mahe 1 | 611 | 615 | 4 | Limestone | Rare oolites | Sf (rare) |
| Mariana 1 | 678 | 691 | 13 | | | Br, Cr, S |
| May River 1 | 478.5 | 488.5 | 10 | – | | Br, Bz |
| Meda 1 | 723 | 726 | 3 | Sandstone | Medium grained, calcareous and fossiliferous with very sandy calcarenite and few beds of fossiliferous limestone | Br, Bz |
| Meda 2 | 768 | 787 | 19 | Sandstone and siltstone | Slightly carbonaceous siltstone and fossiliferous calcarenite and sandstone | Bz |

**Table 6.1. continued**

| *Well* | *Top (m)* | *Base (m)* | *Thickness (m)* | *Lithology* | *Notes* | *Fossils* |
|---|---|---|---|---|---|---|
| Minjin 1 | 819 | 827 | 8 | Limestone | White to light grey, finely crystalline with rare to abundant skeletal material and hard calcilututes | C, Es, Br |
| Moogana 1 | 1159 | 1167 | 8 | Mudstone–packstone | | Br, Cr (debris) |
| Perindi 1 | 867 | 877 | 10 | Skeletal grainstone–packstone | Abundant fossil fragments | Br, Bz, Cr, O, S, possible Bv |
| Puratte 1 | 1496 | 1503.5 | 7.5 | Mudstone – crystalline carbonate | Occasionally fossiliferous mudstone grading to crystalline carbonate | Br, Bz |
| Roebuck Bay 1 | 606 | 624 | 18 | Calcarenite | Coarse grained, fossiliferous | Cr (plates), F, Bz |
| Sunup 1 | 812 | 816 | 4 | – | – | |
| Thangoo 1 | 442 | 449 | 7 | Calcarenite | Coarse, highly fossiliferous | Bz, Br, Cr, E |
| Thompsons 1 | 868 | 877 | 9 | – | – | |
| West Kora 1 | 1000 | 1024 | 24 | Crystalline carbonate | Thin beds, hard, white, buff, occurring below 1000 m | |
| Whistler 1 | 434 | 466 | 32 | Calcarenite | Fossiliferous grainstone at 442.9 m | Bz, C, Es, F? |
| Yarrada 1 | 843 | 859 | 16 | Sandstone | Fossiliferous | |

**NOTE**: Fossil names are abbreviated as follows: Bi – Bivalve; Br – Brachiopod; Bz – Bryozoan; C – Coral; Cr – Crinoid; E – Echinoid; Es – Echinoid Spines; F – foraminifera; O – Ostracod; S – Sponge; Si – Spicule; Sf – Shell fragments (undefined); Sp – Spine (unclassified)

# Appendix 7

## Summary of porosity data from petroleum well reports

**Table 7.1. Summary of porosity data from the Nura Nura Member — wells within a 200 km radius of James Price Point**

| *Well* | *Interval (m)* | *Thickness (m)* | *Average porosity (%)* | *Porosity range (%)* | *Additional information* |
|---|---|---|---|---|---|
| Perindi 1 | 869–877 | 8 | 0.046 | Not recorded | |
| Kambara 1 | 844–852 | 8 | 0.117 | 0 – 0.13 | |
| Booran 1 | 1301–1308 | 7 | 0 | 0 – 0.01 | |

**Table 7.2. Summary of porosity data from P1 — wells within a 200 km radius of James Price Point**

| *Well* | *Interval (m)* | *Thickness (m)* | *Average porosity (%)* | *Porosity range (%)* | *Additional information* |
|---|---|---|---|---|---|
| Perindi 1 | 833–835 | 2 | 0.077 | – | Top of section |
| Minjin 1 | 779.75 – 795.25 | 15.5 | 0.287 | – | Middle ofsection |
| Kambara 1 | 809–844 | 35 | – | 0 – 0.09 | Whole section |
| Moogana 1 | 1118–1167 | 49 | 0.168 | 0 – 0.252 | Whole section |
| Puratte 1 | 1436 – 1503.5 | 67.5 | 0.162 | 0 – 0.212 | Whole section |
| Booran 1 | 1236–1301 | 65 | 0.214 | 0 – 0.234 | Whole section |
| West Kora 1 | 982.75 – 985 | 2.25 | 0.186 | – | Top of section |
| Kora 1 | 998–1098 | 100 | 0.187 | – | Depth range extends 51 m into the top of the Grant Group |
| Langoora 1 | 578.2 | – | 0.013 | – | Base of section |
| Mellany 1 | 436.516 | | 18.7 | – | Whole section. Depth range extends 38 m into the uppermost Grant Group |
| West Terrace 1 | 834–842 | 8 | – | 23–26 | Top of section |
| Pearl 1 | 902–1134 | 232 | – | 20–23 | Whole section. Depth range extends 182.5 m into the top of the Grant Group |
| East Crab Creek 1 | 676–758 | 82 | 25–32 | – | Top of section. Porosity measurement for upper sections, lower section is not porous |
| Freney 1 | 764.3 | – | 26.51 | – | Upper section |

**Table 7.3. Summary of porosity data from the Noonkanbah Formation — wells outside the 200 km radius from James Price Point**

| *Well* | *Interval (m)* | *Thickness (m)* | *Average porosity (%)* | *Porosity range (%)* | *Additional information* |
|---|---|---|---|---|---|
| Scarpia 1 | 484.9 – 497.15 | 12.25 | 29.52 | 25.8 – 33.1 | Porosity increasing with depth |

The Poole Sandstone and Noonkanbah Formation are recognized as part of the first order Late Carboniferous – Permian Megasequence and within it the second-order Early – Late Permian Supersequence I. This Report presents facies analysis and well-log data that allow further subdivision of the stratigraphic section into third-order, fourth -order and high-frequency cycles. The Poole Sandstone displays a major facies variation from northwest to southeast. Five facies associations were identified in outcrop and cored sections: fluvial (FA1), tidal flat (FA2), shoreface (FA5), mid-ramp (FA9) and offshore (FA7). The Noonkanbah Formation is dominated by mudstone facies across the study area. Four major facies associations were identified in cored sections: tidal flat (FA3), shoreface (FA5), offshore transitional (FA6) and offshore (FA7). Facies associations in the Noonkanbah Formation have a consistent stratigraphic position across large areas. Subsurface carbon dioxide ($CO_2$) sequestration is now considered a significant climate change mitigation strategy, as a result of which, a prospective $CO_2$ sequestration site was investigated in the northern Canning Basin near James Price Point. The Permo-Carboniferous Grant Group and Poole Sandstone are possible reservoirs, sealed by the Noonkanbah Formation. This report comments on the suitability of these potential reservoir and seal units based on the findings of facies and stratigraphic analysis.

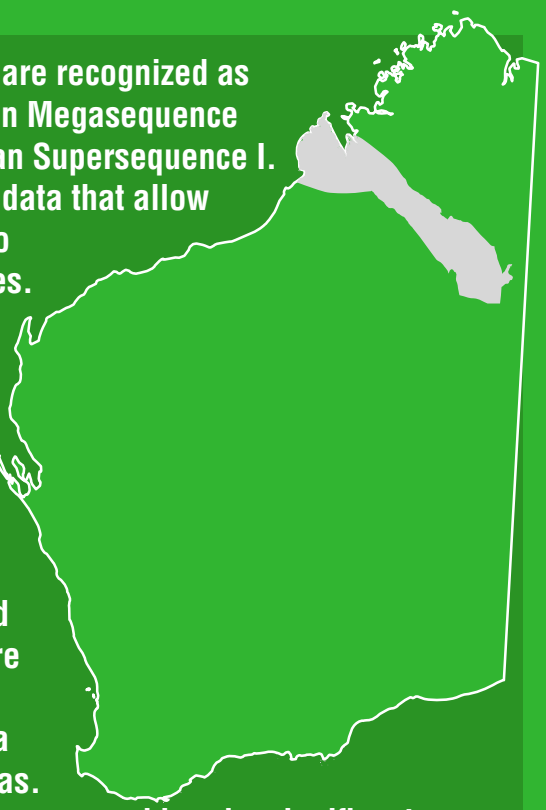

Further details of geological products and maps produced by the Geological Survey of Western Australia are available from:

Information Centre
Department of Mines and Petroleum
100 Plain Street
EAST PERTH WA 6004
Phone: (08) 9222 3459 Fax: (08) 9222 3444

www.dmp.wa.gov.au/GSWApublications

DENT CHARACTERIZATION AND CORRELATION OF LOWER PERMIAN STRATA, CANNING BASIN, WESTERN AUSTRALIA, AND IMPLICATIONS FOR $CO_2$ SEQUESTRATION REPORT 149

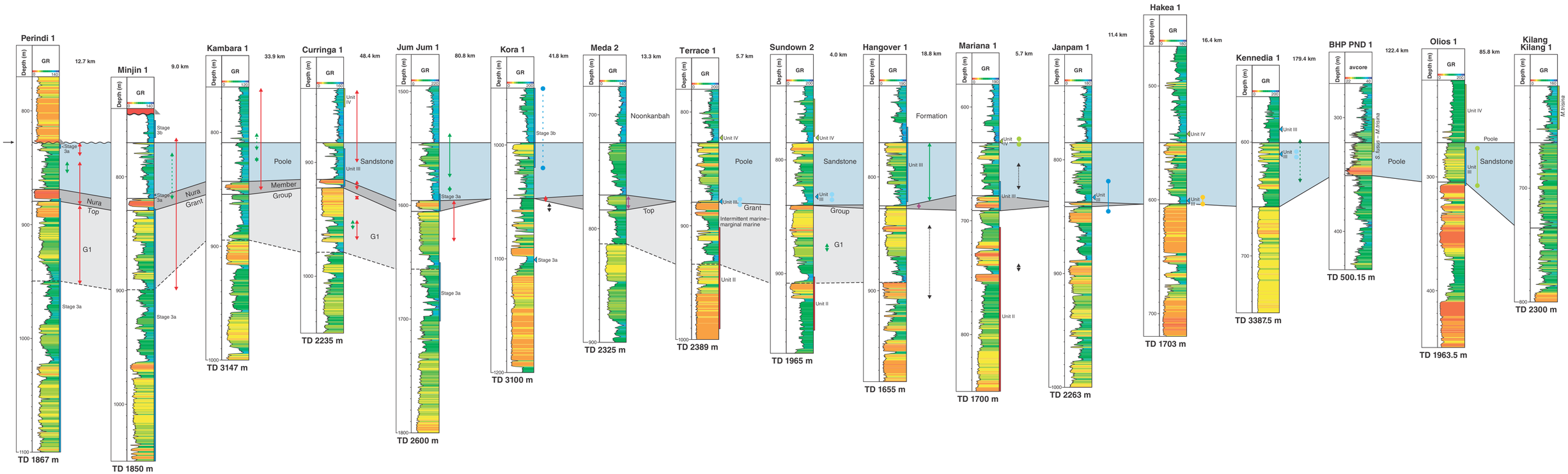


## Legend

- Poole Sandstone
- Nura Nura Member
- G1
- Casing shoe
- Datum – top of Poole Sandstone

**Environmental interpretation**

- Marine – marginal marine
- Nearshore – brackish
- Brackish/fresh – brackish
- Restricted brackish

**Features**

- Glauconite
- Trace glauconite
- Limestone
- Fossils
- Trace coal

**Palynology**

Palynology from Tables 1 and 2, Appendix 5, according to Mory (2010), coloured according to Figure 5

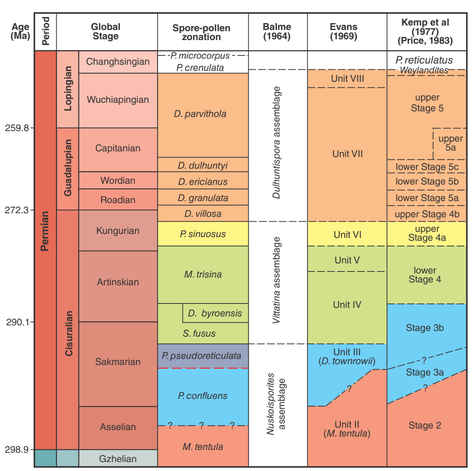


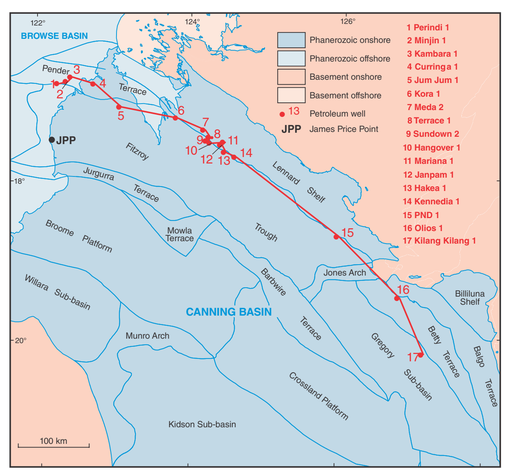


Government of Western Australia
Department of Mines and Petroleum

HON. SEAN K D'ESTRANGE MLA
MINISTER FOR MINES AND PETROLEUM

Geological Survey of Western Australia

RICK ROGERSON
EXECUTIVE DIRECTOR

**Compiled by LM Dent, 2015**
Edited by SR White
Cartography by A Symonds

Published by the Geological Survey of Western Australia. A PDF of this plate can be downloaded free from the GSWA eBookshop <www.dmp.wa.gov.au/GSWApublications>.

The recommended reference for this plate is:
Dent, LM 2016, Stratigraphic correlations of the uppermost Grant Group and Poole Sandstone, Canning Basin, Perindi 1 to Kilang Kilang 1 *in* Characterization and correlation of lower Permian strata, Canning Basin, Western Australia, and implications for $CO_2$ sequestration: Geological Survey of Western Australia, Report 149, Plate 1.

**GEOLOGICAL SURVEY OF WESTERN AUSTRALIA**

**REPORT 149 PLATE 1**

# STRATIGRAPHIC CORRELATIONS OF THE UPPERMOST GRANT GROUP AND POOLE SANDSTONE CANNING BASIN

# PERINDI 1 TO KILANG KILANG 1

June 2016

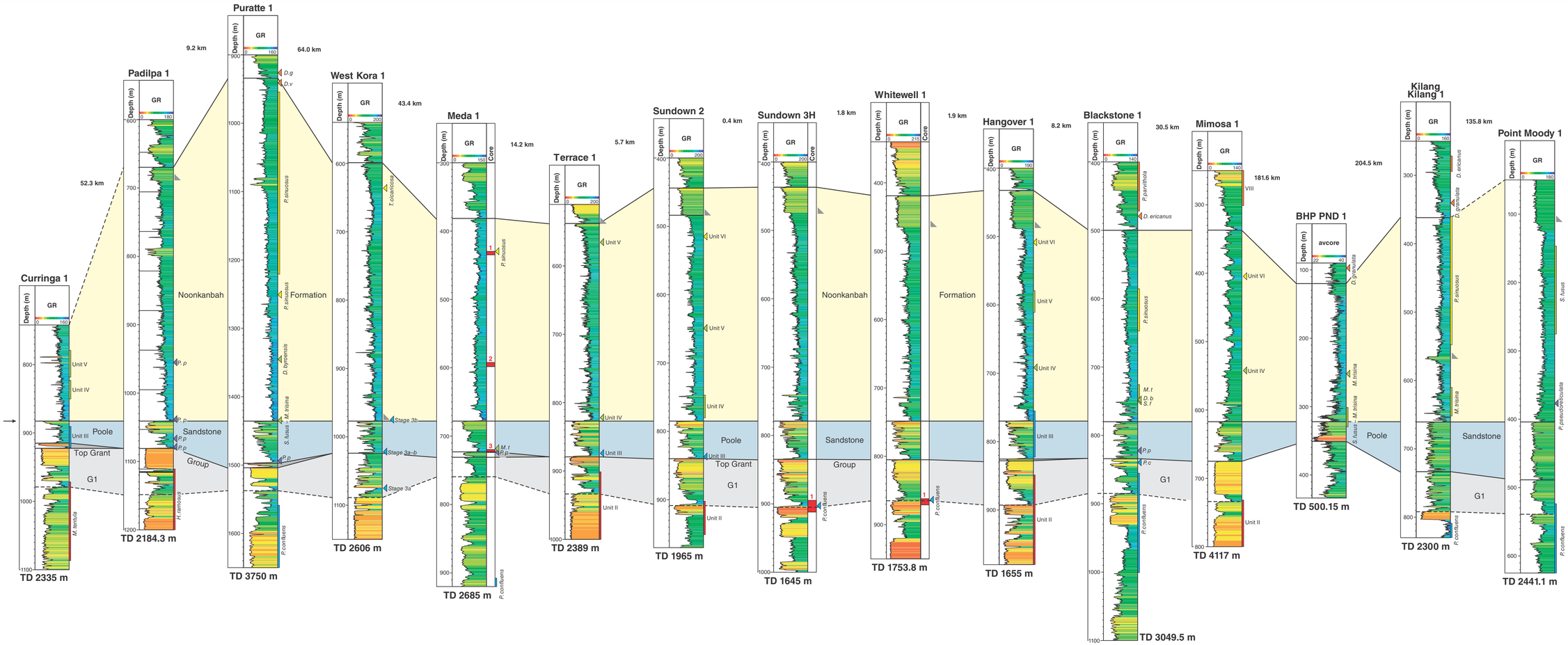


## Legend

- Noonkanbah Formation
- Poole Sandstone
- Nura Nura Member
- G1
- Casing shoe
- Datum – top of Poole Sandstone

**Palynology**

Palynology from Tables 1 and 2, Appendix 5, according to Mory (2010), coloured according to Figure 5

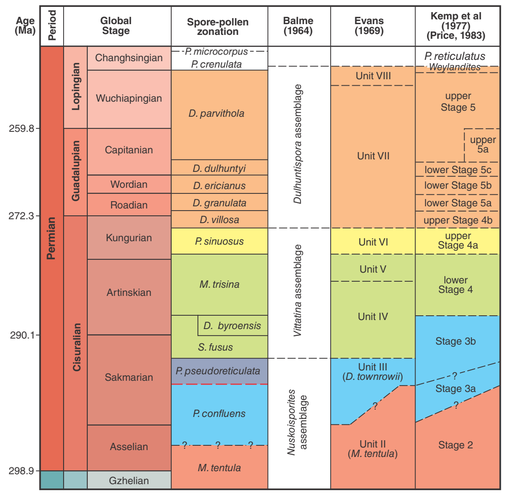


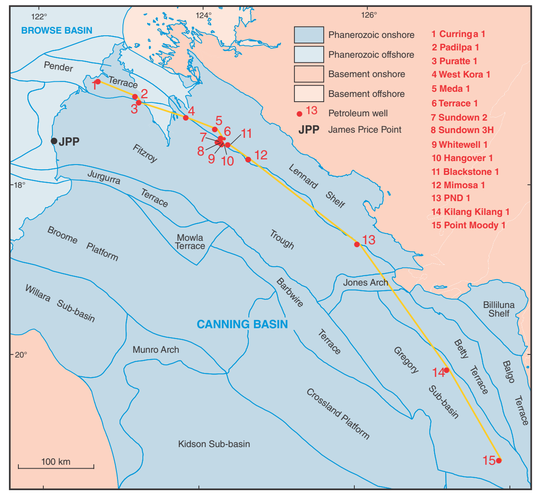


Government of **Western Australia**
Department of **Mines and Petroleum**

HON. SEAN K D'ESTRANGE MLA
MINISTER FOR MINES AND PETROLEUM

Geological Survey of Western Australia

RICK ROGERSON
EXECUTIVE DIRECTOR

**Compiled by LM Dent, 2015**
Edited by SR White
Cartography by A Symonds

Published by the Geological Survey of Western Australia. A PDF of this plate can be downloaded free from the GSWA eBookshop <www.dmp.wa.gov.au/GSWApublications>.

The recommended reference for this plate is:
Dent, LM 2016, Stratigraphic correlations of the uppermost Grant Group to Noonkanbah Formation, Canning Basin, Curringa 1 to Point Moody 1 in Characterization and correlation of lower Permian strata, Canning Basin, Western Australia, and implications for $CO_2$ sequestration: Geological Survey of Western Australia, Report 149, Plate 2.

**GEOLOGICAL SURVEY OF WESTERN AUSTRALIA**

**REPORT 149 PLATE 2**

# STRATIGRAPHIC CORRELATIONS OF THE UPPERMOST GRANT GROUP TO NOONKANBAH FORMATION CANNING BASIN

# CURRINGA 1 TO POINT MOODY 1

June 2016

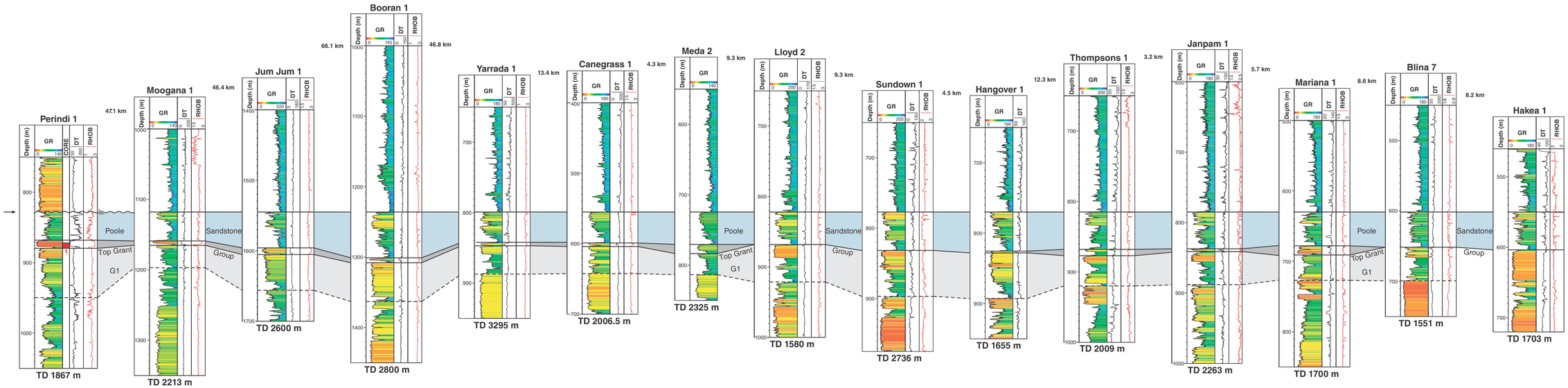


**Legend**

- Poole Sandstone
- Nura Nura Member
- G1
- Casing shoe
- Datum – top of Poole Sandstone

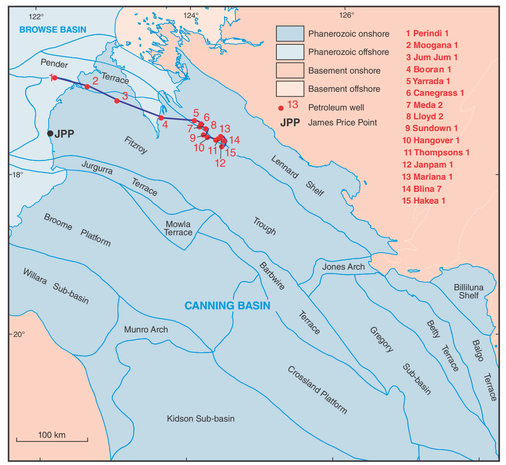


Government of **Western Australia**
Department of **Mines and Petroleum**

HON. SEAN K D'ESTRANGE MLA
MINISTER FOR MINES AND PETROLEUM

Geological Survey of Western Australia

RICK ROGERSON
EXECUTIVE DIRECTOR

**Compiled by LM Dent, 2015**
Edited by SR White
Cartography by A Symonds

Published by the Geological Survey of Western Australia. A PDF of this plate can be downloaded free from the GSWA eBookshop <www.dmp.wa.gov.au/GSWApublications>.

The recommended reference for this plate is:
Dent, LM 2016, Stratigraphic correlations of the uppermost Grant Group and Poole Sandstone, Canning Basin, Perindi 1 to Hakea 1 *in* Characterization and correlation of lower Permian strata, Canning Basin, Western Australia, and implications for $CO_2$ sequestration: Geological Survey of Western Australia, Report 149, Plate 3.

**GEOLOGICAL SURVEY OF WESTERN AUSTRALIA**

**REPORT 149 PLATE 3**

# STRATIGRAPHIC CORRELATIONS OF THE UPPERMOST GRANT GROUP AND POOLE SANDSTONE CANNING BASIN

# PERINDI 1 TO HAKEA 1

June 2016

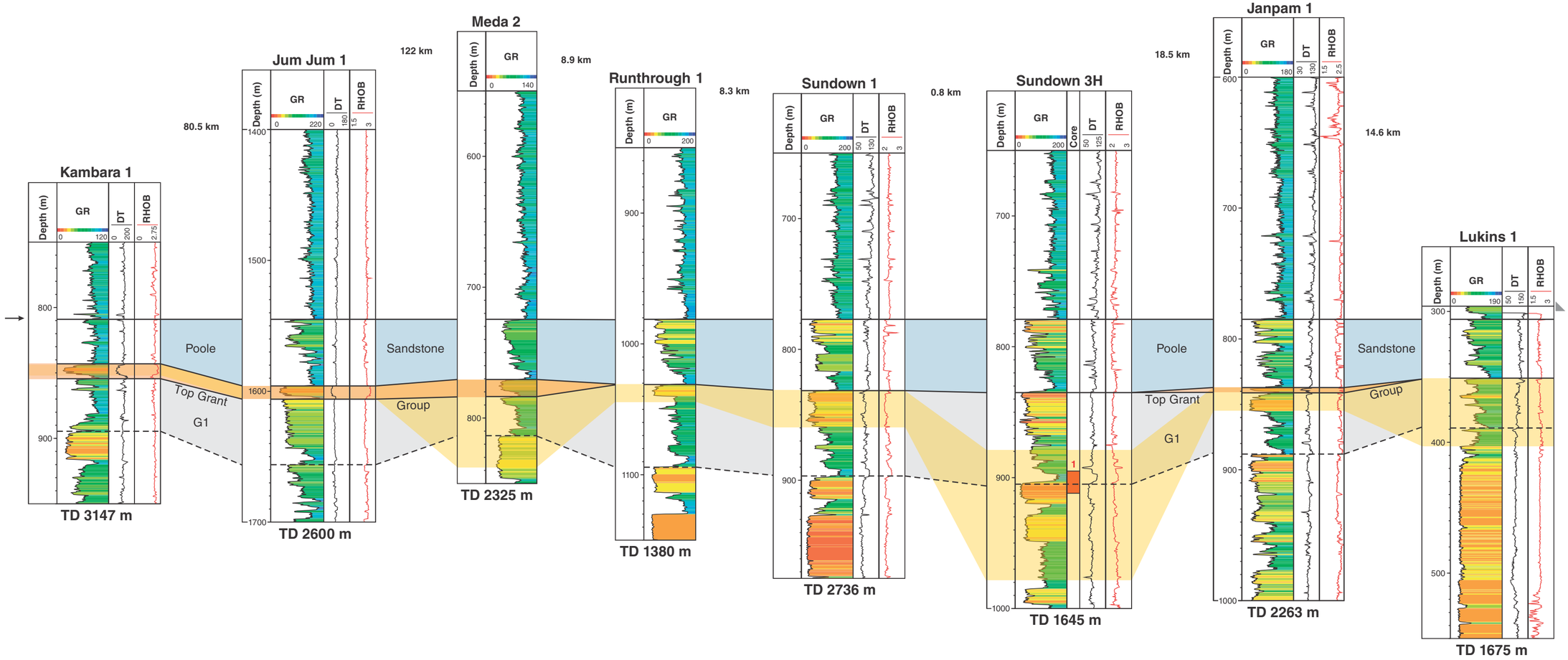


## Legend

- Currently interpreted Nura Nura Member
- Previously interpreted Nura Nura Member
- Poole Sandstone
- G1
- Casing shoe
- Datum – top of Poole Sandstone

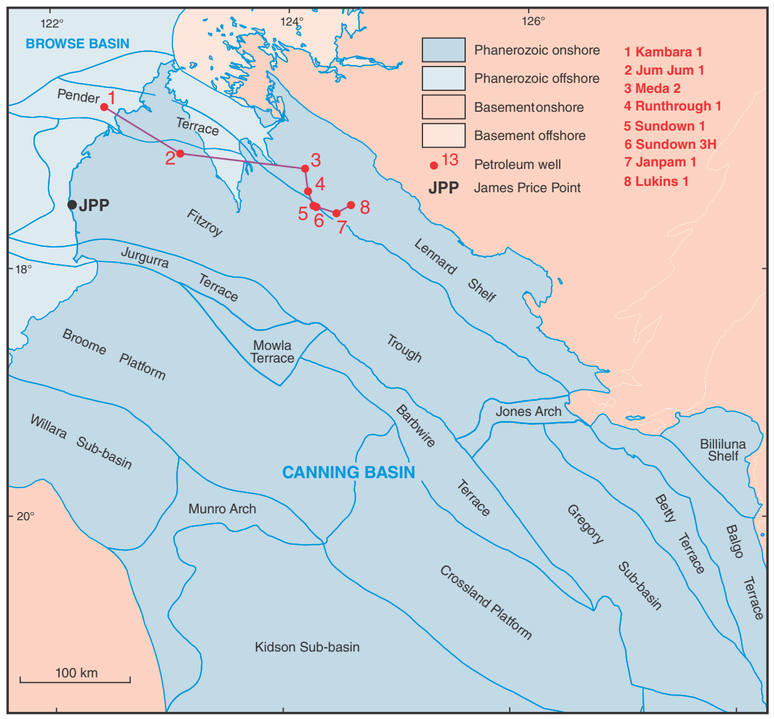


Government of **Western Australia**
Department of **Mines and Petroleum**

HON. SEAN K D'ESTRANGE MLA
MINISTER FOR MINES AND PETROLEUM

Geological Survey of Western Australia

RICK ROGERSON
EXECUTIVE DIRECTOR

**Compiled by LM Dent, 2015**
Edited by SR White
Cartography by A Symonds

Published by the Geological Survey of Western Australia. A PDF of this plate can be downloaded free from the GSWA eBookshop <www.dmp.wa.gov.au/GSWApublications>.

The recommended reference for this plate is:
Dent, LM 2016, Stratigraphic correlations of the Nura Nura Member — previous and current, Canning Basin, Kambara 1 to Lukins 1 *in* Characterization and correlation of lower Permian strata, Canning Basin, Western Australia, and implications for $CO_2$ sequestration: Geological Survey of Western Australia, Report 149, Plate 4.

**GEOLOGICAL SURVEY OF WESTERN AUSTRALIA**

**REPORT 149 PLATE 4**

# STRATIGRAPHIC CORRELATIONS OF THE NURA NURA MEMBER — PREVIOUS AND CURRENT CANNING BASIN

# KAMBARA 1 TO LUKINS 1

June 2016

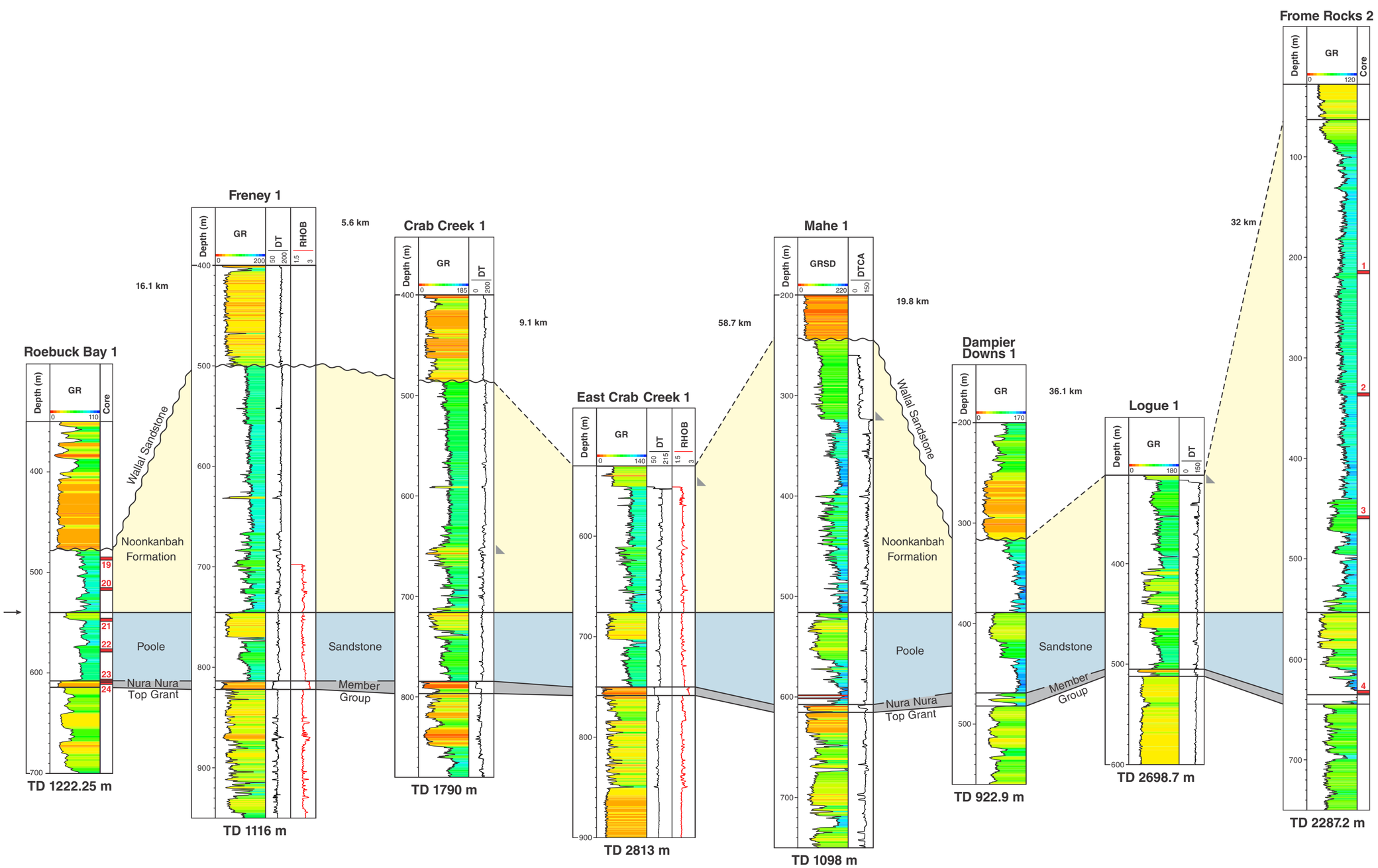


**Legend**

- Noonkanbah Formation
- Poole Sandstone
- Nura Nura Member
- G1
- Casing shoe
- Datum – top of Poole Sandstone

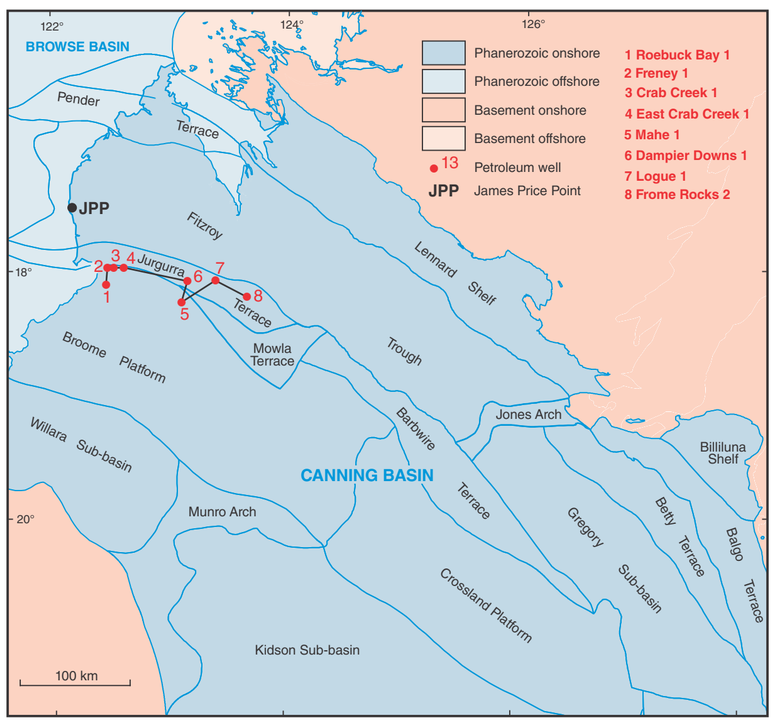


Government of **Western Australia**
Department of **Mines and Petroleum**

HON. SEAN K D'ESTRANGE MLA
MINISTER FOR MINES AND PETROLEUM

Geological Survey of Western Australia

RICK ROGERSON
EXECUTIVE DIRECTOR

**Compiled by LM Dent, 2015**
Edited by SR White
Cartography by A Symonds

Published by the Geological Survey of Western Australia. A PDF of this plate can be downloaded free from the GSWA eBookshop <www.dmp.wa.gov.au/GSWApublications>.

The recommended reference for this plate is:
Dent, LM 2016, Stratigraphic correlations of the Poole Sandstone and Noonkanbah Formation, Canning Basin, Roebuck Bay 1 to Frome Rocks 1 *in* Characterization and correlation of lower Permian strata, Canning Basin, Western Australia, and implications for $CO_2$ sequestration: Geological Survey of Western Australia, Report 149, Plate 5.

**GEOLOGICAL SURVEY OF WESTERN AUSTRALIA**

**REPORT 149 PLATE 5**

# STRATIGRAPHIC CORRELATIONS OF THE POOLE SANDSTONE AND NOONKANBAH FORMATION CANNING BASIN

# ROEBUCK BAY 1 TO FROME ROCKS 1

June 2016

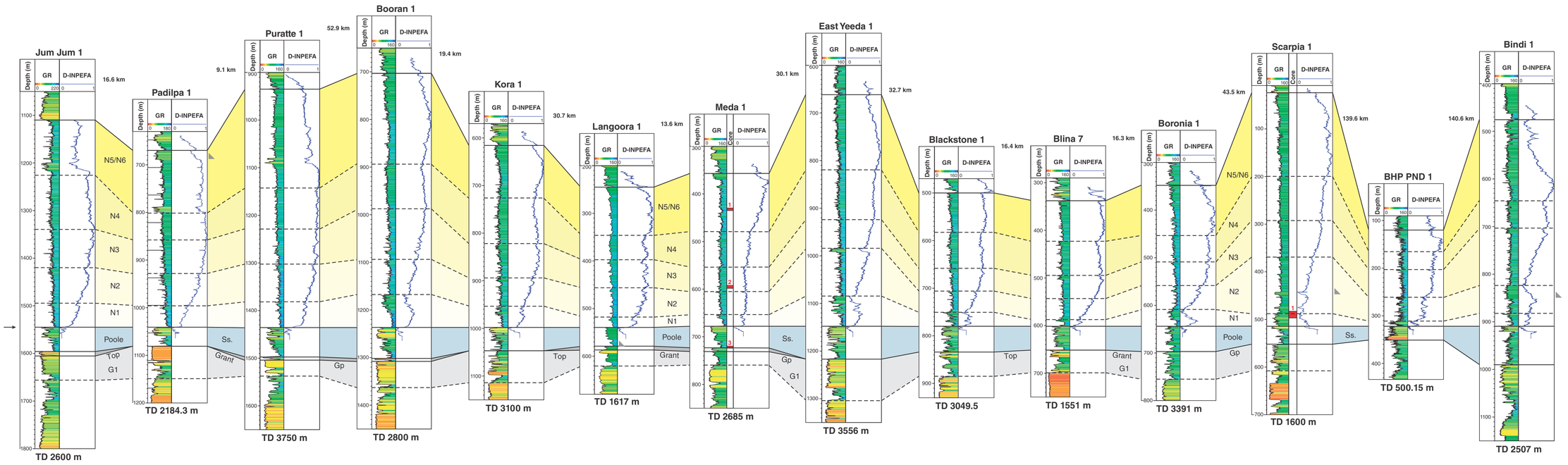


**Legend**

- N5/N6
- N4
- N3
- N2
- N1

Noonkanbah Formation

- Poole Sandstone
- Nura Nura Member
- G1

Grant Group

- Casing shoe
- Datum – top of Poole Sandstone

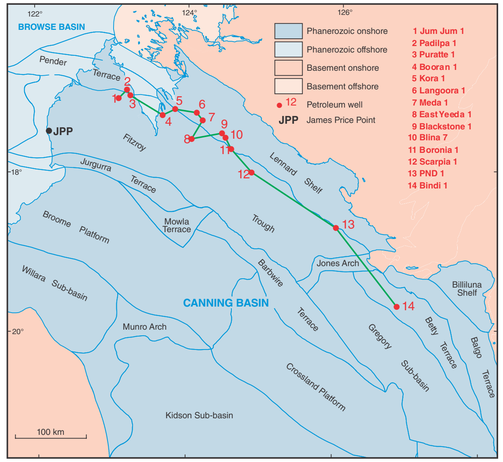


Government of Western Australia
Department of Mines and Petroleum

HON. SEAN K D'ESTRANGE MLA
MINISTER FOR MINES AND PETROLEUM

Geological Survey of Western Australia

RICK ROGERSON
EXECUTIVE DIRECTOR

**Compiled by LM Dent, 2015**
Edited by SR White
Cartography by A Symonds

Published by the Geological Survey of Western Australia. A PDF of this plate can be downloaded free from the GSWA eBookshop <www.dmp.wa.gov.au/GSWApublications>.

The recommended reference for this plate is:
Dent, LM 2016, Stratigraphic correlations of the uppermost Grant Group to Noonkanbah Formation, Canning Basin, Jum Jum 1 to Bindi 1 in Characterization and correlation of lower Permian strata, Canning Basin, Western Australia, and implications for $CO_2$ sequestration: Geological Survey of Western Australia, Report 149, Plate 6.

**GEOLOGICAL SURVEY OF WESTERN AUSTRALIA**
**REPORT 149 PLATE 6**

# STRATIGRAPHIC CORRELATIONS OF THE UPPERMOST GRANT GROUP TO NOONKANBAH FORMATION CANNING BASIN
# JUM JUM 1 TO BINDI 1

June 2016